SYNTHESIS AND ELECTROCATALYTIC PROPERTIES OF POLYMERIZABLE METALLOPHTHALOCYANINES

A thesis submitted in fulfillment of the requirements for the degree of

DOCTOR OF PHILOSOPHY

Of

RHODES UNIVERSITY

By

JOSEPH CHINYE OBIRAI

February 2005

DEDICATION

To all Lovers of Righteousness

ACKNOWLEDGEMENTS

To the making of many books there is no end and much devotion to them is wearisome to the flesh- says the patriarch King Solomon (*Eccl. 12:12)*. I found these words very true, in my case, as I tried to make my little contribution in chemistry. My greatest gratitude goes to the giver and sustainer of life, Jehovah, for seeing me through this wearisome but rewarding thirty-six months. His undeserved kindness has been sufficient for me.

I guess I was just a "good for nothing fellow". All I did was what I ought to have done as a mere tool in the capable hands of a great master. Dear Prof Tebello Nyokong, I hope I did not hurt your hands too much as a tool in your hands. For my part, I enjoyed working under your tutelage much more than my undemonstrative disposition can say- Kea leboha

Dr Fethi Bedioui and colleagues at Unité de Pharmacologie Chimique et Génétique,UMR CNRS n° 8151/ U INSERM n° 640, Ecole Nationale Supérieure de Chimie de Paris,11 rue Pierre et Marie Curie, F-75231 Paris, France. The wealth of knowledge I received from you has been valueless! Merci encore plus!!!

I thank the Department of Chemistry for giving me the opportunity to be a part of the team, as a tutor and demonstrator. My experience for the whole period showed that I was actually the learner. I learnt tolerance, patience and the need to understand and be understood from the undergrad and post grad students alike. All professional advices and comments received from the following are significantly noticed: Prof P. Kissinger, Prof L. Nagels and all reviewers who were involved in the articles published from this thesis.

Bebe, Querida and Elvire, you three constituted the sole of my feet as I walked the rough terrain. I trampled on your emotions and needs, but with good intent. Just know that no discipline seems joyous for the present, but grievous, yet afterward to those who have been trained by it, it yields peaceful fruit, namely righteousness (*Heb 12:11*). Deepest gratitude goes to my family members and friends who stood by me even at very odd times. The following have in no small measure contributed to my success: Mr. & Mrs. Adebowale, Mr. & Mrs. Nwabudike and Mr. & Mrs. Ariomovuoman.

Special thanks go to South African National Research Foundation (NRF), CNRS and EGIDE (France) for financial support.

ABSTRACT

The syntheses, spectral and electrochemical characterization of new family electropolymerizable pyrrole, thiophene and mercaptopyrimidin substituted metallophthalocyanine (MPc) complexes are described. Tetraamino substituted chromium and manganese phthalocyanine complexes were also synthesized and characterized. The spectral and electrochemical results are comparable to literature reports.

The complexes formed stable films when deposited on electrode surfaces. The MPc films were formed by electropolymerization, drop-dry method and self-assembling. Nickel hydroxide-like electrodes were formed by electrotransformation of nickel-tetra-4-(pyrrol-1-yl)phenoxy phthalocyanine polymer films to the corresponding PcNi-O-NiPc modified electrodes in alkaline solution. The thiophene, mercaptopyrimidine functionalized MPcs and amino group containing complexes formed good self-assembled monolayers (SAMs) on gold electrode. The electrode modification processes were reproducible. The conductivities of the electrode were dependent on the surface concentrations of the complexes as a function of electropolymerization scan numbers. The electrodes showed good catalytic responses toward L-cysteine, nitrite, nitric oxide (NO), glycine, phenol and its derivative and oxygen. The results also suggest that the presence of thio groups on the ring substituents lowers the oxidation potential of L-cysteine more compared to literature values.

The stability of the amperometric responses toward the various analytes is used to diagnose the applicability of the materials for electroanalytical purposes. The limits of detection for L-cysteine, nitrite, NO and glycine were in the range of $\sim 10^{-7}$ to 10^{-5} mol dm^{-3}.

Table of Contents

Contents	Page
Title Page	i
Dedication	ii
Acknowledgement	iii
Abstract	iv
Table of Contents	v
List of Abbreviations	xii
List of Symbols	xvi
List of Figures	xix
List of Schemes	xxvi
List of Tables	xxvii

Chapter One

Contents	Page
1.0 Introduction	1
1.1. Background on Electrochemical Techniques	2
1.1.1. Cyclic Voltammetry	2
1.1.1.1. *Reversible Systems*	3
1.1.1.2. *Irreversible Systems*	5
1.1.1.3. *Quasi-reversible Systems*	7
1.1.2. Differential Pulse and Square Wave Voltammetry	7
1.1.2.1. Differential Pulse Voltammetry	8

1.1.2.2.	*Square Wave Voltammetry*	9
1.1.3.	Spectroelectrochemistry	10
1.2	**Types and Properties of Electrodes**	12
1.2.1.	Optically Transparent Electrodes	12
1.2.2.	Glassy Carbon Electrode	13
1.2.3.	Frontier Orbitals and Redox Potentials	14
1.2.4.	Surface Confined Processes	15
1.2.4.1.	*Adsorbed Species*	16
1.2.4.2.	*Deposition process*	18
1.3.	**Modified Electrodes**	19
1.3.1.	Polymer Modified Electrodes	21
1.3.1.1.	*Methods of Polymer Formation on Electrode Surfaces*	23
1.3.1.2.	*Mechanism of Polymer Formation on Electrode Surfaces*	26
1.3.2.	Self-Assembled Monolayers	30
1.3.2.1.	*Preparation of SAMs*	31
1.3.2.2.	*Characterization of SAMs*	32
1.3.3.	Monolayer Annealing	33
1.3.4.	Electrocatalysis at Modified Electrodes	33
1.4.	**Chemistry of Metallophthalocyanines**	35
1.4.1.	Structure and Naming of Phthalocyanines	35
1.4.2	Electronic Structure and Spectroscopy of Metal Phthalocyanines	37
1.4.3.	Electrochemistry of Phthalocyanines	39
1.4.4.	Synthesis of Phthalocyanines	43

1.4.4.1. *Unsubstituted Phthalocyanines*	43
1.4.4.2. *Ring Substituted Phthalocyanines*	45
1.4.4.3. *Synthesis of Substituted Phthalonitrile Precursors*	48
1.4.4.4. *Mechanistic Aspects of the Synthesis of Phthalocyanines*	50
1.4.5. Applications of Metal Phthalocyanines	51
1.4.6 Electrocatalytic Properties of Metal Phthalocyanines	53
1.5. Review of Analytes to be Electrocatalyzed by Metallophthalocyanine Modified Electrodes	55
1.5.1. Aminoacids (L-Cysteine and Glycine)	55
1.5.1.1. *L-Cysteine*	55
1.5.1.2. *Glycine*	57
1.5.2. Oxygen	58
1.5.3. Nitric Oxide and Nitrite	62
1.5.4. Phenols and Chlorinated Phenols	65
1.6. Summary of Aims of Thesis	66

Chapter Two

2.0. Experimental	68
2.1. Solvents	69
2.2. Reagents	69
2.3. Instrumentation	70
2.4. Synthesis	70
2.4.1. 4-Nitrophthalonitrile	70
2.4.2. 5-(Pyrrol-1-yl)pentan-1-ol	72

2.4.3. Synthesis of substituted phthalonitriles	73
2.4.3.1. *4-(pyrrol-1-yl)phenoxy phthalonitrile*	73
2.4.3.2. *5-(pyrrol-1-yl)pentoxy phthalonitrile*	74
2.4.3.3. *4-{2-(2-thienyl)ethoxy}phthalonitrile*	74
2.4.3.4. *4-(2-mercapto)pyrimidinphthalonitrile*	75
2.5. Synthesis of Phthalocyanines	76
2.5.1 Synthesis of Pyrrole Substituted Phthalocyanine Complexes	76
2.5.1.1. *Tetra-4-(pyrrol-1-yl)phenoxy phthalocyanines*	76
2.5.1.2. *Tetra-5-(pyrrol-1-yl)pentoxyphthalocyanine Complexes*	78
2.5.2. Synthesis of Thiophene Substituted Phthalocyanine Complexes	79
2.5.3. Synthesis of Pyrimidin Substituted Phthalocyanine Complexes	81
2.5.3.1. *Cobalt tetra-(2-mercapto)pyrimidyl phthalocyanine*	81
2.5.3.2. *Synthesis of the other metal containing tetramercaptopyrimidyl phthalocyanines*	83
2.5.4. Chromium (OH)CrTAPc and Manganese (OH)MnTAPc Tetraaminophthalocyanine	84
2.6. Electrochemical methods	85
2.6.1. General Conditions	85
2.6.2 Electrode modification	87
Results and Discussions	89
Publications	90

Chapter Three

3.0 Syntheses and Spectral Characterization		91
3.1	**N-Pyrrole Substituted Phthalocyanines**	94
3.1.1	N-Phenoxy Pyrrole	94
3.1.2	N-Pentoxy Pyrrole	105
3.2.	**Metal-tetra-{2-(2-thienyl)ethoxy}phthalocyanine**	106
3.3.	**Mercaptopyrimidine Substituted Metallophthalocyanines**	110
3.4.	**Tetra Substituted Amino-derivatized metallophthalocyanine**	118

Chapter Four

4.0. Electrochemical Properties		122
4.1.	**Pyrrole Substituted Metallophthalocyanine Complexes**	123
4.1.1.	Cyclic and square wave voltammetry	123
4.1.2.	Spectroelectrochemistry	130
4.2.	**Mercaptopyrimidin Substituted Metallophthalocyanine Complexes**	139
4.2.1.	Cyclic voltammetry and square wave voltammetry	139
4.2.2.	Spectroelectrochemistry	143
4.3.	**Amino Substituted Phthalocyanine Complexes**	146
4.3.1.	Cyclic and square wave voltammetry	146
4.3.2.	Spectroelectrochemistry	151
4.4.	**Thiophene Substituted Metallophthalocyanine Complexes**	158
4.4.1.	Cyclic and square wave voltammetry	158
4.4.2.	Spectroelectrochemistry	166

Chapter Five

5.0. Electrode Modification	169
5.1. Pyrrole Substituted Metallophthalocyanines	170
5.1.1. Electropolymerization of cobalt-tetra-4-(pyrrol-1-yl)phenoxy phthalocyanine	170
5.1.2. Electropolymerization of cobalt-tetra-5-(pyrrol-1-yl)pentoxy phthalocyanine	177
5.1.3 Electropolymerization of nickel-tetra-4-(pyrrol-1-yl)phenoxy phthalocyanine	181
5.2. Tetraamino Metallophthalocyanine Complexes	190
5.2.1 Electropolymerization of chromium tetraamino-phthalocyanine	190
5.2.2 Electropolymerization manganese tetraamino-phthalocyanine	195
5.2.2.1. *pH Study of the Redox Processes of Poly-MnTAPc*	198
5.2.2.2. *Spectral Characterization of Poly-MnTAPc film*	204
5.3. Mercaptoyrimidin Substituted Metallophthalocyanine	205
5.3.1. Electropolymerization	205
5.3.2. The Effect of pH on the *Poly*-Mn^{III}TMPyrPc/Mn^{II}TMPyrPc Redox Couples	207
5.4. Thiophene Substituted Metallophthalocyanine Complexes	209
5.5. Self-Assembled Monolayer Formation	211
5.5.1. CoTMPyrPc	212
5.5.2. CoTETPc and CrTAPc	215
Conclusions	217

Chapter Six

6.0. Electrocatalytic Properties	219
6.1. Electrocatalytic Oxidation of Amino Acids (L-cysteine and Glycine)	220
6.1.1. L-Cysteine	220
6.1.1.1. Pyrrole Substituted CoPc	220
6.1.1.2. Thiophene Substituted CoPc	224
6.1.1.3. Mercaptopyrimidin Substituted CoPc	228
6.1.2. Glycine Reduction on MnTAPc-Modified Electrode	230
6.2. Phenol and its Derivatives on NiPc	232
6.2.1. Electrocatalytic Oxidation of p-Chlorophenol	232
6.2.2. Electrocatalytic Oxidation of Phenol	239
6.2.3. Electrocatalytic Oxidation of p- Nitrophenol	241
6.3. Electrocatalytic Reduction of Oxygen	242
6.4. Electrocatalytic Oxidation of Nitric Oxide and Nitrite	250
6.4.1. Nitric Oxide (NO)	250
6.4.2. Nitrite	252

Chapter Seven

7.0. Conclusions	255
References	259

List of Abbreviations

AE	=	Auxiliary electrode
AFM	=	Atomic force microscopy
Ag	=	Silver wire pseudo-reference electrode
Ag|AgCl	=	Silver-silver chloride reference electrode
BAS	=	BioAnalytical Systems
4-CP (p-CP)	=	4-chlorophenol (or para chlorophenol)
CB	=	Conduction band
$CDCl_3$	=	Deuterated chloroform
CH_3CN	=	Acetonitrile
CME	=	Chemically modified electrode
CoP	=	Cobaltporphyrin
CoPc	=	Cobaltphthalocyanine
CoTPOPyPc	=	Cobalt-tetra-5-(pyrrol-1-yl)pentoxyphthalocyanine
CE	=	Counter electrode
COP	=	Conducting organic polymer
CP	=	Conjugated polymer
CV	=	Cyclic voltammetry
DBU	=	1,8-diazabicyclo[5.4.0] undec-7-ene
DCM	=	Dichloromethane
DMEA	=	N,N-Dimethylethanolamine
DMF	=	Dimethylformamide
DMSO	=	Dimethylsulfoxide

$DMSO-d_6$	=	Deuterated dimethylsulfoxide
DPV	=	Differential pulse voltammetry
EQCM	=	Electrochemical quartz crystal microbalance
ETME	=	Electron-transfer-mediated electrocatalysis
FTIR	=	Fourier transform infrared
GCE	=	Glassy carbon electrode
GSC	=	Graphite single crystal
HIV	=	Human immune-deficient virus
^1H NMR	=	Proton nuclear magnetic resonance
HOMO	=	Highest occupied molecular orbital
HOPG	=	Highly oriented pyrolytic graphite
TPhPyPc	=	Tetra-4-(pyrrol-1-yl)phenoxy phthalocyanine
TPOPyPc	=	Tetra-5-(pyrrol-1-yl)pentoxyphthalocyanine
ITO	=	Indium tin oxide
IR	=	Infrared
LB	=	Langmuir-Blodgett
LCDs	=	Liquid crystal displays
LoD	=	Limit of detection
LMCT	=	Ligand-to-metal charge transfer
LUMO	=	Lowest unoccupied molecular orbital
MLCT	=	Metal-to-ligand charge transfer
MOBTPc	=	Metal-octabutylthiophthalocyanine
MOHETPc	=	Metal-octahydroxyethylthiophthalocyanine

MO	=	Molecular orbital
MPc	=	Metallophthalocyanine
MPc-SAM	=	Metallophthalocyanine-Self-assembled monolayer
MPc/gold-SAM	=	Metallophthalocyanine-Self-assembled monolayer on gold
MTAPc	=	Metal-tetraaminophthalocyanine
MTETPc	=	Metal-tetra-{2-(2-thienyl)ethoxy}phthalocyanine
MTMPyrPc	=	Metal-tetra-(2-mercapto)pyrimidinphthalocyanine
MTPhPyPc	=	Metal-tetra-4-(pyrrol-1-yl)phenoxy phthalocyanine
MTPP	=	Metal-tetraphenyl porphyrin
MTSPc	=	Metal-tetrasulfophthalocyanine
NIR	=	Near infrared
NO	=	Nitric oxide
OSWV	=	Osteryoung square wave voltammetry
OTE	=	Optically transparent electrode
OTTLE	=	Optically transparent thin layer electrode
PBS	=	Phosphate buffer solution
Pc	=	Phthalocyanine
PDT	=	Photodynamic therapy
Ppy	=	Poly pyrrole
PG	=	Pyrolytic graphite
RE	=	Reference electrode
R_f	=	Retention factor
RHE	=	Reversible hydrogen electrode

RT	=	Room temperature
SEM	=	Scanning electron microscopy
SWV	=	Square wave voltammetry
$TBABF_4$	=	Tetrabutylammonuim tetrafluorobarate
TEAP	=	Tetraethylammonium perchlorate
THF	=	Tetrahydrofuran
TPP	=	Tetraphenyl porphyrin
VB	=	Valence band
UV-Vis	=	Ultraviolet-Visible
UV-Vis-NIR	=	Ultraviolet-Visible-near infrared
WE	=	Working electrode

List of Symbols

α	=	Rate of electron transfer
α_a	=	Rate of electron transfer of oxidized species
α_c	=	Rate of electron transfer of reduced species
k^{α}	=	Rate of diffusion of species to the electrode surface.
Δ	=	Heat
Γ	=	Surface coverage or surface concentration
Γ_O	=	Surface concentration of oxidized species
Γ_R	=	Surface concentration of reduced species
Γ_T	=	Total surface coverage or surface concentration
Γ_{ibf}	=	Ion barrier factor
ε	=	Extinction coefficient
μ	=	Micro
π	=	Pi bonding
π^*	=	Pi anti-bonding
ν	=	Scan rate
λ	=	Wavelength
[O]	=	Concentration of oxidized species
[R]	=	Concentration of reduced species
A	=	Surface area of electrode
C	=	Concentration
C_s	=	Specific interfacial capacitance
δ[C]	=	Change in concentration

D	=	Diffusion coefficient
DMEA	=	N,N-Dimethylethanolamine
E	=	Potential
$E_{1/2}$	=	Half-wave potential
E_{FWHM}	=	Potential corresponding to full-width at half maximum
E_i	=	Initial potential
E_λ	=	Reversal (or switching) potential
E_p	=	Peak potential
E_{pa}	=	Anodic peak potential
E_{pc}	=	Cathodic peak potential
E^o	=	Standard potential
$E^{o'}$	=	Formal potential
ΔE	=	Change in potential
ΔE_p	=	Anodic-to-cathodic peak potential
$E^{o'}_{Surf}$	=	Formal redox potential of surface confined species
F	=	Faraday's constant
Hz	=	Hertz
I_{ch}	=	Charging current
i_f	=	Forward half-cycle
i_r	=	Reverse half-cycle
I_p	=	Peak current
I_{pa}	=	Anodic peak current
I_{pc}	=	Cathodic peak current

K	=	Kelvin
mV	=	Millivolts
n	=	Number of electrons
n_α	=	Number of electrons transferred
Q	=	Electrical charge
Q_{Bare}	=	Intergrated electrical charge due to bare gold electrode
Q_{SAM}	=	Intergrated electrical charge due to MPc-SAM-modified gold electrode
R	=	Universal gas constant
Subs	=	Substrate
T	=	Temperature
t	=	Time
V	=	volts
V_x	=	Velocity of solution movement perpendicular to disc
x	=	Distance of diffusing electroactive species from electrode surface

List of Figures

Chapter 1

Figure caption		Page
Fig 1.1:	Cyclic voltammogram for a reversible process.	2
Fig 1.2:	Typical cyclic voltammogram of a totally irreversible system	6
Fig 1.3:	Potential waveform for differential pulse voltammetry	8
Fig 1.4:	Potential waveform for square wave voltammetry.	10
Fig 1.5:	Schematic representation of chemical functionalities at edge plane of pyrolytic graphite	13
Fig 1.6:	Energy level diagram for metal (electrode), semiconductor and redox active (MPc) system.	15
Fig 1.7:	A representation of the interfacial electrochemical transformations of immobilized electroactive species.	16
Fig 1.8:	Theoretical cyclic voltammogram for the reduction of adsorbed and reoxidation of the product.	17
Fig 1.9:	Typical cyclic voltammogram for a metal deposition reaction exhibiting a nucleation over potential.	19
Fig 1.10:	A schematic model of the over layer structure formed by alkanethiolate SAMs on Au(111).	31
Fig 1.11:	Numbering scheme of a phthalocyanine system.	36
Fig 1.12:	Representative sketch of phthalocyanine and some related molecules.	37
Fig 1.13:	Molecular orbital diagram of the π-system of an ideal 16 atom, 18 π-electron system showing the origin of the Q and B bands.	38
Fig 1.14:	Typical room temperature electronic absorption spectra of MPc^{-2}.	39
Fig 1.15:	Structure of MPc complexes studied in this work.	42
Fig 1.16:	Examples of some phthalocyanine precursors.	43

Fig 1.17: Structure of a subphthalocyanine.	47
Fig 1.18: Structure of MPc complexes studied in this thesis.	67

Chapter 3

Fig 3.1: List of the tetra- pyrrole, thiophene, pyrimidin and amino functionalized metallophthalocyanine complexes studied in this work	91
Fig 3.2: Electronic absorption spectra of CoTPhPyPc (**7**), FeTPhPyPc (**8**), MnTPhPyPc (**9**), NiTPhPyPc (**10**) and ZnTPhPyPc (**11**) in DMF.	98
Fig 3.3: Changes in the UV-Visible spectra with changes in the concentration of complexes CoTPhPyPc (**7**), FeTPhPyPc (**8**), MnTPhPyPc (**9**), NiTPhPyPc (**10**) and ZnTPhPyPc (**11**) in DMF.	102
Fig 3.4: A representative plot showing Beers law behaviour of the N-pyrrole substituted metallophthalocyanine complexes.	104
Fig 3.5: Electronic absorption spectra of CoTPOPyPc in DCM and DMF.	105
Fig 3.6: Electronic absorption spectra of CoTETPc **(16)**, (Cl)MnTETPc (**17**) and ZnTETPc **(18)** in DMF.	108
Fig 3.7: Changes in the UV-Vis spectra with concentration of complexes **16** (CoTETPc), **17** (MnTETPc) and **18** (ZnTETPc).	109
Fig 3.8: UV-visible spectra of CoTMPyrPc and ZnTMPyrPc MnTMPyrPc in DMF.	112
Fig 3.9: UV-Visible spectral changes observed for MnTMPyrPc in the absence and presence of O_2 or imidazole.	114
Fig 3.10: Changes in the UV-Vis spectra with concentration of complexes **13** (CoTMPyrPc), **14** (MnTMPyrPc) and **18** (ZnTMPyrPc).	117
Fig 3.11: UV-Visible spectra of (i) CrTAPc (**19**) and (ii) MnTAPc (**20**) in DMF.	120

Chapter 4

Fig 4.1:	Cyclic voltammograms of complexes CoTPhPyPc (**7**), FeTPhPyPc (**8**), MnTPhPyPc (**9**), NiTPhPyPc (**10**) and ZnTPhPyPc (**11**) in DMF.	125
Fig 4.2:	Cyclic and square wave voltammograms of CoTPOPyPc in DMF.	129
Fig 4.3:	Spectroscopic changes during controlled potential electrolysis of CoTPhPyPc (**7**) in DMF at various potential values.	131
Fig 4.4:	Spectroscopic changes during controlled potential electrolysis of FeTPhPyPc (**8**) in DMF at various potential values.	135
Fig 4.5:	Spectroscopic changes during controlled potential electrolysis (- 0.2 and – 1.3 V) of complex MnTPhPyPc (**9**) in DMF.	137
Fig 4.6:	Spectroscopic changes during controlled potential electrolysis (OTTLE) of complex NiTPhPyrPc (**10**) in DMF.	138
Fig 4.7:	Cyclic voltammograms of CoTMPyrPc (**13**), MnTMPyrPc (**14**) and ZnTMPyrPc (**15**) in DMF.	140
Fig 4.8:	UV-Visible spectral changes observed during controlled potential electrolysis of CoTMPyrPc (**13**) in DMF at various potential values.	144
Fig 4.9:	Cyclic voltammogram of CrTAPc (**19**) complex in DMF.	147
Fig 4.10:	Cyclic voltammogram of MnTAPc (**20**) in DMF.	149
Fig 4.11:	UV-Visible spectral changes observed during controlled potential reduction and oxidation of Cr^{III}TAPc (**19**) in DMF at various potential values.	152
Fig 4.12:	Electronic absorption spectral changes observed during controlled potential reduction and oxidation of MnTAPc (**20**) in DMF at various potential values.	155
Fig 4.13:	Cyclic voltammograms and OSWV CoTETPc (**16**), MnTETPc (**17**) and ZnTETPc (**18**) in DMF.	159
Fig 4.14:	UV-Visible spectral changes observed during controlled potential (- 0.5 V and - 1.1 V) reduction MnTETPc (**17**) in DMF.	167

Chapter 5

Fig 5.1:	Cyclic voltammogram of CoTPhPyPc (**7**) in DCM.	171
Fig 5.2:	Evolution of the cyclic voltammograms of CoTPhPyPc (**7**) in DCM.	172
Fig 5.3:	Cyclic voltammograms of poly(Co-TPhPyPc) film in fresh DCM.	174
Fig 5.4:	Evolution of the CVs of CoTPhPyPc (**7**) in DCM. Electrode: ITO	176
Fig 5.5:	Absorption spectra of polyCoTPhPyPc films on ITO electrodes	177
Fig 5.6:	Evolution of the cyclic voltammograms of complex CoTPOPyPc (**12**) in DCM.	178
Fig 5.7:	Voltammetric responses and repetitive cycling of *poly*-CoTPOPyPc electrode in blank DCM.	180
Fig 5.8:	Repetitive cyclic voltammograms of NiTPhPyPc (**10**) in DCM.	181
Fig 5.9:	Cyclic voltammograms of *poly*-NiTPhPyPc-GCE in DCM.	183
Fig 5.10:	Repetitive cyclic voltammograms of *poly*-$[NiTPhPyPc]_{20}$ in NaOH.	184
Fig 5.11:	Cyclic voltammograms of unmodified and *poly*-Ni(OH)TPhPyPc GCE electrodes in NaOH.	185
Fig 5.12:	UV-Visible spectra of *poly*-$[NiTPyPhPy]_n$ and *poly*-Ni(OH)TPhPyPc on ITO electrodes.	187
Fig 5.13:	Evolution of cyclic voltammograms during electropolymerization of CrTAPc (**19**) in DMF.	191
Fig 5.14:	Voltammetric profiles of the absorbed CrTAPc polymer on a GCE in a N_2 deaerated pH 4.3 acetate buffer solution.	192
Fig 5.15:	Evolution of cyclic voltammograms during electropolymerization of CrTAPc in DMF on ITO.	193
Fig 5.16:	UV-Visible spectra of *poly*-CrTAPc on ITO.	194
Fig. 5.17:	SEM micrographs showing the morphology of *poly*-CrTAPc	195
Fig 5.18:	Evolution (on GCE) of the cyclic voltammograms of MnTAPc (**20**) in DMF and pH 4-11.	198

Fig 5.19: Changes in cyclic voltammograms of *poly*-MnTAPc film in KCl and KNO_3 solutions.	202
Fig 5.20: Variation of peak potential with pH for couple **II** of poly-MnTAPc.	204
Fig 5.21: Electronic absorption spectra of polymer *poly*-MnTAPc and monomeric (MnTAPc) on ITO.	205
Fig 5.22: Repetitive cyclic voltammetry at a glassy carbon electrode of MnTMPyrPc (**14**) in DCM.	206
Fig 5.23: Cyclic voltammograms of *poly*-MnTMPyrPc in aqueous phosphate buffer solutions.	208
Fig 5.24: Plot of peak separation vs. pH and cathodic peak potential vs. pH for *poly*-MnTMPyrPc in aqueous phosphate buffer solution.	209
Fig 5.25: Cyclic voltammograms of bare GCE and CoTETPc modified GCE in pH 4.0 phosphate buffer.	210
Fig 5.26: Cyclic voltammograms of gold electrode before and after CoTMPyrPc/gold-SAM formation in KOH solution, and $K_4Fe(CN)_6$ in KCl solution..	212
Fig 5.27: Cyclic voltammograms of gold electrode before and after CoTETPc/gold-SAM formation, in KOH solution, and $K_4Fe(CN)_6$ in KCl solution..	215
Fig 5.28: Cyclic voltammograms of gold electrode before and after CrTAPc/gold-SAM formation in $K_4Fe(CN)_6$ in 0.1 M KCl solution.	216

Chapter 6

Fig 6.1 Cyclic voltammograms of a bare GCE and a *poly*-CoTPhPyPc film modified GCE in phosphate buffer solution in the presence of L-cysteine.	221
Fig 6.2: Cyclic voltammetric responses of bare GCE and CoTETPc (**16**) modified GCE in the presence of L-cysteine.	224
Fig 6.3a: Repetitive cyclic voltammogram of 1 mM L-cysteine at CoTETPc (**16**) modified GCE in pH 4.0 phosphate buffer solution.	225
Fig 6.3b: Cyclic voltammogram of 1 mM L-cysteine at CoTETPc (**16**) modified GCE in pH 4.0 phosphate buffer solution, before and after 30	

	repetitive scans.	226
Fig 6.4:	Cyclic voltammetry of CoTETPc (**16**) modified GCE in the presence of varying concentrations of L-cysteine.	227
Fig 6.5:	CV of CoTETPc-GCE in 0.1 M L-cysteine in pH 4 buffer solution, immediately after the electrode fabrication and 8 days after use.	228
Fig 6.6:	Cyclic voltammetric responses of bare GCE and CoTMPyrPc (**13**) modified GCE in the presence of L-cysteine.	229
Fig 6.7:	Cyclic voltammetry of CoTMPyrPc (**13**) modified GCE in the presence of varying concentrations of L-cysteine.	230
Fig 6.8:	Detection of bare GCE and *poly*-MnTAPc-GCE in the presence of glycine.	231
Fig 6.9:	First cyclic voltammogram of p-chlorophenol (p-CPh) at unmodified GCE, *poly*-Ni(OH)TPhPyPc and *poly*-[NiTPhPyPc]$_{20}$ modified GCE.	232
Fig 6.10:	Repetitive cyclic voltammograms of p-CPh at unmodified GCE, *poly*-Ni(OH)TPhPyPc and *poly*-[NiTPhPyPc]$_{20}$ modified GCE.	233
Fig 6.11:	Cyclic voltammograms of p-CPh at passivated electrodes unmodified, *poly*-NiTPhPyPc and *poly*-Ni(OH)TPhPyPc modified GCEs.	235
Fig 6.12:	Cyclic voltammograms of p-CPh in at unmodified and *poly*-Ni(OH)TPhPyPc modified GCEs.	236
Fig 6.13:	Cyclic voltammograms of p-CPh at *poly*-NiTSPc and *Poly*-Ni(OH)TPhPyPc modified GCE, before electrolysis and after controlled potential electrolysis at 0.4 V.	237
Fig 6.14:	Cyclic voltammograms of phenol at unmodified and *poly*Ni(OH)TPhPyPc modified GCEs before and after passivation.	240
Fig 6.15:	Cyclic voltammograms of p-NPh at unmodified GCE and *poly*-Ni(OH)TPhPyPc-GCE before and after passivation.	241
Fig 6.16:	Cyclic voltammogram of [*poly*-CrTAPc]$_{20}$ modified GCE in DCM solution.	243
Fig 6.17:	Cyclic voltammogram of [*poly*-CrTAPc]$_{20}$ modified GCE in oxygen-free and molecular oxygen saturated DCM.	244

Fig 6.18:	Cyclic voltammogram of [*poly*-MnTAPc]$_{20}$ modified GCE in DCM.	246
Fig 6.19:	Cyclic voltammograms of [*poly*-MnTAPc]$_{20}$ modified GCE in oxygen-free, molecular oxygen saturated DCM and in the presence of benzoic anhydride.	247
Fig 6.20:	Cyclic voltammogram of *poly*-MnTMPyrPc modified GCE in oxygen-free; molecular oxygen saturated DCM and in the presence of benzoic anhydride.	248
Fig 6.21:	Cyclic voltammogram of *poly*-CoTPhPyPc modified GCE in oxygen-free, molecular oxygen saturated DCM and in the presence of benzoic anhydride.	249
Fig 6.22:	Voltammetric response for NO at an unmodified GCE and [*poly*-CrTAPc]$_{20}$ modified GCE.	251
Fig 6.23:	Cyclic voltammetric response of NO_2^- on unmodified GCE and [*poly*-CrTAPc]$_{50}$ for varying concentrations of NO_2^-.	252
Fig 6.24:	Plots of (a) Ip vs. $\nu^{1/2}$; (b) E_p vs. log v and (c) $I_p\nu^{1/2}$ vs. ν for 1.4 x 10^{-4}M NO_2^-.	253

List of Schemes

Scheme		Page
Scheme 1.1:	Examples of polymers formed from monomers by electrooxidation.	27
Scheme 1.2:	Proposed mechanistic pathway for the electro polymerization of pyrrole functionalized macro cyclic complexes and MTAPc complexes.	28
Scheme 1.3:	Schematic representation of a mediated electrocatalysis	34
Scheme 1.4:	Redox behaviour of cobaltphthalocyanine in coordinating and non-coordinating media.	40
Scheme 1.5:	Synthesis of MPc using Li-pentanol to achieve cyclotetramerization.	44
Scheme 1.6:	Scheme for the synthesis of metallophthalocyanines.	45
Scheme 1.7:	Route for the synthesis of 4,5-dichlorophthalonitrile and 4-nitrophthalonitrile.	49
Scheme 1.8:	Synthetic route for modification of 4-nitrophthalonitrile and 4,5-dichlorophthalonitrile.	49
Scheme 1.9:	Mechanistic scheme for cyclotetramerization of phthalonitriles during synthesis of MPcs.	51
Scheme 1.10:	A general scheme for the series (consecutive)-parallel reactions of O_2 and H_2O_2.	59
Scheme 3.1:	Synthetic route for N-pyrrole substituted pentanol.	94
Scheme 3.2:	Synthetic route for the functionalized phthalonitriles used in synthesis of the MPcs studied in this thesis.	95
Scheme 3.3:	Synthetic routes for the preparation of pyrrole substituted phthalocyanine complexes.	97
Scheme 3.4:	Synthetic routes for the preparation of thiophene and mercaptopyrimidin substituted phthalocyanine complexes.	107
Scheme 3.5:	A simplified synthetic route for the preparation of CrTAPc and MnTAPc.	119

List of Tables

Table		Page
Table 1.1:	Diagnostic tests for electrochemical reversibility of a redox couple.	5
Table 1.2:	Diagnostic tests for electrochemical irreversible redox systems.	7
Table 1.3:	Diagnostic tests for electrochemical quasi-reversible redox systems.	7
Table 1.4:	Comparative peak potential and limit of detection (LoD) for cysteine electrooxidation using selected cobalt and iron phthalocyanines.	57
Table 1.5:	Comparative peak potential for the electrocatalytic reduction of O_2 using some phthalocyanine related species.	61
Table 1.6:	Comparative peak potential and limit of detection (LoD) for the electrocatalysis of NO and NO_2^- using some phthalocyanine species.	63
Table 3.1:	List of MPc complexes studied in this thesis: their abbreviations, complex numbers and IR vibrations.	92
Table 3.2:	List of MPc complexes studied in this thesis: their abbreviations, complex numbers and IR vibrations.	93
Table 3.3:	List of MPc complexes studied in this thesis: their abbreviations, wavelength of absorption maxima (λ_{max}/nm) and extinction coefficients in DMF.	100
Table 4.1:	Redox potentials $E_{1/2}$ E_{pa}/V for CoTPhPyPc, FeTPhPyPc, MnTPhPyPc, NiTPhPyPc, ZnTPhPyPc and CoTPOPyPc complexes in DMF.	124
Table 4.2:	Summary of absorption maxima (λ_{max}) of the various central metal oxidation states of the MPc complexes.	133
Table 4.3:	Summary of redox potentials of MTMPyrPc in DMF.	143
Table 4.4.	Redox potentials of the CrTAPc and MnTAPc in DMF.	148
Table 4.5:	Redox potentials for CoTETPc, MnTETPc and ZnTETPc complexes measured in DMF.	163

Table 5.1:	Total surface coverage of the polymer modified electrodes using complexes **7**, **10** and **12.**	175
Table 5.2:	Summary of ion-barrier factor (Γ_{ibf}) and interfacial capacitance (C_s) of the MPc-SAM on gold studied in this work.	217
Table 6.1:	Summary of peak potential (E_p) for the electroassisted reactions of the analytes at the modified electrodes using the MPc complexes studied in this work	223

Chapter One

Introduction

This thesis dwells on the electrochemistry and electrocatalytic properties of metallophthalocyanines (MPcs). In this chapter, a review of the basic concepts of electrochemical techniques, including the nature of electrodes, electrode modification and characterization and electrocatalysis is presented. The synthesis, general properties and applications of metallophthalocyanines will also be discussed in this chapter.

1.1 Background on Electrochemical Techniques

1.1.1 Cyclic Voltammetry

Electrochemical techniques have in the last decades become standard tools for inorganic and bioorganic chemists in the study of redox reactions of a large variety of compounds. In particular, cyclic voltammetry (CV) has been vastly used to elucidate electron transfer mechanisms and to study the products resulting from the electron transfer. During *cyclic voltammetry*, the potential is swept from an initial potential E_i to a final potential, and at the end of its linear sweep, the direction of the potential is reversed, usually stopping at E_i (or may commence an additional cycle). The potential at which the reversal occurs is called the *switch potential* (E_λ) (Fig 1.1).

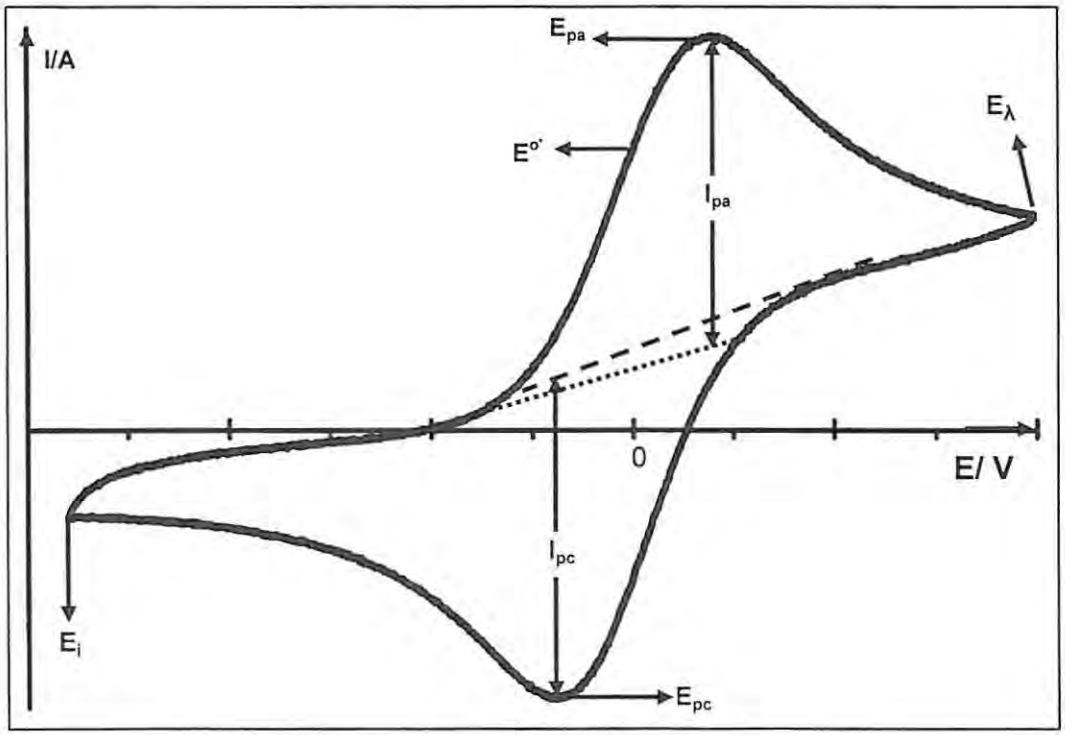

Fig 1.1: Cyclic voltammogram for a reversible process. I_{pa} = anodic peak current, I_{pc} = cathodic peak current, E_i = initial potential, E_λ = reversal (or switching) potential, E_{pa} = anodic peak potential, E_{pc} = cathodic peak potential, $E^{o'}$ = formal potential.

Furthermore, the rate of potential scan can be varied over a wide range allowing coupled chemical reactions and transient intermediates to be investigated. CV not

only has the power to study products of initial electrode reaction and unstable intermediates, but can also be used to investigate coupled chemical reactions and their rates, rates of electron transfer, disproportionation reactions and adsorption of reactants or products.[1-4] The measure of the current, I_{pa} (anodic peak current) or I_{pc} (cathodic peak current) (i.e. *Faradaic current*), is indicative of the rate at which electrons are being transferred between the redox species and the electrode.

Assuming that the rate of electron transfer is fast when a redox species comes into contact with the electrode surface, the current that flows is dependent on the rate at which the species reach the electrode surface. The potential at which the peak current occurs is known as the peak potential (E_p). At this potential, the redox species has been depleted at the electrode surface and the current is diffusion limited. The further the redox species is from the electrode, the longer the time needed for diffusion to the electrode and the lower the Faradaic current becomes.

In addition to *Faradaic* processes that obey Faraday's Law, *non-Faradaic* processes may also occur. Typically these are processes such as adsorption. Charging current and ion migration can also contribute to non-Faradaic processes. They originate mostly from the electrical capacitance present at the interface. The non-Faradaic current is the region between E_i and the onset (or foot) of the wave labelled I_{pa} in Fig 1.1.

1.1.1.1 *Reversible Systems*

Peaks are observed for both forward and reverse sides of the cyclic voltammogram for reversible systems. These peaks are of similar shape and, if fully *reversible*, the magnitude of the current is proportional to concentration, and the forward current (I_{pa}) and the reverse current (I_{pc}) are equal. For an electrochemical

process involving the oxidation of a species **O**, and reduction of the oxidation product **R**, (shown in Equation 1.1), a reversible cyclic voltammogram can only be observed if (1) both **O** and **R** are stable, (2) the kinetics of the electron transfer process are fast and (3) at all potentials and potential scan rates, the electron transfer process on the surface is in equilibrium.

$$O + ne^- \rightleftharpoons R \qquad 1.1$$

For a planar diffusion[5-7] the value of I_p can be obtained using the Randles- Sevćik equation (Equation 1.2)

$$I_p = 0.4463nF\left(\frac{nF}{RT}\right)^{1/2}[O]A(D\nu)^{1/2} \qquad 1.2$$

This becomes equation 1.6 at 25°C.

$$I_p = (2.69\text{x}10^{-5})n^{3/2}[O]A(D\nu)^{1/2} \qquad 1.3$$

where I_p = the peak current (Amperes), A = electrode area (cm^2), [**O**] = concentration (mol cm^{-3}) and ν = scan rate (Vs^{-1}), D = diffusion coefficient, n = number of electrons, R = gas constant, T = temperature (K), F = Faraday's constant.

Thus the peak current is proportional to the concentration of the electroacative species, the square root of the sweep rate and to the diffusion coefficient. Provided that the system is reversible and not complicated by side reactions, the half-wave potential ($E_{1/2}$) will be equal to the formal potential ($E^{o'}$) and related to the standard potential (E^o) as follows (Equation 1.4):

$$E_{1/2} = E^{o'} = E^o + \frac{RT}{2F}\ln\frac{[O]}{[R]} \qquad 1.4$$

The formal potential can easily be calculated from equation 1.5:

$$E^{o'} = \frac{E_{pa} + E_{pc}}{2} \qquad 1.5$$

The difference between the anodic peak (E_{pa}) and cathodic peak (E_{pc}) potentials ($\Delta E_p = E_{pc} - E_{pa}$) is given by Equations 1.6a and 1.6b:

$$E_{pc} - E_{pa} = \frac{RT}{nF} \qquad 1.6a$$

$$\text{At } 25\ ^{\circ}C\ \Delta E = \frac{0.059V}{n} \qquad 1.6b$$

Table 1.1 shows a complete list of diagnostic conditions for reversibility.

Table 1.1: *Diagnostic Tests for Electrochemical Reversibility of a Redox Couple*[8]

1. $I_{pa} = I_{pc}$, i.e. $I_{pa}/I_{pc} = 1$
2. The peak potentials, E_{pa} and E_{pc}, are independent of the scan rate v
3. The *formal electrode* potential, $E^{o'}$, is midway between E_{pa} and E_{pc}, so that $E^{o'} = (E_{pa} + E_{pc})/2$
4. $I_p \propto \upsilon^{1/2}$
5. The peak separation, ($|E_{pa} - E_{pc}|$) is 59/n mV for an n-electron couple.

1.1.1.2 Irreversible Systems

For totally irreversible systems the rate of electron transfer is insufficient to maintain surface equilibrium. Unlike a reversible system (where electron transfer rates are significantly greater than the rate of mass transport at all potential scan rates), at low potential scan rates, the rate of electron transfer is greater than that of mass transport, and a reversible cyclic voltammogram is observed. However as the scan rate is increased, the rate of mass transport increases and becomes comparable to the rate of electron transfer. This phenomenon results in a noticeable increase in the peak separation. The surface concentration of the reactant changes more slowly with potential so that the peak for an irreversible process is drawn out, and the surface

concentration eventually reaches zero. The most marked feature of a cyclic voltammogram of a totally irreversible system is the absence of a reverse peak (Fig. 1.2).

However, the absence of a reverse peak does not imply an irreversible electron transfer, but might mean a fast chemical reaction following electron transfer.

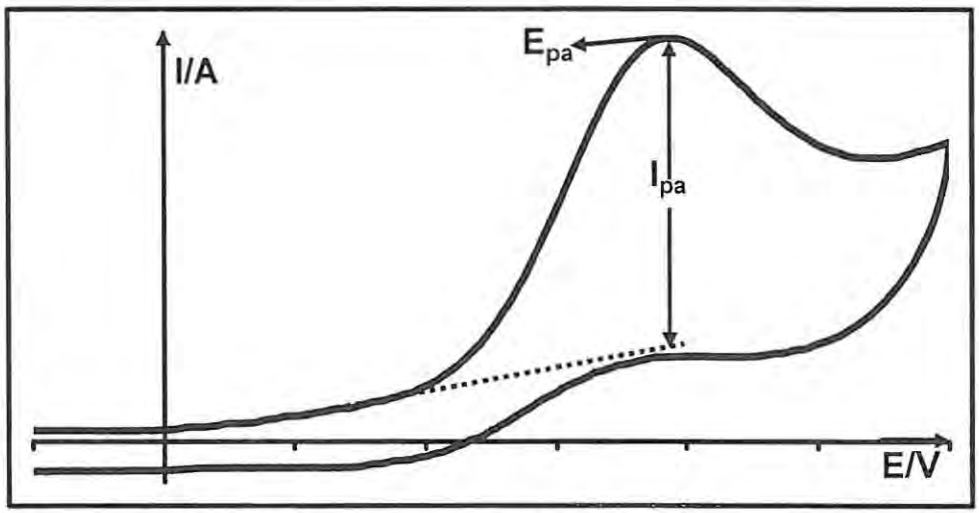

Fig. 1.2: Typical cyclic voltammogram of a totally irreversible system.

The value of the peak potential E_p, for irreversible processes varies with the sweep rate according to equation 1.10:

$$E_p = \mathrm{K} - \frac{2.3RT}{2\alpha n_a F}\log\nu \qquad 1.7$$

where $$\mathrm{K} = \mathrm{E}^{o'} - \frac{RT}{\alpha n_a F}\left[0.78 - \frac{2.3}{2}\log\left(\frac{\alpha n_a FD}{(k^{\alpha})^2 RT}\right)\right] \qquad 1.8$$

α = rate of electron transfer, n_a = number of electrons transferred in the rate determining step and k^{α} is rate of diffusion of species to the electrode surface. The other symbols are as defined previously in Equations 1.2 and 1.3 (see also the list of symbols). Table 1.2 shows a summary of the diagnostic tests for irreversibility.

Table 1.2: *Diagnostic Tests for Electrochemical Irreversible Redox Systems*[8]

1. No linked reverse peak (in some cases)
2. $I_{pc} \propto \upsilon^{1/2}$
3. E_{pc} shifts by $30/\alpha_c n_a$ mV for each increase in υ
4. $|E_p - E_{p/2}| = 48/\alpha_c n_a$ mV

1.1.1.3 Quasi-reversible Systems

This is the intermediate between reversible and irreversible systems. The transition from reversibility occurs when the relative rate of electron transfer with respect to that of mass transport is insufficient to maintain Nernstian equilibrium at the electrode surface. In the case of quasi-reversible regions both the forward and reverse reactions make a contribution to the observed current.

Table 1.3: *Diagnostic Tests for Electrochemical Quasi-reversible Redox Systems*

1. $|I_p|$ increases with $\upsilon^{1/2}$ but not proportional to it
2. $|I_{pa}/I_{pc}| = 1$ provided $\alpha_a = \alpha_c = 0.5$
3. $|E_{pa} - E_{pc}| > 59/n$ mV and increases with increasing υ
4. I_p shifts with increasing υ.

1.1.2 Differential Pulse and Square Wave Voltammetry

The basis of all pulse techniques is that the difference in current is measured hence minimizing charging currents.[9] The important parameters for pulse techniques are as follows:

1. *Pulse amplitude* is the height of the potential pulse. This may or may not be constant depending upon the technique.
2. *Pulse width* is the duration of the potential pulse.
3. *Sample period* is the time before and after application of pulse.

1.1.2.1 Differential Pulse Voltammetry

This is a popular quantitative pulse technique. The potential waveform for differential pulse voltammetry (DPV) is shown in Fig. 1.3. The potential waveform consists of small pulses (of constant amplitude) superimposed upon a staircase waveform (increase in step). The current is sampled twice in each Pulse Period (once before the pulse, and at the end of the pulse), and the difference between these two current values is recorded and displayed as a single symmetrical peak.

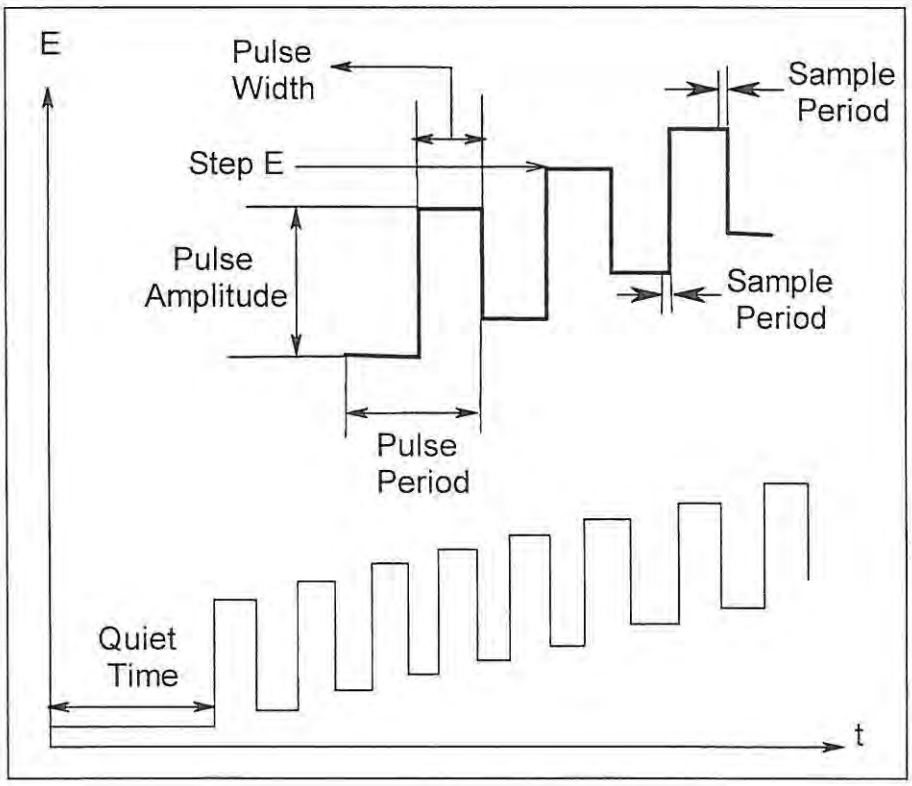

Fig 1.3: Potential waveform for differential pulse voltammetry.

1.1.2.2 Square Wave Voltammetry

The potential waveform for square wave voltammetry (SWV) is shown in Fig. 1.4. The potential waveform consists of a square wave of constant amplitude superimposed on a staircase.[10] The current is measured at the end of each half-cycle, and the current measured on the reverse half-cycle (i_r) is subtracted from the current measured on the forward half-cycle (i_f). This difference in current (i_f - i_r) is displayed as a function of the applied potential.

There are two advantages of measuring the difference in current; (a) it increases the discrimination against the charging current, since any residual charging current is subtracted, (b) the shape of the current response is a symmetric peak. If we consider a reduction, then at the potential well positive of the redox potential, both the forward and reverse currents are zero, so the difference in current is also zero. At potentials well negative of the redox potential, the current is diffusion-controlled, and the potential pulse has no effect; hence, the forward and reverse currents are equal, and the difference in current is again zero. The largest difference between the forward and reverse currents (and hence the largest current response) is at the redox potential. SWV gives excellent detection limits and it is better than DPV in some cases. Also DPV is slow, hence not suitable for some applications. However, both SWV and DPV are techniques of choice for determining trace concentrations (10^{-9} to 10^{-11} M) of metals, anions and selected adsorbates.

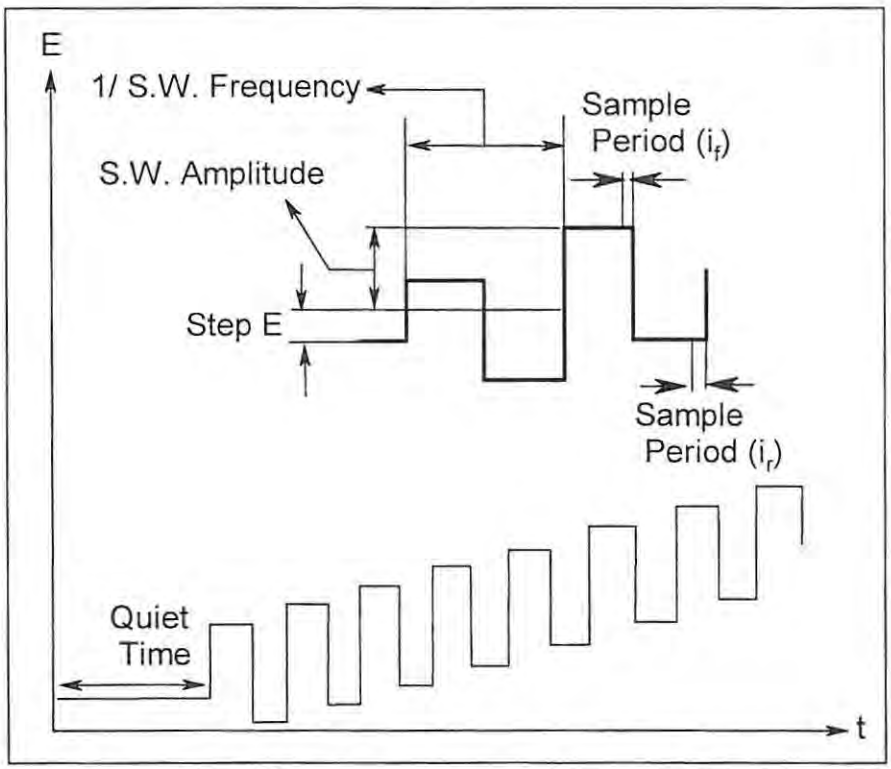

Fig. 1.4: Potential waveform for square wave voltammetry. SW = square wave

1.1.3 Spectroelectrochemistry

Spectroelectrochemistry is the in situ coupling of a spectroscopic technique with an electrochemical technique and this may be subdivided into those methods which focus on the spectroscopic characterization of the electrode surface and those which focus on the spectroscopic characterization of the electrogenerated solution species.[11] The field of spectroelectrochemisry dates back to 1964, when the first work was reported by Kuwana *et al.*[12] Many spectroelectrochemical techniques rely on the existence of electrodes that are transparent to radiation in a particular spectral range. An ideal optically transparent electrode (OTE) combines the characteristics of high optical transparency with low electrical resistivity. Very few materials are both optically transparent and excellent electrical conductors. Hence, compromise between optical transparency and electrical conductance is typified in an OTE.[13] Tin

oxide films on glass or quartz, for example, show unique properties such as good optical transparency, high electrical conductivity, high mechanical strength, resistance to corrosion, high hydrogen and oxygen overpotential, low background current and absence of electroactive oxide layer.[14-19] These properties make tin oxide ideally suited for certain photoelectrochemical studies.[20] The use of indium tin oxide (ITO) coated glass, as an optically transparent electrode for UV-Visible spectroelectrochemical measurements of inorganic and organic redox analytes is common. The technique has evolved over the years to encompass research on a variety of topics: new electrode development, thin-layer cell design and construction, evaluation of reaction mechanisms, delineation of kinetic and thermodynamic parameters,[9] material characterization, structure-formation studies of biomolecules, and environmental contaminant monitoring.[21-24] Several different OTEs have been reported, with the most common type being ITO.[1,25-30] The others include (a) thin films of semiconductors (e.g. SnO_2 or In_2O_3), prepared by an electrodeposition procedure,[12,31-33] on a glass, quartz, or plastic substrate, (b) fine wire mesh "minigrids", (e.g. Pt, Au, Ag etc.), with several hundred wire per centimeter, have also been used as OTEs,[34,35] (c) other OTEs have been constructed from conductive materials, such as germanium[36,37] that are highly transparent in the spectral range of interest, thereby obviating the necessity of using thin films or holes to give transparency.

1.2 Types and Properties of Electrodes

1.2.1 Optically Transparent Electrodes

A brief description of optically transparent electrodes (OTEs) has been given in section 1.1.3 (under spectroelectrochemistry). Thin layer cells incorporating these electrodes are generically referred to as *optically transparent thin-layer electrode* (OTTLE) cells. The choice of OTE for the fabrication of an OTTLE cell is governed by; (1) optical and electrochemical properties. For example, ITO while highly functional for many applications has variable optical and electrochemical properties from source to source; (2) tolerance to cathodic and anodic polarization in different chemical environments; (3) the allowed optical window; and (4) effects of aggressive electrochemical environments.[38,39] The working volume of OTTLE cells range from 30 –50 μL.[38-40] The attractive features of OTTLE include the high sensitivity which can be achieved with very small volumes, the ease of achieving steady state conditions at the electrode, a ready adaptability to simultaneous optical observation of the electrolyzing solution, the very low current densities which permit highly irreversible reactions to be studied, and the relatively simple and inexpensive electronic control circuit.[41] Also, bulk electrolysis is achieved in few seconds. Spectroelectrochemisry has been primarily developed for obtaining spectra, and electron stiochiometries (n values) of redox couples.[42,43] The technique is based on the control of the ratio [**O**]/[**R**] of the redox couple in the thin layer solution by an applied potential. The redox couple is incrementally converted from one oxidation state to another by a series of applied potentials for which each corresponding value of [**O**]/[**R**] is determined separately.[13] Thin layer spectroelectrochemistry is a useful technique for monitoring electron transfer processes, rate constants and stability

constants.[44-47] The number of electrons transferred during a redox process can be determined using Faraday Law, given by Equation 1.9:

$$n = \frac{Q}{FVC} \qquad 1.9$$

Where Q = amount of charge passed (Coulombs), V = volume of OTTLE cell (dm^3). C = concentration.

1.2.2 Glassy Carbon Electrode

Carbon has been described as a natural field in which to plant covalent bonds for electrode modification.[48] For example pyrolytic graphite consists of the basal and plane-edge surfaces shown in Fig 1.5

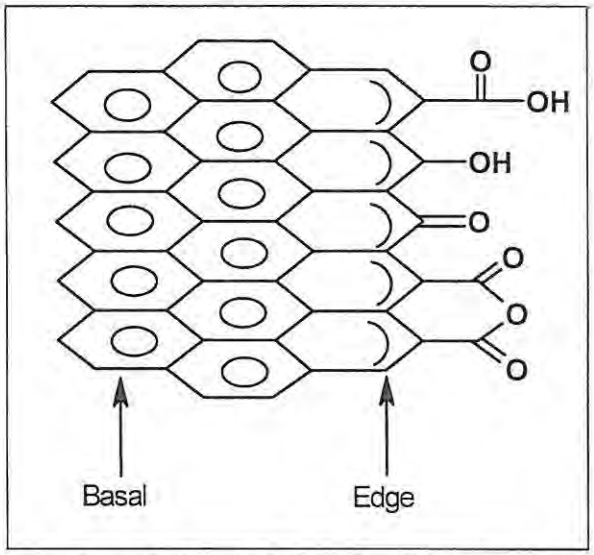

Fig 1.5: Schematic representation of chemical functionalities at edge plane of pyrolytic graphite.

Carbon exists in a variety of physical and chemical forms, e.g., graphite single crystal (GSC), pyrolytic graphite (PG), highly oriented pyrolytic graphite (HOPG), glassy (vitreous) carbon, compacted polycrystalline structures of varying porosity (such as high density spectroscopic rods), powders, whiskers, fibers, yarn, cloth etc. Pyrolytic graphite may be described as random tangles of graphite stripes such that

each exposed surface exhibits a mixture of basal and edge plane characteristics (Fig 1.5). An uninterrupted basal plane surface is non-ionic, with low polarity, hydrophobic, and rich in π-electron density. A low population of chemical functionalities is likely concentrated along the surface imperfections exposing the edge plane.[48] Under normal conditions the basal plane is barren to synthetic coupling reactions. On the other hand, the high π-electron density is conductive to strong chemisorptive interactions, especially with unsaturated compounds.[48] Usually, the portion of edge and basal plane characteristics exposed on a surface depends on the pre-treatment steps. For example, mechanical polishing of the basal plane of PG will expose edge plane sites while polished edge plane surfaces will display some basal plane areas if structural folding of the graphitic sheets occurs during polishing.[48] The useful carboxylic acid and hydroxyl groups on the edge plane can be enhanced by some proposed chemical pre-treatment procedures such as heating in air (at 400-500 ^{o}C),[49-52] or treatment in radio frequency oxygen plasma.[52] Whichever procedure used for the pre-treatment leaves the surface oxidized. Upon activation, it is possible to attach electroactive species on carbon electrodes. For instance, Lennox and Murray[50] demonstrated that tetraaminoporphyrins could be attached on thermally oxidised glassy carbon electrode using thionyl choride as activator.

1.2.3 Frontier Orbitals and Redox Potentials.

The electrode materials used in electrochemistry are made of metals, or metal-like (semiconductor) materials in which there is a continuous band of energy which electrons can occupy. The analogous energy level to the highest occupied molecular orbital (HOMO), in a molecule (e.g. a metallophthalocyanine (MPc) molecule), is called the Fermi level in a metal. All the energy levels below the Fermi level are

occupied at O K. If a negative potential is applied to the electrode, the Fermi level moves to higher energy and is able to reduce a molecule in its vicinity. On the other hand, if a positive potential is applied, the Fermi level moves to lower energy so that the metal is able to accept electrons from the molecule in solution (i.e. can oxidize the molecule) (Fig. 1.6). For a reversible system, at equilibrium, the rates of the forward and reverse electron transfer must be equal, suggesting that the distribution functions for the oxidized and reduced species are situated symmetrically about the Fermi energy in the metal.

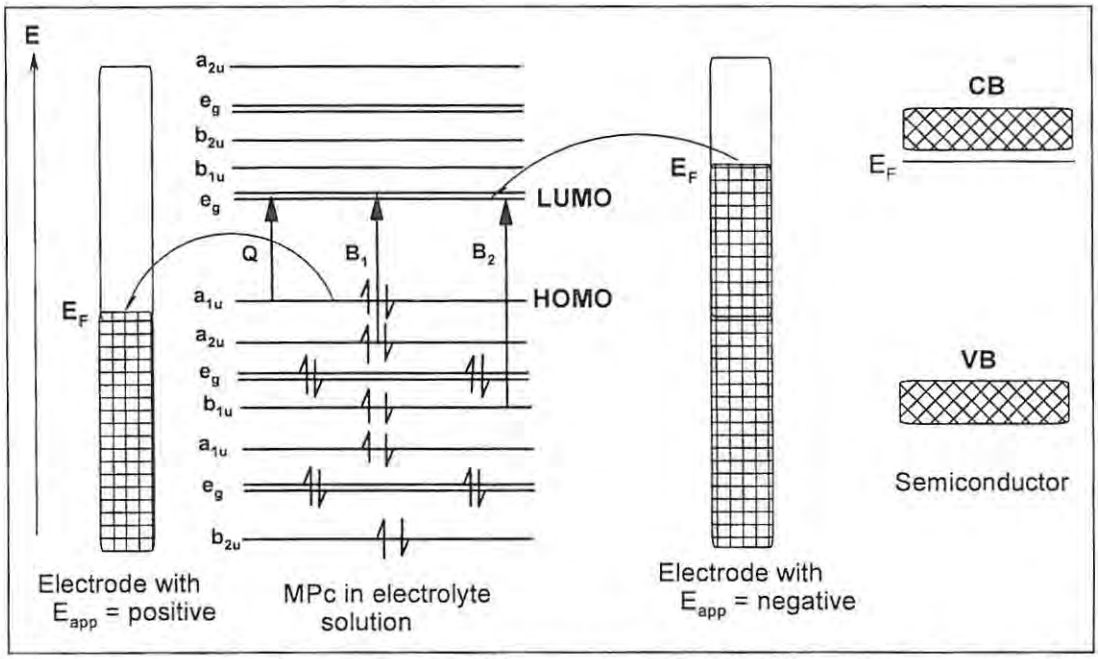

Fig. 1.6: Energy level diagram for metal (electrode), semiconductor and redox active (MPc) system. CB = conduction band, VB = valence band, E_F = Fermi level, LUMO = lowest unoccupied molecular orbital.

1.2.4 Surface Confined Processes

It is vital to investigate the electrochemical manifestations of molecules attached to electrode surfaces so that the extent of success of an immobilization procedure could be ascertained. Some electrochemical experiments used in studying modified surfaces include cyclic voltammetry, differential pulse voltammetry (DPV), chronoamperometry and chronocoloumetry, chronopotentiometry, coulosatics, AC

voltammetry and measurement of electron-transfer-mediated electrocatalysis (ETME). However, only a brief discussion on CV and ETME will be highlighted in this work. An electrochemical experiment may give cyclic voltammetric results that are not expected for electrode reactions in which the reactants and products are freely soluble in the electrolyte solution. In such situations the voltammogram could be a good indication that some surface processes may be involved. Some surface processes include *adsorption*, *deposition process*, and *passivation.*

1.2.4.1 Adsorbed Species

The most interesting and most studied electrode-surface-immobilized chemicals are those that are electrochemically reactive.[53] If the molecular attachment scheme is such that the immobilized substance can (directly or indirectly) exchange electrons with the electrode surface, the electrode displays electrochemical responses for oxidation or reduction of the substance (Fig. 1.7).

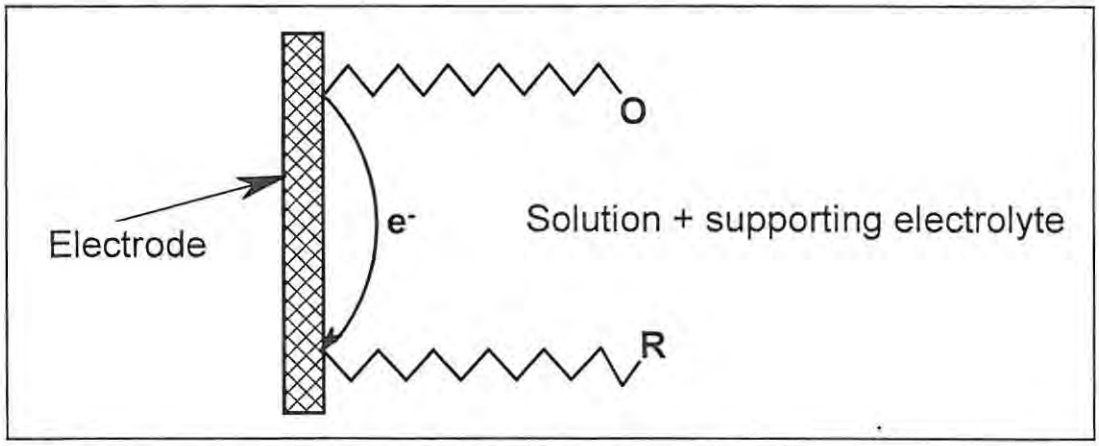

Fig 1.7: A representation of the interfacial electrochemical transformations of immobilized electroactive species. Where **O** and **R** are the oxidized and reduced forms of the immobilized molecule and the wiggle link between the electrode and **O** and **R** represents the link between the immobilized species and the electrode.

The simplest case of an electrode reaction involving adsorption is where the adsorbed forms of **O** and **R** are electroactive in the potential range under investigation, giving a cyclic voltammogram shown in Fig 1.8. The reasons for the

observed shape of the voltammograms (Fig 1.8) include the fact that the reduction potential of the adsorbed **O** is shifted more positive of the reduction potential of dissolved **O**. The analysis of such a system is very straightforward as mass transport effects can be ignored.[53] The quantities that are of interest in CV experiments for the electrode reaction above are schematically illustrated in Fig 1.8.

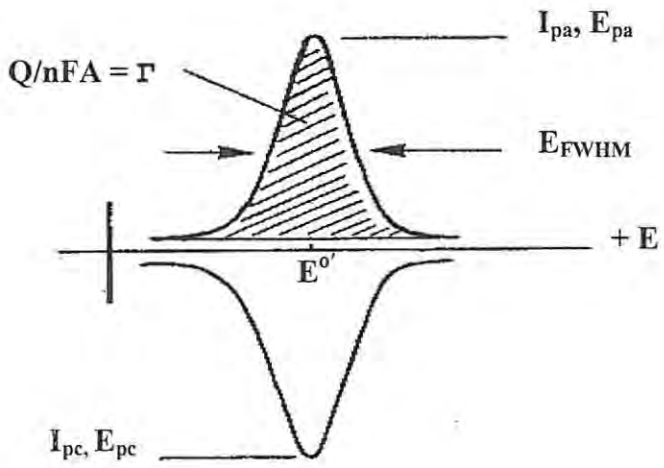

Fig 1.8: Theoretical cyclic voltammogram for the reduction of adsorbed O and reoxidation of the product where the free energies of adsorption of O and R are equal and adsorption follows a Langmuir isotherm.[8,54] E_{FWHM} = potential corresponding to full-width at half maximum, $E^{o'} = (E_{pa} + E_{pc})/2$; Γ = total electroactive coverage (i.e. $\Gamma_O + \Gamma_R$) and $E^{o'} = E_{FWHM}$. All other symbols are as described before (see list of symbols).

For this reversible system, a direct proportionality exists between I_p and the scan rate, υ. Also shapes of the cathodic and anodic waves are identical, $\Delta E_p = E_{pc} - E_{pa} = 0$ and $E_{FWHM} = 90.6/n$ mV. The most sensitive criterion for rapid kinetics in the electron transfer process for adsorbed species is that $\Delta E_p \approx 0$ irrespective of the scan rate.

The major differences (compared to a voltammogram for a reaction in which both **O** and **R** are dissolved in solution) are that the peaks are sharp and symmetrical, the current rising from zero and then falling back to zero on the reverse scan, and as

mentioned above, there is little or no peak separation (i.e. $\Delta E_p \approx 0$). The symmetrical shape of the peaks arises because of the fixed amount of the reactant (i.e. only **O** on the surface of the electrode at the start of the sweep can be reduced). The actual value of I_p, E_p, and the peak width all depend on the type of adsorption isotherm involved and the relative strengths of adsorption of **O** and **R**. The area under the cathodic or anodic peak, Q, corresponds to the charge associated with the reduction or oxidation of the adsorbed layer of **O** and this enables the surface concentration of **O** to be determined by Equation 1.10:

$$\Gamma_O = \frac{Q}{nF} \qquad 1.10$$

For non-Nernstian (adsorbed) systems the shapes of the cyclic voltammogram change. For irreversible systems, the forward peak is not symmetric and there is no reverse peak. For a quasi-reversible system there is an asymmetrical reverse peak and the peak potentials are not coincident.[8,55-56]

1.2.4.2 Deposition process

Fig. 1.9 depicts the cyclic voltammogram observed for the deposition of metals, or other phases from dilute solution onto a foreign substrate, e.g. Hg on carbon. The forward peak (deposition) is similar to voltammograms observed for a process involving only solution soluble species, except that the leading edge is slightly steeper. The major differences are seen upon sweep reversal. The current trace crosses over the forward sweep (at E_e, Fig 1.9), whilst the reverse peak is sharp and symmetrical. The shape of the reverse wave is explained by the fact that the reacting material is deposited on the electrode and therefore does not need to diffuse there in order to react. It thus behaves like an adsorbed species.

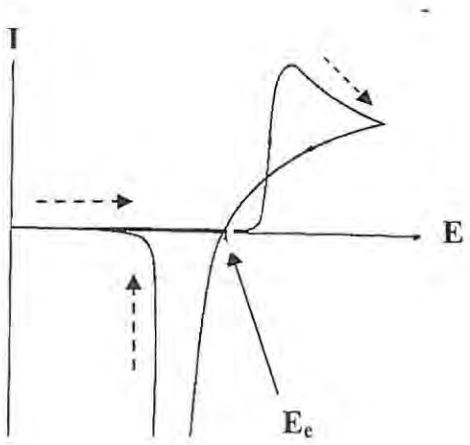

Fig 1.9: Typical cyclic voltammogram for a metal deposition reaction exhibiting a nucleation over potential.[8] The dashed arrows show the direction of scan.

This process is a prerequisite for the growth of metal on an electrode, which is favoured by the thermodynamically stable nuclei on the electrode surface. Usually nucleation overpotential on the first sweep is generally greater than that on the second and subsequent sweeps.[8]

1.3 Modified Electrodes

An electrode is an electronic conductor in contact with an ionic conductor, the electrolyte. A drawback in all electroanalytical methods is an intrinsic lack of substrate selectivity because many substrates, notably biologically active species, have similar redox potentials and many are difficult to discern because of Nernstian irreversibility and adsorption effects on solid electrodes.[58] This problem has been successfully solved using ion-selective electrodes and other types of substrate selective membrane.[59-62] Chemically modified electrodes can be designed to have versatile properties and they have attracted wide interest, in recent years, in analytical chemistry. Polymer layers on electrodes can serve several purposes namely: (a) as preconcentration medium, (b) acting as class specific redox catalyst or (c) as substrate

selective layer.[63] Basically the main interest in chemically modified electrodes stems from the various possible applications in which these materials could be used. Of primary interest is the quest for electrocatalysis. For example, an electrode made of an inexpensive and rugged material that could reduce oxygen to water effectively (and efficiently) at a potential near the thermodynamic value would find wide use in fuel cells, batteries, and other electrochemical systems.[38,64,65] Electrochromic devices such as displays or "smart" windows and mirrors can be made from modified electrodes involving materials that change color upon oxidation and reduction.[66-69] In recent years the search for electrochemical systems capable of mimicking the behavior of diodes, transistors and electrical networks (molecular electronic devices) has intensified.[70-72]

Modified electrodes can be prepared in different several ways. These include irreversible adsorption, covalent attachment of a monolayer and coating the electrode (substrate) with films of polymers or other materials. There has been a lot of research on the methods of preparation, characterization and electrochemical behaviour of these chemically modified electrodes.[73-79] The strong and frequently irreversible, adsorption of species at electrode surfaces will often change the electrochemical behaviour of an electrode.[3,38] Electrode modification can also result in increase in electron transfer rates at the resulting electrode surface compared with the bare electrode.[80] Redox reaction at bare electrodes usually involves slow electron transfer kinetics and therefore occurs at an appreciable rate only at potentials higher than its thermodynamic redox potential. Such reactions can be catalyzed by immobilizing suitable electron-transfer mediators on the electrode surfaces.[38] Chemically modified electrodes incorporating transition metal complexes provide strategies for improving the performance of solid electrodes by incorporating catalytic sites at the

electrode/solution interfaces.[63,81] The metallic redox couples present in the macrocycle have an oxidative (or reductive) capability that promotes the indirect electrooxidation (or electroreduction) of organic compounds. Thus, metalloporphyrins (MPs), metallophthalocyanines (MPcs), metal Schiff bases and metal tetraazamacrocyclic complexes, among others, have been immobilized on different electrode surfaces and these have shown catalytic activities for a great number of electrode reactions.[82]

1.3.1 Polymer Modified Electrodes

Background on Conducting Organic Polymers

Conducting organic polymers (COPs) have the unusual property of possessing high electrical conductivity, and can exhibit a range of properties from semi conductivity to near metallic behaviour. The major interest shown by electrochemists in these materials is based on the utilization of the properties possessed by organic conducting polymers in fabrication of potential electrode materials. The current interest in COPs began in the 1970s when it was found that the electrical properties of polyacetylene, a semiconductor when pristine, could be radically altered by treating it with an oxidizing agent such as iodine.[83] Research devoted to gas sensors is based on the conducting properties of metallophthalocyanine (MPc) films.[84-86] For example the semiconducting properties of nickel phthalocyanine (NiPc) has been employed for building field-effect transistors for the detection of ozone in air.[87-89]

Three major electrochemical areas are considered when studying COPs:[83]

1. the electrochemistry of the materials themselves (i.e. doping reactions, intercalation etc),

2. the electrochemistry occurring at the electrodes made from or coated with these materials (e.g. the electrochemistry of couples such as ferrocene/ferrocinium at COP electrodes and electrocatalytic properties of the electrodes),
3. Structural and morphological study of the materials may also be considered since this has a significant effect both on the electrical and electrochemical properties of the polymer electrodes.

The conducting (charge carrier) properties of conjugated polymers arise from the doping process occurring during the synthesis of the polymer from the monomer. Doping occurs when the oxidation (or reduction) state of conjugated polymers, (CPs), is altered with a concomitant change in the electronic properties of the material (e.g. to increase their conductivity). Doping reaction is essentially a charge transfer reaction resulting in the partial oxidation or reduction of the polymer.[83] When a CP is partially oxidized, the resulting polymer is termed 'p-doped'. It involves the removal of electrons from the monomer units as shown in Equation 1.11:

$$(\text{Monomer unit})_x \rightarrow [(\text{Monomer unit})^{y+}]_x + xye^- \qquad 1.11$$

n-doping occurs when there is a partial reduction of the polymeric material (Equation 1.12):

$$(\text{Monomer unit})_x + xye^- \rightarrow [(\text{Monomer unit})^{y-}]_x \qquad 1.12$$

Doping process can be achieved with gas phase reagents such as AsF_5 and I_2, solution species such as $FeCl_3$ and electrochemical oxidation and reduction. Electrochemical doping is fast becoming the preferred technique in many applications as it provides a potentially highly controllable and reproducible result with accurately

monitored and regulated transfer of charge. Electrochemical doping is conveniently achieved in the presence of an electrolyte serving as the source of counter ion.[83]

1.3.1.1 Methods of Polymer Formation on Electrode Surfaces

The following techniques have been used to modify electrode surfaces with polymers.

a. Dip Coating

The electrode is exposed to a dilute solution of the polymer for some time, during which an adsorbed polymer film forms on the electrode surface. The polymer may already contain the redox moiety or may be bound subsequently to the film.[90-93]

b. Spin Coating

This technique has been used for a series of preformed redox polymers. It involves the evaporation of a few drops of a large number of monolayers of the polymer (in solution) on an electrode surface by rotating at high speed using centrifugal force. The films obtained in this technique are usually pinhole free.[94-96] The simplicity of spin coating has been extended to metallophthalocyanine-type polymer derivatives.[96,97]

c. Droplet Evaporation

This involves spreading and evaporating a few micro litres of a dilute solution of a polymer on the electrode surface. Films formed from this manner can be topologically rough, but can be improved by spinning the solution off or removing it only after partial evaporation.[93,97-100]

d. *Oxidative or Reductive Deposition*

This is based on the solubility of the polymer as a function of its ionic state, which can be changed by oxidation or reduction. It is also known as electroless deposition. The method has been used to deposit polyvinyl ferrocene films from CH_2Cl_2 solutions, oxidizing the polymer to its less soluble (and more absorbable) ferrocenium form.[101-104]

e. *Composite*

It is obtained by mixing a polymeric chemical modifier (e.g. metallophthalocyanine) with an electrode matrix (e.g. activated carbon) to form a carbon paste electrode.[105-109] The constituents retain their identity such that they can be physically identified.

f. RF Plasma Polymerization

The polymeric material is formed by exposing vapours of monomers to a radio-frequency (RF) plasma discharge. Upon exposure to air, plasma films typically take up oxygen and other unknown functionalities as a result of chemical damage in the RF discharge.[110-113]

g. *Electrochemical Polymerization*

A solution of monomer is oxidized (as with phenols,[114] anilines, [115,116] pyrrole[117-120]) or reduced (as with activated carbon[121-123]), to intermediates that polymerize sufficiently rapidly so as to form a polymer directly on the electrode. To grow films of sufficient thickness, the polymer film must be redox active and capable of electrocatalytically oxidizing or reducing fresh

monomer, or the polymer film must be permeable (which is rarely the case) to fresh monomer. Otherwise electrode passivation soon occurs and film growth is prevented. In most cases the electrochemical polymerization is performed under potentiodynamic conditions (e.g. cyclic voltammetry) in such a way that the potential window for the experiment must be within the oxidation or reduction potential of the polymerizable moiety of the monomer. The increase in the peak current (and formation of new peak in some cases) is usually indicative of the growth of the polymer on the electrode as voltammetric scans continue.

Electropolymerization, like the well-known radical polymerization is a chain process. While the growing end groups in radical polymerization are electrically neutral, they are charged in electropolymerization. During synthesis, charge transfer also takes place. The polymerizing systems are electrically neutral. Hence some negatively charged ions are present in cationically polymerized systems, while positively charged ions are present in anionically grown species. Many electropolymerization processes are conducted in solutions containing supporting electrolytes to provide the anions or cations. The participation of these counter-ions makes this polymerization intrinsically more complex than radical polymerization. Conducting and semi-conducting phthalocyanine polymers can be synthesized and deposited onto a conductive surface of a given substrate from monomer solutions by electrochemical polymerization. The advantage of electropolymerization is that precise film thickness and rate of film deposition can be maintained by varying the potential/current conditions of the working electrode. Use of this method yields a high-quality thin film and has great prospects in biosensing.[124-126] Polymerization of MPc has mainly been induced electrochemically.

1.3.1.2 Mechanism of Polymer Formation on Electrode Surfaces

Considerable work devoted to a better understanding of the role played by various experimental parameters, towards the growth of various conducting polymers such as polyaniline, polypyrrole, polythiophene and polyfluorines have been reported.[54,127-134] Conjugated organic polymers have been greatly exploited in various applications and a lot of effort has been devoted to their synthesis and the understanding of their physicochemical properties.[135-139] Polymer growth mechanism, kinetics of the polymerization reaction rate and related quantitative characteristics of polymerization of polypyrrole, polythiophene, polyaniline, polyfluorine have been studied using cyclic voltammetry, electrochemical quartz crystal microbalance (EQCM) and spectroelectrochemical.[140-143] Electropolymerization of pyrrole and thiophene substituted metallophthalocyanine complexes (both of interest in this work) follow the same mechanism for the polymerization of the monomeric pyrroles and thiophene heterocycles. For tetraaminometallophthathocyanines (MTAPcs, also of interest in this work), the electropolymerization would be similar to the mechanistic pathway for the polymerization of anilines to form polyaniline. The overall mechanism for anodic polymerization of metallophthalocyanine complexes, containing pyrrole, thiophene and amino substituents follows a similar pattern as indicated in Scheme 1.1:

The generally accepted mechanism of polymerization of heterocyclic polymers follows the $E(CE)_n$ mechanism, (where E = electron transfer, C = chemical step).[144-148] Scheme 1.2 (a) shows the proposed mechanistic pathway for the electropolymerization of pyrrole functionalized macrocyclic complexes on solid electrodes. The first step is suggested to involve the electrochemical oxidation of the monomer (A) to a delocalized radical cation (B to E) (Step I, Scheme 1.2 (a)). The

delocalized radical cation has the highest spin density at the α-position so that (E) is the most stable radical cation out of the possible resonance forms ([C], [D] and [E]) (Scheme 1.2 (a)).[147]

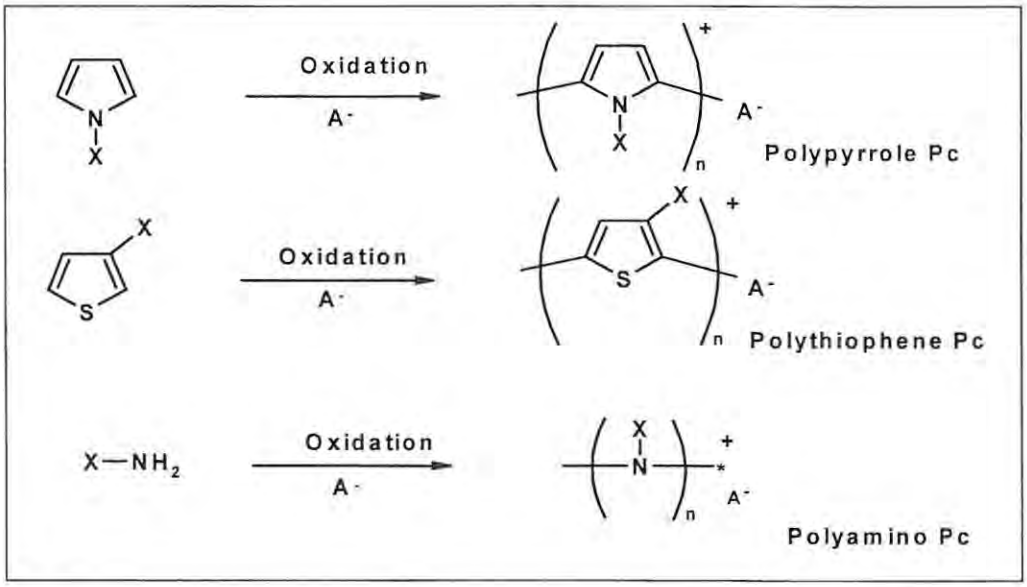

Scheme 1.1: Examples of polymers formed from monomers by electrooxidation. A^-= counter ion from electrolyte, X = Pc macrocycle.

The second step is the dimerization of the monomer radicals via a radical-radical coupling at the α-positions (or between the radical and A) (Steps II and III). The radical-radical coupling is then followed by the expulsion of two H^+ ions affording the neutral dimer (Step IV). This dimerization process is facilitated by the return to aromaticity. Chain extension is achieved via oxidation of the neutral dimer (or oligomer) to form the radical, (Step V) that combines chemically with other monomer, dimer or oligomer radicals to form a further extended polymer radical (Step VI). The return to aromaticity similar to step IV is repeated in step VII through the loss of two H^+ ions. It is accepted that the chemical coupling/electrochemical oxidation process repeats itself until the chain growth is terminated; hence the mechanism is represented as an $E(CE)_n$ mechanism.

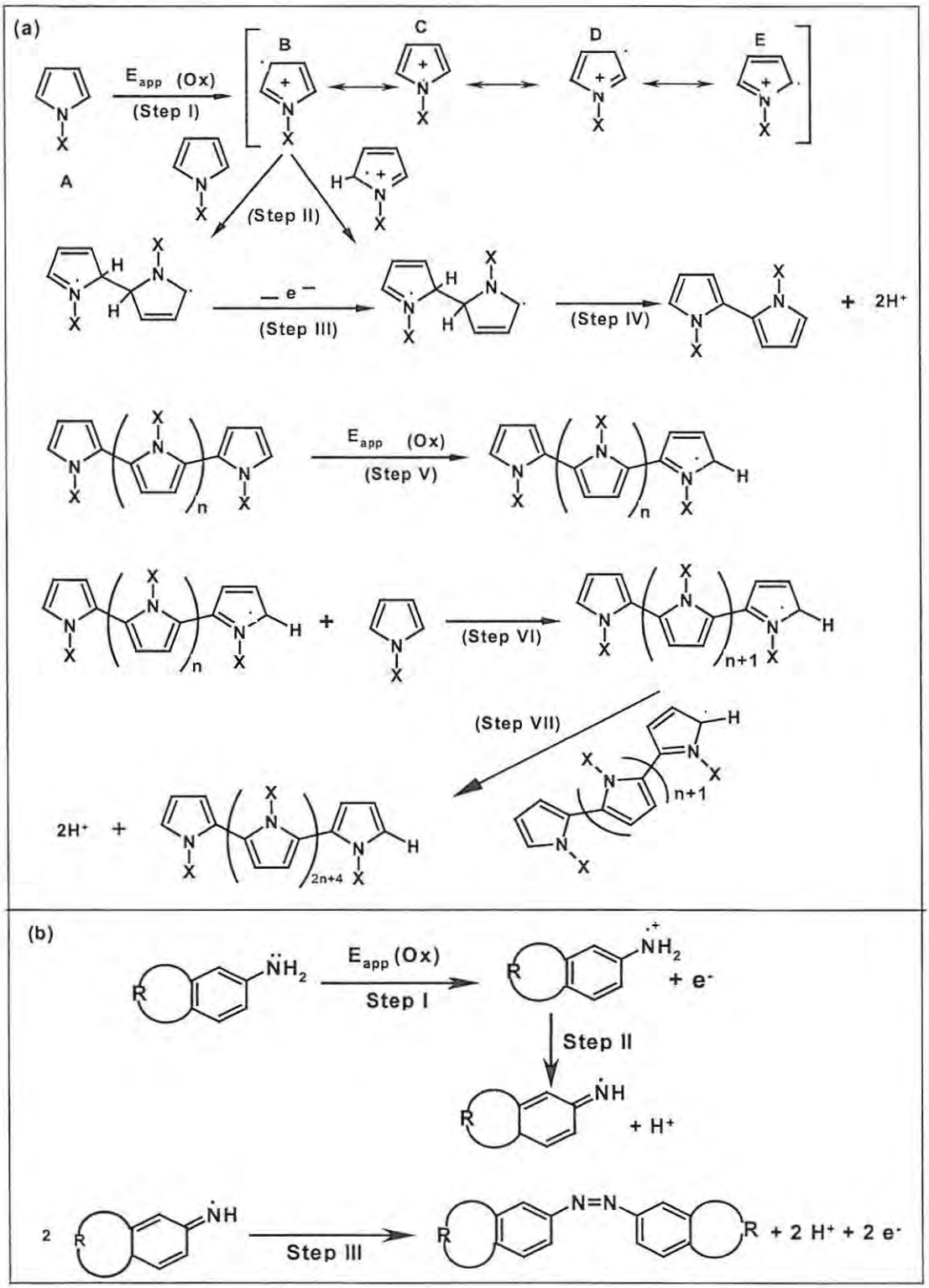

Scheme 1.2: Proposed mechanistic pathway for the electro polymerization of (a) pyrrole functionalized macro cyclic complexes and (b) MTAPc complex.[149] R = the rest of the MPc macrocycle.

John and Wallace[150] showed that critical chain lengths of the oligomeric intermediates were required for precipitation to occur at the electrode surface. Their

work also showed that nucleation followed by the precipitation on top of the polymeric nuclei was favored since the monomers/oligomers in solution are more readily oxidized at the polymer surface than at the bare substrate, the same way as in metal deposition.

The electropolymerization of tetraaminometallophthalocyanine complex follows the mechanism depicted in Scheme 1.2b. The polymerization process occurs via the oxidation of the (Step I) followed by the N-N oxidative coupling of the monomers (Step III) after the loss of a proton from the radical cation (Step II). Again the driving force to the stability and hence the formation of oligomers and polymers from the radicals is the desire to return to aromaticity. The following experimental variables govern the polymer growth mechanism:[150]

i. the nature of monomer employed, in particular its solubility.
ii. nature of the counter ion employed and the ability to form an insoluble polymer salt,
iii. the polymerization solvent. The monomer should have an oxidation potential which is accessible via a suitable solvent system,
iv. electrode nature and size: large surfaces provide greater probability of higher energy point on the electrode,
v. the monomer must produce radical cations which react more quickly with other monomers to form the polymer, than with other nucleophiles in electrolyte solution,
vi. the monomer should produce a polymer with a lower oxidation potential than that of the monomer if the material is to be produced in a state that has a higher conductivity.

1.3.2 Self-Assembled Monolayers

Molecular *Self-assembly* encompasses phenomena whereby small chemical units are introduced into an environment, reach an equilibrium state, and produce much larger-scale structures and patterns by the spontaneous formation.[2] Self-assembly strongly mimics *natural* mechanisms that form stable and complex architectures from simple building blocks.

Chemisorption (or *chemical adsorption*) is adsorption in which the forces involved are valence forces. It is an irreversible adsorption of electroactive substances on electrode surfaces through a covalent bond-like interaction.[74,151-153] It involves the formation of strong chemical bonds between adsorbate molecules and specific surface locations known as chemically active sites.

Common examples of self-assembled chemical structures include liquid crystals, self-assembled monolayers (SAMs), organization of lipids into micelles and membrane vesicles, block copolymer micro phase separation, and polymers adsorbed onto surfaces in layers. SAMs of alkanethiols and thiol substituted phthalocyanines[96,154-160] (on gold) form organic layers in which their properties are largely controlled by the end groups of the molecules comprising the films. SAMs provide a unique link between the science of organic surfaces and technologies that seek to exploit their adaptable character. SAMs exhibit a type of collective order dominated by end-group packing that overwhelms the substrate topography and generates interfaces with a higher degree of perfection. For example it has been shown that SAMs with an alkane chain length of 12 or more methylene units form well-ordered and dense monolayers on Au(111) surfaces. The thiols are believed to attach primarily to the threefold hollow sites of the gold surface, losing the proton in the process and forming an overlayer structure (Fig 1.10).

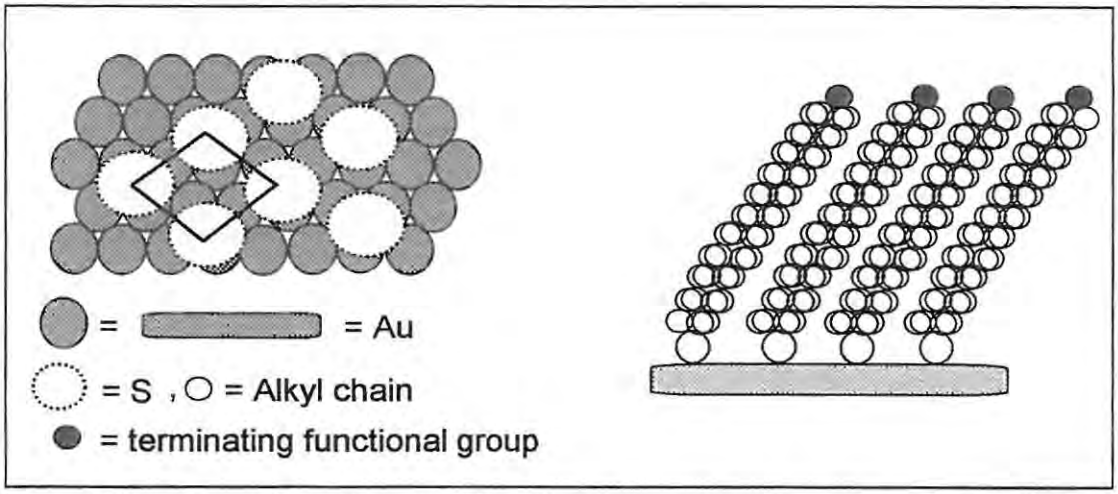

Fig 1.10: A schematic model of the over layer structure formed by alkanethiolate SAMs on Au(111).

The thiols and thiol substituted phthalocyanine molecules have been shown to readily form SAM films on gold surfaces with thickness ranging from 100 nm to 500 nm depending on the length of the CH_2 chain (either in alkane thiols or thiol substituted phthalocyanines).[157-161] The thiol molecules adsorb readily from solution onto the gold, creating a dense monolayer with the tail group pointing outwards from the surface. By using thiol molecules with different tail groups, the resulting chemical surface functionality can be varied within wide limits.

Depending on chain length and chain-terminating group, various super lattice structures are superimposed on the overlayer structure. The most commonly seen super lattice is the c(4×2) reconstruction, (Fig 1.10), where the four alkanethiolate molecules of a unit cell display slightly different orientations when compared with each other.

1.3.2.1 Preparation of SAMs

Different solvents may be employed for the preparation of SAMs. The nature and composition of the SAM is directly related to the solvent and deposition

solution.[162,163] The most commonly used solvent is ethanol because of its ability to reduce gold oxide and ease of evaporation. However the use of ethanol is limited by the lack of solubility of thiols. Although, a SAM can form very rapidly on the substrate, it is useful to employ adsorption times of 15 h or more to obtain well-ordered, defect-free SAMs. Multilayers do not form, and adsorption times of two to three days are optimal in forming highest-quality monolayers.

As mentioned above, the tail group that provides the functionality of the SAM can be widely varied. CH_3-terminated thiols are commercially available; other functional groups can be synthesized, providing almost infinite possibilities of variation. In addition, chemical modification of the tail group is entirely possible after formation of the SAM, expanding the available range of functionalities even further. Examples of some reported functionalities include:[164-166] $-CH_3$, -OH, $-(C=O)OCH_3$, $-O(C=O)CH_3$, $-O(C=O)CF_3$, $-O(C=O)C_6H_5$, -COOH, $-OSO_3H$, -Cl, MPcs.[96,154-156,158-160] SAMs can also be prepared by the formation of two-component molecular gradients, as first described by Liedberg and Tengvall.[167]

1.3.2.2 Characterization of SAMs

SAMs have been thoroughly characterized using different surface analytical tools. Among the most frequently used techniques are FT-Raman and infrared spectroscopy,[157-166] ellipsometry, study of wetting by different liquids,[168] X-ray photoelectron spectroscopy,[169] electrochemistry,[164,169-172] and scanning-probe measurements.[173]

Electrochemical techniques, particularly cyclic voltammetry have been employed to investigate the integrity of SAMs on gold electrodes. Since the chemisorbed species in SAMs are surface confined, the results obtained from cyclic

voltammetric experiments are similar to that described in Sections 1.2.4.1 and 1.2.4.2 such that I_p is defined by equation 1.13:[163]

$$I_p = \frac{n^2F^2A\Gamma\nu}{4RT} \qquad 1.13$$

where A = surface area of the electrode (cm^2), Γ = total surface coverage by electroactive species and all other symbols have their usual meaning (see list of symbols).

1.3.3 Monolayer Annealing

The influence of surface orientation of organic molecules has received increasing attention in recent years.[163,714-178] Thermal annealing involves heating a deposited molecule (e.g. on an electrode) such that the metastable disordered state of the molecules can be reconstructed.[162] The reconstruction can also be achieved using electrochemical method by repeatedly cycling the adsorbed layer under potentiodynamics conditions such as cyclic voltammetry. It is believed that this approach helps to improve the surface properties of the adsorbed layer (such as reducing the interfacial capacitance, pinhole area and defects) by changing the structural orientation and molecular transition within the adsorbed layer.[179]

1.3.4 Electrocatalysis at Modified Electrodes

When an electrode is coated with a monomer or conducting polymer film, the following modes of reaction of electroactive solutes are possible: (1) reaction at the film-solution interface via electronic conduction, (2) diffusion through pores and channels to react at the electrode-film interface and (3) electron transfer mediation by the film (electrocatalysis).[180]

Electrocatalysis occurs when the surface of an electrode acts both as a source of electrons and as a reaction site. It is the study of how reactions may be accelerated at electrode surfaces. The process usually requires the surface of the electrode to be modified, in some way, for there to be a mediating molecule close to the electrode or in solution. Electrocatalysis at a modified electrode is ordinarily a mediation of electron transfer, by the immobilized electroactive species (the **O/R** couple), between the electrode and a substrate (**S**) (Scheme 1.3) which would otherwise undergo a slow electrochemical reaction at an unmodified electrode.

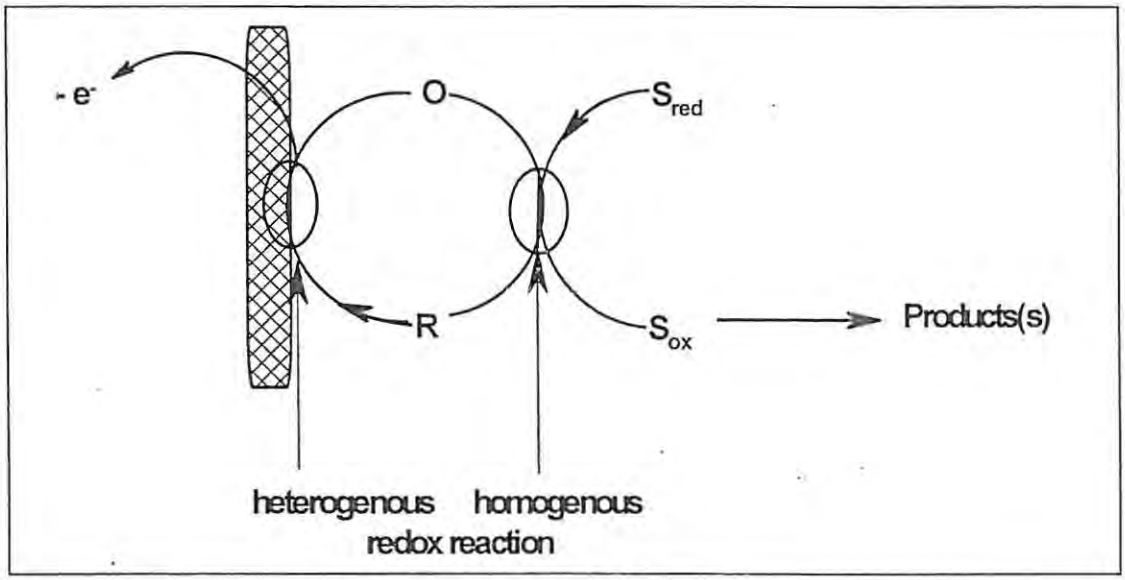

Scheme 1.3: Schematic representation of a mediated electrocatalysis.

If the rate of mediated reaction is fast, and the rate of reduction of **O** faster, the substrate becomes reduced at a potential near that of **O/R** formal potential, $E^{o'}$ (i.e. formal potential of the surface confined redox mediator). The catalysis of the rate of electrode reaction of a dissolved substrate by an electrode bearing an immobilized redox species (Scheme 1.3) accounts for most of the recent interest in modified electrodes.[91,180-191]

1.4 Chemistry of Metallophthalocyanines

Since the serendipitous discovery and identification of phthalocyanines (Pcs) in the early 1900s,[192-196] they have been extensively used as dyes and pigments in paints, textiles, biomedical materials and paper industries. In 1934, Linstead[193] deduced the complex macro cyclic structure and coined the name phthalocyanine (phthalo from naphtha (meaning oil) and cyanine meaning blue). The areas of application of phthalocyanine owe credit to the intense blue-green coloration, high dyeing power, photostability, insolubility in most solvents and their chemical inertness.[197] The structure of phthalocyanines was first confirmed by Robertson[194-196] using X-ray crystallography. Most of the applications of Pcs are concerned with the large, flat π-conjugation system, as well as with the type of central metal of the macro cycle.

The unique chemical properties of Pcs have been extensively exploited in their use as electrocatalysts and photocatalysts. Only a few members of this class of compounds have both electrocatalytic and photocatalytic properties. Electrocatalytic properties of MPcs are related to the central metal in that mainly electroactive metals have been found to efficiently catalyse electrochemical reactions. On the other hand, photocatalysis requires diamagnetic metal centres that are not electroactive and do not rapidly quench the metastable excited state, since the existence of a transient but relatively long-lived excited state is vital in photocatalysis. Such a metastable state could be rapidly "quenched" in the presence of features that promote charge (electron) transfer.

1.4.1 Structure and Naming of Phthalocyanines

Phthalocyanine (Pc) molecule is a macrocycle derived from tetraazaporphyrin by fusion with four benzene units. The phthalocyanine molecule contains four

isoindole groups; linked by four nitrogen atoms to form a symmetrical 18π electron conjugated aromatic macrocycle, which is related to the naturally occurring porphyrin. Pc (**1**) is known systematically as tetraazatetrabenzoporphyrin (Fig. 1.11). There are sixteen hydrogen atoms on the outer benzene ring (Fig. 1.11) that can be substituted. Substitution at positions 2, 3, 9, 10, 16, 17, 23 or 24 is referred to as peripheral, while substitution at positions 1, 4, 8, 11, 15, 18, 22 or 25 is non-peripheral. It is usually simpler to refer to these positions in the nomenclature of the compound. In the presence of a metal salt metallophthalocyanines (MPc, **2**) is formed. Pc is structurally related to other synthetic porphyrins analogues such as tetraphenylporphyrin (**3**, TPP), porphyrin (**4**), tetrabenzoporphyrin (**5**, TBP) and tetraazaporphyrin (**6**, TAP) (Fig. 1.12).

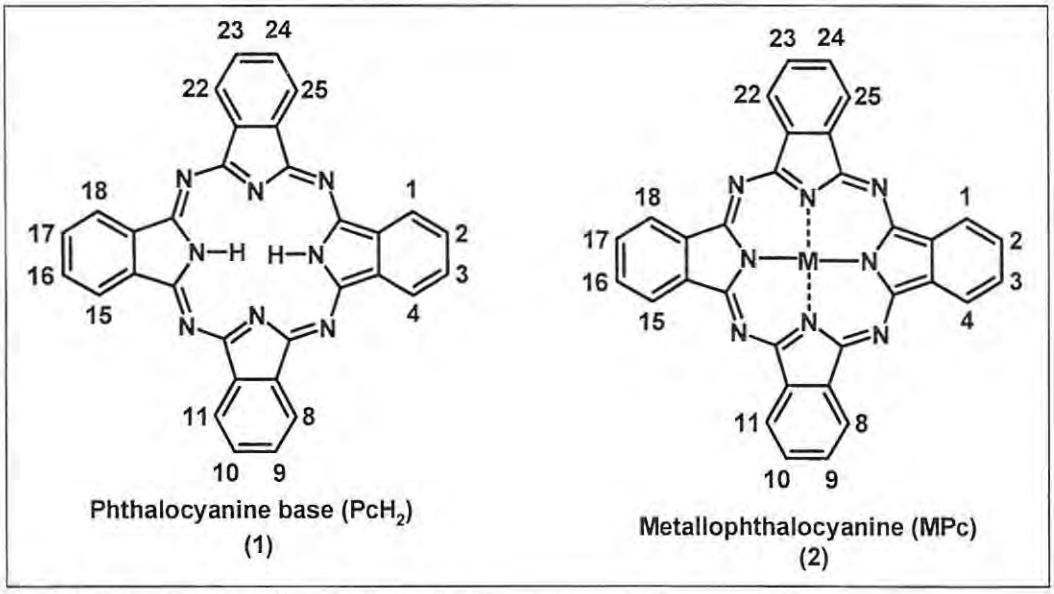

Fig 1.12: Numbering scheme of a phthalocyanine system.

MPcs are relatively small planar molecules containing 56 atoms (per molecule) in an arrangement with D_{4h} symmetry. The closed inner system consists of 16 carbon and 8 nitrogen atoms with great stability.[198-200] The Pc ring itself can be symmetric. Perturbations to the geometry from D_{4h} to C_{4v} of the central metal due to

axial ligands or solvents, and the size effects of different central metals have been extensively studied.

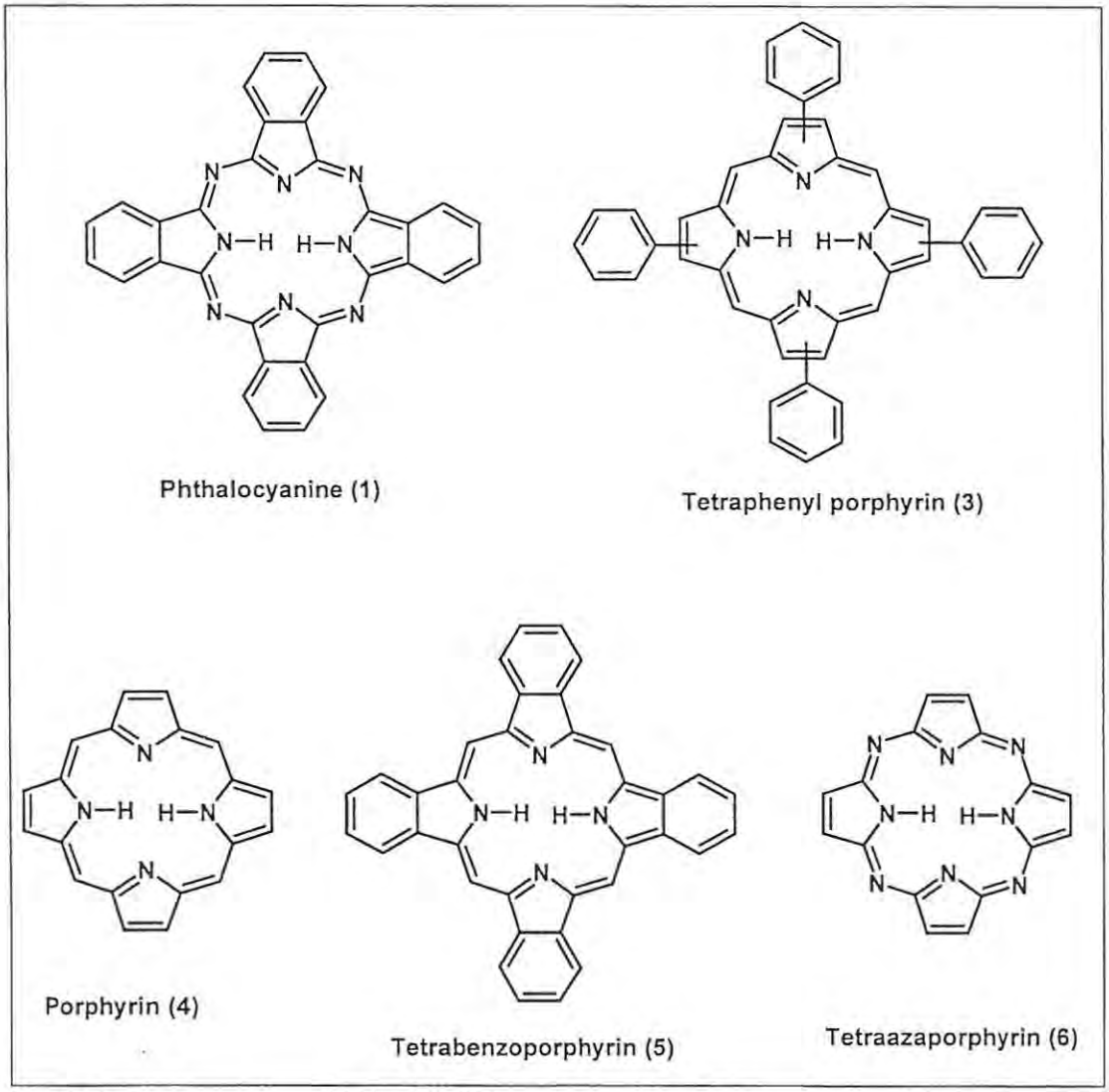

Fig. 1.12: Representative sketch of phthalocyanine and some related molecules.

1.4.2 Electronic Structure and Spectroscopy of Metal Phthalocyanines

A major interest in metallophthalocyanines and related macrocycles arise from a combination of their intense coloration and their diverse redox chemistry, properties that are associated with both the heteroatomic π-systems of the Pc ligand and the central metal. UV-Visible absorption and associated magnetic circular dichroism

(MCD) spectra provide direct information about energies and degeneracies of the states that are responsible for the major spectral bands in the UV-Visible and near IR spectral region.[197]

Fig 1.13 shows the origin of the UV-Visible spectrum as presented by Gouterman's 4-orbital linear combination of atomic orbitals model.

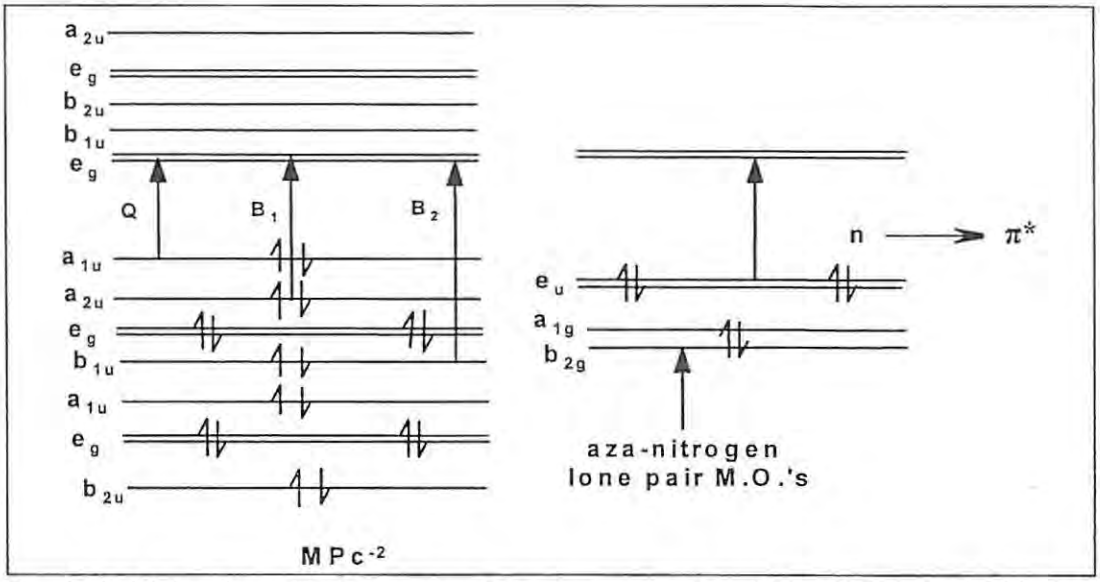

Fig. 1.13: Molecular orbital diagram of the π-system of an ideal 16 atom, 18 π-electron system showing the origin of the Q and B bands in Gouterman's 4-orbital linear combination of atomic orbitals model.

The UV-Visible spectrum of unsubstituted metallophthalocyanines (MPcs) is typified by a Q band near 670 nm (Fig 1.14) with extinction coefficients greater than 10^5 L mol^{-1} cm^{-1}, originating from $a_{1u} \rightarrow e_g$ ($\pi \rightarrow \pi^*$) (Fig 1.13), in addition to a series of vibrational bands (Fig. 1.14). The Soret band of MPcs results from a superimposition of two bands B_1 and B_2 (Figs 1.14) in the 350 nm regions in the absence of strong axial ligands.[201-205] Three other high-energy transitions which may be observed below 300 nm in the ground state electronic absorption spectra of diamagnetic MPcs such as ZnPc and MgPc,[206] are referred to as N, L and C bands (with increasing order of energy). The non-bonding electrons on the azomethine nitrogens of the Pc macrocycle in MPcs also contribute to the observed spectra. The n

orbitals are very close (in energy), to the π orbitals (highest occupied molecular orbital, HOMO) and consequently, the n→π* transitions are expected to be coupled with π→π* transition. Huang *et al.*[207,208] have suggested that the band around 605 nm in the optical spectra of MPcs may have a partial contribution from the n→π* transition.

The band around 500 nm (usually observed in some transition metal MPcs) is characterized as charge transfer transition,[199,200] from metal to ligand (MLCT) or from ligand to metal (LMCT).

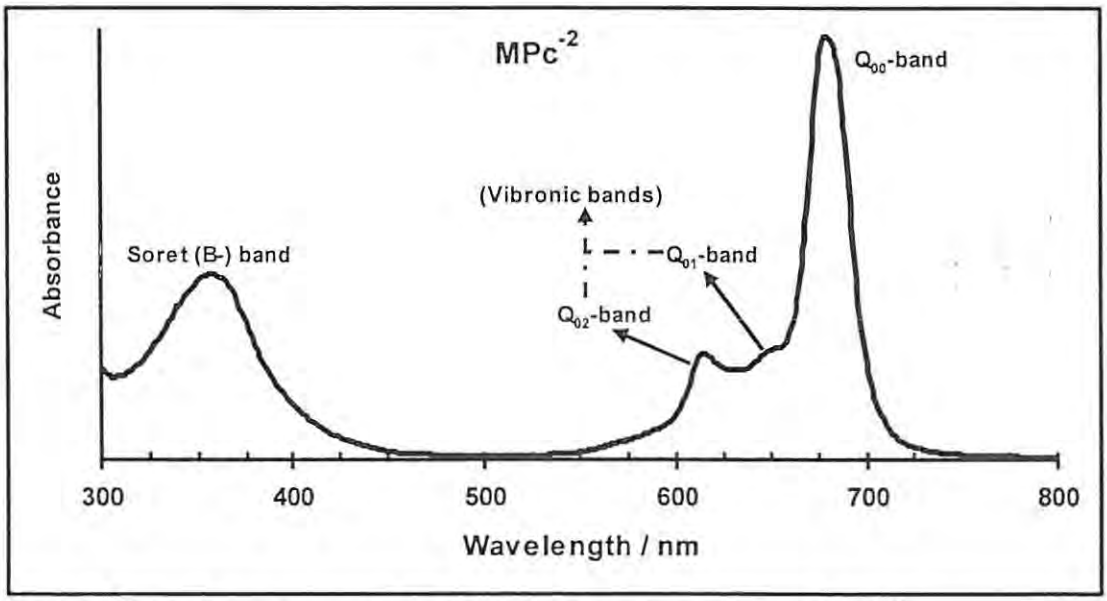

Fig. 1.14: Typical room temperature electronic absorption spectrum of MPc^{-2}.

1.4.3 Electrochemistry of Phthalocyanines

The electrochemistry of phthalocyanines did not receive much attention as did the parent compound, (the porphyrins), owing to the influence of poor solubility and purity of phthalocyanine on their physicochemical studies.[209] Since the development of substituted phthalocyanines with more fine-tuned molecular properties, and with increased solubility and purity, electrochemistry of phthalocyanines has gained increasing interest. Most electrochemical techniques require solution concentrations

ranging from 10^{-4} to 10^{-3} M. Non-aqueous solvents are often employed. Otherwise, specially synthesized water soluble MPcs are employed. As is the case for porphyrins and metalloporphyrins,[210] the electrochemistry of Pcs and MPcs in nonaqueous media occurs at different cites depending on the nature of the Pc. The redox activity of the Pc ring is directly linked with the frontier orbitals (i.e. HOMO) and lowest unoccupied molecular orbital (LUMO)) in the molecule. Oxidation is the removal of electron(s) from the HOMO while reduction is the addition of electron(s) to the LUMO. The Pc skeleton exists as a dianion, Pc^{-2}, so that successive removal of up to two electrons from the HOMO (a_{1u}) results in the formation of Pc(-1) and Pc(0), respectively. In a similar manner, the successive addition of up to four electrons to the LUMO (e_g) results in the formation of Pc^{-3}, Pc^{-4}, Pc^{-5} and Pc^{-6}.

In non-aqueous media, free base (Pcs without a central metal) and MPcs with "inactive" metals (eg Zn^{2+}, Mg^{2+}) usually undergo up to two reversible single electron oxidations leading to the corresponding π-cation radicals and dications, and up to four reversible single electron reductions, yielding π-anion radical (for first reduction) and dianions (for second reduction). The metal centered redox processes are also observed for a number of MPcs containing electro-active metals. For MPcs containing electroactive metals, (e.g. Co, Fe, Mn, Cr), the reduction and oxidation of the central metal occurs before ring-based processes. For example, Scheme 1.4 shows the redox behaviour of cobalt phthalocyanine in coordinating and non-coordinating media.

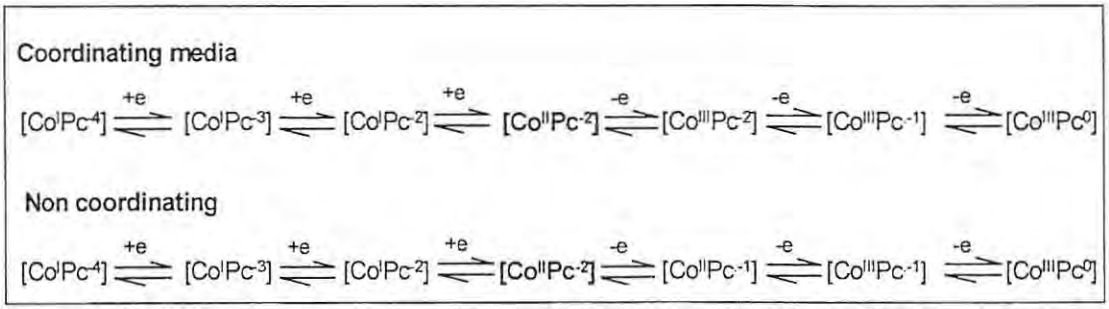

Scheme 1.4: Redox behaviour of cobaltphthalocyanine in coordinating and non-coordinating media.[209]

Electron transfer to and from MPcs may involve reactions at an axially bound 5^{th} or 6^{th} ligand. Specifically, such ligand-centred redox process may occur for (1) Pcs containing various bound oxo or peroxo groups, (2) Pcs containing bound catechol or thiol donor groups, (3) Pcs with bound diatomic molecules such as NO and O_2, (4) Pcs containing a σ-bonded alkyl or aryl group, and (5) bimetallic complexes where a metal-carbon unit is σ-bonded to the MPc. Often, spectroelectrochemistry has been employed in assigning the redox processes of MPc complexes. The electrochemistry and spectroelectrochemistry of new pyrrole, thiophene and pyrimidin tetra substituted phthalocyanines containing cobalt, iron, manganese, nickel and zinc are presented in this work (Fig 1.15).

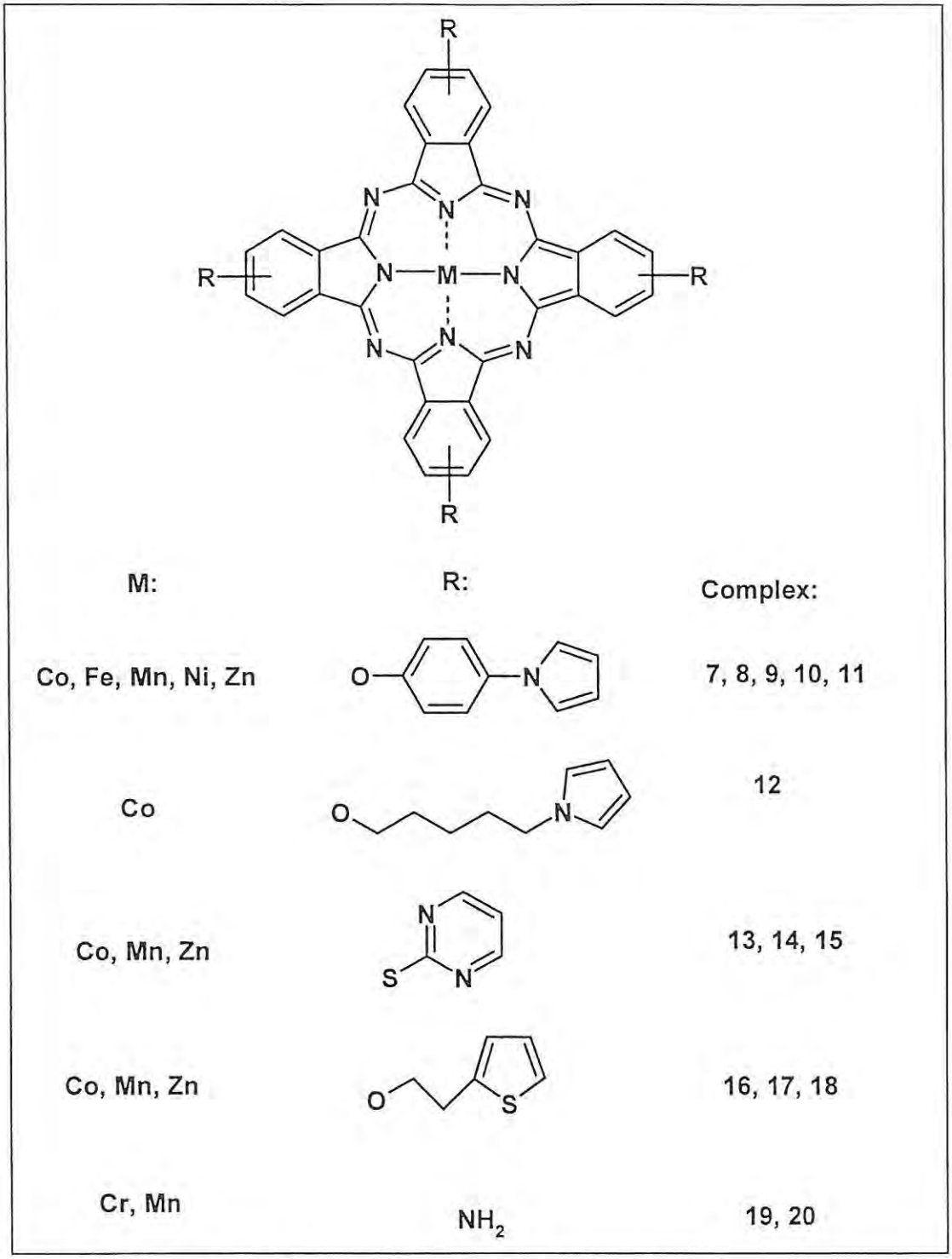

Fig 1.15: Structure of MPc complexes studied in this work.

1.4.4 Synthesis of Phthalocyanines

1.4.4.1 Unsubstituted Phthalocyanines

A variety of precursors (**21-26**, Fig 1.16) have been employed for synthesis of phthalocyanines. Phthalonitriles (**22**) are among the most useful Pc precursors, since they readily yield Pc complexes in good yields with most metals.[211] The condensation of phthalonitriles often occurs upon heating in the presence of a metal ion source (e.g. metal halides) either as a melt of metal reagent or in a suitable high boiling solvent such as 1-pentanol or similar alcohols in the presence of organic base such as 1,8-diazabicyclo[5.4.0]undec-7-ene (DBU), piperidine or cyclohexylamine.[212-214]

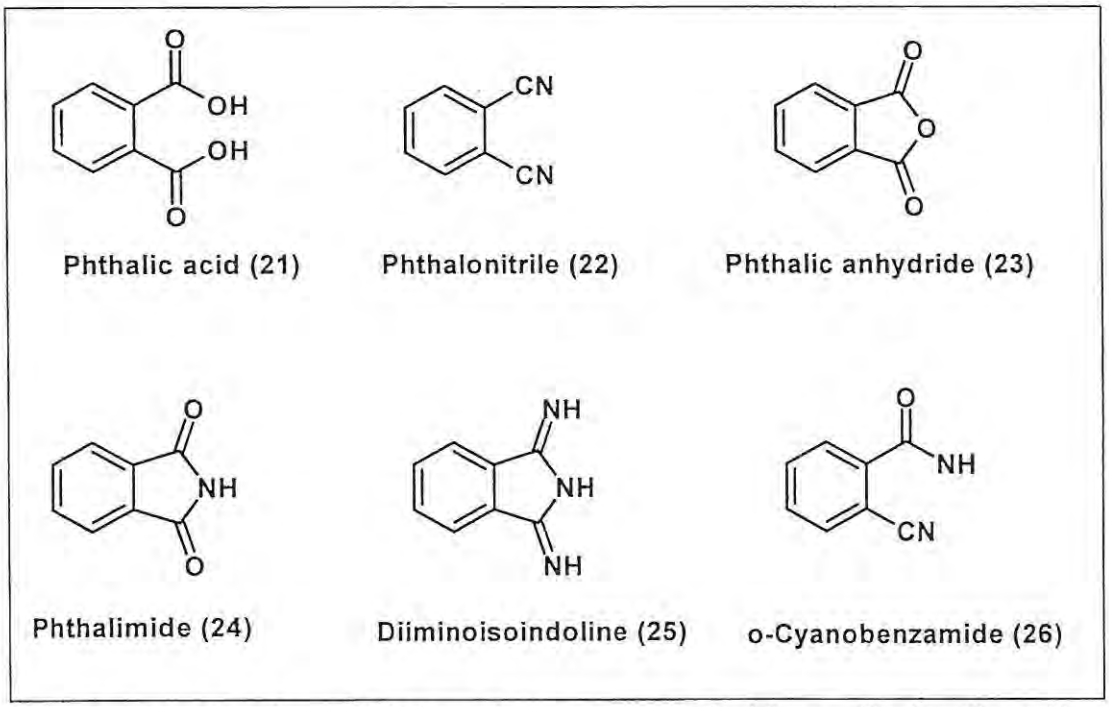

Fig. 1.16: Examples of some phthalocyanine precursors derived from *o*-dicarboxylic acid.

Lithium metal has also been used instead of the above-mentioned organic bases to facilitate cyclotetramerization via the lithium pentanolate or lithium pentoxide route[215,216] (Scheme 1.5). Cerium-induced cyclotetramerization of phthalonitriles has also been reported by Lee and Ng.[217]

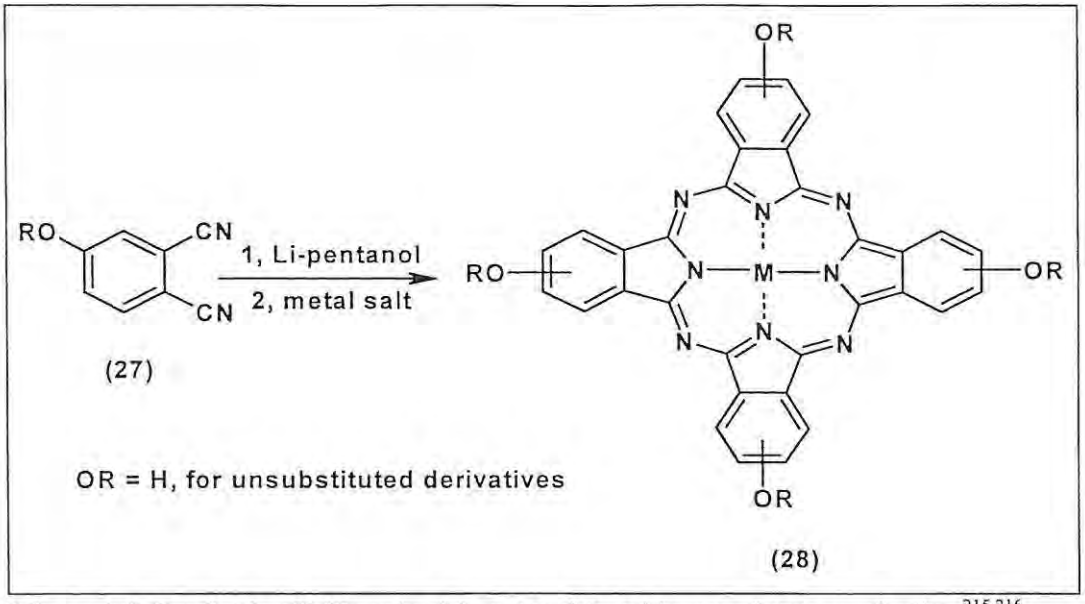

Scheme 1.5: Synthesis of MPc using Li-pentanol to achieve cyclotetramerization.[215,216]

As stated above Pcs formed from phthalonitriles are generally much cleaner than those obtained from other Pc precursors and are known to give best yields, typically in the range of 30-50% and some times 90%.[218] On the other hand, synthesis using Pc precursors such as phthalic anhydride (**23**) and phthalimide (**24**) require the presence of nitrogen source such as urea and a catalyst such as ammonium molybdate or boric acid.[219] The various 1,2-disubstituted benzene precursors used to obtain metallophthalocyanine are summarized in Scheme 1.6.

For each of the methods, the reactants and conditions favour a cyclotetramerization of the precursor or its substituted derivative to form the phthalocyanine macrocycle.[220] As can be seen, the methods applied for the MPcs syntheses are not discrete as one type of precursor is often an intermediate in the cyclotetramerization reaction of another.

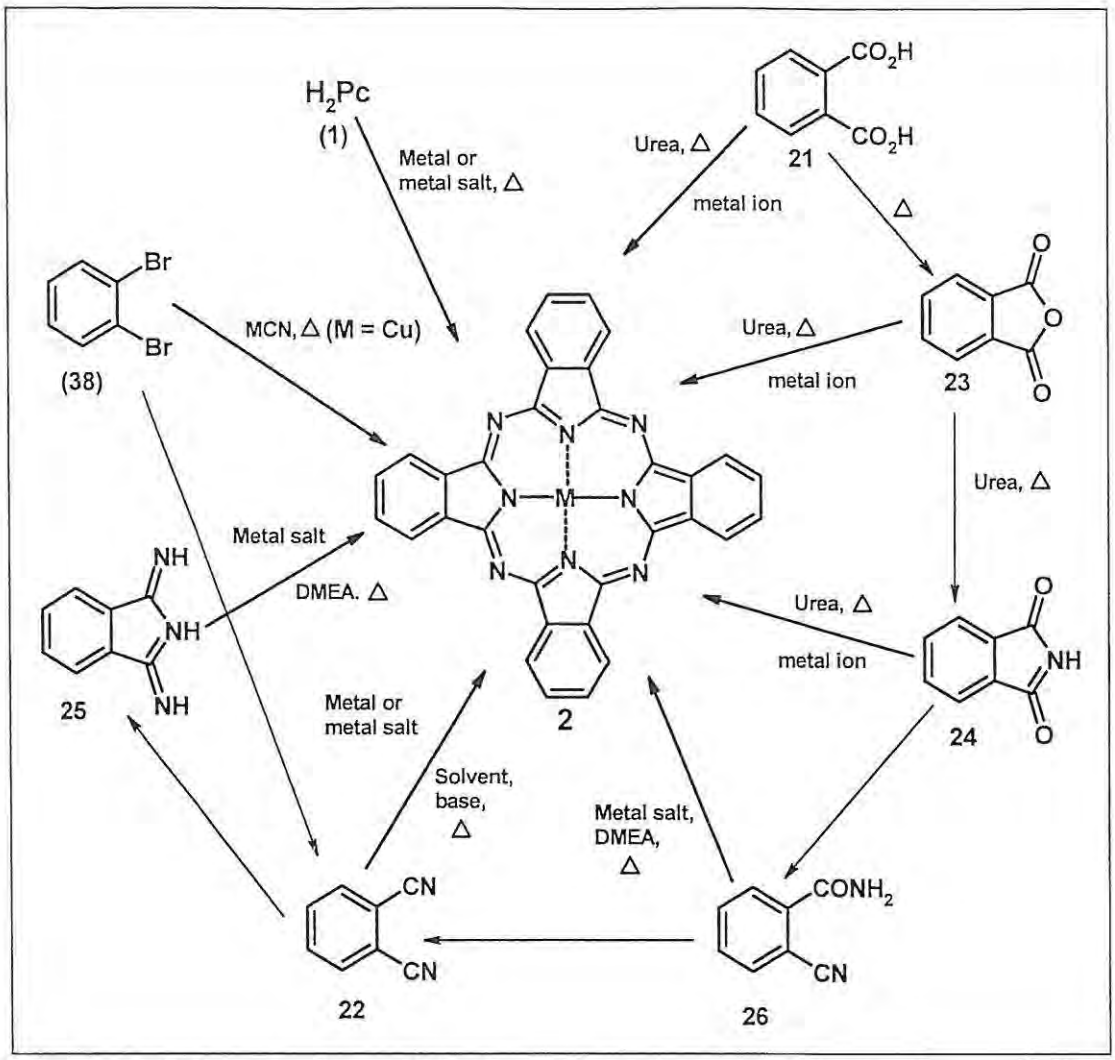

Scheme 1.6: Scheme for the synthesis of metallophthalocyanines. The dotted arrows indicate the connectivity between the precursors. DMEA = N,N-Dimethylethanolamine

1.4.4.2 Ring Substituted Phthalocyanines

Ring substituted Pcs are usually obtained by one of two basic routes. The first involves the direct substitution onto a pre-existing Pc as demonstrated in the case of sulphonation of Pcs that is accomplished by heating a Pc macro cycle in oleum.[221] This approach generally results in complex isomeric mixtures and varying degrees of substitution with substituents added at any or all of the 16 available positions on the MPc (Fig. 1.11). The major set-back in this approach is that the resulting Pc mixture lacks a distinct structure and isolation and purification of the desired product is

extremely difficult, thereby limiting the utility of this methodology in application requiring well-defined Pcs.[218,222] More often than not, Pc complexes are formed from precursors via a metal-templated cyclotetramerization reaction of the starting material(s). The addition of substituents to the Pcs in order to improve their properties is easier to control using appropriately substituted starting material rather than adding them to pre-existing macrocycles.

Thus a second method of synthesizing ring substituted Pc involves condensation of substituted precursors (Scheme 1.5). The resulting Pcs in this methodology are purer in terms of degree of substitution. The basic positions of the substituents are easily predictable and in most cases are known precisely. For instance a 4,5-disubstituted phthalonitrile would condense to form 2,3,9,10,16,17,23,24-octasubstituted Pc. Mono substituted phthalonitriles at 4 or 5 position condense to form constitutional isomers[223-225] of the corresponding Pc: 3,10,17,24-(C_{4h}); 3,10,16,24- (C_s); 3,9,16,24- (C_{2v}); 3,9,17,23- (D_{2h}) tetra substituted Pcs. Although isomeric mixtures may be desired for some applications, fields such as non-linear optics require distinct molecular geometries. As such, new synthetic protocols and specially designed Pc precursors for preparation of single isomers have been studied. While condensation of substituted precursors has certain drawbacks, it remains the preferred method for adding substituents to Pcs and as such, the syntheses of substituted precursors is a vital route in the preparation of new Pc derivatives with improved properties and chemical architecture.[219]

Another major challenge facing Pc synthetic chemists is in the case of asymmetrically substituted Pc[226] synthesis for varying applications. Langmuir-Blodget films for example require different substituents in order to achieve the molecular orientations necessary to ensure that transferred films have similar

orientation.[227-230] Pcs bearing amphiphillic moieties have shown high potency as photosensitizers for photodynamic therapy (PDT).[230-234] The asymetrically substituted Pcs formed are rather difficult to isolate according to the constituent isomers. Column and high performance liquid chromatography (HPLC) can be used to isolate the desired substituted products in most cases, but often this is a very tedious task and is fraught with contamination with differently substituted Pcs.[235]

Different Pc precursors have been designed with the ultimate aim of improving yields of exclusively single isomer or tailored substitution pattern. Some degree of success has also been achieved using some polymer-supported precursors[236] and boron subphthalocyanine (**29**)[237] (Fig 1.17). Subphthalocyanine (SubPc, **29**), (Fig 1.17) was first synthesized in 1972[238] and has received attention as a precursor for MPc synthesis.

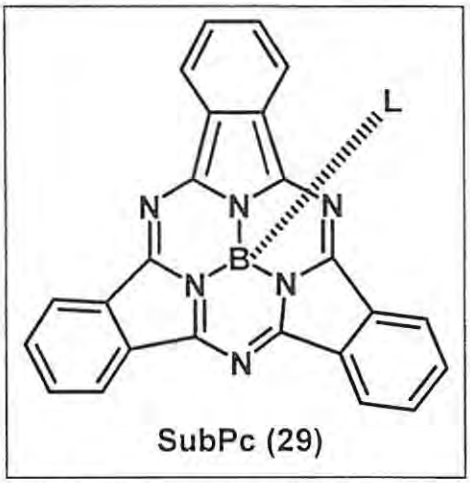

Fig. 1.17: Structure of a subphthalocyanine.

SubPcs can be synthesized by reacting phthalonitrile (**22**) with boron trichloride in 1-chloronaphthalene under reflux.[238,239] The major interest in the application of SubPcs in MPc syntheses is the need for asymmetrically substituted MPcs. When an unsubstituted SubPc is reacted with a substituted diiminoisoindoline or phthalonitrile molecule, different degrees of substitution on the resulting MPc are

achieved.[240] Symmetrically substituted Pc containing pyrrole, thiophene, pyrimidine and amino groups are reported in this work using phthalonitrile and phthalimide precursors.

1.4.4.3 Synthesis of Substituted Phthalonitrile Precursors

Phthalonitriles are usually synthesized from phthalic acid derivatives by stepwise progression through the anhydride, imide, diamide, and finally to the desired phthalonitrile. Many substituted phthalonitriles bearing versatile functional groups can be synthesized from relatively inexpensive commercially available starting materials (Scheme 1.7). The routes employed to obtain 4,5-dichlorophthalonitrile (**34**) and 4-nitrophthalonitrile (**37**) are shown in Scheme 1.7 (a and b).[224,225,240] Generally, the nitro group or the chloro group serves as the leaving groups while alcohols, phenols, thiols[225,241,242,243] and amines have been used as the nucleophiles in a nucleophilic aromatic substitution (S_NAr) reaction mechanism.

Scheme 1.8 shows the route employed to obtain modified phthalonitrile from 4-nitrophthalonitrile (a) and 4,5-dichlorophthalonitrile (b). The conditions necessary for the substitution reactions are also indicated in the reaction Scheme.

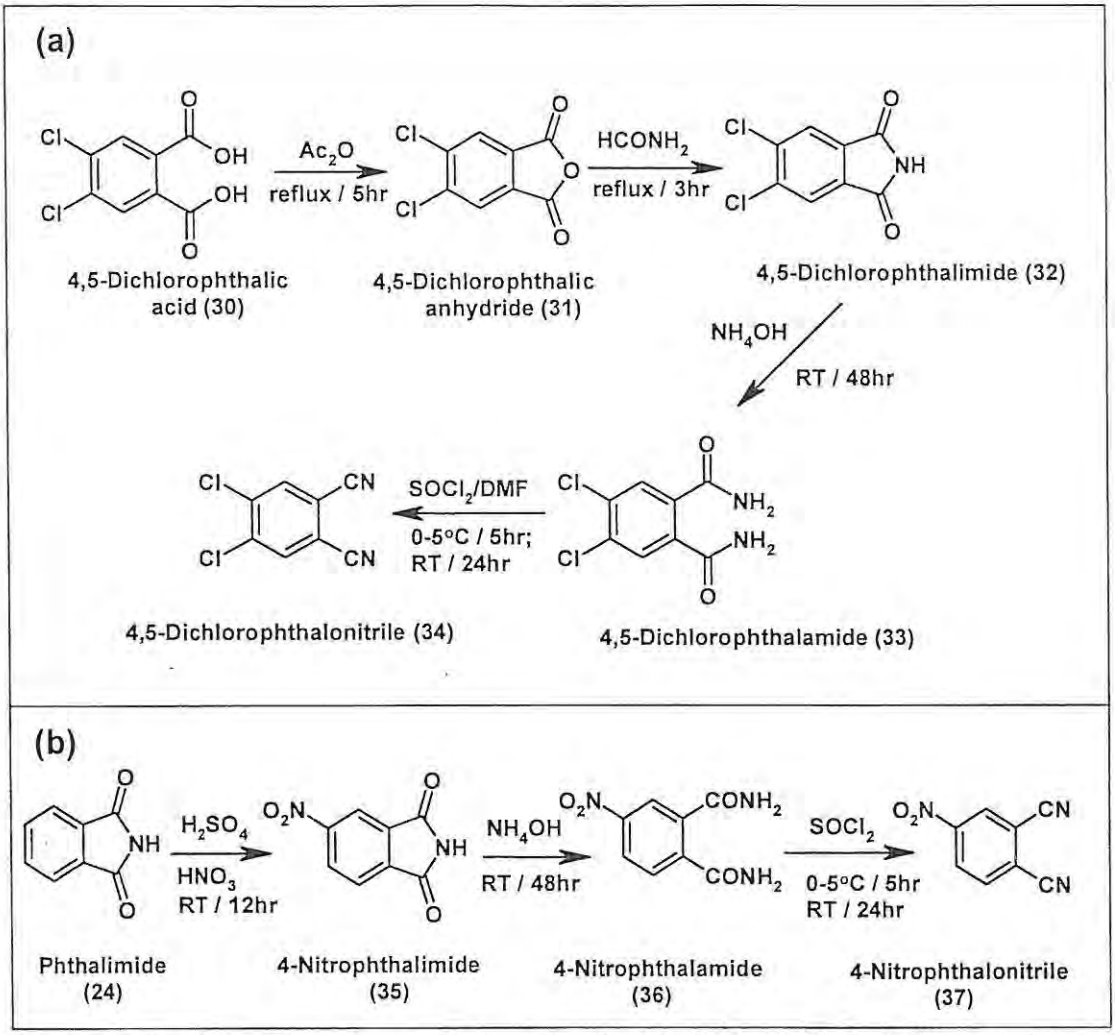

Scheme 1.7: Route for the synthesis of (a), 4,5-dichlorophthalonitrile and (b), 4-nitrophthalonitrile.

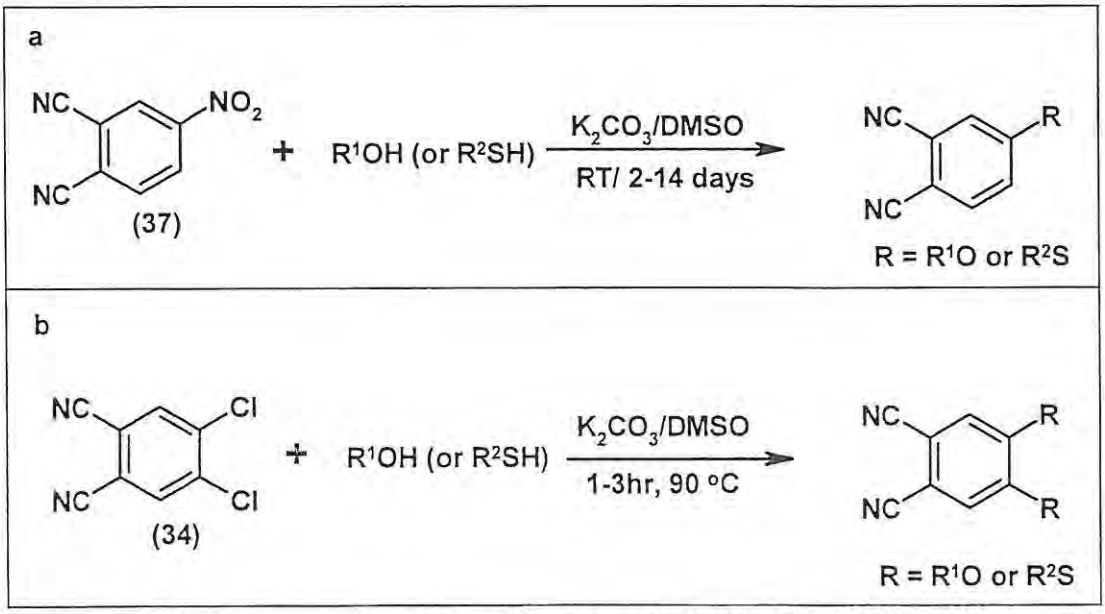

Scheme 1.8: Synthetic route for modification of 4-nitrophthalonitrile (a) and 4,5-dichlorophthalonitrile (b)

Both 3- and 4-nitrophthalonitrile are readily hydrogenated to the corresponding aminophthalonitrile in the presence of catalysts. Although halogens have been shown to be preferred leaving groups in certain S_NAr reactions involving both NO_2 and Cl, the popularity of the NO_2 leaving group in terms of the preparation of mono substituted phthalonitriles is probably linked to the commercial availability of both the 3- and 4-nitrophthalonitrile and/or their facile synthesis via nitration of phthalimide (**24**) and subsequent conversion to the phthalonitrile Scheme 1.6b.

1.4.4.4 Mechanistic Aspects of the Synthesis of Phthalocyanines

The mechanism of condensation reaction involves a stepwise polymerization of Pc precursors or reactive intermediates followed by coordination of the central metal ion and rigid closure to the macrocycle. The mechanistic aspect of Pc formation is depicted in Scheme 1.8.[218] The driving force of the ring closure is not only the template effect of the metal ion and the inherent stabilization implied by the coordination but also by the thermodynamic stabilization and added aromaticity involved in the formation of the Pc ring.[219]

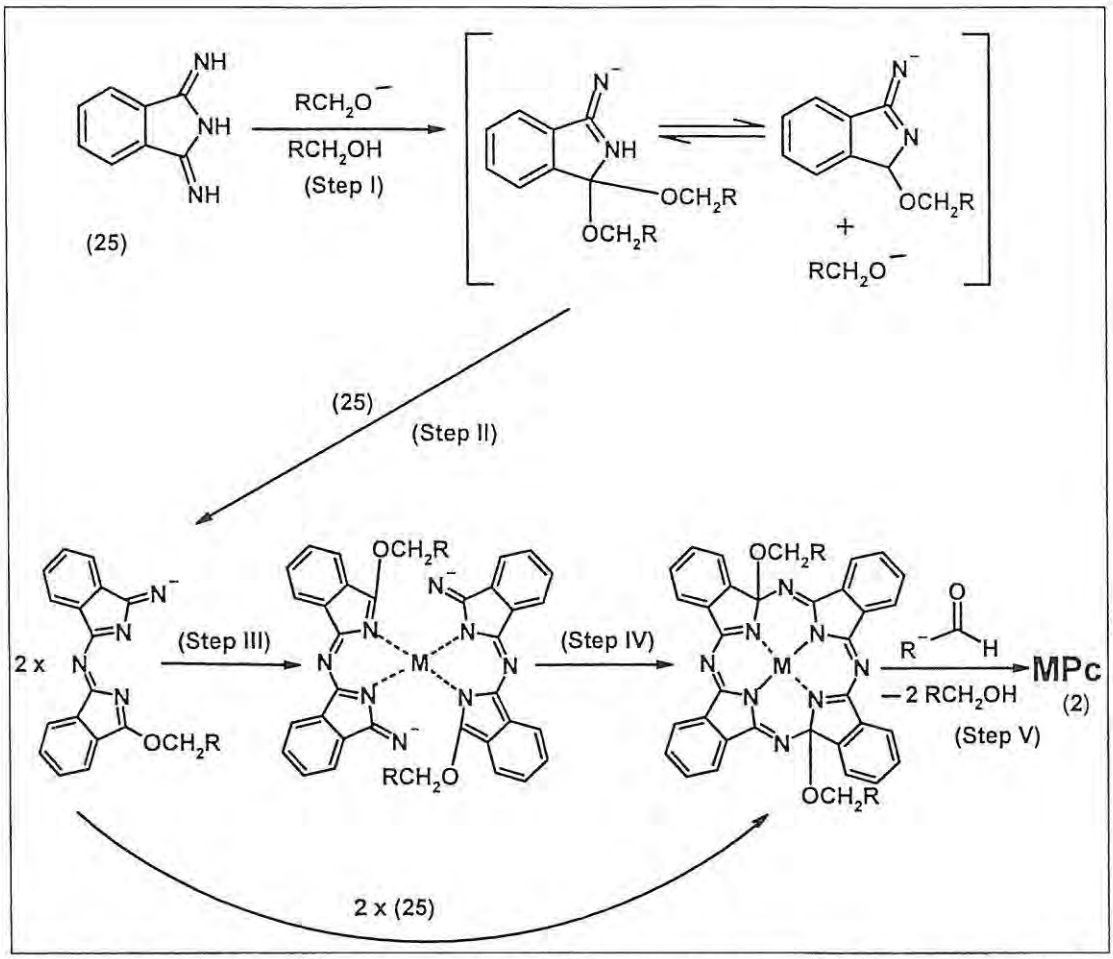

Scheme 1.9: Mechanistic scheme for cyclotetramerization of phthalonitriles during synthesis of MPcs.[218]

Up to 70 different metals can be placed in the central cavity of Pcs whereby the choice of the cation can strongly influence the physical properties of the resulting MPc. Many metal ions (e.g. Cu^{2+}, Co^{2+}, Fe^{2+}) are held so tightly that they cannot be removed without destructing the macrocycle.[245] Unlike their porphyrin analogues, which can be found as natural products, Pcs and MPcs are purely synthetic.

1.4.5 Applications of Metal Phthalocyanines

MPcs are widely used in industries in a variety of applications ranging from conventional dyes to catalysts or from coatings for read/write CD-RWs to anti-cancer agents.[220] MPcs have been used as deodorants and as drugs for inactivation of

bacteria or viruses,[246-248] and the ability to create different ring substituted MPcs, thereby adjusting the main band (Q band) position of Pc, has helped in preparing Pcs that are used in the surface of read/write compact disks,[220,249-251] Langmuir-Blodgett (LB) films,[251-254] photodynamic therapy (PDT),[231,247,255] dyes,[193,256-259] electrochemiluminescent displays,[260,261] for photocopiers and laser printers by xerography.[262] It has been suggested that cobalt phthalocyanine (CoPc) and cobalt porphyrin (CoP) may be suitable candidates for denitrification and as gas sensors owing to their ability to bind small molecules such as nitric oxide (NO) and oxygen.[263,264] Collman and coworkers[265] demonstrated that stacks of MPc complexes can serve as good organic conductors. Moreover, MPcs have been employed as active ingredients in liquid crystal displays (LCDs), electronics, opto-electronics and iono-electronics.[266-268]

The search for therapeutically effective, safe, cost-effective and socially acceptable microbicide in treatment and prevention of human immunodeficient virus (HIV) has led to scores of research papers being published in recent years. Of special interest is the fact that certain levels of success have been demonstrated in this area of research using phthalocyanines. For instance, Zmudzka and co-workers[269] showed that silicon phthalocyanine SiPc) is effective in photosensitised decontamination of blood. Similarly Ben-Hur *et al*[270] showed that SiPc and red light caused apoptosis in HIV-infected cells. More recently, the inactivation of HIV by Pcs via processes that do not involve exposure to light has been reported.[271] The study showed that the structure of MPcs plays a significant role in the efficacies of the MPcs against HIV-IIIB. Sulphonated Pcs were the most promising class of MPcs for development of microbicides to prevent HIV transmission. Specific structural features, particularly central metal and the extent and placement of the sulphonic groups, also played a role

in determining the activity of these compounds. It was also shown that planar or near-planar MPcs are more effective than MPcs with axial ligands, both in inhibition of fusion and blocking of viral infection.

Electrodes modified with Pcs with different central metals and ring substituents have been vastly employed in the electrocatalysis of many systems including biologically important molecules.[272-277] This thesis is concerned with the use of MPcs as electrocatalyts, hence a review of electrocatalytic properties of MPcs will be considered next.

1.4.6 Electrocatalytic Properties of Metal Phthalocyanines

As mentioned earlier, electrocatalysis occurs when the surface of an electrode acts both as an electron source and as a reaction site. The interest in the catalytic properties of MPcs is derived not only from the advantages they have over metal and metal oxide but also because their catalytic actions can be related to their chemical structure, chemical and physical properties.[278] It is well known that the presence of π donors as a fifth ligand on metallophthalocyanines[109, 278-284] increases their catalytic activity. The electrocatalytic activity of MPcs has been[285-288] related to redox potentials of the central metal, for example in the reduction of oxygen, equations 1.14 - 1.16:

$$M^{(II)}\,Pc^{-2} + O_2 \rightarrow [M^{(III)}{-}O_2{-}Pc^{-2}] \qquad 1.14$$

$$[M^{(III)}{-}O_2{-}Pc^{-2}] \rightarrow \text{Product} + M^{(III)}Pc^{-2} \qquad 1.15$$

$$M^{(III)}Pc^{-2} + e^- \rightleftharpoons M^{(II)}Pc^{-2} \qquad 1.16$$

And the general mechanism for the metal oxidation-mediated catalytic oxidation of a species (A) to a product (B) is given by equations 1.20 and 1.21.[283, 289-292]

$$M^{(II)}Pc^{-2} \rightarrow M^{(III)}Pc^{-2} + e^{-} \quad 1.17$$

$$M^{(III)}Pc^{-2} + A \rightarrow M^{(II)}Pc^{-2} + B \quad 1.18$$

Sekota and Nyokong[289] have reported electrooxidation of L-cysteine mediated by ring-based processes using rhodium, ruthenium and osmium phthalocyanine complexes ($(CN)_2RhPc^{-}$, $(DMSO)(Cl)RhPc$, $(DMSO)_2RuPc$ $(DMSO)_2OsPc$) according to equations 1.19-1.21):

$$MPc^{-2} \rightarrow [MPc^{-1}]^{+\cdot} + e^{-} \quad 1.19$$

$$2[MPc^{-1}]^{+\cdot} \rightarrow ([MPc^{-1}]^{+\cdot})_2 \quad 1.20$$

$$([MPc^{-1}]^{+\cdot})_2 + A \rightarrow MPc^{-2} + B \quad 1.21$$

Methods of Electrode Modification Using Metal Phthalocyanines

Electrodes modified with metallophthalocyanines have been extensively used in electrocatalytic reactions. The electrodes modified with MPcs include glassy carbon, carbon fibres, graphite, gold, platinum, indium tin oxide on glass. However, carbon is the most widely used electrode material. The methods employed to attach the MPcs on the electrodes include electropolymerization,[283,293] adsorption by drop-dry,[283] chemisorption (as in SAMs).[157-159] In some cases where the intention is to design a sensor, the electrodes have been modified by screen printing. Co, Fe, Ni and Sn phthalocyanines have been shown to adsorb on graphitized carbon black, containing 15% platinum for use as co-catalyst.[294] MPcs have been deposited on electrode surfaces, incorporated in a polymer.[295-297] Zeolites modified with MPcs in which the MPcs were mixed with graphite to get a conductive catalytic phase have

been reported.[297-300] Electropolymerization of MPcs is a convenient way to obtain thick and stable catalytic film on the surface of the electrode. This has been made possible in the presence of counter-ions during the formation of MPc based conducting polymer.[301-303]

A wide range of species is catalyzed by MPc-modified electrodes, however, only selected amino acids, nitric oxide, nitrite, phenols and oxygen will be considered in this thesis. The next section will give a brief overview of the electrocatalytic behaviour of MPc-modified electrodes toward some of the species mentioned above.

1.5 Review of Analytes to be Electrocatalyzed by Metallophthalocyanine Modified Electrodes

1.5.1 Aminoacids (L-Cysteine and Glycine)

1.5.1.1 L-Cysteine

L-Cysteine is a neutral, genetically coded amino acid that can be found in many proteins throughout the body. Cysteine is a nonessential amino acid. It is made in the body from serine and methionine. It is one of the few amino acids that contain sulphur. This allows cysteine to bond in a special way and maintain the structure of proteins in the body. Cysteine is a component of the antioxidant, glutathione. The body also uses cysteine to produce taurine, another amino acid. N-acetyl-L-cysteine (NAC), a modified form of cysteine, helps break down mucus and detoxify harmful substances in the body.

The biochemical importance of cysteine is related to the presence of a sulphur-containing thiol group in its side chain. This group participates in the catalytic reactions of certain enzymes, such as that of papain, the enzyme from papaya latex

used to make commercial meat tenderisers. Kidney malfunction is related to a major complication of cystinuria, an inherited metabolic disease, one of whose symptoms is a twenty-fold to thirty-fold increases in urinary excretion of cystine, a relatively insoluble amino acid in the kidney.[304,305] Other diseases associated with cysteine include multiple sclerosis,[306,307] cancer and lung diseases,[308,309] Sjogren's syndrome (an autoimmune disorder characterized by dry mouth and dry eyes), cataracts and macular degeneration,[310,311] hepatitis C,[312-315] amyotrophic lateral sclerosis[316] (ALS, often called Lou Gehrig's disease, a rapidly progressive neuromuscular disease caused by the destruction of nerve cells in the brain and spinal cord) are also related to abnormality in cysteine level in the body.

Abnormal amounts of cysteine may be toxic to nerve cells and have been associated with Alzheimer's, Parkinson's diseases[317-320] and epileptic seizures.[321-323] Low levels of cysteine may be linked to an increased risk of cervical dysphasia[324] (the appearance of precancerous abnormal cells on the surface of the cervix, the lowest part of the uterus). When left untreated, dysplasia sometimes progresses to an early form of cancer known as cervical carcinoma in situ, and eventually to invasive cervical cancer. HIV infection is considered to be a condition of excessive oxidative stress (caused by free radicals) where the antioxidant glutathione is depleted significantly.[310,325-327]

Different methods have been employed to determine thiols. These include chromatography, fluorimetry, and electrochemistry.[328,329] Most of the electrochemical methods used are limited as a result of the fouling of the bare electrodes used in the analysis of thiols. The use of transition-metal phthalocyanines, adsorbed on graphite electrodes, have been shown to have a substantial electrocatalytic activity for the oxidation of several thiols like cysteine, reduced glutathione, 2-mercaptoethanol and

2-mercaptoethanesulfonic acid[279,289,330-332] The advantage offered by MPc modified electrodes is the decrease in the oxidation potential of the thiols and the significantly improved rate of electron transfer.[293,333]

The lower the potential for thiols, the better, thus Table 1.4 shows that substituted MPc complexes lower the potential for cysteine oxidation more than the unsubstituted MPc complexes.

Table 1.4: Comparative peak potential and limit of detection (LoD) for cysteine electrooxidation using selected cobalt and iron phthalocyanines.

MPc	Electrode material	E_p / V (Ag | AgCl)	LoD/ mol dm^{-3}	References
CoPc	C-cement	0.74	1.0×10^{-7}	334
CoOBTPc	SAM-Au	0.42	3.1×10^{-7}	157
FeOHETPc	SAM-Au	0.38	5.2×10^{-7}	158
CoOHETPc	SAM-Au	0.50	5.2×10^{-7}	159
FeOBTPc	SAM-Au	0.33	3.0×10^{-7}	335

Aim of Thesis

Pyrrole, thiophene and pyrimidin functionalized metallophthalocyanine complexes have been synthesized in this thesis. Part of the aims of this thesis therefore, is to study the electrocatalytic activity of these newly synthesized CoPc complexes towards the analysis of L-cysteine, with particular reference to oxidation potential and stability of the electrodes.

1.5.1.2 Glycine

Glycine is also a neutral, genetically coded amino acid. It is the only protein-forming amino acid without a centre of chirality. It is structurally the simplest of the

α-amino acids, having merely a hydrogen atom for a side chain, and is thus very unreactive when incorporated into proteins. Nevertheless, in the free state glycine participates in several important reactions, including the biosynthesis of heme, (an important constituent of haemoglobin), and the biosyntheses of bile acids, cretin phosphate and serine (another amino acid), purines (constituents of genetic material), and glutathione (a coenzyme)). Glycine is not essential to the diet since it can be made from other substances in the body. Glycine was the first amino acid to be isolated from a protein, in this case gelatine. Glycine is also similar to *gamma*-aminobutyric acid and glutamic acid in the ability to inhibit neurotransmitter signals in the central nervous system. It enhances the activity of chemical messengers (neurotransmitters) in the brain that are involved in memory and cognition.[336] It is present in considerable amounts in prostate fluid and has been reported to play a role in maintaining the health of the patients with benign prostatic hyperplasia (BPH).[337,338]

Aim of Thesis

Within the scope of available literature, in this work, there is no report on the analysis of glycine at metallophthalocyanine-modified electrodes. We aim at investigating the electrocatalytic property of manganese tetraamino phthalocyanine for the determination of glycine in this thesis.

1.5.2 Oxygen

The electrochemistry of oxygen is of major importance to energy conversion and storage and conservation. Oxygen-consuming cathodes are used in fuel cell systems and in metal-air batteries. Oxygen electroreduction is a multielectron reaction

and is suggested[339] to include a number of elementary steps forming various parallel-consecutive combinations (Scheme 1.10).

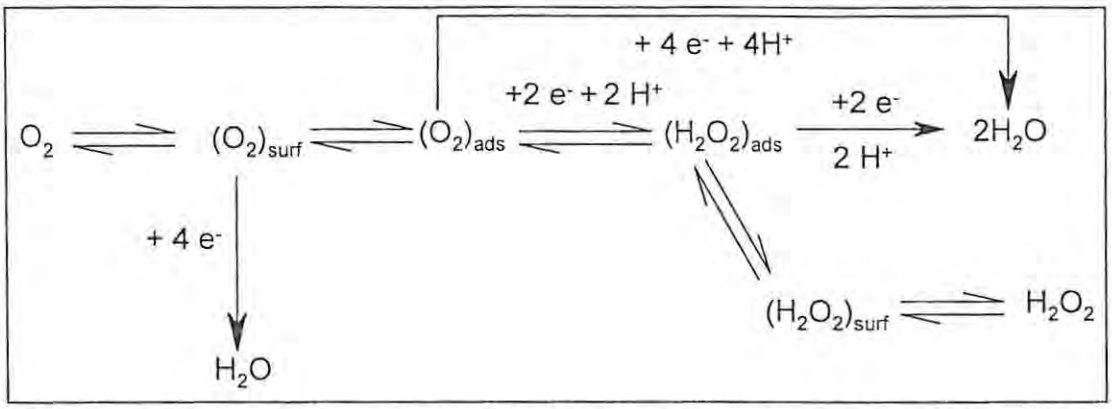

Scheme 1.10: A general scheme for the series (consecutive)-parallel reactions of O_2 and H_2O_2.

Where O_2, $(O_2)_{sur}$, and $(O_2)_{ads}$ correspond to the molecular O_2 in the bulk solution, in the solution adjacent to the electrode surface, and in the adsorbed state, respectively.

Many transition metal macrocyclic complexes have substantial catalytic activity for O_2 reduction.[340] Oxygen reduction has been studied on thin films of macrocyclic complexes attached on a carbon, graphite, or metal substrates.[287,288,305,341-344] In particular, Jasinski's[287,288] discovery that CoPc catalyses oxygen reduction at a potential close to that at platinum, provoked a large amount of interest in the possible application of MPcs in cathode reaction of fuel cells. The electrocatalytic reduction of O_2 on thin films is influenced by:

(a) *the ligand structure*: Phthalocynines,[342,345] tetraphenylporphyrins,[346] and dibenzotetraazoannulenes display different activity for oxygen electroreduction both in acid and in alkaline solutions. Alt and coworkers[345] showed that introduction of electron donors into the phenyl groups of cobalt tetraphenylporphyrin (CoTPP) decreases its activity (for O_2 reduction) in the series of OCH_3 > Phenyl > SCH_3 > H.

(**b**) *central metal ion*: With polymeric metallophthalocyanines, the use of electroactive central metals such as Mn, Fe and Co not only increases the possibility of the O_2 reduction to water but also accelerates the whole reduction process.[347] The dependence of the mechanism and kinetics on the nature of the central metal ion indicates that the metal is the active site where electrocatalysis occurs. Randin[340] reported a correlation of electrochemical activity for O_2 reduction with the first redox potential of MPc and the value of the magnetic moment of the MPc, implying that the local interaction rather than the collective one plays a major role with these metal organic complexes.

(**c**) *Electrolyte*: The effect of pH on the electro reduction of oxygen has been reported.[348] The reduction of oxygen in alkaline solution by cobalt tetrasulfonated phthalocyanine (CoTSPc), CoPc and cobalt tetraphenylporphyrin (CoTPP) modified electrodes have been shown to proceed in two stages (Equations 1.22 and 1.23) with the formation of a peroxide as intermediate.

$$(L\text{-}M) + O_2 \longrightarrow (L\text{-}M)\text{-}O_2 \qquad 1.22$$

$$(L\text{-}M)\text{-}O_2 + e^- \longrightarrow (L\text{-}M)\text{-}O_2^- \qquad 1.23$$

where L = Pc ligand and M = central metal

The behavior in acidic medium was different since the reduction occurred at less negative potentials. This was explained by the need for a simultaneous proton transfer as shown in equation 1.24.

$$(L\text{-}M)\text{-}O_2 + H_2 + e^- \longrightarrow (L\text{-}M)\text{-}O_2H \qquad 1.24$$

Manganese Schiff bases[347] and MPcs such as cobalt tetraaminophthalocyanine (CoTAPc),[348] cobalt tetrasufophthalocyanine (CoTSPc),[339] CoTSPc/polypyrrole

(CoTSPc-Ppy)[334] have been demonstrated to lower the reduction potential of oxygen. Table 1.5 shows the oxygen reduction potential on some modified electrodes. The reduction potential is generally closely related to the redox potentials of the central metal. For example the redox potential of Co^{II}/Co^{I} in poly-CoTAPc-GCE electrode, in pH 7, is reported at + 0.05 V which is very close to - 0.23 V related to the oxygen reduction potential on the same electrode. Similarly the table shows that the redox potential of the manganese central metal in Mn-salen (- 0.275 V) is very much associated with the potential (- 0.45 V) at which the oxygen reduction occurs on the electrode modified with this catalyst. The objective of this thesis is thus to extend the range of possible electrocatalysts for oxygen reduction using the newly synthesized MPc derivatives.

Table 1.5: Comparative peak potential for the electrocatalytic reduction of O_2 using some phthalocyanine related species.

MPc	$E_p(O_2)$(V vs. SCE)	Medium	$E_{1/2}$(MPc)/V vs. SCE
CoTAPc	- 0.23	pH 7	+ 0.05[348]
CoTSPc	~ - 0.42	0.05M H_2SO_4	not stated[339]
CoTSPc-PPy	- 0.15 (vs. RHE)	0.05M H_2SO_4	+ 0.05[334]
Mn-salen	~ - 0.45	CH_3CN	- 0.275[347]

RHE = Reversible hydrogen electrode

Aim of Thesis

This study focuses on the electrocatalytic activity of manganese phthalocyanines (MnPcs) complexes modified electrodes towards reduction of molecular oxygen. The interaction of molecular oxygen with the MnPcs in solution is also investigated. The report also includes attempts made towards activation of molecular oxygen using cobalt-tetra-{4-(pyrrol-1-yl)}phenoxyphthalocyanine

(CoTPhPyPc, 7) and chromium tetraamoniphthalocyanine (CrTAPc). This is the first time a CrTAPc-modified GCE is used for oxygen reduction.

1.5.3 Nitric Oxide and Nitrite

Nitric oxide is a highly reactive gas that participates in many chemical reactions. NO is synthesized within cells by an enzyme NO synthase (NOS) from arginine with the aid of molecular oxygen and nicotinamide adenine dinucleotide (NADPH).[349-351] NO diffuses freely across cell membranes[352,353] and it can interact with so many molecules, that it is quickly consumed close to where it is synthesized. Thus NO acts in a paracrine or even autocrine fashion — affecting only cells near its point of synthesis. NO has many physiological functions including smooth muscle relaxation,[275,354] inhibition of the aggregation of platelets,[276,355-357] inhibition of inflammation,[277,358,359] neurotransmission,[248,353,355,356] and antibacterial activity.[360-363]

Methods of detecting NO are often indirect in that the measurements are based on secondary species such nitrite and nitrate, after removal from biological systems. There is a growing interest in electrochemical sensors for direct analysis of NO in biological systems.[364-368] Electrochemical reduction or oxidation of NO has been achieved on metalloporphyrins and related metalloproteins modified electrodes with varying degrees of success in terms of reduction or oxidation potentials and detection limits.[368-372] NO binds axially with MPc complexes and the driving force for the catalytic activity of MPcs towards NO has been linked with the axial ligation and peripheral substitution on the MPc macrocycle.[373-376] Metallophthalocyanine complexes have been shown to lower the reduction and oxidation overpotentials (with increased current) for activation of NO.[377-380] Table 1.6 shows an abbreviated list of reduction or oxidation potentials of MPc complexes and their relation to the reduction

or oxidation potentials of NO, at the respective MPc modified electrodes. New MPc complexes which can lower the potentials further are desirable.

Table 1.6: Comparative peak potential and limit of detection (LoD) for the electrocatalysis of NO and NO_2^- using some phthalocyanine species.

MPc	E_p (NO) / V vs. SCE[a]	Medium/ LoD[b] (mol dm^{-3})	$E_{1/2}$(MPc) V vs. SCE
NO			
Oxidation			
$[CoTSPc]^{4-}$	+ 1.04[378]	pH 4 ($1x10^{-9}$)	+ 0.43 Co^{III}/Co^{II}
CoPc	+ 0.90[379]	pH 4	+ 0.80 Co^{III}/Co^{II}
CoPc	+ 0.67[372]	Blood serum	+ 0.80 Co^{III}/Co^{II}
FePc	+ 0.74[372]	pH 7.4	+ 0.38 Fe^{III}/Fe^{II}
NiTSPc	+ 0.70[380]	pH 7.4($1x10^{-6}$)	+ 0.40 Ni^{III}/Ni^{II}
NiTSPc	+ 0.75[381]	pH 7.4	+ 0.50 Ni^{III}/Ni^{II}
Reduction			
$[CoTSPc]^{4-}$	- 1.01[290]	pH 4 ($1x10^{-9}$)	- 0.50 Co^{II}/Co^{I}
$[CoTSPc]^{4-}$	- 1.15[290]	pH 7	- 0.50 Co^{II}/Co^{I}
CoPc	- 0.98[379]	DMSO/TEAP	- 0.37 Co^{II}/Co^{I}
CoPc	- 0.98[379]	pH 4	- 0.37 Co^{II}/Co^{I} –
H_2Pc	- 0.90[382]	pH 3	- 0.72 Pc^{-2}/Pc^{-3}
NO_2^-			
$[CoTSPc]^{4-}$	+ 0.93[378]	pH 7 ($2x10^{-7}$)	+ 0.75 Co^{III}/Co^{II}
CoPc	+ 0.87[273]	pH 7.3	+ 0.45 Co^{III}/Co^{II}

[a] References given as superscripts

[b] LoD given in brackets

Nitrites are a major constituent of fertilizers and have been used for many years in lawn treatments. Without the addition of nitrites, crops would deplete nitrogen from soil. Unfortunately, when nitrogen fertilizers are used, they can get into wells and contaminate them. Nitrites from fertilizers also seep into groundwater, especially shallow wells thereby creating cause for environmental concern.

Nitrites are a cause for concern in infants under 6 months of age and farm animals. They affect the blood's ability to carry oxygen. Nitrites get into the body when nitrates are ingested, both from food and water, and nitrate-reducing bacteria in an infant's digestive tract converts the nitrate to nitrite. Once the nitrite enters the blood stream and binds to the hemoglobin, oxygen cannot be carried, and "blue-baby" syndrome (bluish tint to skin due to lack of oxygen) occurs, as well as shortness of breath, increased sensitivity to illness, heart attacks, and possibly death by asphyxiation. However, as the infant ages, stomach acid becomes stronger, and bacteria that cause the conversion of nitrate to nitrite are reduced. Older children and adults generally do not have a problem with nitrites. Since the dawn of recorded human history, nitrites have been used to preserve meat from bacterial spoilage.

Most recorded methods for the determination of nitrite involve spectrophotometry with related complications and are time-consuming.[383-386] MPc and related complexes, such as porphyrins, hemoglobin and myoglobin have been used for determination of nitrites.[274,371,387-391] Table 1.6 shows the oxidation potential of nitrite at some MPc modified electrodes.

Aim of Thesis

CrPc complexes have not been employed in electrocatalysis of NO and nitrites. This work aims at investigating the electrocatalytic activities of

electropolymerized chromium tetraaminophtalocyanine (CrTAPc) as catalyst for the oxidative determination of NO and nitrite. Thus extending the use of MPc type catalysts to the electrooxidation of NO and nitrite.

1.5.4 Phenols and Chlorinated Phenols

Chlorophenols and phenols are introduced in the environment, through their use as biocides or as by-products of other industrial operations, such as pulp bleaching with chlorine and waste incineration. Chlorophenols and phenols have also been used as general purpose disinfectants, and it has been found that they can also appear as degradation products of other chlorinated xenobiotics.[392]

Chlorophenols, with at least two chlorine atoms, either have been used directly as pesticides or converted into pesticides. Also, chlorophenols, especially 4-chlorophenol, have been used as antiseptics. Phenols and chlorophenols accumulate in the environment (soil and water) as incalcitrant contaminants and this is of concern to the environmental scientists.[393,394] They constitute a major class of organic pollutants that contaminate the ecosystem and accumulate in the food chain.[395] Several chlorinated phenols such as 2-chlorophenol, 2,4-dichlorophenol, 2,4,6-trichlorophenol, and pentachlorophenol have been classified as priority pollutants.[394]

Monitoring and detection of chlorophenols are of particular importance in environmental control and food analysis for the investigation of human and animal exposure. The electrooxidation of chlorophenols on glassy carbon electrodes modified with nickel based cyclam, porphyrin and tetrasulfonated phthalocyanine has been reported.[83,396-398] The electrode modification was found to minimize fouling of the electrode by the oxidation product.

Aim of Thesis

As has been mentioned above, Ni(II) macro cycles have been shown to be good electrocatalysts for the oxidation of phenols and chlorophenols.[396-398] However, the electrooxidation products easily foul electrodes within a short time. Electropolymerizable pyrrole substituted nickel phthalocyanine has been synthesized in this study. The thesis will look at the potential application of the newly synthesized complex for the electrocatalytic oxidation of phenol and its derivatives with the aim of reducing electrode fouling by the oxidation products.

1.6 Summary of Aims of Thesis

The overall aims of this thesis are as follows:

- To synthesize and characterize pyrrole, thiophene, mercaptopyrimidin and amino substituted metallophthalocyanines namely: metal-tetra-4-(pyrrol-1-yl)phenoxy phthalocyanine (MTPhPyPc), metal-tetra-{2-(2-thienyl)ethoxy}phthalocyanine (MTETPc), metal-tetra-(2-mercapto)pyridinphthalocyanine (MTMPyrPc) and metal-tetraaminophthalocyanine (MTAPc) (Fig 1.18. The complexes will be characterized using spectroscopic, electrochemical and spectroelectrochemical techniques. These molecules are chosen since they should be electropolymerizable.
- To prepare metallophthalocyanine modified electrodes (by electropolymerization, drop-dry and self-assembly (SAM)) and characterise them using electrochemical techniques.
- To investigate the electrocatalytic properties of the MPcs (shown in Fig 1.18 modified electrodes toward detection of some biological and

environmentally important molecules. The catalytic properties of chosen MPc complexes (Fig 1.18) toward L-cysteine, glycine, nitric oxide nitrite, oxygen and phenol and its derivatives will be investigated.

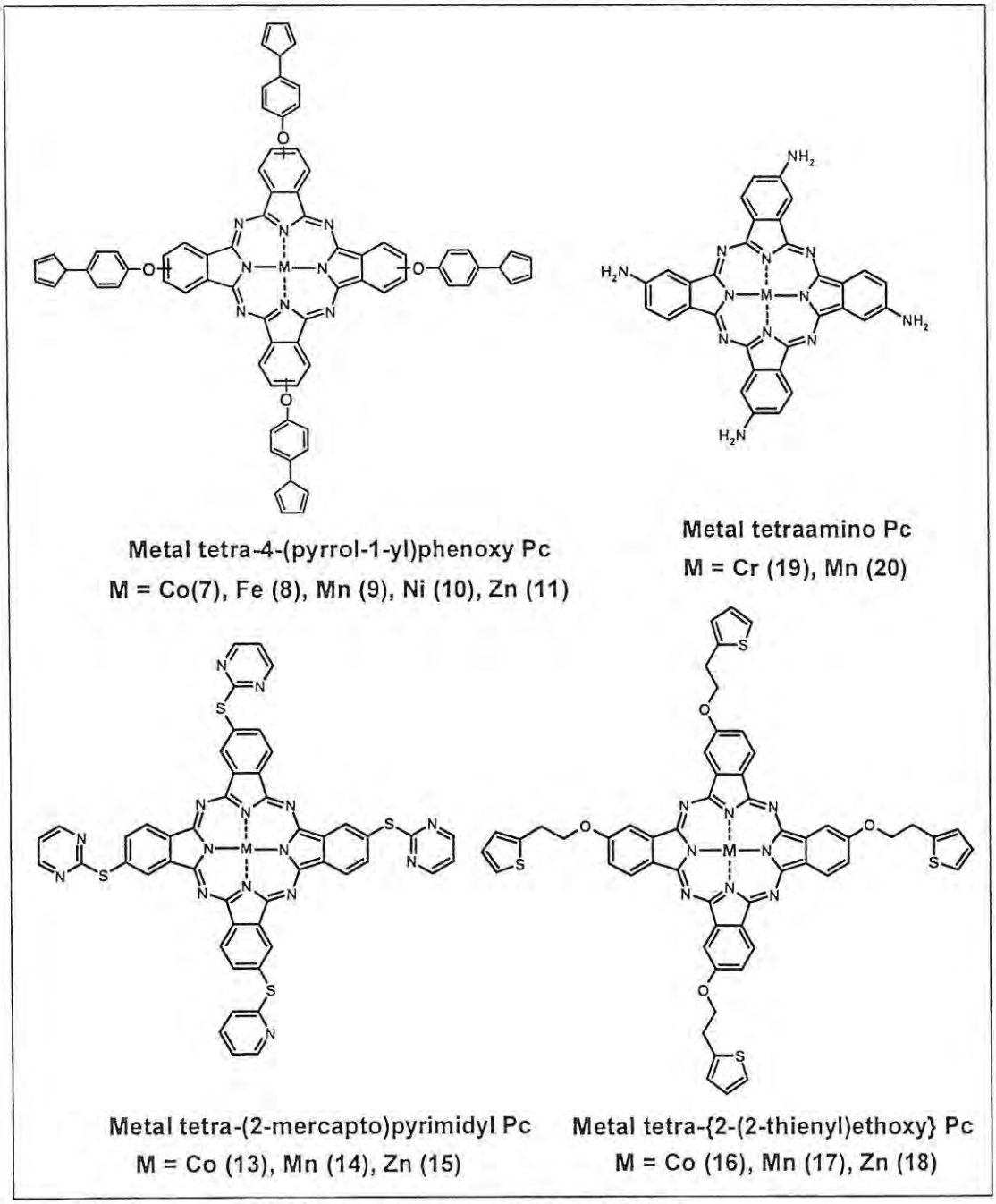

Fig 1.18: Structure of MPc complexes studied in this thesis

Chapter Two

Experimental

This chapter describes the general experimental procedures employed in this work. The synthetic route adopted to obtain the metallophthalocyanine complexes studied in this work is presented. The synthesis of a series of N-pyrrole substituted phthalocyanines in which either a phenoxy group or a pentoxy group separates the pyrrole ring from the phthalocyanine is described. The complexes are denoted: MTPhPyPc (**7-11,** for phenoxy link Pc) and CoTPOPyPc (**12,** for pentoxy linked Pc), where M is the respective metal cation. Also the first report of the synthesis of a mercaptopyrimidin (denoted: MTMPyrPc, **13-15**) and thiophene (denoted: MTETPc, **16-18**) substituted MPcs is presented. The syntheses of chromium and manganese tetraaminophthalocyanine complexes (CrTAPc, **19,** and MnTAPc, **20**) are also described here.

2.1 Solvents

N N dimethyl formamide (DMF), dimethylsulfoxide (DMSO), dichlororomethane (DCM), tertrahydrofuran (THF), diethyl ether, methanol, ethanol, acetone, DMSO-d_6 and $CDCl_3$ were purchased from SAARCHEM (Pty) Ltd (South Africa). DMF, DCM and DMSO were freshly distilled before use. THF was distilled and dried over molecular sieves. 1--entanol was obtained from Aldrich. Deionized water was collected from Milli-Q Millipore water purification system and used to prepare all buffered solutions.

2.2 Reagents

Phthalimide, L-cysteine, tetrabutylammonuim tetrafluorobarate ($TBABF_4$), 4-(*1-H*-pyrrol-1-yl)phenol, 2-mercaptopyrimidin, zinc acetate and thionyl chloride were used as received from Aldrich. 2-Thienyl-2-ethanol was obtained from Fluka and used as received. Phenol, 4-chlorophenol (4-CP), 4-nitrophenol and sodium nitrite were obtained from BDH. Glycine, potassium carbonate, manganous chloride ($MnCl_2$), chromium chloride, nickel acetate, ferric acetate, cobalt acetate, sodium hydroxide, hydrochloric acid, nitric acid and sulphuric acid were purchased from SAARCHEM (South Africa). Tetraethylammonium perchlorate (TEAP) was recrystallized from ethanol. All other chemicals and reagents were of analytical grade and were used as received. Phosphate and acetate buffer tablets and powders were obtained form SAARCHEM (South Africa).

2.3 Instrumentation

UV-Visible spectra were recorded on either Varian 500 UV-Vis/NIR or Cary 1E spectrophotometer. IR spectra (KBr pellets) were recorded on a Perkin-Elmer spectrum 2000 Fourier Transform Infrared (FTIR) spectrometer. ^{1}H-nuclear magnetic resonance (^{1}H-NMR, 400MHz) spectra were obtained in $CDCl_3$ or DMSO-d_6 using Bruker EMX 400 NMR spectrometer. Adsorption column chromatography was performed using silica gel 60 (0.040-0.063 mm) obtained from Merck. Elemental analyses were performed with a Carlo Erba NA 1500 Nitrogen analyzer at the University of the Western Cape, Cape Town, South Africa. MALDI-TOF spectra were collected with Perseptive Biosystems Voyager DE-PRO Biospectrometry Workstation with Delayed Extraction Technology. In some cases Finnigan LCQ-MS electron spray ionization mass spectra was employed for analysis of starting phthalonitrile. Scanning electron micrographs were obtained using JOEL JSM 840 scanning electron microscope. A WTW pH meter was used for pH measurements.

2.4 Synthesis

2.4.1 4-Nitrophthalonitrile (37) (Scheme 1.6)[225]

4-Nitrophthalonitrile (**37**) was synthesized according to reported procedure[225] starting from phthalimide **(24)**. The synthesis is as shown in Scheme 1.7 (Chapter One) and was used as the starting reagent for the synthesis of other substituted phthalonitriles.

4-nitrophthalimde (35)

Fuming HNO_3 (30 mL) was slowly added to 180 mL of H_2SO_4. The mixture was allowed to cool, to ~ 12 °C, in an ice bath. Phthalimide **(24)**, 50.0 g (0.3 mol) was added to the acid mixture while stirring as quickly as possible and maintaining the temperature between 10 °C and 15 °C in an ice bath. The solution was allowed to stand overnight at room temperature. The resulting yellow product was poured on ice (~ 1.2 kg) while rapidly stirring the solution to yield a beige suspension which was isolated by filtration under reduced pressure. The solid was washed six times with 150 mL ice water to afford the 4-nitrophthalimide **35**. Yield: 42%. ^{1}HNMR $CDCl_3$: δ (ppm): 8.71(d, 1H, Ar-H); 7.94(s, 1H, N-H); 8.10(d, 1H, Ar-H); 8.70(dd, 1H, Ar-H). IR (KBr) v/cm^{-1}: 1781 (s), 1720 (s) (CO-NH-CO), 1535 (vs) (NO_2 assym.), 1350 (vs) (NO_2 sym.).

4-nitrophthalamide (36)

4-Nitrophthalimide **(35)** (20 g, 0.1 mol), was stirred in 300 mL of 25% ammonia solution for 24 hours before another 100 mL 25% ammonia solution was added. The stirring was continued for another 24 hours and the resulting yellowish product was filtered off under reduced pressure and washed 4 times with 200 mL of water. The solid product, 4-nitrophthalamide **(36)** was dried in the oven at 100 °C. Yield: 85%. ^{1}HNMR $CDCl_3$: δ (ppm): 8.10 (d, 1H, Ar-H); 8.26 (dd, 1H, Ar-H); 8.42(d, 1H, Ar-H). IR (KBr) v/cm^{-1}: 3343 (NH_2 str), 1680 (s) (C=O str), 1615 (vs) (NH_2 def.).

4-nitrophthalonitrile (37)

Freshly distilled thionyl chloride, 25 mL (0.035 mol) was added, while stirring at 0 °C, to 100 mL of dry dimethylfomamide (DMF) in a nitrogen atmosphere. The stirring was continued for 2 hours and then 8.5 g (0.04 mol) of **36** was added to the mixture while stirring. The mixture was stirred for 5 hours at 0 °C and then at room temperature overnight. The product was poured into 300 mL of ice water, filtered under reduced pressure and washed 6 times with 80 mL of water. The product was recrystallized twice from methanol to yield yellow 4-nitrophthalonitrile **(37)**. Yield: 70%. ^{1}HNMR $CDCl_3$: δ (ppm): 8.10 (d, 1H, Ar-H); 8.60 (dd, 1H, Ar-H); 8.72(d, 1H, Ar-H). IR (KBr) v/cm^{-1}: 2230 (s) (C≡N) 1540 (vs) (NO_2 assym.), 1360 (vs) (NO_2 sym.).

2.4.2 5-(Pyrrol-1-yl)pentan-1-ol (40), (Scheme 3.1)[399]

This molecule was used for the formation of pentoxy pyrrole substituted phthalonitrile. The N-pyrrole substituted pentan-1-ol was synthesized according the procedure reported for the synthesis of the ethanol analogue.[399] 5-Aminopentanol (50 g, 0.817 mol) was added to 100 mL of glacial acetic acid (while stirring) then cooled in an ice bath containing sodium chloride (NaCl), in such a way that temperature of the solution was kept below 20 °C since the reaction is exothermic. One portion of 25 g (0.19 mol) of 2,5-dimethoxytetahydrofuran (**39**) was then added to the solution while stirring and left to stand for 10 minutes. The acetic acid was distilled off under reduced pressure and the residue was treated with 200 mL of water. The product was extracted five times from water with dichloromethane (DCM). The extracted organic solution was treated, three times, with a saturated aqueous solution of sodium sulfate followed by

distilling off of the DCM. The residue was stirred overnight with a mixture of 30 mL methanol and 30 mL 20% aqueous solution of NaCl. Then the mixture was saturated with NaCl while stirring and left to stand for 30 minutes. The mixture was then transferred into a separating funnel and the organic product was extracted with DCM. Since traces of water will be present in the DCM extract the product was dried with calcium chloride. Finally, the DCM was distilled off under reduced pressure. Yield: 30%. IR (KBr) ν/cm^{-1}: 3097, 2939, 1655, 1503, 1430, 1280, 1087, 1070, 982, 866, 730. ^{1}HNMR d-DMSO; δ (ppm): 3.2 (d, 1H, pyrrole); 4.0-3.6 (m, 10H, pentane); 6.30(t, 2H, pyrolle); 6.91(t, 2H, pyrrole).

2.4.3 Synthesis of substituted phthalonitriles (Scheme 3.2)

All the functionalized phthalonitriles used for the preparation of the phthalocyanine complexes were synthesized via the nucleophilic aromatic substitution (S_NAr) reaction of 4-nitrophthalonitrile as described below using the desired substituting reagent. The synthetic route is summarized in Scheme 3.2.

2.4.3.1 4-(pyrrol-1-yl)phenoxy phthalonitrile (42)[399]

4-(Pyrrol-1-yl)phenoxy phthalonitrile (**42**) was synthesized by following literature[399] reports for similar complexes: 4-(pyrrol-1-yl)phenol (**41**) (0.3 g, 1.9 mmol) and 0.27 g (1.56 mmol) of 4-nitrophthalonitrile (**37**) were added to 0.6 g dry K_2CO_3 in 15 mL dry DMSO. The mixture was stirred under nitrogen for 48 hrs at room temperature. The precipitated product was washed with cold water (four times) and finally with methanol (two times). The resulting solid (**42**) was dried in the oven at 50°C. IR (KBr)

v/cm^{-1}: 3442, 3106, 3063, 2229 (C≡N), 1598, 1516, 1486, 1244(C-O-C), 1205, 1076, 840, 727. ^{1}HNMR d-DMSO; δ (ppm): 6.29(s, 2H); 7.30(d, 2H); 7.38(d, 2H); 7.44(m, 1H); 7.50(d, 2H); 7.85(d, 1H); 8.10(d, 1H).

2.4.3.2 5-(pyrrol-1-yl)pentoxy phthalonitrile (43)[399]

5-(Pyrrol-1-yl)pentoxy phthalonitrile (**43**) was synthesized by following literature[399] reports for similar complexes: 5-(pyrrol-1-yl)pentan-1-ol **(40)** (0.3 g, 1.9 mmol) and 0.27 g (1.56 mmol) of 4-nitrophthalonitrile (**37**) were added to 0.6 g dry K_2CO_3 in 15 mLdry DMSO. The mixture was stirred under nitrogen for 48 hrs at room temperature. The product was poured into 100 mL of 0.1 M HCl solution to afford a yellowish-brown precipitate. The precipitated product was washed with cold water (four times) and finally with methanol (two times). The resulting solid (**43**) was dried in the oven at 50 °C. IR (KBr) v/cm^{-1}: 3442, 3106, 3063, 2229 (C≡N), 1598, 1516, 1486, 1244 (C-O-C), 1205, 1076, 840, 727. ^{1}HNMR d-DMSO; δ (ppm): 6.29(s, 2H), 7.30(d, 2H); 7.38(d, 2H); 7.44(m, 1H); 7.50(d, 2H); 7.85(d, 1H); 8.10(d, 1H).

2.4.3.3 4-{2-(2-thienyl)ethoxy}phthalonitrile (45)

Complex **45** was synthesized by stirring a mixture of 4-nitrophthalonitrile **(37)** (0.4 g, 2.3 mmol), 2-(2-thienyl)ethanol **(44)** (1.5 mL, 10 mmol) and dry K_2CO_3 (0.8 g, 5.8 mmol) in 20mL dry DMSO under nitrogen atmosphere at room temperature (RT) for two days. Another portion of dry K_2CO_3 (0.6 g, 4.3 mmol) was added after 2 days and the mixture was stirred under nitrogen for another 5 days at RT. The product was precipitated out of solution by neutralizing the solution using 0.1 M HCl to yield a

greenish gelatinous precipitate. The precipitated product was finally washed twice with distilled water and recrystalized from acetone. The resulting green solid was dried over P_2O_5 in a desiccator. Yield: 73%. IR (KBr disk) λ_{max}/cm^{-1}: 3460, 3099, 2228, 1561, 1486, 1471, 1406, 1308, 1250 (C-O-C), 1097, 1019, 850, 712, 522. ^1H NMR /ppm: 4.37 (t, 2H); 6.96 (m, 2H); 7.35 (d, 2H); 7.47 (m, 1H); 7.80 (d, 1H); 8.02 (d, 2H). Electron spray mass spectra: Calc: 254.31m/z. Found: 254.30.

2.4.3.4 4-(2-mercapto)pyrimidinphthalonitrile (47)

2-mercaptopyrimidin (**46**) (4 g, 35.7 mmol), 3.8 g (21.85 mmol) of 4-nitrophthalonitrile **(37)** and 5.5 g (39.86 mmol) of dried potassium carbonate were added to 37 mL dry DMSO under dry, inert gas (N_2). The mixture was stirred for 24 hrs at RT and another 4 g (30 mmol) of K_2CO_3 was added. The mixture was stirred for another 6 days at RT. Ice water (400 mL) was added and pH was adjusted to 7. The precipitated product was thoroughly washed with distilled water and twice with cold methanol. The product was finally recrystalized from methanol and dried in vacuum for 3 days. The purity of the product **(47)** was confirmed by thin layer chromatography, (TLC), and NMR. Yield: 82%. IR (KBr) ν\cm^{-1}: 3441, 3093, 3030, 2372 (S-C), 2229 (C≡N), 1554, 1478, 1382, 1176, 834, 804, 759, 523. ^{1}H-NMR/ppm: 7.36 (t, 1H); 8.12 (d, 2H); 8.48 (s, 1H); 8.71 (d, 2H).

2.5 Synthesis of Phthalocyanines

2.5.1 Synthesis of Pyrrole Substituted Phthalocyanine Complexes (Scheme 3.3)

2.5.1.1 Tetra-4-(pyrrol-1-yl)phenoxy phthalocyanines (Scheme 3.3)[399]

A procedure similar to that reported[399] for the synthesis of tetrakis(3-pyrrol-1-yl)propoxy) phthalocyanine was adopted for the preparation of (H_2TPhPyPc) **(48)**. A solution of 0.15 g (0.6 mmol) of **42** in 5 mL dry pentanol/DMSO (4:1) was refluxed for 20 minutes in the presence of nitrogen. Lithium (4 mg, 0.57 mmol) was added to the refluxing solution. The solution immediately turned blue-green on addition of lithium metal. Refluxing was continued for another 1 hour. The UV-Visible spectrum of the refluxing solution was recorded at different time intervals to monitor the formation of the characteristic Q-band of phthalocyanine ring (Pc). The pentanol was removed by blowing out with nitrogen while the heating continued. The product was transferred into 10mL of water and the pH adjusted to 5 using dilute HCl. The product was then filtered and the unreacted phthalonitrile was removed by Soxhlet extraction with methanol. The purity of the Pc was checked using thin layer chromatography (TLC). TLC revealed two different spots (impurities) that were removed using diethylether and chloroform. The Pc complex **48** was eluted with tetrahydrofuran (THF).

H_2TPhPyPc **(48):** Yield: 50%. IR (KBr) ν/cm^{-1}: 3430, 3300, 2922, 2853, 1612, 1513, 1467, 1328, 1230 (C-O-C), 1093, 1011, 923, 801, 725. ^{1}HNMR d-DMSO; δ (ppm): 6.30 (d, 8H, pyrolle); 7.40 (d, 8H, pyrrole); 7.5-7.9 (m, 16H, phenoxy); 8.61 (s, 4H, Pc);

9.12 (s, 8H, Pc). UV-Vis (DMF), λ_{max}/nm (log ε): 344 (4.50), 609 (4.41), 637 (4.45), 670 (4.95), 700 (4.69).

Cobalt-tetra-4-(pyrrol-1-yl)phenoxy phthalocyanine **(CoTPhPyPc) (7).**

Cobalt (II) acetate (0.027 g, 0.023 mmol) was added to a solution of 0.03 g (0.026 mmol) of the unmetallated phthalocyanine (**48**) in pentanol and stirred under reflux for 90 minutes. The pentanol was removed by bubbling nitrogen and the residue was treated with a 1:1 mixture of water-methanol to remove unreacted acetate. The product was washed three times with methanol. The purity of the product was confirmed using TLC.

CoTPhPyPc **(7):** Yield: 21 %. IR (KBr disk) v/cm^{-1}: 2923, 2852, 1606, 1515, 1462, 1236 (C-O-C), 1096, 835, 724. UV-Visible (DMF) λ_{max}/nm (log ε) (DMF): 328 (3.67), 603 (1.47), 665 (4.88). MS (FAB): m/z 1200 (M +1). Calculated: 1199 gmol^{-1}.

Iron (FeTPhPyPc) (8,) Manganese (ClMnTPhPyPc) (9), Nickel (NiTPhPyPc) (10) and Zinc (ZnTPhPyPc) (11) Tetra-4-(pyrrol-1-yl)phenoxy) phthalocyanine Complexes **(Scheme 3.3)**

These compounds were prepared using a similar procedure as for CoTPhPyPc, using ferric acetate, manganous chloride, nickel acetate and zinc acetate, respectively, instead of cobalt acetate. Same amounts (in moles) of reagents were used as for the cobalt complex.

FeTPhPyPc **(8):** Yield: 35 %. IR (KBr disk) v/cm^{-1}: 3436, 2955, 2922, 2859, 1610, 1510, 1472, 1233 (C-O-C), 1077, 831, 726. UV-Visible (DMF) λ_{max}/nm (log ε) (DMF): 327 (6.36), 457 (1.85), 628 (4.38), 701 (3.12).

(Cl)Mn^{III}TPhPyPc **(9):** Yield: 20 %. IR (KBr disk) v/cm^{-1}: 3437, 2944, 2859, 1606, 1514, 1468, 1234 (C-O-C), 1071, 808, 720, 285 (Mn^{III}-Cl). UV-Visible (DMF) λ_{max}/nm (log ε) (DMF): 380 (2.57), 497(0.84), 649 (0.95), 720 (4.80).

NiTPhPyPc **(10):** Yield: 20 %. IR (KBr disk) v/cm^{-1}: 3423, 2958, 2923, 2845, 1609, 1514, 1461, 1236 (C-O-C), 1096, 808, 720. UV UV-Visible (DMF) λ_{max}/nm (log ε) (DMF): 329 (4.43), 621 (5.06), 671 (4.45).

ZnTPhPyPc **(11):** Yield: 20 %. IR (KBr disk) v/cm^{-1}: 3433, 2924, 2845, 1609, 1511, 1478, 1232 (C-O-C), 1090, 833, 728. UV UV-Visible (DMF) λ_{max}/nm (log ε) (DMF): 352 (2.27), 609 (4.55), 678 (5.04).

2.5.1.2 Tetra-5-(pyrrol-1-yl)pentoxyphthalocyanine Complexes[399] (Scheme 3.3)

The synthesis of H_2TPOPyPc was achieved by dissolving 1.2 g (4.30 mmol) of 5-(pyrrol-1-yl)pentoxyphthalonitrile **(43)** in 15 mL dry pentanol and stirring under reflux for 15 mins. Following this, 10 mg lithium was added to the stirring mixture while stirring and the solution turned green immediately. UV-Visible spectra of the product were used to monitor the formation of the Pc. After 1hr, the product was allowed to cool to room temperature and methanol was added to the solution to afford the product. The solid product was treated in a Soxhlet extractor with methanol, for 24 hrs, to remove unreacted phthalonitrile. After this treatment, the product was found to be predominantly metal free Pc (**49**). No further purification was done. The metal free Pc (hereinafter referred to as H_2TPOPyPc **(49)**), was used for the synthesis cobalt derivative. The CoTPOPyPc **(12)** was obtained by reaction of 0.4 g (0.36 mmol) H_2TPOPyPc with 0.027

g (0.023 mmol) of cobalt acetate in dry DMSO under reflux for 1 hr. The solution was transferred into distilled water to precipitate out the solid CoTPOPyPc **(12)**. Finally, the product was purified by column chromatography using dichloromethane as eluting solvent. The purity of **12** was confirmed by thin layer chromatography. The characterization of the products gave satisfactory results.

H_2TPOPyPc (**49**): Yield: 60%. IR (KBr) v/cm^{-1}: 3280, 3097, 2930, 2865, 1615, 1487, 1235 (C-O-C), 1090, 940, 826, 721. UV-Visible (DMF) λ_{max}/nm (log ε) (DMF): 330 (4.48), 635 (4.01), 670 (4.65), 700 (4.65). ^{1}HNMR d-DMSO; δ (ppm): 6.19(d, 8H, pyrolle); 7.32(d, 8H, pyrrole); 8.41(s, 4H, Pc); 9.00(s, 8H, Pc);.

CoTPOPyPc **(12):** Yield: 92%. IR (KBr) v/cm^{-1}: 3330, 3080, 2935, 2880, 1610, 1490, 1235 (C-O-C), 1190, 1088, 960, 723. UV-Visible (DCM) λ_{max}/nm: 675, 615, 375, 323, 290. UV-Visible (DMF) λ_{max}/nm (Log ε) (DMF): 670 (4.40), 615 (1.95). Elemental analysis $C_{68}H_{68}CoN_{12}O_4$ (1175 gmol^{-1}): Calculated: C, 69.63%; H, 5.83%; N, 14.29%. Found: C, 68.7%; H, 5.64%; N, 13.56%.

2.5.2 Synthesis of Thiophene Substituted Phthalocyanine Complexes (Scheme 3.4)

Cobalt tetra-{2-(2-thienyl)ethoxy}phthalocyanine, (CoTETPc), (16)

Complex **45** (0.06 g, 0.24 mmol) was added to 10 mL of dry pentanol and stirred for 15 minutes. Lithium metal (15 mg, 2.14 mmol) was added to the solution while stirring then the solution was left to reflux for 30 mins. The solution turned deep green as soon as Li metal was added (possibly forming Li_2Pc). Cobalt acetate (0.035 g, 0.03

mmol) was then added to the solution and stirred for one hour. The solution turned deep blue within 10 minutes upon addition of the cobalt salt. The complete conversion of the Li_2Pc to the corresponding cobalt complex was monitored by the UV-Visible spectra obtained in the DMF solution of the complex by checking the disappearance of the Q-band due to Li_2Pc and the formation of the Q band of the cobalt complex. The reaction mixture was allowed to cool to room temperature and then poured into distilled methanol to precipitate out the CoTETPc. The product was subjected to Soxhlet extraction (using methanol) overnight to remove unreacted phthalonitrile and cobalt acetate. CoTETPc was purified by using column chromatography and THF as elution solvent and silica gel 60 (0.040-0.063 mm) as the stationary phase. The column was first eluted using DCM to remove some yellowish substance that had higher retention factor (R_f) values than the CoTETPc in DCM but eluted at the same rate as the CoTETPc in THF. The purity of the product was confirmed using TLC.

CoTETPc **(16):** Yield: 47%. IR (KBr disk) ν/cm^{-1}: 3417, 1610, 1482, 1390, 1338, 1235, 1080, 1040, 826, 695, 620. UV-Visible (DMF) λ_{max}/nm (log ε) (DMF): 333 (4.67), 603 (4.45), 673 (4.96). Elemental analysis ($C_{55}H_{40}CoN_8O_4S_4$); Expected %: C: 62.50; N: 10.41; H: 3.75. Found %: C: 61.63; N: 10.95; H: 3.70.

For the preparation of Mn and Zn-containing phthalocyanine complexes, the same procedure used for the synthesis of the cobalt complex was adopted, except that $MnCl_2$ and Zn acetate were employed for $(Cl)Mn^{III}$TETPc **(17)** and ZnTETPc **(18)** formation instead of cobalt acetate employed for CoTETPc. The same mole ratio used for CoTETPc described above was used for the respective metal salts.

(Cl)Mn^{III}TETPc **(17):** Yield: 40%. IR (KBr) ν/cm^{-1}: 3410, 1612, 1489, 1387, 1340, 1235, 1080, 1041, 826, 700, 625, 287. UV-Visible (DMF) λ_{max}/nm (log ε) (DMF):368 (4.5), 500 (4.0), 667 (3.3), 723 (4.7). MALDI-TOF: $C_{55}H_{40}MnN_8O_4S_4Cl$. Calc. for [(Cl)MnTETPc - Cl]$^+$: 1072.2 m/z, found (m/z) = 1072.1.

ZnTETPc **(18):** Yield: 40%. IR (KBr) ν/cm^{-1}: 3416, 1610, 1482, 1386, 1333, 1232, 1081, 1043, 823, 694, 620. UV-Visible (DMF) λ_{max}/nm (log ε) (DMF): 353 (4.1), 610 (4.5), 676 (5.1). ^{1}H NMR (DMSO-d_6) /ppm: 3.72 (m 8H, ethylene), 4.51 (d, 8H, ethylene), 7.15 (s, 4H, Pc), 7.25 (d, 4H, thiophene), 7.63 (m, 8H, thiophene), 8.51 (t, 4H, Pc), 8.92 (d, 4H, Pc). Elemental analysis ($C_{55}H_{40}ZnN_8O_4S_4$ = 1082.62 g mol^{-1}), Expected %: C: 62.13; N: 10.35; H: 3.72. Found %: C: 61.52; N: 11.01; H: 3.56.

2.5.3 Synthesis of Pyrimidin Substituted Phthalocyanine Complexes (Scheme 3.4)

2.5.3.1 Cobalt tetra-(2-mercapto)pyrimidylphthalocyanine (CoTMPyrPc) (13), Scheme 3.4, route (a and b).

Two different approaches were followed to obtain **13**. Firstly (route a) 0.3 g (0.31 mmol) of **47** was dissolved in 15 mL dry DMF. Cobalt acetate (0.07 g, 0.06 mmol) was added to the solution and refluxed in the presence of DBU for 5 hours under inert atmosphere. The reaction mixture was allowed to cool and 100 mL distilled water was added to yield a precipitate of the crude CoTMPyrPc. The solid product was isolated and washed with water 5 times and then treated in a Soxhlet extraction apparatus with

methanol to remove unreacted phthalonitrile and cobalt acetate. Finally the product was purified by column chromatography using distilled THF as the eluting solvent. The product was dried in vacuum over P_2O_5. The product gave the same results as those prepared following the second approach described next.

Alternatively, (route b), 0.3 g (0.31 mmol) of **47** was added to dry 15 mL of pentanol and reflux for 45 mins. Lithium metal (5 mg, 0.71 mmol) was added after 15 mins of refluxing. The colour of the reacting mixture turned green upon addition of Li metal. Cobalt acetate (0.07 g, 0.06 mmol) was added and the mixture refluxed for 1 hr. The complete conversion to CoTMPyPc was monitored using the UV-Visible spectrum for the formation of CoTPhPyPc at 665 nm and disappearance of absorption band due to Li_2Pc at 685 nm. The product was allowed to cool to room temperature and 50 mL methanol was added to precipitate out the CoTMPyrPc. The product was then purified following the procedure described for route (a) above. Route (b) was used for synthesizing the other metal Pcs since it was less time consuming and the reaction conditions were milder than the former, which required higher temperatures and longer heating time. Also it should be noted that the yield was higher for route (b). In both cases, the purity of the CoTMPyPc (**13**) was confirmed by TLC.

CoTMPyrPc **(13)** Yield: 40%, IR (KBr) ν/cm^{-1}: 2931, 2863, 2377, 1549, 1374, 1306, 1184, 1091, 920, 758. UV-Visible (DMF) λ_{max}/nm (log ε) (DMF): 668 (5.06), 603 (4.54), 333 (4.93). Elemental analysis: $C_{48}H_{24}CoN_{16}S_4$ **(13)** (1175 $gmol^{-1}$): Cald: C, 56.97%; H, 2.39%; N, 22.14%. Found: C, 56.23%; H, 2.40%; N, 21.85%.

2.5.3.2 *Synthesis of the other metal containing tetramercaptopyrimidyl-phthalocyanines (Metal-TMPyrPc).*

A method similar to route b (Scheme 3.4) was followed, with a slight modification. A solution of 0.3 g (0.31 mmol) of **47** in dry DMF was heated under reflux for 15 mins. Li metal (5 mg, 0.71 mmol) was added and the reacting mixture was refluxed for another 30 mins. Metal salt (zinc acetate or manganous chloride, ~ 0.06 mmol) was added and the mixture was stirred under reflux for one hour. After cooling, the product was poured into a beaker containing 60 mL methanol. The precipitated MPcs were centrifuged and treated with Soxhlet extraction using methanol for 24 hrs. The products were finally purified by column chromatography using THF as eluting solvent. The purity of the various MPcs was confirmed by TLC. The products were dried in vacuum over P_2O_5.

MnTMPyrPc **(14):** Yield, 50%. IR (KBr) ν\cm^{-1}: 3437, 2928, 2855, 2368, 1555, 1379, 1318, 1177, 1059, 620. UV-Visible (DMF) λ_{max}/nm (log ε) (DMF): 720 (4.62), 626 (4.40), 500 (3.75), 350 (4.43). Mixture of complexes hence no elemental analysis was done (see Chapter Three).

ZnTMPyrPc **(15):** Yield, 55%. IR (KBr) ν\cm^{-1}: 3437, 2931, 2863, 2374, 1641, 1556, 1377, 1185, 1082, 895, 750. UV-Visible (DMF) λ_{max}/nm (log ε) (DMF): 678 (5.35), 615 (4.64), 356 (4.9). ^{1}H NMR: 7.36 (t,8H), 7.95 (d,4H), 8.29 (s,4H), 8.72 (s, 8H). Elemental analysis: $C_{48}H_{24}ZnN_{16}S_4$ (1175 gmol^{-1}): Calculated: C, 56.61%; H, 2.38%; N, 22.00%. Found: C, 55.67%; H, 2.12%; N, 23.00%.

2.5.4 Chromium {(OH)CrTAPc} (19) and Manganese {(OH)MnTAPc} (20) Tetraaminophthalocyanine[400] (Scheme 3.5)

Complexes, **19** and **20,** were made by first synthesizing chromium tetranitrophthalocyanine (**50**) and manganese tetranitrophthalocyanine (**51**) and then converting them to desired MTAPc species. 4-Nitrophthalimide **(35)** (2.0 g, 0.01 mol), 0.0025 mol metal chloride, 0.04 g (0.4 mmol) ammonium molybdate and excess urea (about 3 g, 0.05 mol) were finely ground together and added to a round bottom flask containing 10 mL nitrobenzene. The mixtures were heated under reflux for 5 hours between 180-190 °C. The solid products were filtered and washed with methanol and then transferred into a thimble. The products were subjected to Soxhlet extraction overnight using methanol to remove the remaining nitrobenzene. The resulting deep green solids were treated with 1 M HCl (30 mL) saturated with sodium chloride (NaCl) by boiling for 5 minutes. The solid products were isolated by centrifuge and transferred into a beaker containing 1 M NaOH saturated with NaCl. The mixtures were heated at 90 °C for 30 minutes and isolated, after cooling, by centrifuge. The isolated products were treated two times (each), with 1.0 M HCl and NaOH. The resulting dark solids (**50** and **51**) were washed with water until free from NaOH and dried at 100 °C overnight. Complexes **50** and **51** were then converted to (OH)Cr^{III}TAPc (**19**) and (OH)Mn^{III}TAPc (**20**) by addition of sodium sulphide monohydrate to slurries of CrTNPc (or MnTNPc), respectively, and stirred for 5 hrs. The products were isolated by centrifuge and treated with 1.0 M HCl (180 mL). The products were isolated again by centrifuge and transferred into 120 mL of 1.0 M NaOH and stirred for one hour. Finally, the solid products were

isolated by centrifuge and washed with water until free from NaOH and dried overnight at 100 °C. Scheme 3.5 shows a simplified synthetic route for the preparation of chromium and manganese tetraaminophthalocyanine complexes.

CrTNPc **(50):** Yield: 40%. IR (KBr disk) v/cm^{-1}: 3444(ν_{OH}), 1626, 1536, 1333, 1144, 1082, 759,728.

Cr^{III}TAPc **(19):** Yield: 88%. IR (KBr disk) v/cm^{-1}: 3442 (NH), 3350 (ν_{-OH}), 3282, 3190, 1608, 1415, 1348, 1306, 1254, 1138, 1099, 1055, 860 (ν_{Cr-O}), 826, 826, 760, 730. UV-Visible (DMF) λ_{max}/nm (log ε) (DMF): 363 (4.54), 450 (3.01), 502 (3.01), 665 (3.19), 735 (4.8).

MnTNPc **(51):** Yield: 40%. IR (KBr disk) v/cm^{-1}: 3440(ν_{-OH}), 1624, 1530, 1353, 1140, 1079, 755, 725.

(OH)Mn^{III}TAPc **(20)**: Yield: 85%. IR (KBr disk) v/cm^{-1}: 3438 (NH), 3340 (ν_{-OH}), 3282, 3190, 1608, 1415, 1348, 1306, 1254, 1138, 1099, 1057, 870 (ν_{Mn-O}), 826, 760, 730 UV-Visible (DMF) λ_{max}/nm (log ε) (DMF): 350 (4.80), 500 (4.44), 780 (4.71).

2.6 Electrochemical methods

2.6.1 General Conditions

Electrochemical data were collected from either BioAnalytical Systems (BAS) model 100B/W electrochemical workstation or BAS CV-50W voltammetric analyzer or Voltalab® PGZ 301 (Radiometer analytical). A conventional three-electrode electrochemical cell was used. The working electrodes were either a BAS glassy carbon electrode (GCE, 3 mm) or indium tin oxide (ITO) on glass, platinum wire and Ag|AgCl served as counter and pseudo-reference electrodes, respectively. The type of working electrode, GCE or ITO will be indicated where employed in the discussion. Electrical contact between the ITO electrode and the potentiostat was achieved by attaching a

copper foil containing conducting glue on the reverse side to the conducting side of the ITO. All electrochemical experiments involving organic solutions were performed in freshly distilled DMF or DCM containing 0.1 M tetrabutylammoniumtetraflouoroborate ($TBABF_4$) or 0.1 M tetraethylammoniumperchlorate (TEAP) (depending on availability), while phosphate or acetate buffered solutions were used for all experiments in aqueous media. Prior to all electrochemical experiments, the solutions were flushed with dry nitrogen or argon to remove oxygen from the solution. A N_2, or argon atmosphere was maintained throughout the duration of the electrochemical experiments. The working electrode (GCE) was polished with alumina on a Buehler-felt pad followed by washing thoroughly with deionized water collected from Milli-Q Millipore water purification system. The electrode was then washed with a generous supply of methanol and finally with DMF, DCM or phosphate or acetate buffer solution (depending on the medium in which the experiment is to be carried out) before transferring to the electrochemical cell. An optically transparent thin-layer electrochemical (OTTLE) cell, described by Hartl and Daněk[401] was employed for spectroelectrochemical studies. The OTTLE cell was connected to a BAS CV 27 voltammograph and the spectral changes of the electrolyzed species was monitored with Cary 500 UV-Vis-NIR or Cary 1E spectrophotometer. The OTTLE cell contained Pt minigrid working and counter electrodes and silver wire pseudo reference electrode. The experiments were performed by recording each spectral trace following application of the appropriate potential for a known time period, or by continuously recording the spectra while potential is applied. The method employed for each experiment will be stated in the Figure caption.

2.6.2 Electrode modification

Electrode modification was achieved by employing either the drop dry method, electropolymerization or self-assembled monolayer (SAM) technique. For the drop dry method, two drops of 1 mM of the MPc were placed on the surface of a polished GCE. The electrode was allowed to dry in air. It was finally kept in the oven (at ~ 80 ℃) for three hours. The electrode was finally rinsed in THF or DMF or DMSO (depending on the solvent in which the phthalocyanine solution was prepared), before it was used for electrocatalytic studies. The ITO electrodes were modified by either, dipping the electrodes into monomer solutions of the respective MPcs and drying in air after removal from the solution, or by electropolymerization.

Electropolymerization was achieved by repetitively scanning a solution containing monomeric MPc in DCM or DMF at a scan rate of 200 mV s^{-1}, using cyclic voltammetry, in the presence of $TBABF_4$ or TEAP (~ 0.1 M) as electrolytes. The specific scanning potential range and concentration of MPc will be presented in the relevant sections.

For the formation of self-assembled monolayers, the gold electrodes (radius = 0.8mm) were first polished with slurries of alumina (<10 μm) and SiC-emery paper (type 2400 grit), and then on a Buehler felt pad. The electrode was then placed in ethanol and subjected to ultrasonic vibration to remove possibly trapped particles at the surface. The electrode was then etched in a hot "piranha" solution {1:3 (v/v) 30% H_2O_2 and concentrated H_2SO_4} to remove trace organic contaminants on the electrode surface. Following this, the electrode was cycled, in 0.05 M H_2SO_4 solution, between - 0.5 V and 1.2 V vs. Ag|AgCl at a scan rate of 100 mVs^{-1} until a steady reproducible voltammogram

was obtained. This potential scanning ensures the removal of gold oxides and it prepares the electrode for the best possible adsorption of the MPcs.[162,402] The electrode was then immediately transferred into a 1 mM solution of the MPc in THF for 24 hours at room temperature. Upon removal from the deposition solution, the electrodes were thoroughly rinsed with THF (or ethanol, depending on the deposition solvent) and stored in pH 7.0 phosphate buffer solution for further electrochemical experiments. Self-assembly could also be done in solvents such as DCM, DMSO, ethanol and $CHCl_3$.

Results and Discussions

Publications

Some of the results presented in this thesis have been published in the following journals and are not referenced further:

1. Synthesis, Spectral and Electrochemical Properties of a new Family of Pyrrole Substituted Cobalt, Iron, Manganese, Nickel and Zinc Phthalocyanine Complexes, **J. Obirai,** N. P.-Rodrigues, F. Bedioui and T. Nyokong, *J. Porphyrins Phthalocyanines*, 2003, **7**, 508.
2. Electrochemical Studies of Manganese tetraaminophthalocyanine monomer and polymer, **J. Obirai** and T. Nyokong, *Electrochim. Acta*, 2004, **49**, 1417.
3. Electrochemical and Catalytic Properties of Chromium tetraaminophthalocyanine, **J. Obirai** and T. Nyokong, *J. Electroanal. Chem,* 2004, **573**, 77.
4. Electrooxidaton of Phenol and its Derivatives on *Poly*-Ni(OH)TPhPyPc Modified Vitreous Carbon Electrodes, **J. Obirai,** F. Bedioui and T. Nyokong, *J. Electroanal. Chem,* 2005, **576**, 323
5. Synthesis, Spectral and Electrochemical Characterization of Mercaptopyrimidine Substituted Cobalt, Manganese and Zn (II) Phthalocyanine Complexes, **J. Obirai** and T. Nyokong, *Electrochim. Acta* (In press)
6. Electropolymerized Pyrrole-substituted Manganese Phthalocyanine Films for the Electroassisted Biomimetic Catalytic Reduction of Molecular Oxygen, N. P. Rodrigues, **J. Obirai**, F. Bedioui and T. Nyokong, *Electroanalysis,* 2005, **17**, 186
7. Synthesis, Electrochemical and Electrocatalytic Behaviour of Thiophene-appended Cobalt, Manganese and Zinc Phthalocyanine Complexes, **J. Obirai** and T. Nyokong, *Electrochim. Acta* (In press)

Chapter Three

Syntheses and Spectral Characterization

The following metallophthalocyanine (MPc) complexes were synthesized in this thesis - Fig 3.1 shows the structures and Table 3.1 the names, abbreviations and numbers of the complexes:

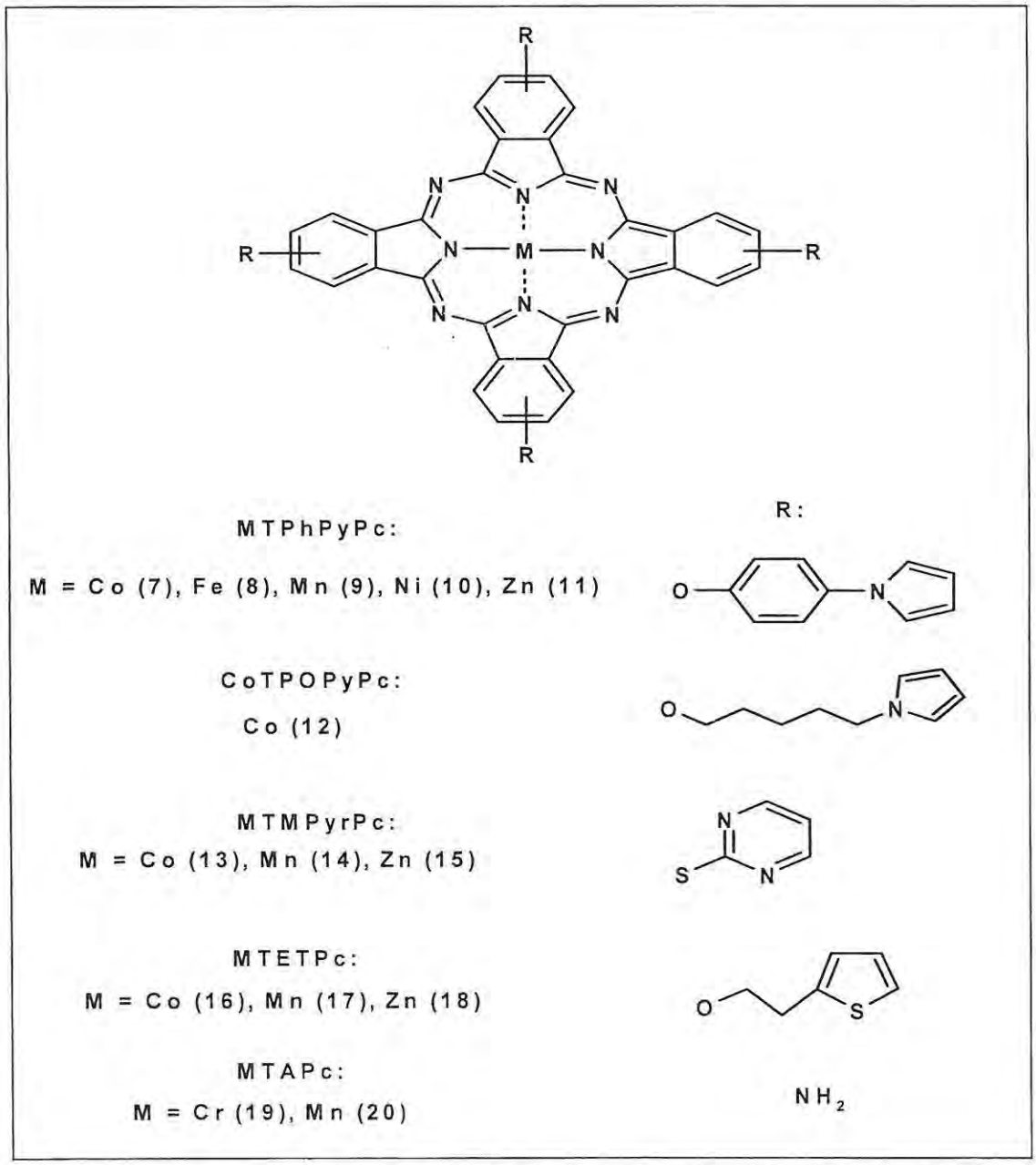

Fig 3.1: Summary of the tetra- pyrrole, thiophene, pyrimidin and amino functionalized metallophthalocyanine complexes studied in this work.

Table 3.1: List of the MPc complexes synthesized.

Name of MPc complex	Abbreviation	Number
Cobalt-tetra-{4-(pyrrol-1-yl)}phenoxyphthalocyanine.	**CoTPhPyPc**	**7**
Iron-tetra-{4-(pyrrol-1-yl)}phenoxyphthalocyanine.	**FeTPhPyPc**	**8**
Manganese-tetra-{4-(pyrrol-1-yl)}phenoxyphthalocyanine.	**MnTPhPyPc**	**9**
Nickel-tetra-{4-(pyrrol-1-yl)}phenoxyphthalocyanine.	**NiTPhPyPc**	**10**
Zinc-tetra-{4-(pyrrol-1-yl)}phenoxyphthalocyanine.	**ZnTPhPyPc**	**11**
Cobalt-tetra-{5-(pyrrol-1-yl)}pentoxyphthalocyanine.	**CoTPOPyPc**	**12**
Cobalt-tetra-(2-mercapto)pyrimidinephthalocyanine.	**CoTMPyrPc**	**13**
Manganese-tetra-(2-mercapto)pyrimidinephthalocyanine.	**MnTMPyrPc**	**14**
Zinc-tetra-(2-mercapto)pyrimidinephthalocyanine.	**ZnTMPyrPc**	**15**
cobalt-tetra-4-{2-(2-thienyl)ethoxy}phthalocyanine.	**CoTETPc**	**16**
Manganese-tetra-4-{2-(2-thienyl)ethoxy}phthalocyanine.	**MnTETPc**	**17**
Zinc-tetra-4-{2-(2-thienyl)ethoxy}phthalocyanine.	**ZnTETPc**	**18**
Chromium-tetraaminophthalocyanine.	**CrTAPc**	**19**
Manganese-tetraaminophthalocyanine.	**MnTAPc**	**20**

This chapter will dwell on the synthesis spectroscopic properties of the synthesized metallophthalocyanine complexes. Table 3.2 shows the list of IR vibration peaks for the complexes studied in this work.

Table 3.2: List of MPc complexes studied in this thesis: their abbreviations, complex numbers and IR vibrations

Complex	No	IR vibration (KBr disk) v/cm^{-1}
CoTPhPyPc	**7**	2923, 2852, 1606, 1515, 1462, 1236(C-O-C), 1096, 835, 724.
FeTPhPyPc	**8**	3436, 2955, 2922, 2859, 1610, 1510, 1472, 1233(C-O-C), 1077, 831, 726.
(Cl)Mn^{III}TPhPyPc	**9**	3437, 2944, 2859, 1606, 1514, 1468, 1234(C-O-C), 1071, 808, 720, 285 (Mn^{III}-Cl).
NiTPhPyPc	**10**	3423, 2958, 2923, 2845, 1609, 1514, 1461, 1236(C-O-C), 1096, 808, 720.
ZnTPhPyPc	**11**	3433, 2924, 2845, 1609, 1511, 1478, 1232(C-O-C), 1090, 833, 728.
CoTPOPyPc	**12**	3330, 3080, 2935, 2880, 1610, 1490, 1235(C-O-C), 1190, 1088, 960, 723.
CoTMPyrPc	**13**	2931, 2863, 2377, 1549, 1374, 1306, 1184, 1091, 920, 758.
MnTMPyrPc	**14**	3437, 2928, 2855, 2368, 1555, 1379, 1318, 1177, 1059, 620.
ZnTMPyrPc	**15**	3437, 2931, 2863, 2374, 1641, 1556, 1377, 1185, 1082, 895, 750.
CoTETPc	**16**	3417, 1610, 1482, 1390, 1338, 1235(C-O-C), 1080, 1040, 826, 695, 620.
(Cl)Mn^{III}TETPc	**17**	3410, 1612, 1489, 1387, 1340, 1235(C-O-C), 1080, 1041, 826, 700, 625, 287 (Mn^{III}-Cl).
ZnTETPc	**18**	3416, 1610, 1482, 1386, 1333, 1232(C-O-C), 1081, 1043, 823, 694, 620.
(OH)CrTAPc	**19**	3442 (NH), 3350 ($\nu_{\text{-OH}}$), 3282, 3190, 1608, 1415, 1348, 1306, 1254, 1138, 1099, 1055, 860 ($\nu_{\text{Cr-O}}$), 826, 826, 760, 730.
(OH)MnTAPc	**20**	3438 (NH), 3340 ($\nu_{\text{-OH}}$), 3282, 3190, 1608, 1415, 1348, 1306, 1254, 1138, 1099, 1057, 870 ($\nu_{\text{Mn-O}}$), 826, 760, 730.

3.1 N-Pyrrole Substituted Phthalocyanines (7-12)

3.1.1 N-Phenoxy Pyrrole (7-11)

Pyrrole-substituted porphyrins have been synthesized and used to form well structured multi-layer films through their direct electropolymerization onto electrodes.[403-405] In the various reported cases, the pyrrole groups were separated from the porphyrin ring via spacer chains. Recently there has been a report on the synthesis of the unique example of a pyrrole substituted phthalocyanine complexes.[399] The electropolymerizable pyrrole group was separated from the phthalocyanine macrocycle by an insulating alkylene spacer. In this work electropolymerizable N-pyrrole-substituted metallophthalocyanine complexes separated by phenoxy or pentoxy groups are reported.

The 4-(pyrrol-1-yl)phenol (**41**) was commercially available, however, the 5(pyrrol-1-yl)pentanol (**40**) had to be synthesized from **39** following literature methods,[399] Scheme 3.1. 5-(Pyrrol-1-yl)pentoxy phthalonitrile **(43)** and 4-(pyrrol-1-yl)phenoxy phthalonitrile (**42**) used for the synthesis of the CoTPOPyPc (**12**) or MTPhPyPc (**7-11**) were synthesized from 5-pyrrole-1-ylpentan-1-ol **(40)** and 4-(pyrrol-1-yl)phenol **(41)**, respectively, by reacting with nitrophthalonitrile following the method employed by Trombach *et al*,[399] Scheme 3.2 (a) and 3.2 (b), respectively.

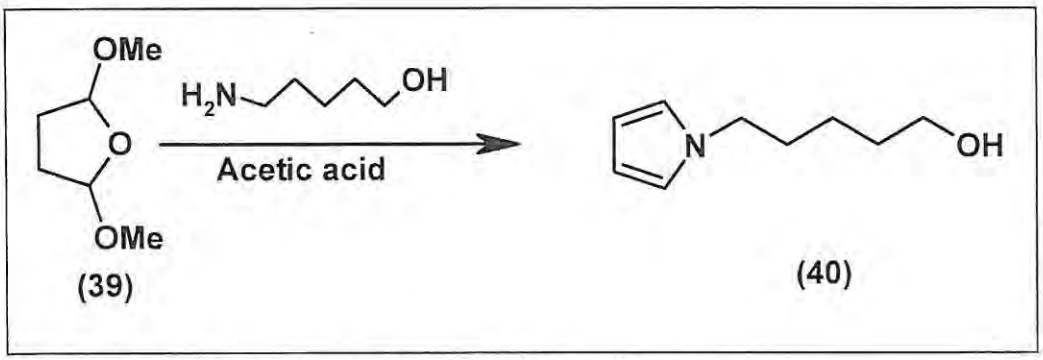

Scheme 3.1: Synthetic route for N-pyrrole substituted pentanol

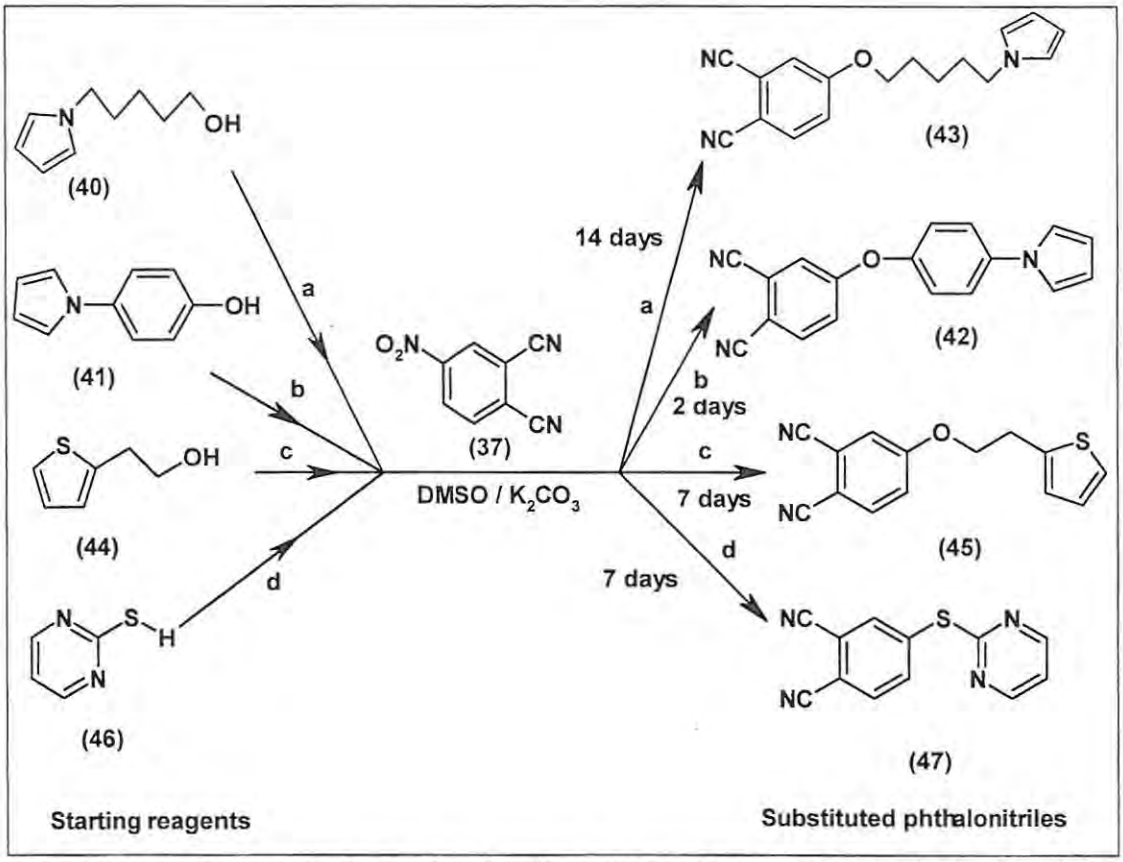

Scheme 3.2: Synthetic route for the functionalized phthalonitriles used in synthesis of the MPcs studied in this thesis.

The characteristic nitrile (C≡N) stretch at 2229 cm^{-1} of **42** and **43** disappeared upon formation of the phthalocyanine. The ether stretching frequencies are prominent in the phthalonitriles (**42** and **43**) and the resulting phthalocyanines, Table 3.2. The synthesis of the 4-(pyrrol-1-yl)phenoxy substituted metallophthalocyanine (H_2TPhPyPc, **48**) complex was achieved using a method different from that previously reported,[399] in that a metal free derivative was synthesized first, then metallated using the metal acetate, (Scheme 3.3), instead of direct reaction of the phthalonitrile with the metal salt. Also a solvent mixture of 1-pentanol/DMSO (4:1 v/v) was used instead of the single solvent (pentanol). Preparation of the complexes via the metal free derivative (**48**) resulted in high yield and purer compound. The cobalt complex CoTPhPyPc (**7**) was used as an

example for mass spectral analysis, and the results obtained (m/z 1200 (M +1)) confirmed the formation of the pyrrole substituted derivatives. CoTPhPyPc **(7)**, FeTPhPyPc **(8)**, MnTPhPyPc **(9)**, NiTPhPyPc **(10)** and ZnTPhPyPc **(11)** complexes were found to be soluble in common organic solvents such as DMF, DCM, THF and DMSO. The complexes were further characterized by UV-Visible, infrared (IR) and NMR spectra. The ether stretching vibrations for these Pcs was observed in the range of 1230-1236 cm^{-1}, Table 3.2. Also the Mn^{III}-Cl stretching vibration was observed at 285 cm^{-1} confirming Cl coordination to the central metal in the (Cl)Mn^{III}TPhPyPc (**9**) complex.

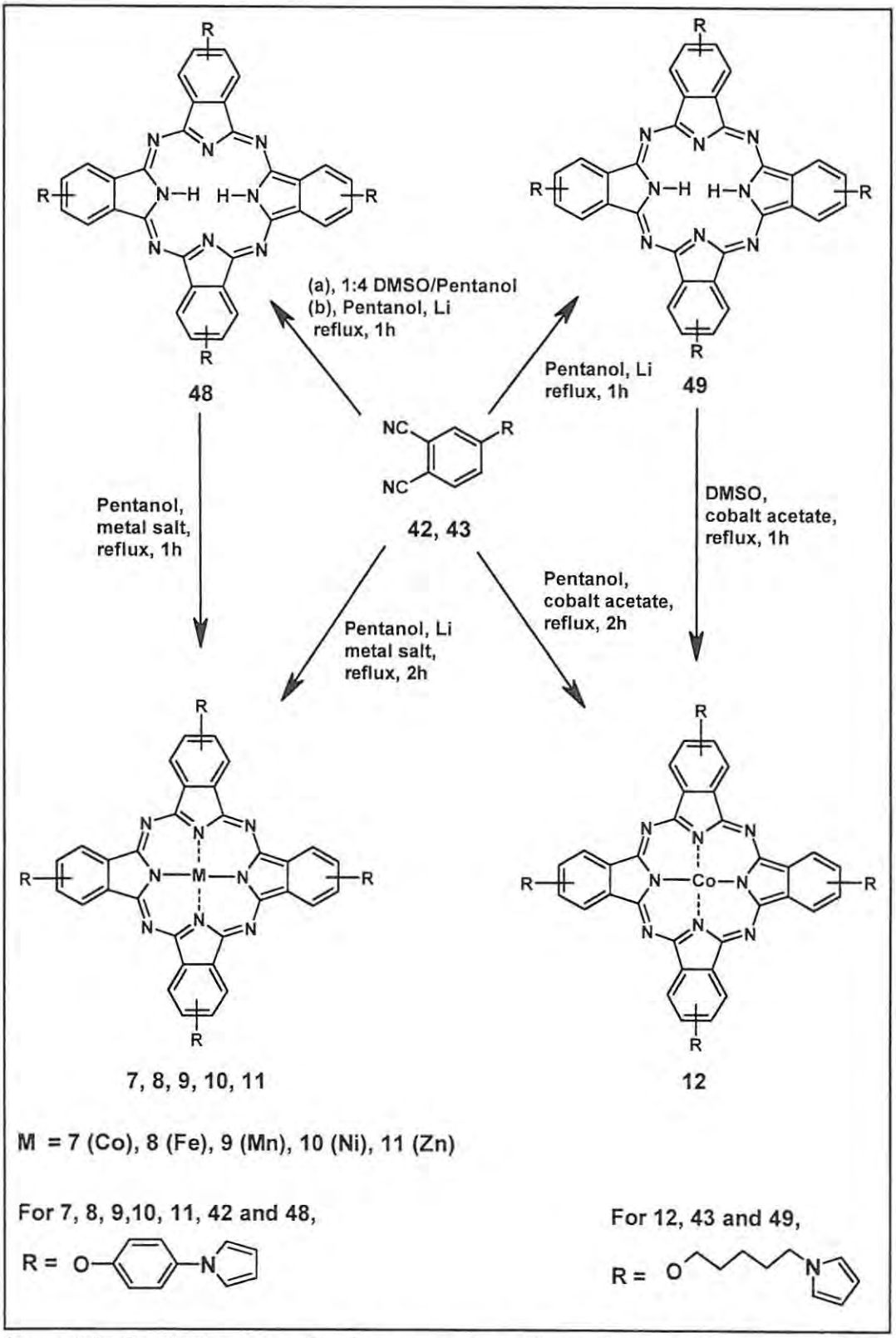

Scheme 3.3: Synthetic routes for the preparation of pyrrole substituted phthalocyanine complexes.

^{1}H NMR spectra of the free-base ligand **48** which was used in synthesizing all the metallated complexes, gave characteristic resonances due to the peripheral (1,4 positions) protons of the phthalocyanines. These were observed as singlets at 9.12 ppm, integrating for a total of 8 protons. In addition, 2,3 protons for the phthalocyanine ring were observed at 8.61 ppm and integrated for four protons. The protons for the pyrrol-phenoxy substituents integrated correctly.

Fig. 3.2 shows electronic absorption spectra of the 4-(pyrrol-1-yl)phenoxy substituted phthalocyanine cobalt, iron, manganese, nickel and zinc complexes. Table 3.3 shows a summary of the UV-Visible spectra of the complexes studied in this thesis.

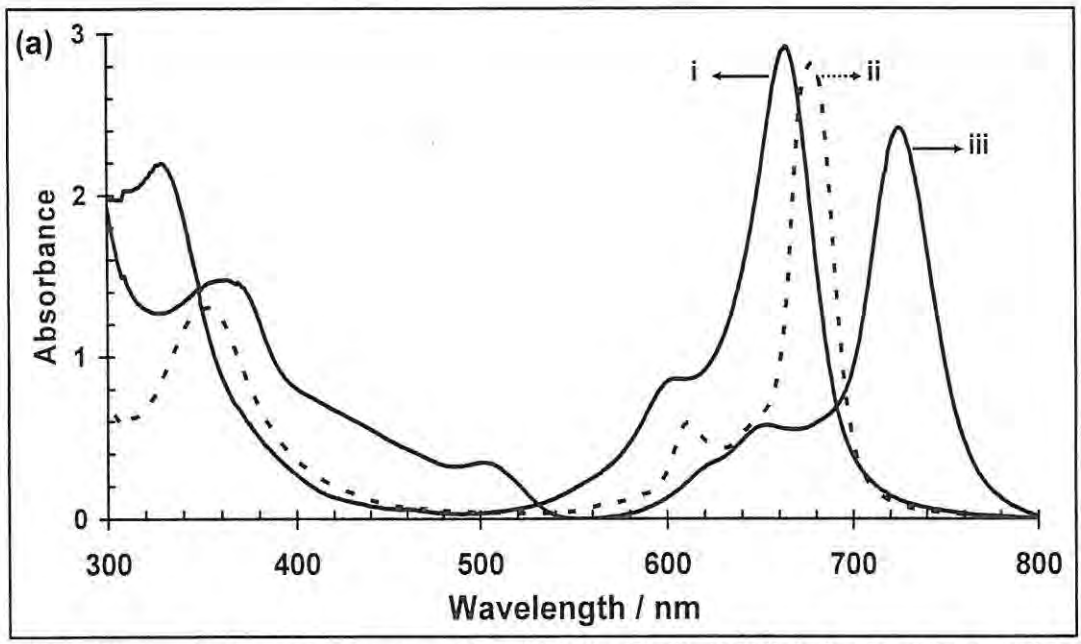

Fig 3.2a: Electronic absorption spectra of CoTPhPyPc (**7**) (i), ZnTPhPyPc (**11**) (ii), MnTPhPyPc (**9**) (iii) in DMF. Concentration = ~ 1 x 10^{-6} M.

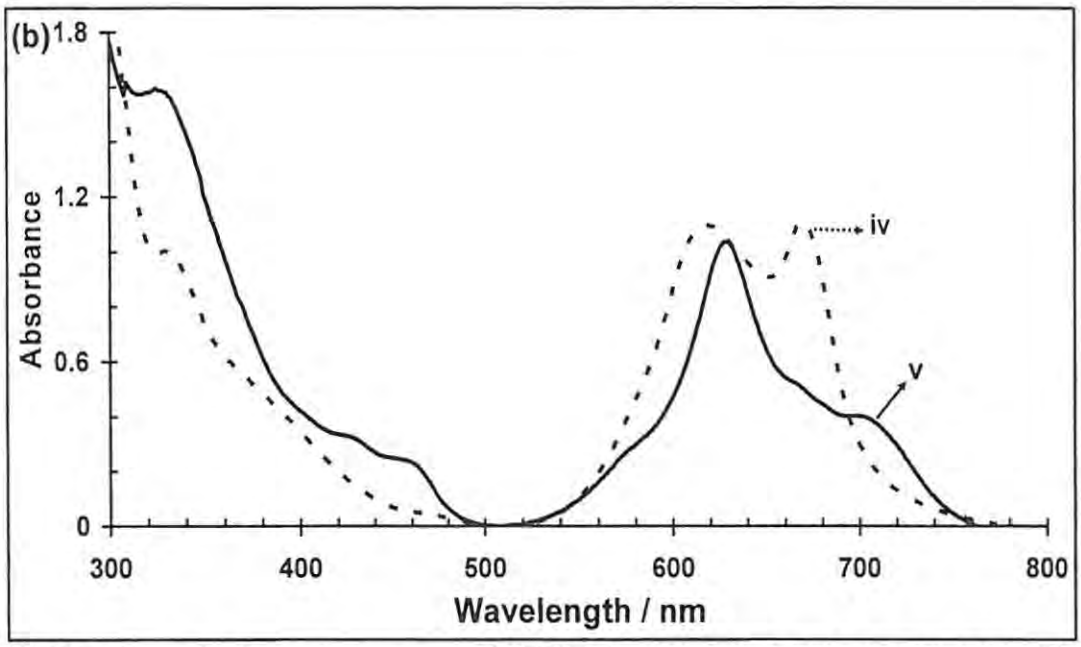

Fig 3.2b: Electronic absorption spectra of NiTPhPyPc (**10**) (iv), FeTPhPyPc (**8**) (v) in DMF. Concentration = $\sim 1 \times 10^{-6}$ M.

The iron and nickel complexes show aggregation as evidenced by the splitting of the Q band region observed in Fig 3.1b. In the case of FeTPhPyPc **(8)**, Fig 3.2b (curve V), the high energy band at 628 nm may be attributed to the aggregated species thus showing that **8** is mainly aggregated. In the case of the NiTPhPyPc **(10)**, Fig 3.2b, the high energy peak due to the aggregated species is observed at 621 nm and the peak due to the monomeric species at 671 nm. For Ni (**10**) and Fe (**8**) complexes, upon dilution, the peak due to the aggregates decreases more in intensity relative to the peak due to the monomer (Fig. 3.3a and b), confirming that the monomeric species predominates in dilute solutions. Note that in the case of the iron phthalocyanine and its derivatives, the UV-Visible spectra analysis have been a subject of extensive research due to the complexity and the wide variety of species that may be formed in solution. For example, perchlorinated iron (II) phthalocyanine dissolved in DMF is known[406,407] to react with oxygen, resulting in oxidation and formation of a μ-oxo species, $Pc^{-2}Fe^{III}$-O-$Fe^{III}Pc^{-2}$,

which changes back to the original monomeric species upon reduction. In this study, the spectra shown in Fig 3.2b and Fig 3.3a for complex **8** were obtained with freshly prepared oxygen-free solutions, showing that they are not related to the μ-oxo species, but only to the presence of monomeric species as well as cofacially aggregated species.

Table 3.3: List of MPc complexes studied in this thesis: their abbreviations, complex numbers, wavelength of absorption maxima (λ_{max}/nm) and extinction coefficients (log ε) in DMF.

Complex	No	λ_{max}/nm (log ε) (DMF)
CoTPhPyPc	**7**	328 (3.67), 603 (1.47), 665 (4.88).
FeTPhPyPc	**8**	327 (6.36), 457 (1.85), 628 (4.38), 701 (3.12).
(Cl)Mn^{III}TPhPyPc	**9**	380 (2.57), 497(0.84), 649 (0.95), 720 (4.80).
NiTPhPyPc	**10**	329 (4.43), 621 (5.06), 671 (4.45).
ZnTPhPyPc	**11**	352 (2.27), 609 (4.55), 678 (5.04).
CoTPOPyPc	**12**	615 (1.95), 670 (4.40).
CoTMPyrPc	**13**	333 (4.93), 603 (4.54), 668 (5.06).
(Cl)Mn^{III}TMPyrPc	**14**	350 (4.43), 500 (0.85), 626 (4.40, μ-oxo dimer), 686 (2.38, Mn^{II}) 720 (4.38, Mn^{III}).
ZnTMPyrPc	**15**	356 (4.9), 615 (4.64), 678 (5.35).
CoTETPc	**16**	333 (4.67), 603 (4.45), 673 (4.96).
(Cl)Mn^{III}TETPc	**17**	368 (4.5); 500 (4.0); 667 (3.3); 723 (4.7).
ZnTETPc	**18**	353 (4.1); 610 (4.5); 676 (5.1).
(OH)CrTAPc	**19**	363 (4.54), 450 (3.01), 502 (3.01), 665 (3.19), 735 (4.8).
(OH)MnTAPc	**20**	350 (4.80), 500 (4.44), 780 (4.71).

It should be noted that the spectral features are indicative of M^{II}TPhPyPc species except in the case of the manganese (MnTPhPyPc) complex **(9)**, Fig 3.2a (curve iii), which exhibits the characteristic features of Mn^{III} species, such as red-shifted Q band and a band at 497 nm,[407-409] see Table 3.3. The presence of Cl^- axial ligand was confirmed by a Mn-Cl vibration, as indicated above. This is further discussed below in the spectroelectrochemical characterization section. The Q band of the cobalt, manganese and zinc complexes in DMF was typical of non-aggregated species, as it can be observed in Fig 3.2a, at concentrations lower than 1×10^{-4} M. Figs 3.3 (c, d and e) show that there are no dilution effects on the solution containing species for the cobalt, manganese and zinc complexes, as no aggregates have been observed. Beer's law behaviour for the cobalt, manganese and zinc complexes was observed at concentrations less than 10^{-4} M and deviation was observed for the iron (**8**) and nickel (**10**) complexes at these concentrations. A representative Beer's Law plot for the complexes is shown in Fig 3.4, which shows a deviation from Beer's Law for the aggregated NiTPhPyPc complex (**10**). Deviations from Beer's Law was also observed for complex **8** (FeTPhPyPc) at concentrations of Fig 3.4.

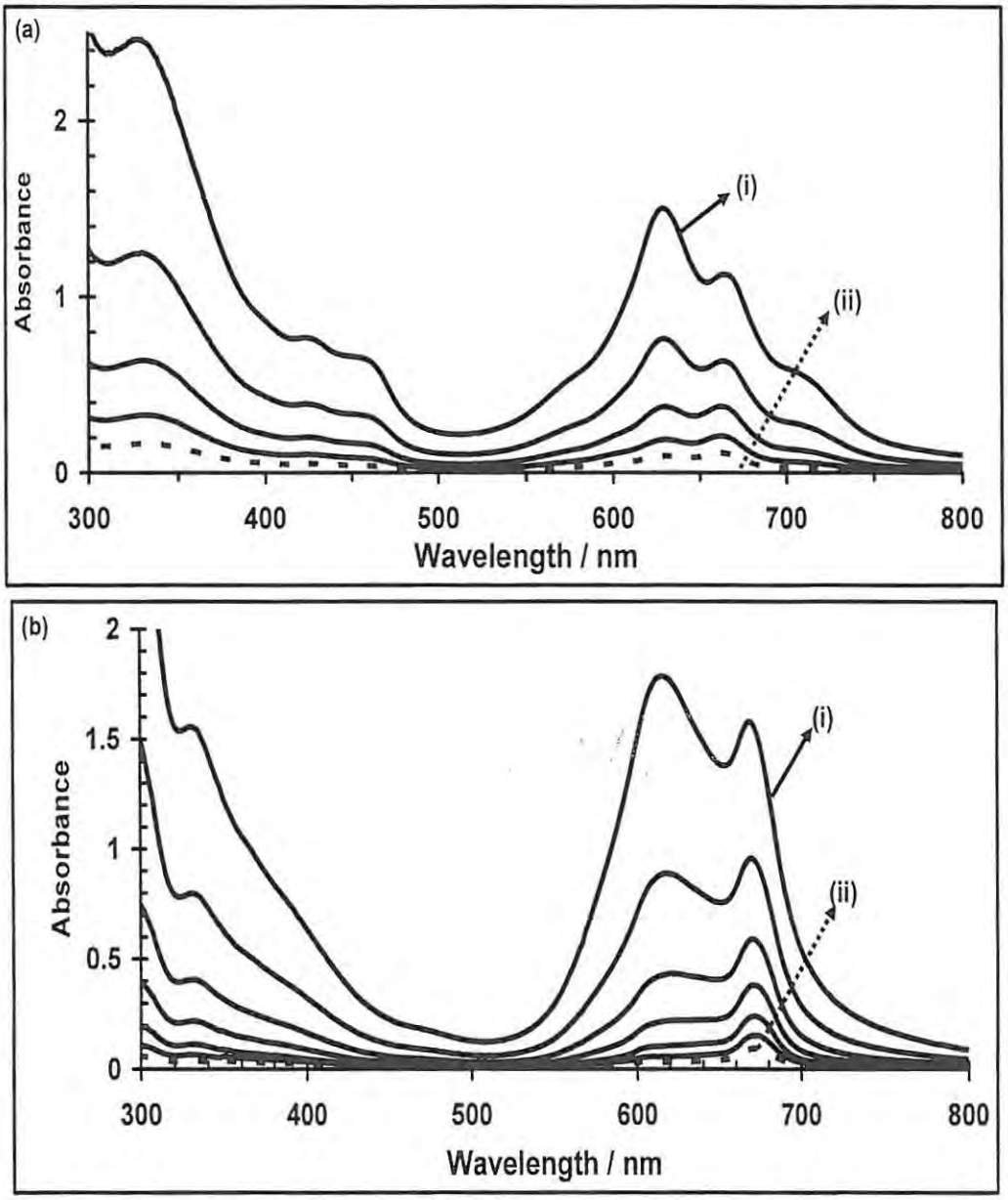

Fig 3.3 (a and b): Changes in the UV-Visible spectra with changes in the concentration of complexes **8** (FeTPhPyPc), (a) and **10** (NiTPhPyPc), (b,): (i) at the start (most concentrated) and (ii) at the end (least concentrated). Starting concentration ~ 1 x 10^{-5} M.

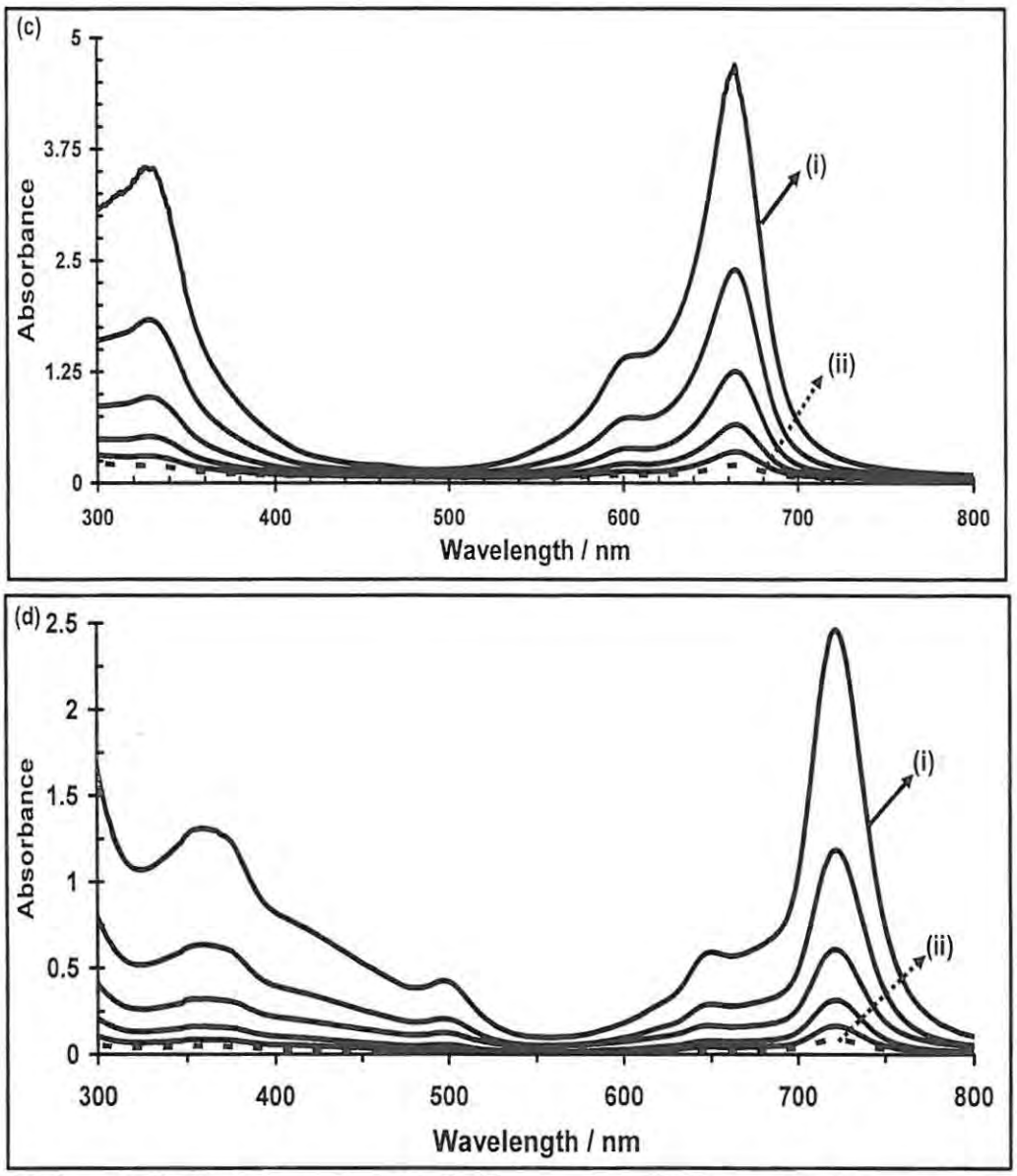

Fig 3.3 (c and d): Changes in the UV-Visible spectra with changes in the concentration of complexes **7** (CoTPhPyPc), (c) and **9** (MnTPhPyPc), (d): (i) at the start (most concentrated) and (ii) at the end (least concentrated). Starting concentration ~ 1 x 10^{-5} M.

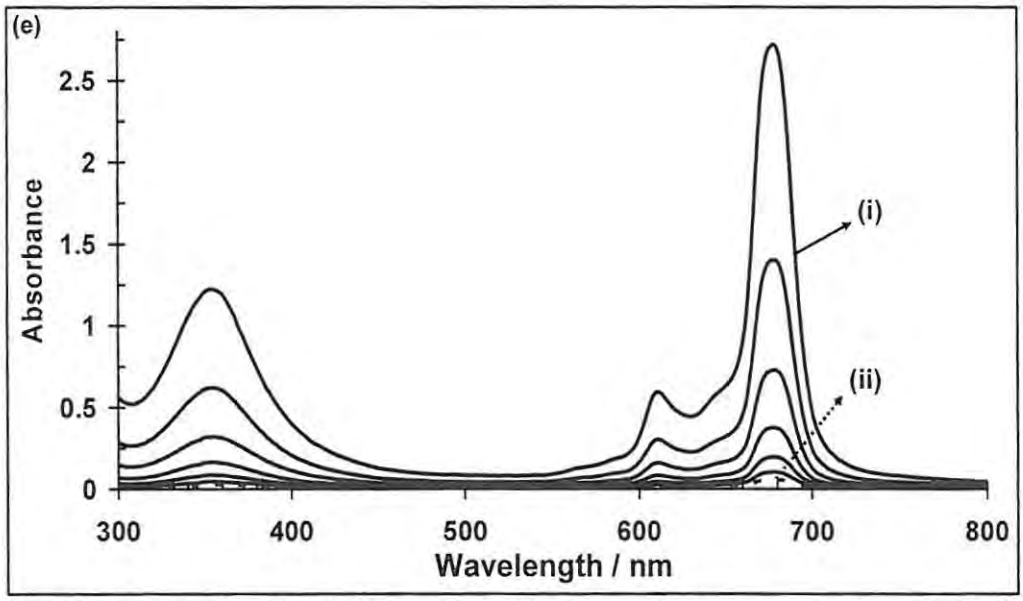

Fig 3.3e: Changes in the UV-Visible spectra with changes in the concentration of complex **11** (ZnTPhPyPc). (i) at the start (most concentrated) and (ii) at the end (least concentrated). Starting concentration ~ 1 x 10^{-5} M.

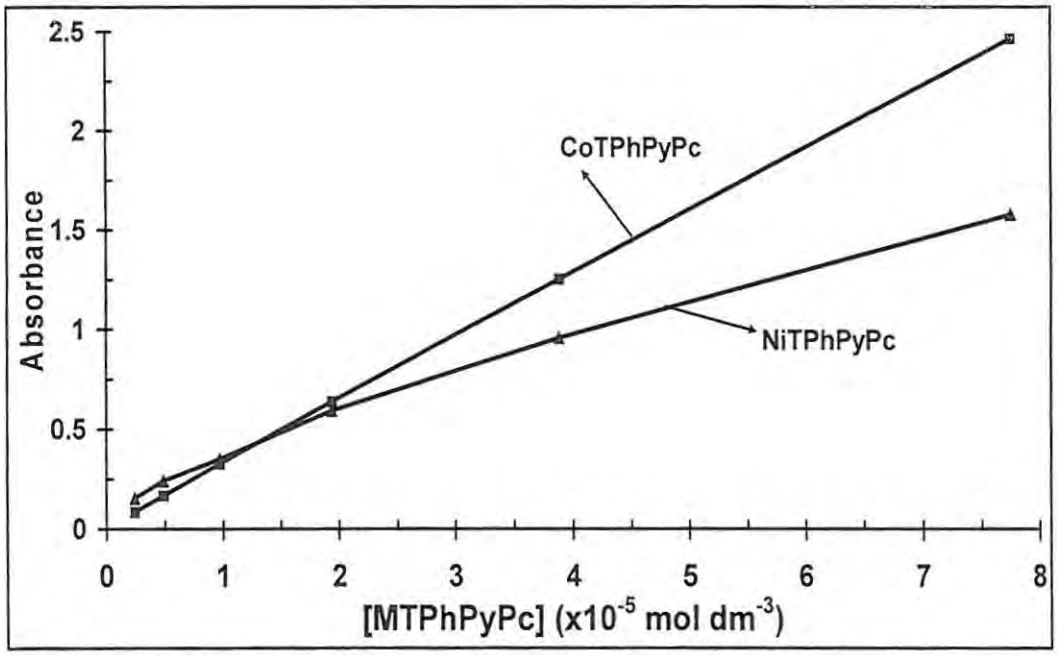

Fig 3.4: A representative plot showing Beers law behaviour of the N-pyrrole substituted metallophthalocyanine complexes. A similar behaviour was observed for **7**, **9** and **11** while the **8** and **10** followed the same pattern.

3.1.2 N-Pentoxy Pyrrole (12)

The metal-free pentoxypyrrole substituted Pc complex H_2TPOPyPc **(49)** was synthesized in dry pentanol while the metallation of the resulting product was achieved in DMSO to afford the CoTPOPyPc **(12),** Scheme 3.4. The ^{1}H NMR spectra of the H_2TPOPyPc **(49)** showed 1,4 protons at 9.00 and 2,3 protons at 8.41 ppm. IR for both **49** and **12** showed ether stretching vibrations at 1235 cm^{-1}, Table 3.2. Elemental analysis confirmed the formation of complex **12**. The UV-Visible spectra of complex **12** in DMF and DCM are shown in Fig 3.5, Table 3.3. The spectra show that there is a tendency for aggregation in the solvents used judging by the height of the peak at 615 nm. It can be seen that while the characteristic Q-bands are unaffected, the effect of the solvent is well pronounced in the B-band region, in that there is essentially no Soret band peak in DMF while the complex showed ill-defined peaks at the same region in DCM (Fig 3.5).

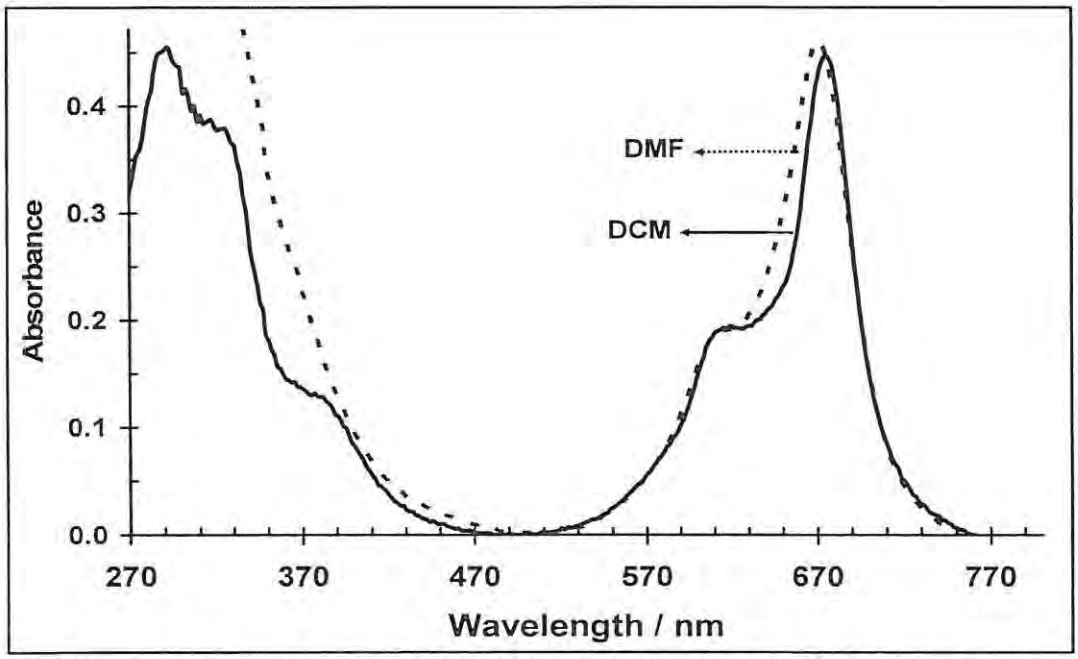

Fig 3.5: Electronic absorption spectra of CoTPOPyPc in DCM and DMF. Concentration = ~ 1 x 10^{-6} M.

3.2 Metal-tetra-{2-(2-thienyl)ethoxy}phthalocyanine (MTETPc) (16-18) (Scheme 3.4)

The synthesis of 4-{2-(2-thienyl)ethoxy}phthalonitrile (**45**) was achieved by reaction of 2-(2-thienyl)ethanol (**44**) with 4-nitrophthalonitrile (**37**) in dry DMSO, Scheme 3.2c. The aromatic nucleophilic substitution of the nitro group was facilitated in the presence of K_2CO_3 as a base. The ether bond formation was confirmed (IR spectra) by the disappearance of the NO_2 symmetric and asymmetric stretch bands at 1360 cm^{-1} and 1540 cm^{-1} respectively (for **45**) and the appearance of the ether bond stretches at 1250 and 1561 cm^{-1}. The formation of the respective metallophthalocyanine complexes was confirmed by the disappearance of the characteristic C≡N stretch at 2228 cm^{-1} of complex **45**. Cyclotetramerization of the substituted phthalonitrile was achieved in a lithium pentanolate medium.[399] The direct conversion of the Li_2Pc complex to the various MPcs was achieved without isolating the unmetallated Pc, Scheme 3.4. IR spectra of the Co (**16**) Mn (**17**) and Zn (**18**) complexes gave ether vibrations at 1235 (**16**) 1235 (**17**) and 1232 cm^{-1} (**18**), Table 3.2.

ZnTETPc (**18**) (containing a diamagnetic central metal) was also characterized using ^1H NMR, which gave characteristic resonances due to the peripheral protons of the Pc ring at 8.51 ppm as triplets, integrating for 4 protons. Non-peripheral proton peaks were observed at 7.15 and 8.92 ppm integrating for 8 protons in total. The protons corresponding to the ethylene and thiophene substituents integrated correctly and were found at 3.70 and 4.5 ppm, and 7.25 and 7.63 ppm, respectively.

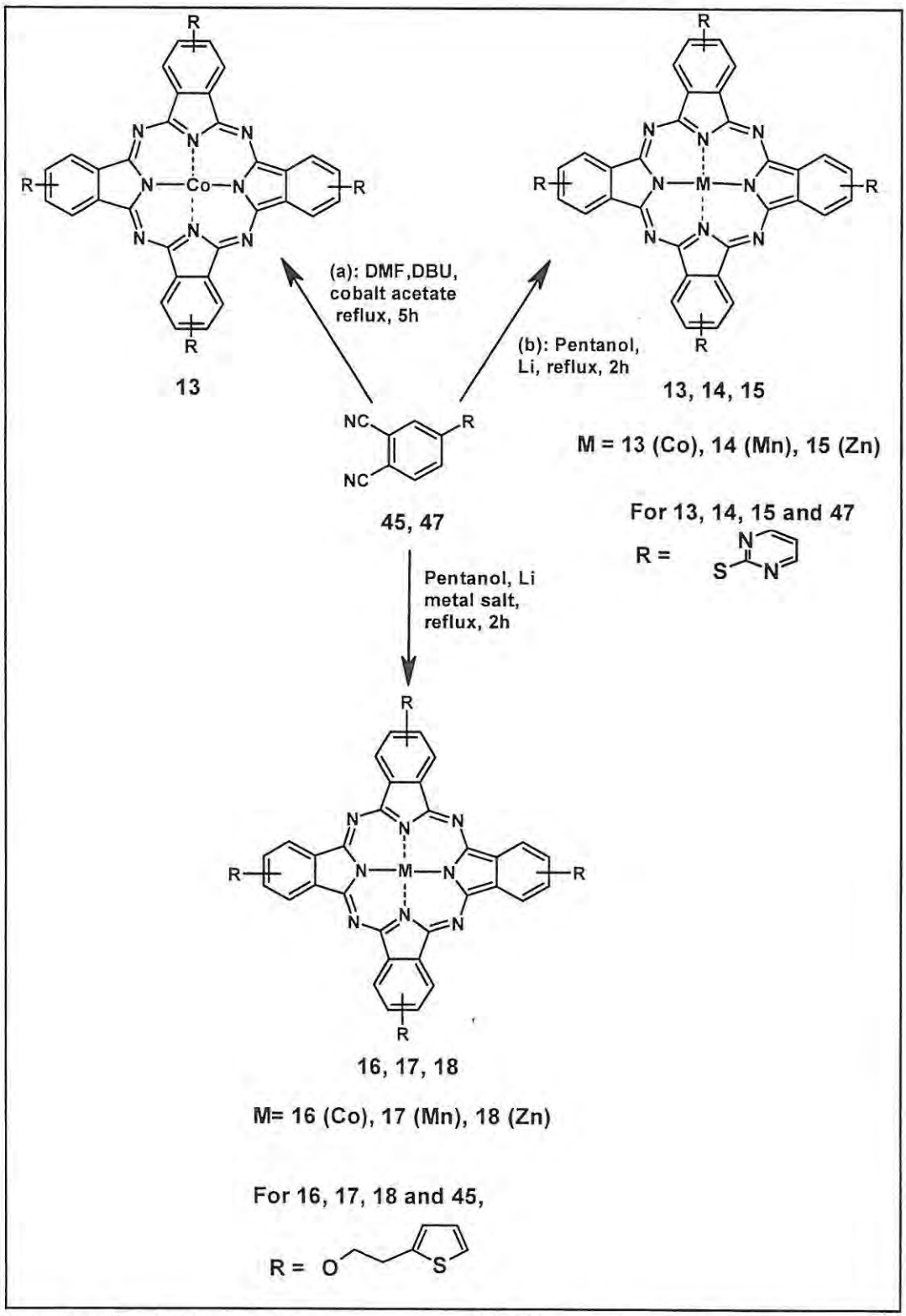

Scheme 3.4: Synthetic routes for the preparation of thiophene and mercaptopyrimidin substituted phthalocyanine complexes.

Fig 3.6 shows the electronic absorption spectra of the complexes (**16-18**) studied in this report and Table 3.3 lists the UV-Visible data.

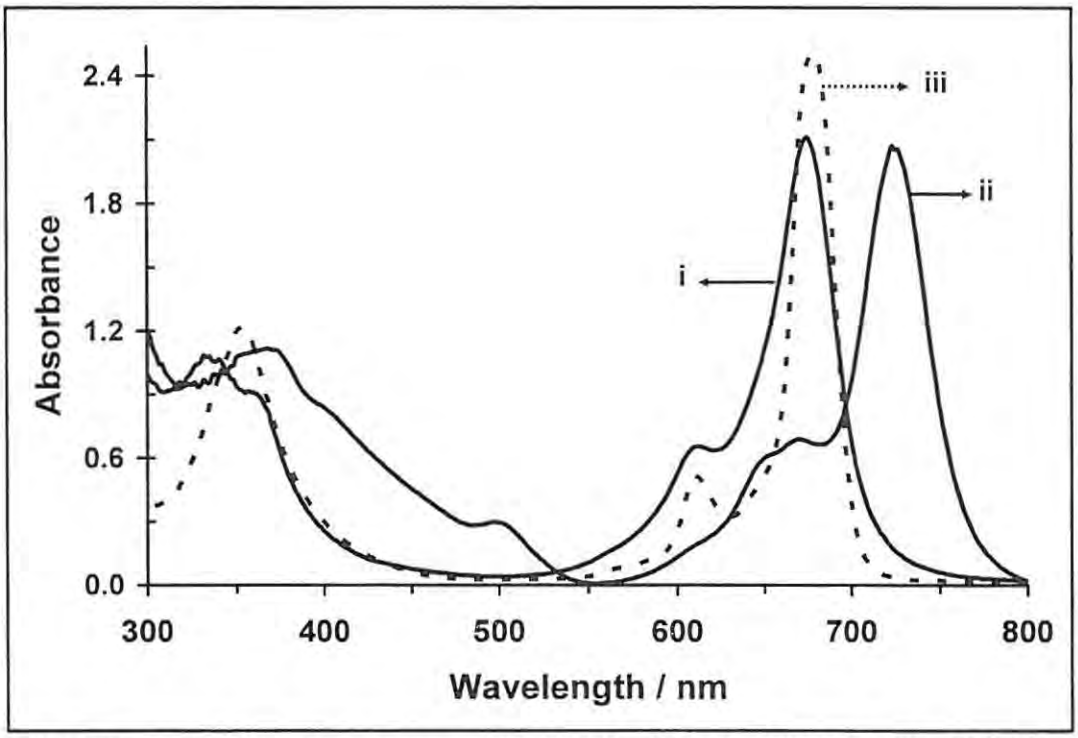

Fig 3.6: Electronic absorption spectra of CoTETPc **(16)** (i), (Cl)MnTETPc (**17**) (ii) and ZnTETPc **(18)** (iii) in DMF. Concentration: ~ 2 x 10^{-5} M.

The spectrum of the Mn complex is typical[409] of $Mn^{III}Pc$ complexes with a red shifted Q band, and a band near 500 nm. The presence of the axial chloride ligand was confirmed by the presence of the Mn^{III}-Cl vibration at 287 cm^{-1}. For all the other thiophene substituted complexes, the central metal is of M^{II} oxidation state. All the complexes exhibited Beer's Law behavior at low concentrations ($\leq 10^{-5}$ M) as shown in the insets of Fig 3.7.

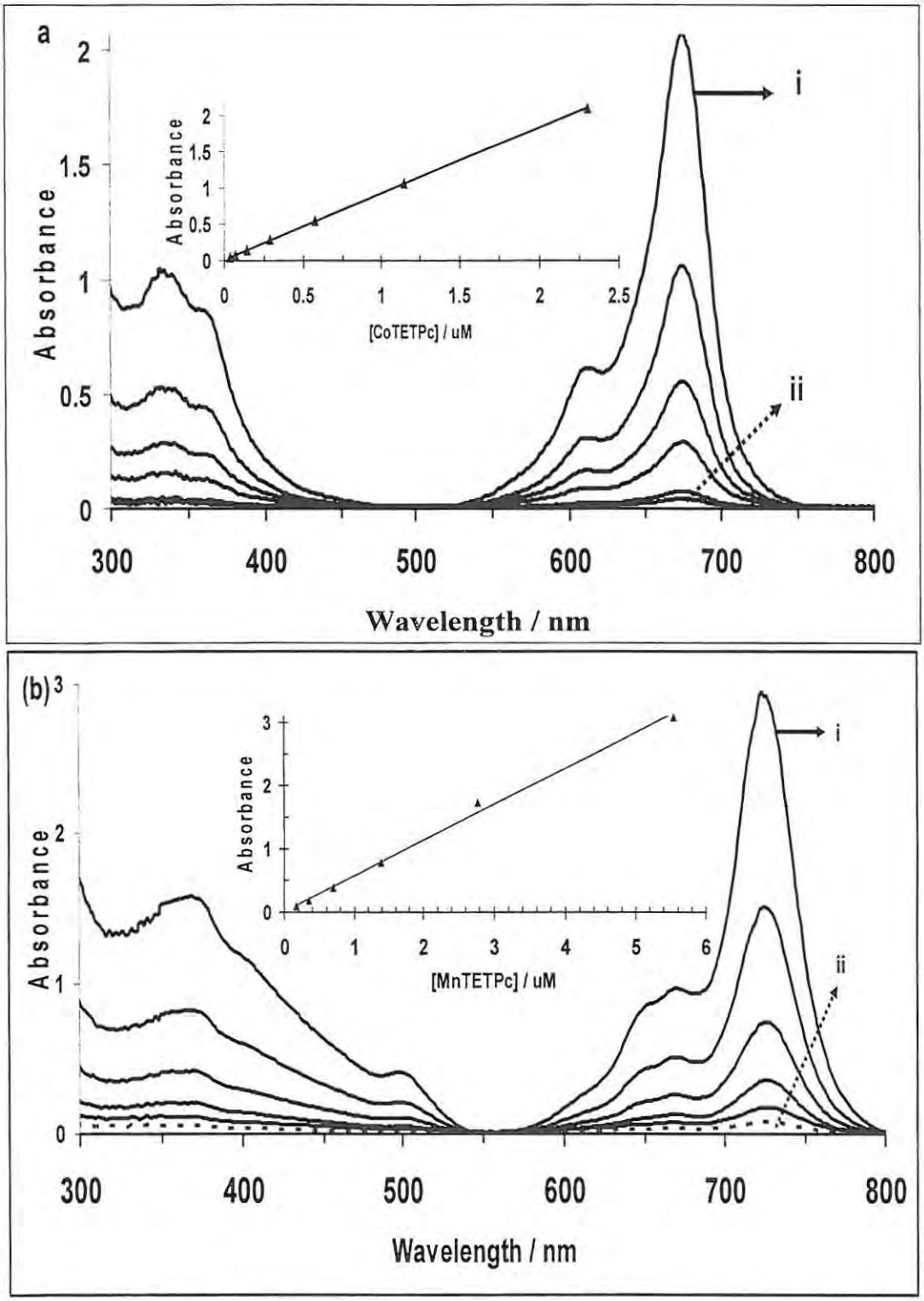

Fig 3.7 (a and b): Changes in the UV-Visible spectra with concentration for complexes **16** (CoTETPc) (a) and **17** (MnTETPc). (i): most concentrated, (ii): least concentrated. Inset shows the Beer-Lambert Law behavior of the complexes.

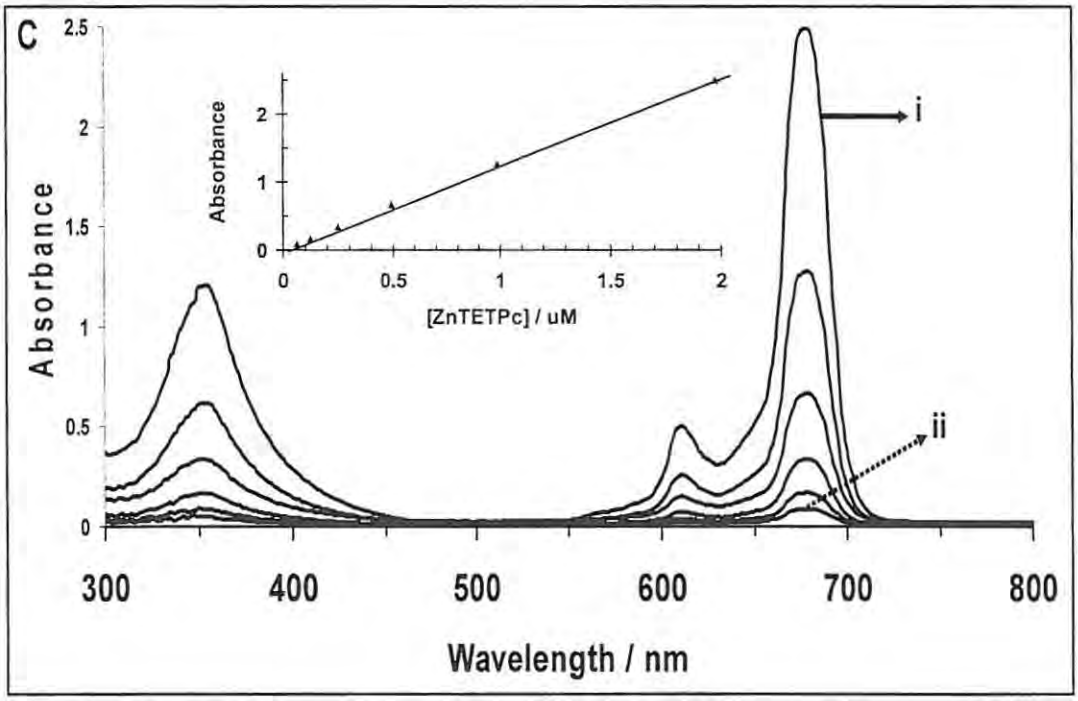

Fig 3.7c: Changes in the UV-Visible spectra with concentration for complex (**18**) (ZnTETPc). (i): most concentrated, (ii): least concentrated. Inset shows the Beer-Lambert Law behavior of the complexes.

3.3 Mercaptopyrimidine Substituted Metallo-phthalocyanine (MTMPyrPc) Complexes (13-15) (Scheme 3.4)

The phthalonitrile (**47**) was synthesized from compound **46** and shown in Scheme 3.2. The different metallo mercaptopyrimidin substituted Pcs (complexes **13, 14** and **15**) were synthesized by the cycloteramerization of 4-(-mercaptopyrimidyl)phthalonitrile (**47**) in pentanol or DMF, Scheme 3.4. For the reactions carried out in pentanol, the tetramerization was achieved in the presence of lithium pentanolate, Scheme 3.4 (route b). The cobalt and zinc complexes gave satisfactory elemental analysis as shown in the experimental section. Since the manganese complex exists as a mixture of compounds,

elemental analysis was not employed, only spectroscopic methods were employed for its characterization. In all cases the disappearance of the characteristic nitrile (C≡N) stretch at 2229 cm^{-1} of the phthalonitrile, **47**, was indicative of the formation of the MPcs. Attempts to obtain a metal free Pc were not successful. ZnTMPyrPc **(15)** was employed for ^{1}H-NMR characterization since it contains a diamagnetic central metal. The ^{1}H-NMR spectrum of ZnTMPyrPc **(15)** gave characteristic resonances due to peripheral and non-peripheral protons of the Pc ring. The peripheral resonances were observed as singlets at 8.29 ppm, integrating for four protons. The non-peripheral protons of the Pc ring were observed at 8.72 ppm integrating for eight protons. The protons related to the pyrimidine rings also integrated correctly at 7.36 and 7.95 ppm.

The UV-Visible spectra of compounds **13-15** are represented in Fig. 3.8 (a and b) and their absorption maxima are listed in Table 3.3. The electronic spectra of **13** (CoTMPyrPc) and **15** (ZnTMPyrPc) in DMF are typical of monomeric MPc species, with Q bands at 668 and 680 nm, respectively, Fig. 3.8a.

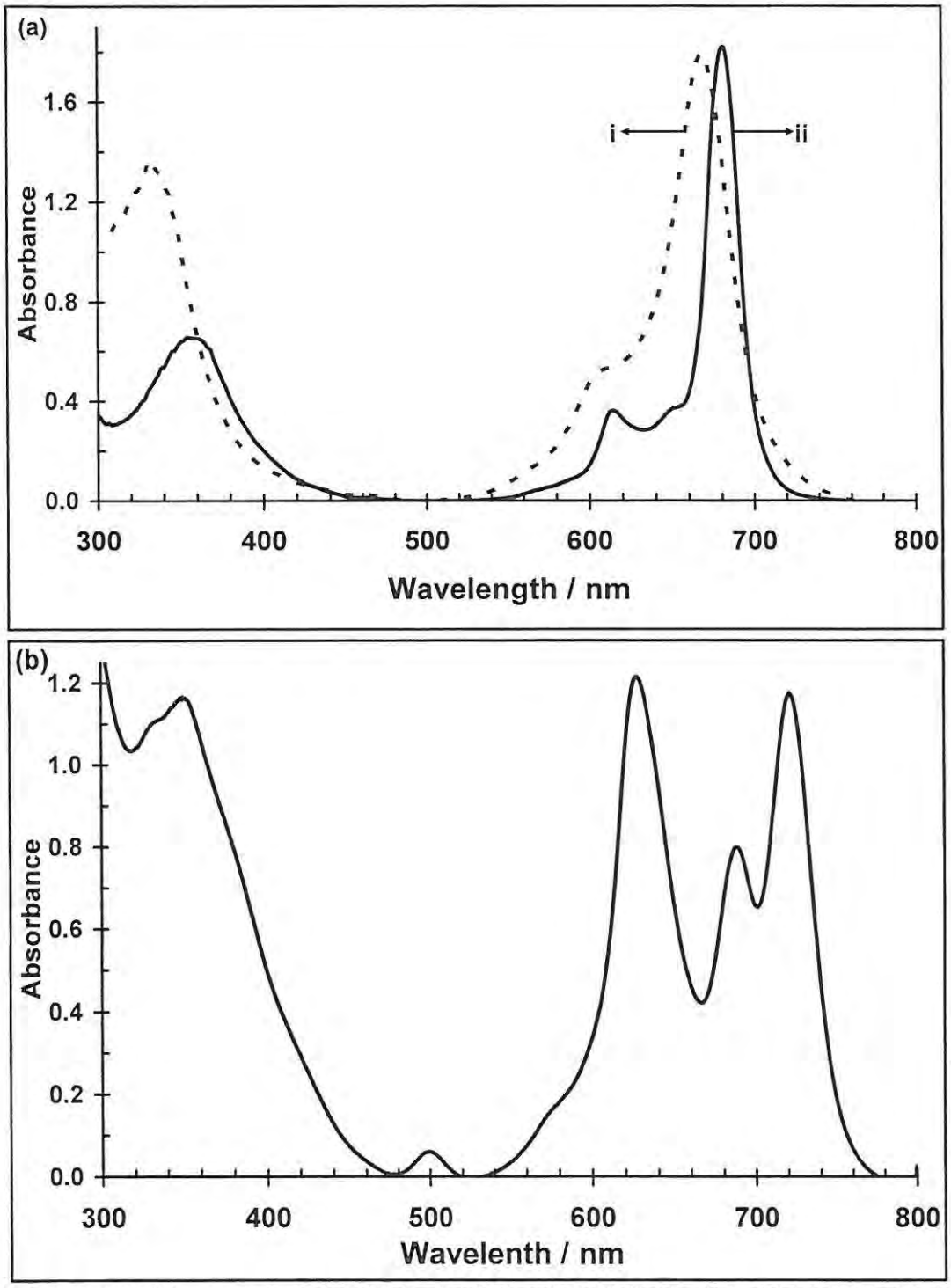

Fig.3.8: UV-Visible spectra of (a) CoTMPyrPc (**13**) and ZnTMPyrPc (**15**); (b) MnTMPyrPc (**14**) in DMF. Concentrations: ~ 5 x 10^{-6} M.

The UV-Visible spectrum for the MnTMPyrPc (complex **14**) is shown in Fig. 3.8b. The spectrum consists of three bands corresponding to three different species in solution. This is typical of the following MnPc species in equilibrium in DMF that has not been deaerated, as suggested by Lever *et al*[408] (Equation 3.1-3.5):

$$PcMn^{II} + O_2 \rightleftharpoons PcMn^{III}(O_2) \quad 3.1$$

$$PcMn^{III}(O_2) + PcMn^{II} \rightleftharpoons PcMn^{III}\text{-}O_2\text{-}Mn^{III}Pc \quad 3.2$$

$$PcMn^{III}\text{-}O_2\text{-}Mn^{III}Pc \rightleftharpoons 2\ PcMn^{IV}O \quad 3.3$$

$$2\ PcMn^{IV}O + 2\ PcMn^{II} \rightleftharpoons 2\ PcMn^{III}\text{-}O\text{-}Mn^{III}Pc \quad 3.4$$

$$\textbf{net}\ 4\ PcMn^{II} + O_2 \longrightarrow 2\ PcMn^{III}\text{-}O\text{-}Mn^{III}Pc \quad 3.5$$

The presence of the Mn^{II}, Mn^{III} and μ-oxo MnPc species was confirmed by monitoring the transformations of the MnTMPyrPc in DMF solution when not de-aerated and when de-aerated with dry N_2 gas.

Fig 3.9a (i) shows the UV-Visible spectra recorded for the MnTMPyrPc complex in DMF before de-aerating. In the presence of O_2, $Mn^{II}Pc$ forms an oxygen adduct which has been described[408] as a $(O_2^-)Mn^{III}Pc$ species and absorbs near 705 nm. Thus the absorption band at 719 nm is typical of Mn^{III} complex with a characteristic charge transfer (CT) band at 497 nm. The peak at 626 nm is typical of μ-oxo ($PcMn^{III}$-O-$Mn^{III}Pc$) species and the peak at 686 nm is due to $Mn^{II}Pc$ in comparison with literature,[408] see listed assignment in Table 3.3.

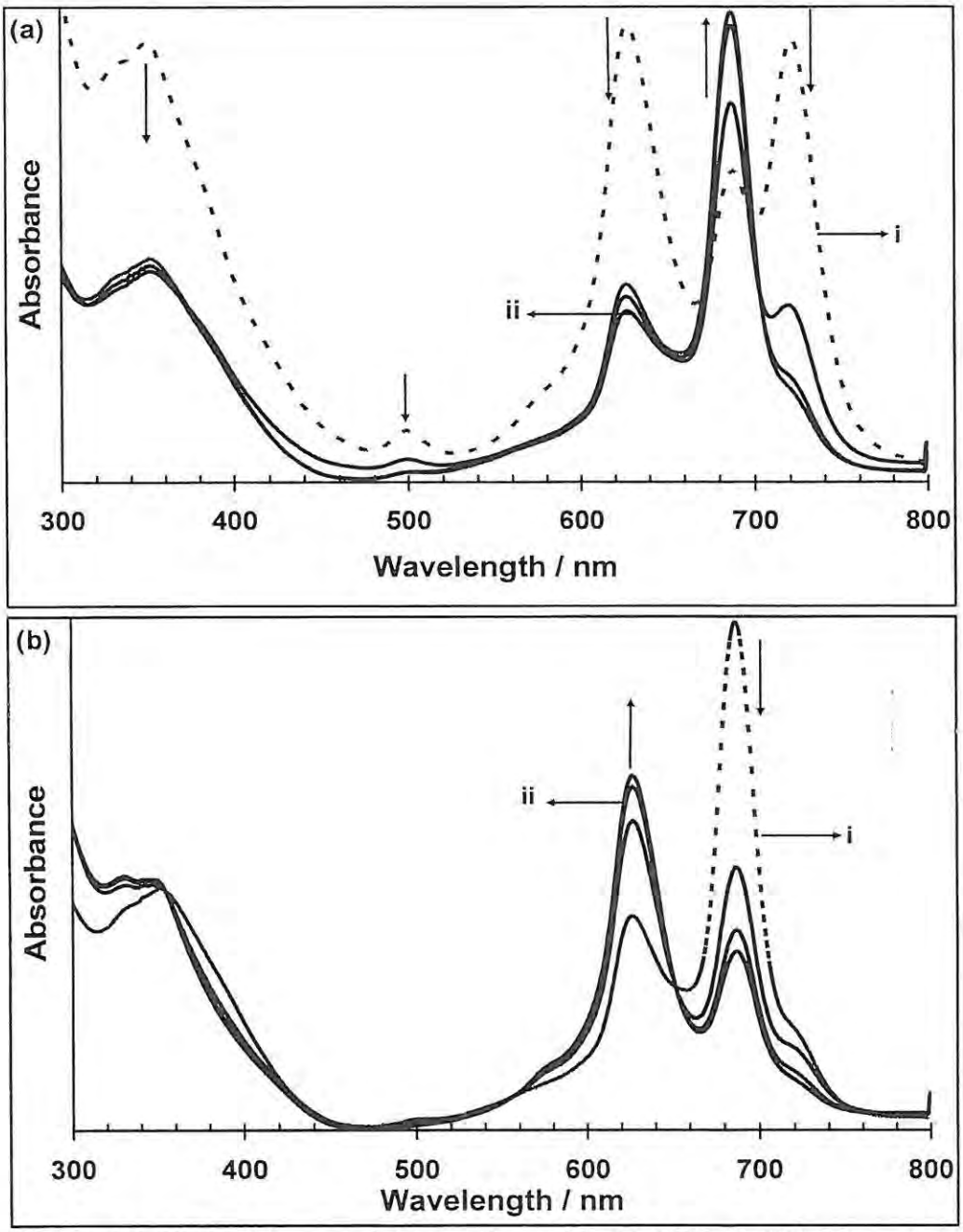

Fig. 3.9 (a and b): UV-Visible spectral changes observed for MnTMPyrPc (**14**): (a) spectra before (i) and 15 minutes (ii) after de-aerating with N_2. (b): spectra before (i) and 30 minutes (ii) after bubbling O_2. The initial spectrum in (b) (i) is the same as the final spectrum in (a) ii. The concentration of MnTMPyrPc is ~ 5 x 10^{-6} M.

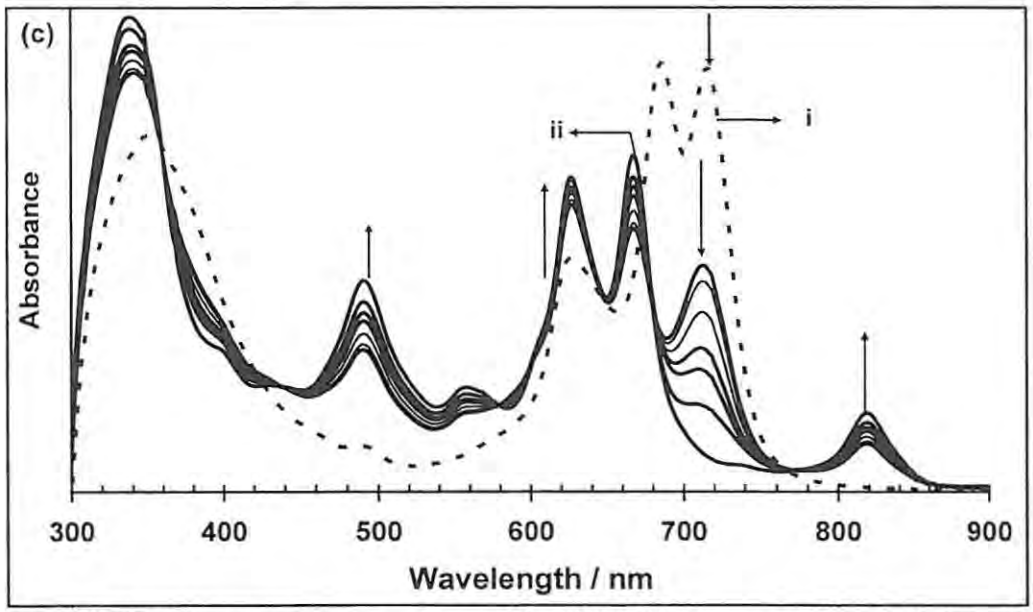

Fig. 3.9c: UV-Visible spectral changes observed for MnTMPyrPc upon addition of imidazole (1 x 10^{-3} M) to solutions of solutions of MnTMPyrPc. (i) is a freshly deaerated solution of MnTMPyrPc and (ii) is the spectrum 10 min after addition of imidazole. The concentration of MnTMPyrPc is ~ 5 x 10^{-6} M.

When the solution was deaerated with dry N_2, the peaks due to Mn^{III} at 719 and 497 nm decreased in intensity accompanied by an increase in the intensity of the peak characteristic of Mn^{II}Pc species at 686 nm, Fig. 3.9a. Also note that the peak at 626 nm (associated with μ-oxo MnPc species) decreased in intensity with time on bubbling nitrogen. No further spectral changes were observed on bubbling nitrogen for prolonged periods, Fig 3.9a (ii) was the final spectrum obtained. Fig. 3.9b shows the spectral changes observed when oxygen was bubbled through the solution formed from Fig. 3.9a (ii). It can be seen that the peak associated with μ-oxo MnPc species adduct increased in intensity relative to the other peaks showing the involvement of molecular oxygen in the transformations of the MnTMPyrPc.

Addition of electron donors such as imidazole is expected to result in the reduction of the μ-oxo dimer. Since as observed in Fig. 3.9a, bubbling nitrogen did not

completely monomerize the dimer, imidazole was added with the aim of converting the dimer to an (imidazole)$_2$MnPc species. Fig. 3.9c shows spectral changes observed on addition of imidazole to the solution of MnTMPyrPc in deaerated solutions. The peak due to the μ-oxo dimer is still observed at 626 nm and peaks at 666 and 820 nm are typical of axially ligated (imidazole)$_2$Mn^{II}Pc species.[408] The peak in the 500 nm region has been observed for both Mn^{II}Pc and Mn^{III}Pc species.[409-411] Addition of imidazole derivatives to (O_2)MnPc has been reported[408] to initially result in the formation of (imidazole)$_2$ Mn^{II}Pc species (with a band at 816 nm) followed by the formation of the μ-oxo dimer, and spectral changes in Fig. 3.9c are consistent with the presence of both μ-oxo dimer and an axially ligated Mn^{II}Pc species. Thus it was not possible to form only the Mn^{II}Pc species.

Beer's law behavior was observed for the Co (**13**) and Zn (**15**) complexes. For the Mn complex, the peak attributed to the Mn^{III}Pc species at 719 nm decreased with concentration to a larger extent than the μ-oxo peak, Fig 3.10. Comparing Fig 3.10b with 3.8b shows that the peak due to Mn^{II}Pc is nonexistent in the former. This may be due to the complicated nature of MnPc complexes which may change from one species to another with time. Fig 3.10b was obtained months after the synthesis of complex **14** while Fig 3.8b was obtained from a freshly prepared complex. Fig 3.10 (a-c) shows the UV-Visible spectral features of the pyrimidin substituted complexes upon dilution in DMF. It can be seen in the case of the Mn complexes that the peak associated with the μ-oxo dimer species persisted in terms of its intensity compared to the other peaks in the spectra.

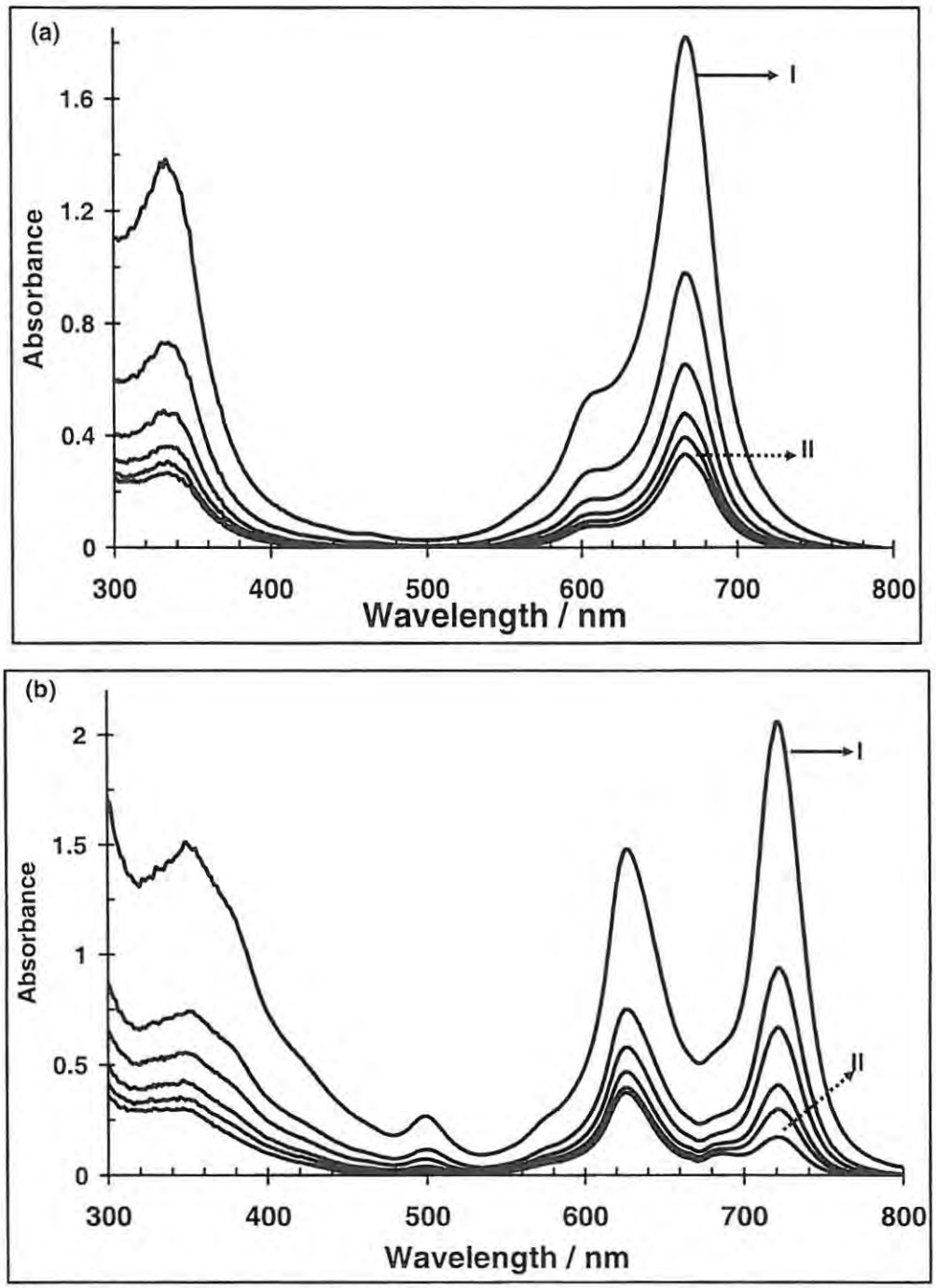

Fig 3.10 (a and b): Changes in the UV-Visible spectra with concentration of complexes **13** (CoTMPyrPc) and **14** (MnTMPyrPc). (i): most concentrated, (ii): least concentrated.

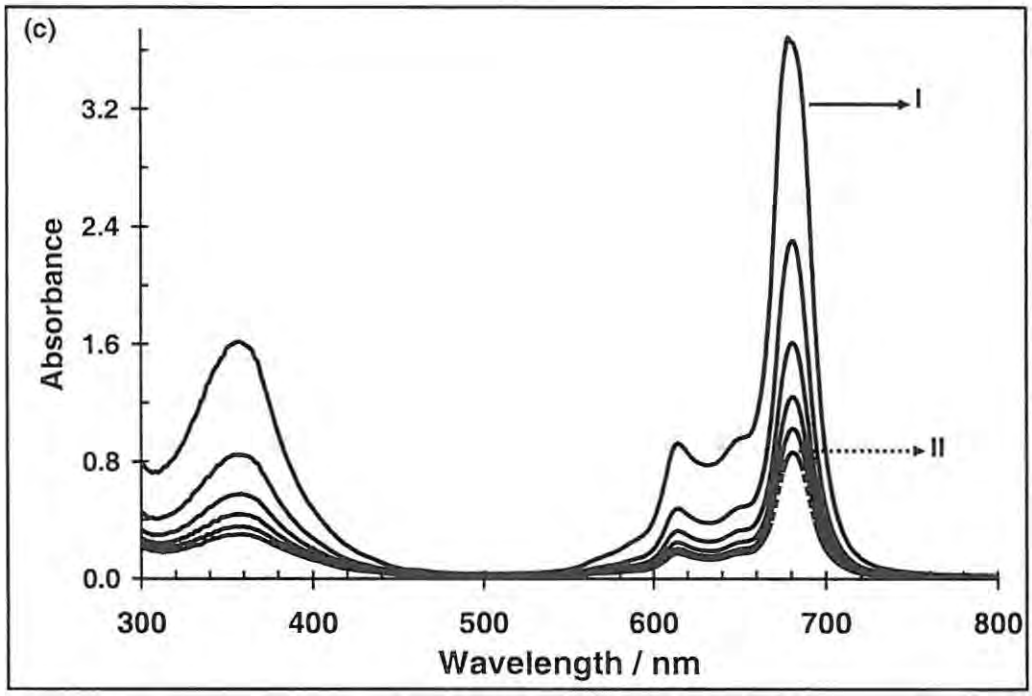

Fig 3.10c: Changes in the UV-Visible spectra with concentration of complex **18** (ZnTMPyrPc). (i): most concentrated, (ii): least concentrated.

3.4 Tetra Substituted Amino-derivatized metallophthalocyanine (MTAPc) Complexes

The precursors for the MTAPc complexes are the tetranitrophthalocyanine complexes **50** and **51** which were synthesized and characterized according to procedures published for the synthesis of the cobalt derivative.[400] The complexes gave satisfactory spectroscopic characterization. The synthetic procedure involved the conversion of 4-nitrophthalimide **(35)** to the chromium or manganese tetranitrophthalocyanine (CrTNPc or MnTNPc) **(50** or **51)** in the presence of chromium chloride (or manganous chloride) and urea, using ammonium molybdate as catalyst (Scheme 3.5).

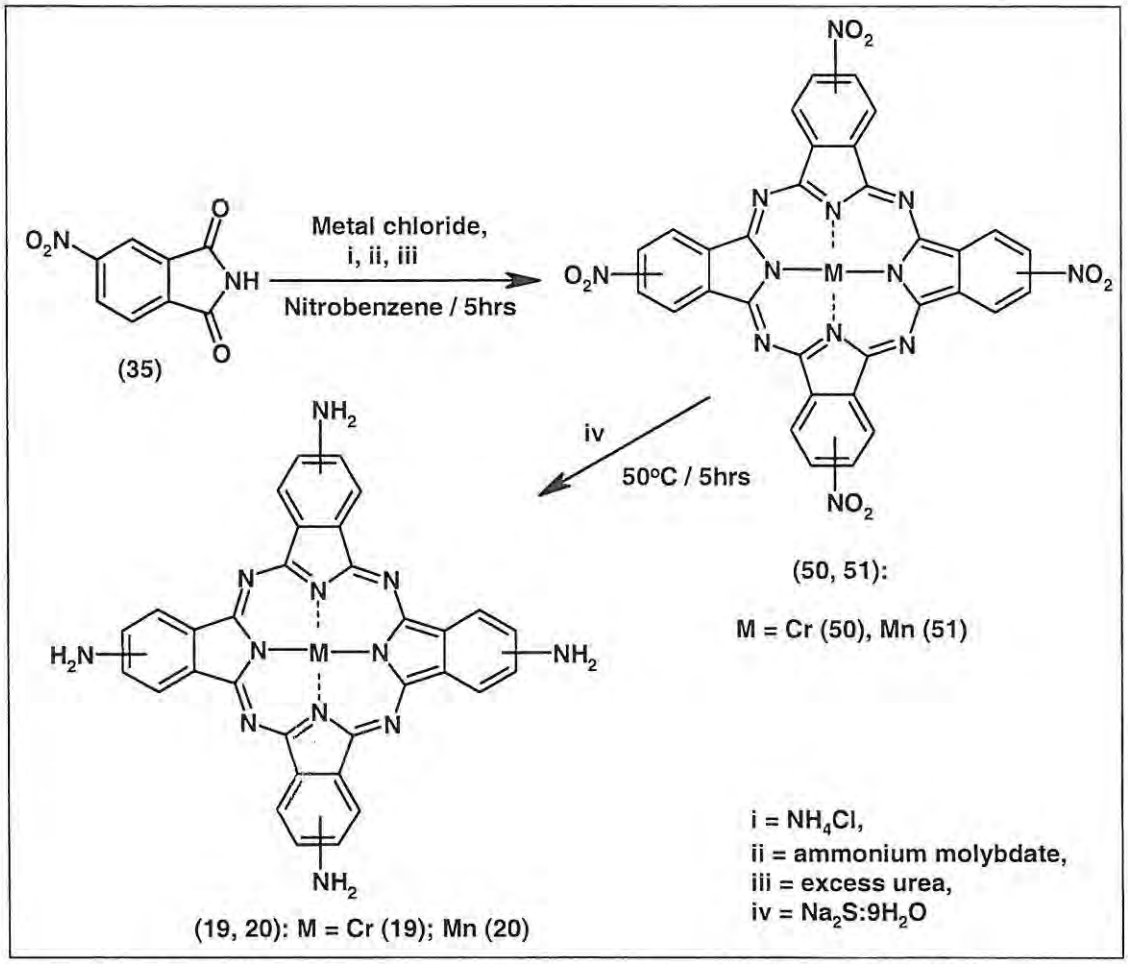

Scheme 3.5: A simplified synthetic route for the preparation of CrTAPc and MnTAPc.

Fig 3.11 shows the UV-Visible spectra of the synthesized chromium, (CrTAPc) **(19),** and manganese, (MnTAPc) **(20),** tetraaminophthalocyanine complexes. The spectrum in Fig 3.11 (curve i) is typical of $Cr^{III}Pc$ species. The band in the 500 nm region has been assigned to ligand to metal charge transfer (LMCT) transition in $Cr^{III}Pc$ complexes.[409] Thus the presence of this band in Fig 3.11 (curve i) suggests that the complex synthesized in this work is the $Cr^{III}TAPc$ species. An OH^- ligand balanced the charge in this molecule to form $(OH)Cr^{III}TAPc$. The presence of OH^- as an axial ligand was confirmed by IR spectra which showed NH vibration at 3442 cm^{-1}, O-H vibration at

3350 cm^{-1} and a Cr-OH vibration at 860 cm^{-1}, Table 3.2. The presence of hydroxide as an axial ligand is an artifact of purification which included treatment with NaOH. The presence of OH as an axial ligand was confirmed by IR as stated above.

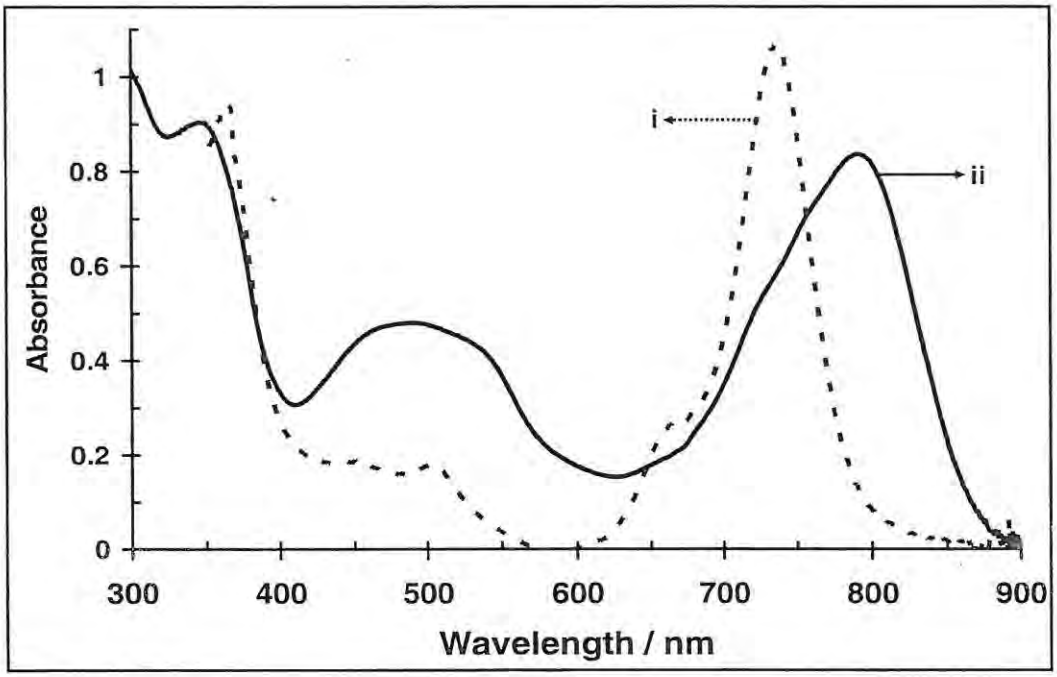

Fig 3.11: UV-Visible spectra of (i) CrTAPc (**19**) and (ii) MnTAPc (**20**) in DMF. Concentration: ~10^{-5} M.

Both complexes, CrTAPc and MnTAPc, were synthesized and purified following the same procedure. The presence of OH^- as an axial ligand is not surprising on the MnTAPc. The IR spectrum which showed NH vibration at 3438 cm^{-1}, OH vibration at 3340 cm^{-1} and a Mn-OH vibration at 870 cm^{-1}, Table 3.2. Therefore the complex synthesized is represented as $(OH)Mn^{III}TAPc$. Fig 3.11 (curve ii) shows the typical UV-Visible spectrum of $(OH)Mn^{III}TAPc$ in de-aerated DMF. The color of the $(OH)Mn^{III}TAPc$ in DMF was reddish-brown. This unusual color may explain the "extended" red shifting of the Q-band of the complex in the UV-Visible spectrum to 780 nm (Fig 3.11 (curve ii)), Table 3.3. The spectrum of the MnTAPc complex is typical[407] of

$Mn^{III}Pc$ complexes with a red-shifted Q band, and a band near 500 nm. The presence of a band in the 500 nm region before reduction suggests that the oxidation state of the central metal is + 3, hence the complex synthesized may be represented as $(OH)Mn^{III}TAPc^{-2}$.

Chapter Four

Electrochemical Properties

In this chapter, the electrochemical characterizations of the synthesized metallophthalocyanine complexes are discussed in detail. The techniques employed for the characterization include: cyclic voltammetry (CV) and Osteryoung square wave voltammetry (OSWV). Also spectroelectrochemistry was used to further confirm the assignments of the redox processes based on the results obtained from the CV and OSWV. The experimental set-ups are as described in Chapter Two under electrochemical techniques.

4.1 Pyrrole Substituted Metallophthalocyanine Complexes (7-12)

4.1.1 Cyclic and square wave voltammetry

Fig 4.1 shows the cyclic voltammograms of the prepared pyrrole substituted phthalocyanine (TPhPyPc) complexes of Co (**7**), Fe (**8**), Mn (**9**), Ni (**10**) and Zn (**11**) in DMF containing 0.1 M TEAP. Table 4.1 summarizes the redox potential values for all the examined phenoxypyrrole and pentoxypyrrole substituted MPc complexes. Three redox processes labelled **I**, **II** and **III** are observed in the case of CoTPhPyPc (**7**) (Fig 4.1a). It is known that the electrochemical behaviour of cobalt phthalocyanine complexes is dependent on the media and that in coordinating solvents such as DMF, the first oxidation process occurs at the central metal[407] and it is irreversible.[407-412] Thus, the process labelled **I** observed at 0.75 V (vs. Ag|AgCl) is due to metal oxidation and the formation of Co^{III}TPhPyPc species. The two redox couples labelled **II** and **III** observed at - 0.13 V and - 1.19 V (vs. Ag|AgCl), respectively, may be assigned to $Co^{II}TPhPyPc^{-2}/Co^{I}TPhPyPc^{-2}$ and to $Co^{I}TPhPyPc^{-2}/Co^{I}TPhPyPc^{-3}$ in comparison with literature data.[407] For these redox couples, the cathodic to anodic peak currents are near unity, but cathodic to anodic peak separations (ΔE) are 150 mV (**III**) and 200 mV (**II**), suggesting quasi-reversible behaviour. Also, the peak currents increased linearly with the square root of scan rates, for scan rates ranging from 50 to 800 mVs^{-1} suggesting diffusion controlled electrode process. The oxidation of the pyrrole groups attached to macrocyclic N_4 ligands has been reported to be near 1.0 V (vs. SCE) in several solvents[399,403-405] and for complex

7, the pyrrole oxidation peak was observed it at a potential around 1.2 V (vs. Ag|AgCl) as indicated by the peak labelled (*) in the OSWV (Fig 4.1a). label

Table 4.1: Redox potentials $E_{1/2}$ E_{pa}/V (vs. Ag|AgCl) for CoTPhPyPc, FeTPhPyPc, MnTPhPyPc, NiTPhPyPc, ZnTPhPyPc and CoTPOPyPc complexes measured in DMF containing 0.1 M TEAP solution. Electrode: GCE. Scan rate = 100 mVs^{-1}.

Complex	Couple **I** $M^{III}Pc^{-2}$ / $M^{II}Pc^{-2}$	Couple **II** $M^{II}Pc^{-2}/M^{II}Pc^{-3}$[a] $(M^{II}Pc^{-2}/M^{I}Pc^{-2})$[b]	Couple **III** $M^{II}Pc^{-3}/M^{II}Pc^{-4}$[a] $(M^{I}Pc^{-2} / M^{I}Pc^{-3})$[b]	Other processes
CoTPhPyPc (7)	0.75[c]	- 0.13	- 1.19	1.2: Pyrrole
FeTPhPyPc (8)	0.37	- 0.33	- 0.87	
MnTPhPyPc (9)	0.15	- 0.65	- 1.23	
NiTPhPyPc (10)		- 0.53	- 0.88	
ZnTPhPyPc (11)		- 0.53	- 0.88	
CoTPOPyPc (12)	0.34	- 0.52		0.76: $Co^{III}Pc^{-1}/Co^{III}Pc^{-2}$, 0.98: Pyrrole

[a]observed for Mn^{II}, Ni^{II} and Zn

[b]observed for Co^{II}, and Fe^{II} species

[c]E_{pa} since the redox process is irreversible

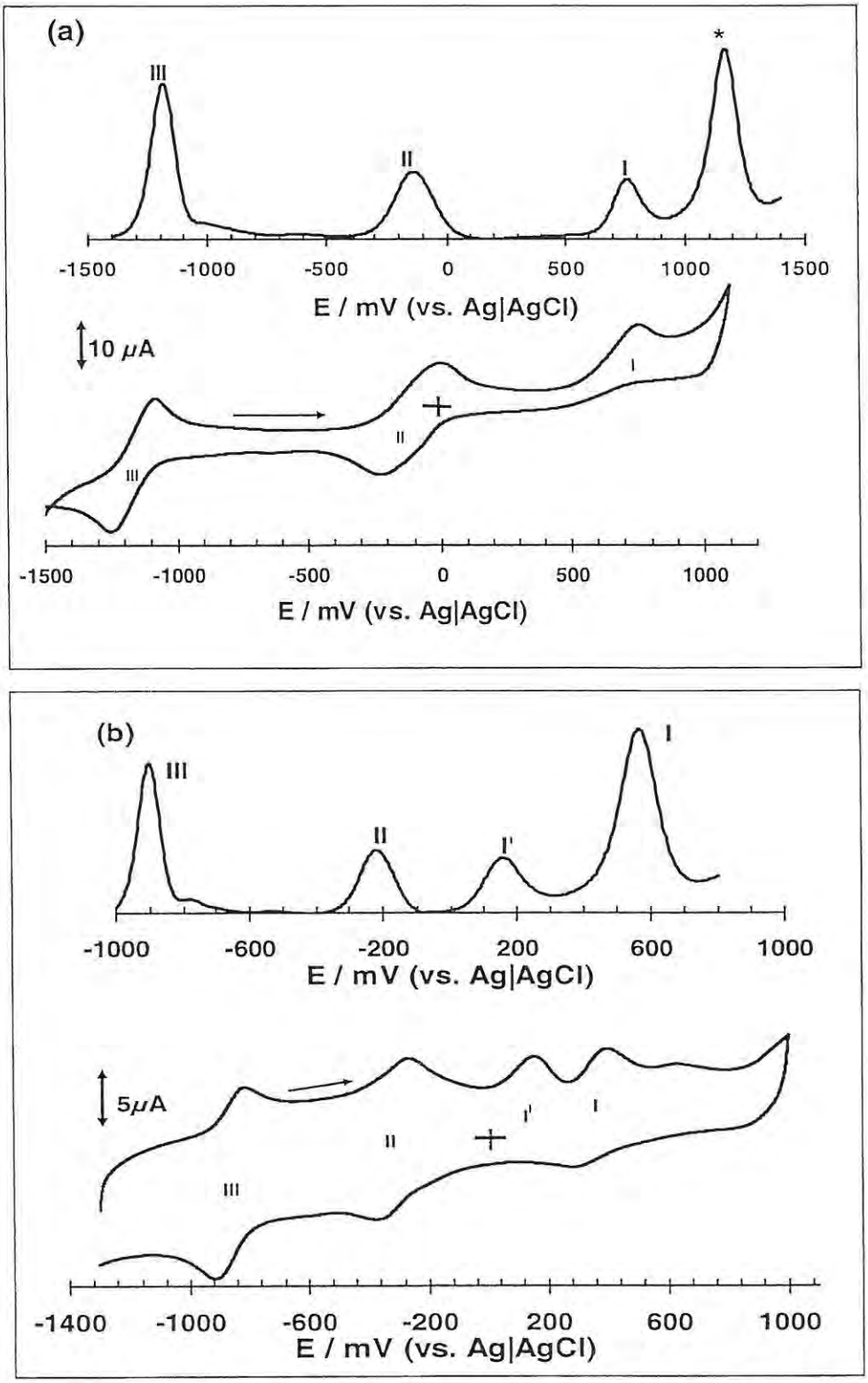

Fig 4.1 (a and b): Cyclic voltammograms of (a) CoTPhPyPc (**7**) and (b) FeTPhPyPc (**8**) in DMF containing 0.1 M TEAP. Scan rate = 100 mVs^{-1}, concentration = ~1 x 10^{-4} M. Electrode: GCE. Curves above the CVs are the square wave voltammograms.

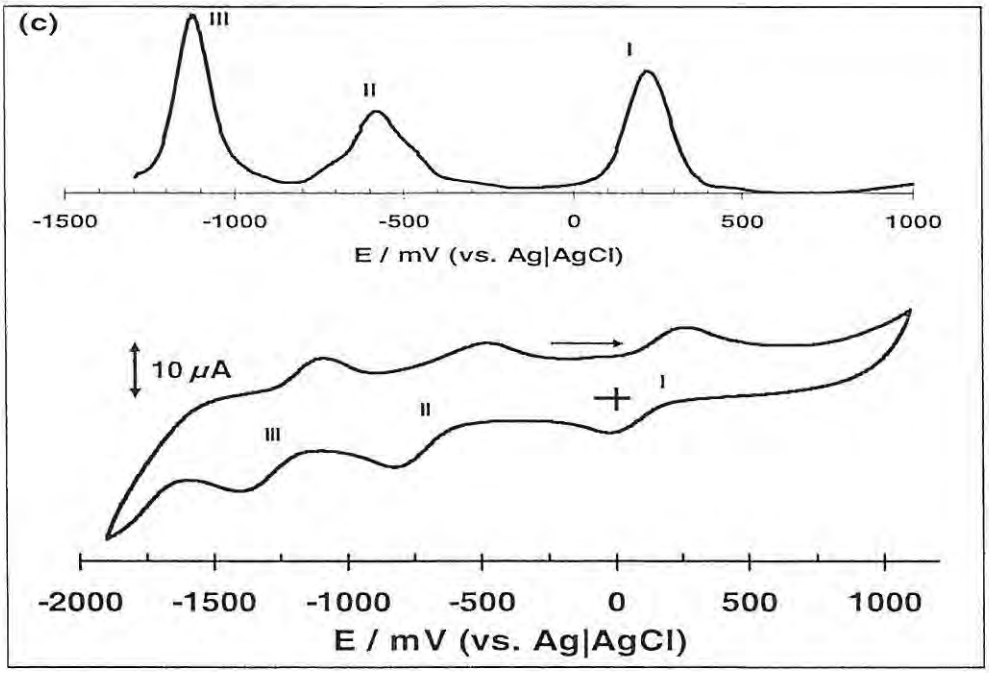

Fig 4.1c: Cyclic voltammograms of MnTPhPyPc, **9** in DMF containing 0.1 M TEAP. Scan rate = 100 mVs^{-1}, concentration = ~1 x 10^{-4} M. Electrode: GCE. The curve above the CV is the square wave voltammogram for complex **9** under the same condition at the CV.

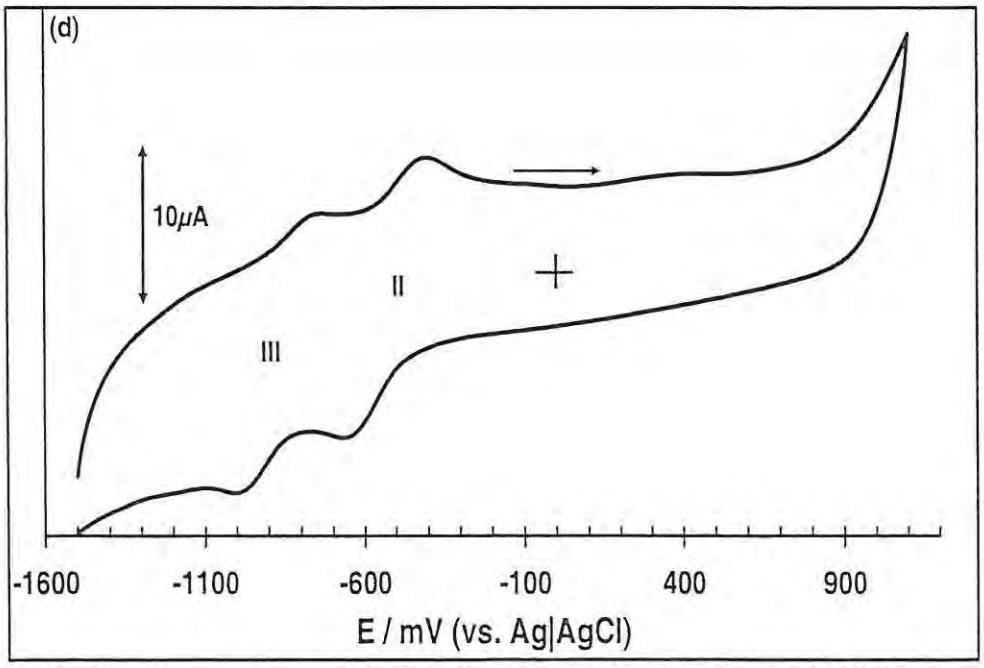

Fig 4.1d: Cyclic voltammograms of NiTPhPyPc, **10** in DMF containing 0.1 M TEAP. Scan rate = 100 mVs^{-1}, concentration = ~1 x 10^{-4} M. Electrode: GCE.

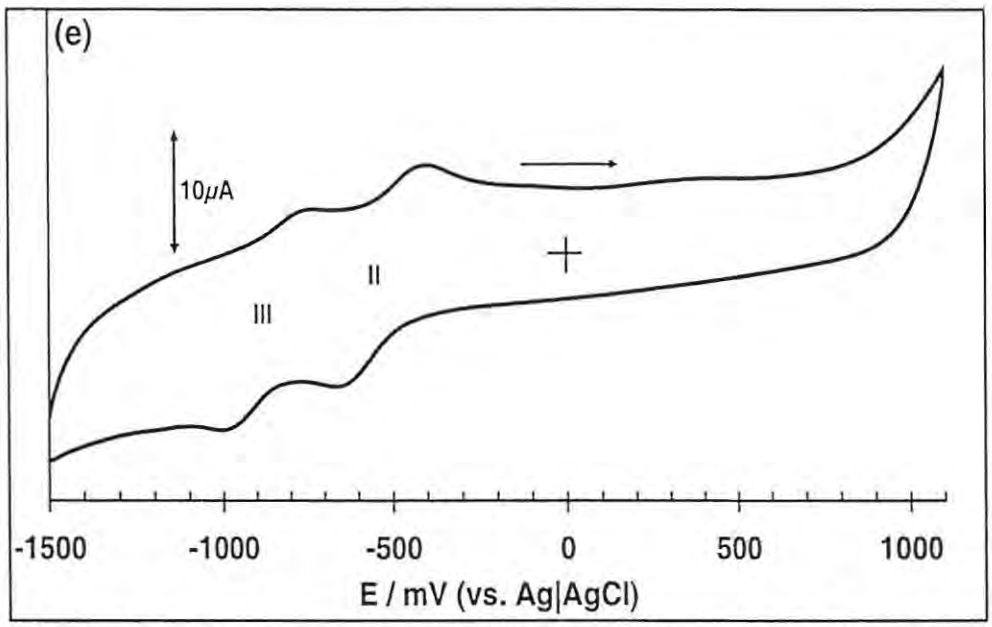

Fig 4.1 (e): Cyclic voltammograms of ZnTPhPyPc (**11**) in DMF containing 0.1 M TEAP. Scan rate = 100 mVs^{-1}, concentration = ~1 x 10^{-4} M. Electrode: GCE.

Fig 4.1b shows the cyclic and square wave voltammograms of the iron complex, FeTPhPyPc (**8**). As shown in Chapter Three, this complex is highly aggregated, and will be more aggregated at the concentrations used for cyclic voltammetry, hence the observed voltammetric peaks in Fig 4.1b are mainly due to the aggregated species, with some contribution from the monomeric component. As observed for the cobalt complex, three main redox processes (**I** to **III**) are observed for FeTPhPyPc. The oxidation process **I** (at 0.37 V) shows a return peak, which is weaker than the forward one. It can be assigned to the $Fe^{III}TPhPyPc^{-2}/Fe^{II}TPhPyPc^{-2}$ process, since it is the potential range for Fe^{II} oxidation in phthalocyanine complexes.[407] The origin of the weak peak negative of the anodic component of process **I**, (labelled **I'**) cannot be easily assigned, but it is noticeable that it decreased in intensity upon repeated successive scans. Couples **II** and **III** observed at - 0.33 V and - 0.89 V (vs. Ag|AgCl), respectively are found to be reversible with the ratio of cathodic to anodic peak currents being near unity, and

cathodic to anodic peak separation (ΔE) of 100 mV, (ΔE = for 90 mV ferrocene/ferrocenium couple). They can be assigned to $Fe^{II}TPhPyPc^{-2}/Fe^{I}TPhPyPc^{-2}$ and $Fe^{I}TPhPyPc^{-2}/Fe^{I}TPhPyPc^{-3}$, respectively, in comparison with literature data.[404]

Figs 4.1 (c-e) show cyclic voltammograms of MnTPhPyPc, NiTPhPyPc and ZnTPhPyPc complexes, respectively. In the case of MnTPhPyPc (**9**) (Fig 4.1c), three clearly defined redox couples (**I** to **III**) are observed. Mn^{II}-Pc complexes are known to undergo redox activity both at the metal and at the ring. They are readily oxidized,[404] at oxidation potentials ranging from 0.1 V to – 0.23 V (vs. SCE). Thus, couple **I** at 0.15 V (vs. Ag|AgCl) can be assigned to the $Mn^{III}TPhPyPc^{-2}/Mn^{II}TPhPyPc^{-2}$ redox process. As will be shown later, spectroelectrochemistry confirmed this assignment. Couples **II** (- 0.65 V vs. Ag|AgCl) and **III** (- 1.23 V vs. Ag|AgCl), Table 4.1, can be assigned to $Mn^{II}TPhPyPc^{-2}/Mn^{II}TPhPyPc^{-3}$ and $Mn^{II}TPhPyPc^{-3}/Mn^{II}TPhPyPc^{-4}$ respectively. These assignments will be confirmed below using spectroelectrochemistry.

For the nickel complex NiTPhPyPc **(10)** (Fig 4.1d), all the observed couples are ring based since the central metal is known[407] to be electrochemically inactive for nickel phthalocyanine complexes. Thus, couples **II** (- 0.53 V) and **III** (- 0.88 V) in Fig 4.1d can be assigned to $Ni^{II}TPhPyPc^{-2}/Ni^{II}TPhPyPc^{-3}$ and $Ni^{II}TPhPyPc^{-3}/Ni^{II}TPhPyPc^{-4}$, respectively. Zinc phthalocyanine complexes are also not known to show redox activity at the central metal. Hence, the redox couples observed for ZnTPhPyPc (**II**, - 0.53 V) in Fig 4.1e are associated with ring based processes, $Zn^{II}TPhPyPc^{-2}/Zn^{II}TPhPyPc^{-3}$ (**II**) and $Zn^{II}TPhPyPc^{-3}/Zn^{II}TPhPyPc^{-4}$ (**III**, - 0.88 V), respectively. All the observed redox couples showed quasi-reversible behaviour.

The electrochemical behaviour of the pentoxypyrrole substituted CoPc (CoTPOPyPc, **12**) was also investigated. It was found that the complex was soluble in DCM and most organic solvents such as DMSO, THF and chloroform. Fig 4.2 shows the typical cyclic voltammogram obtained for complex **12** in de-aerated DMF containing 0.1 M $TBABF_4$ at a glassy carbon electrode (GCE).

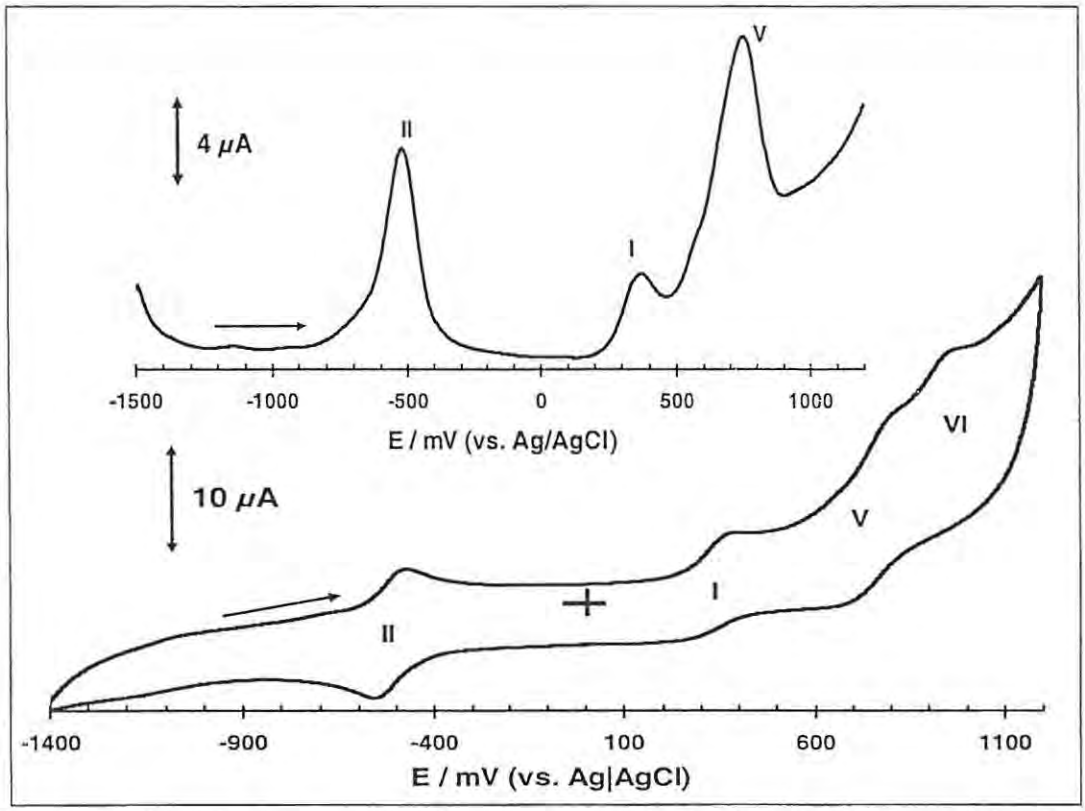

Fig 4.2: Cyclic and square wave voltammograms of CoTPOPyPc in DMF containing 0.1 M $TBABF_4$. Scan rate = 100 mVs^{-1}.

Four redox processes labelled **I, II, V** and **VI** are observed (Fig 4.2). Table 4.1 lists the redox potentials. The quasi-reversible process labelled **I** (0.34 V) is observed at potentials typical for metal oxidation in $Co^{II}Pc$ complexes in coordinating solvents such as DMF[404] and is thus assigned to $Co^{III}TPOPyPc^{-2}/Co^{II}TPOPyPc^{-2}$ redox process. The oxidation process labelled **V** ($E_{½}$ = 0.76 V) is due to the first ring oxidation and is

assigned to $Co^{III}TPOPyPc^{-1}/Co^{III}TPOPyPc^{-2}$ in comparison with literature.[404,409] The redox couple labelled **II** observed at $E_{½}$ = - 0.52 V vs. Ag|AgCl is assigned to $Co^{II}TPOPyPc^{-2}/Co^{I}TPOPyPc^{-2}$ in comparison with literature[407] while **VI** has been assigned to the pyrrole oxidation redox process.[399,405,413,414] Process **II** exhibited reversible behaviour, whereas **I** and **V** were quasi-reversible in that the anodic to cathodic peak separation (ΔE) for couple **II** was 90 mV (ΔE = 90 for ferrocene/ferrocenium couple) while for couple **V**, ΔE was 156 mV (vs. Ag|AgCl). The anodic to cathodic peak ratios for the redox couples were near unity for **II**. Fig 4.2 also shows the square wave voltammogram (SWV) of CoTPOPyPc obtained under the same conditions as the CV, which clearly shows the three couples due to CoTPOPyPc (**12**). The peak currents increased linearly with the square root of scan rate for the scan rates ranging from 50 mVs^{-1} to 500 mVs^{-1}, confirming diffusion-controlled processes.

4.1.2 Spectroelectrochemistry

Spectroelectrochemistry experiments using optically transparent thin layer electrochemical (OTTLE) cell were performed to provide further insight into the nature of the redox activity observed by cyclic voltammetry. Fig 4.3a shows the UV-Visible spectral changes observed during controlled potential reduction of $Co^{II}TPhPyPc^{-2}$ complex at - 0.4 V (vs. Ag|AgCl), which is more negative than the potential value of the first reduction process (**II**) in Fig 4.1a. It is noticeable that the Q band centered at 665 nm decreases in intensity, while new bands at 700 nm and 475 nm appear. See Table 4.2 for the list and assignment of UV-Visible data.

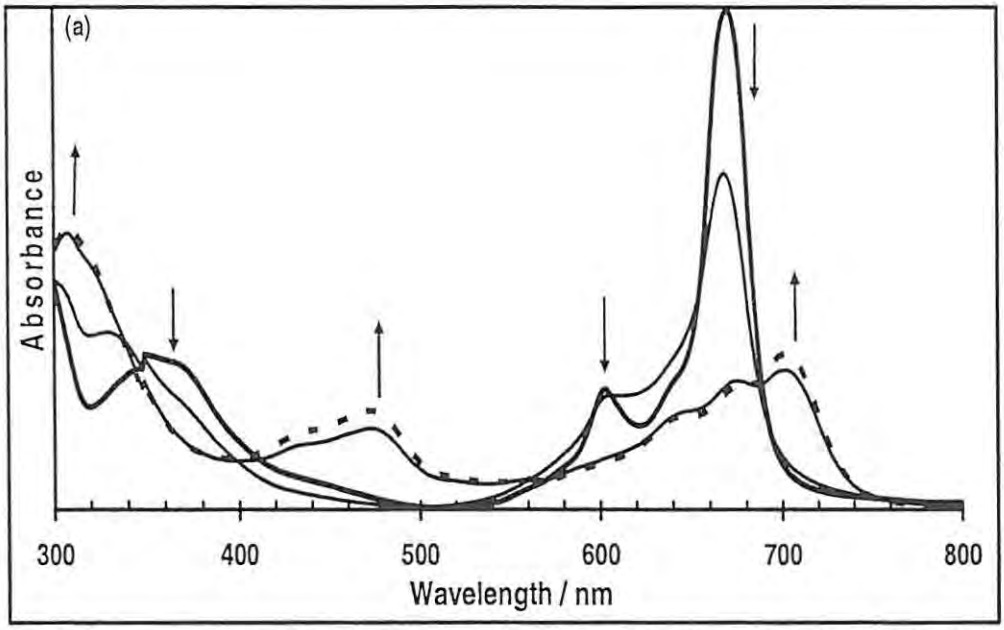

Fig 4.3a: Spectroscopic changes during controlled potential electrolysis (OTTLE) of complex CoTPhPyPc (7) in DMF containing 0.1 M TEAP. Applied potential = - 0.4 V (vs. Ag|AgCl), concentration ~ 1 x 10^{-5} M. In all cases the spectral were recorded while continuously applying the specified potential.

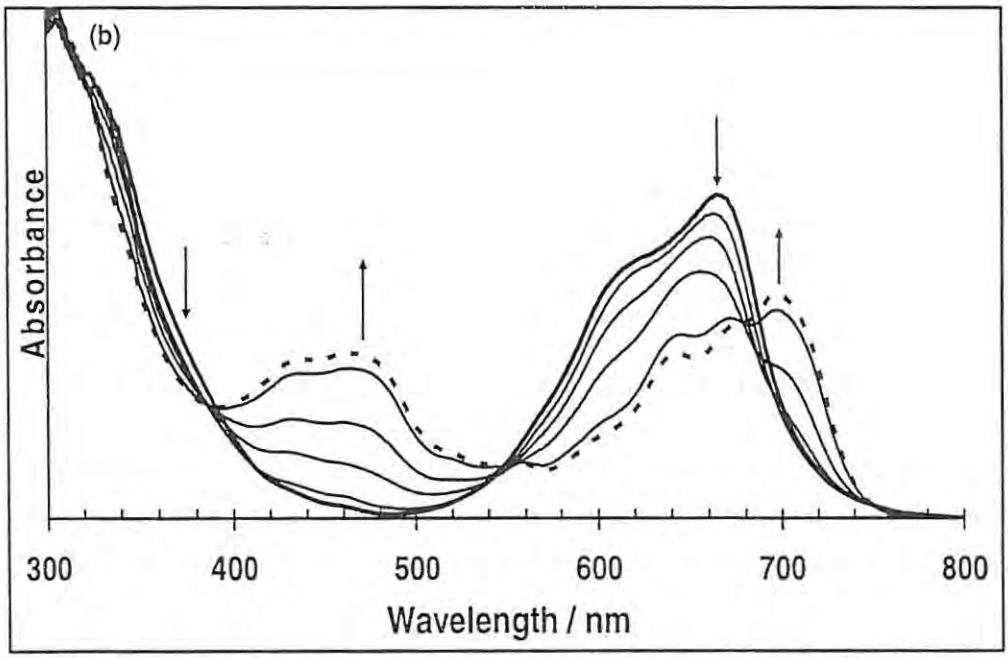

Fig 4.3b: Spectroscopic changes during controlled potential electrolysis (OTTLE) of complex CoTPhPyPc (7) in DMF containing 0.1 M TEAP. Applied potential = - 0.4 V (vs. Ag|AgCl), concentration ~ 1 x 10^{-4} M. In all cases the spectra were recorded while continuously applying the specified potential.

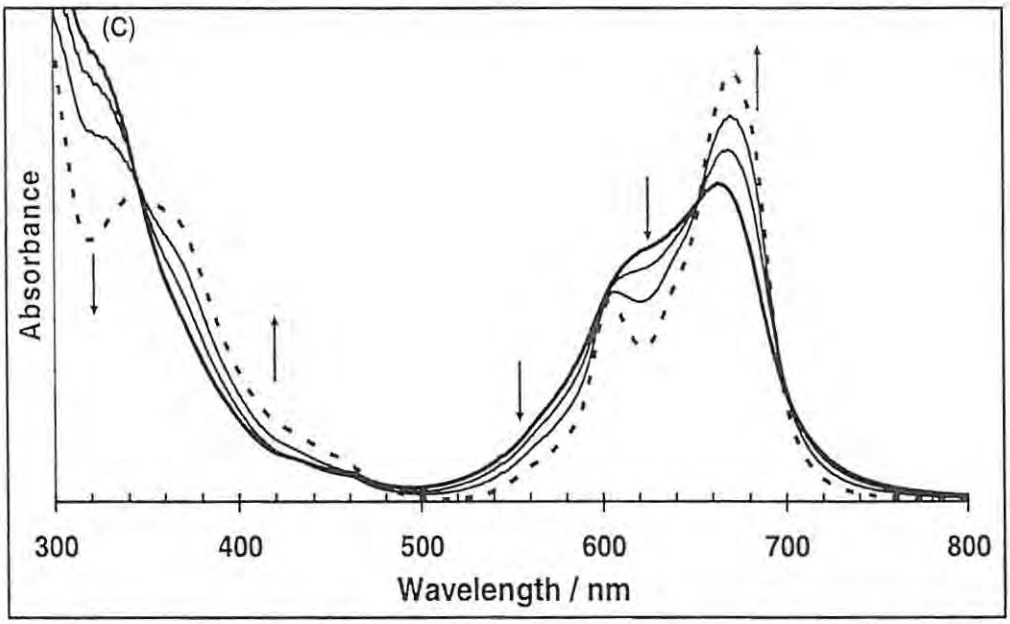

Fig 4.3c: Spectroscopic changes during controlled potential electrolysis (OTTLE) of complex CoTPhPyPc (7) in DMF containing 0.1 M TEAP. Applied potential = + 0.9 V (vs. Ag|AgCl) and concentration ~ 1 x 10^{-4} M. In all cases the spectra were recorded while continuously applying the specified potential.

The band at 475 nm is typical[409,415] of the formation of reduced $Co^{I}Pc^{-2}$ species and it is then assigned to a metal-to-ligand charge transfer. The Q band for Co^{I}-Pc species is generally weaker than that of the Co^{II} and it is red shifted, hence the absorption at 700 nm is due to the Q band for the $Co^{I}TPhPyPc^{-2}$ species. It can also be observed that the formation of the $Co^{I}TPhPyPc^{-2}$ species is accompanied by diffuse isosbestic points. This could be due to the presence of isomers or some aggregation in the complex. The number of moles of electrons transferred was found to be near unity, confirming a one electron reduction process. The application of 0 V (vs. Ag|AgCl) resulted in > 90 % regeneration of the spectra of the starting species, hence showing that the reduction of $Co^{II}TPhPyPc^{-2}$ complex is reversible.

Table 4.2: Summary of absorption maxima (λ_{max}) of the various central metal oxidation states of the MPc complexes in DMF + TEAP (or $TBABF_4$).

Complex	λ_{max}/nm ($M^{I}Pc^{-2}$)	Q-band λ_{max}/nm ($M^{II}Pc^{-2}$)	λ_{max}/nm ($M^{III}Pc^{-2}$)	λ_{max}/nm ($M^{IV}Pc^{-2}$)
CoTPhPyPc (**7**)	475, 700	665	670	
CoTPOPyPc (**12**)		670		
CoTETPc (**16**)	450, 701[a]	673	680	
CoTMPyrPc (**13**)	478, 709	671[b]	676	
CrTAPc (**19**)		720	502, 735	668, 741
FeTPhPyPc (**8**)	670	665		
MnTAPc (**20**)		710	500, 780	667
MnTETPc (**17**)		682	500, 723	
MnTMPyrPc (**14**)		687	500, 720	
MnTPhPyPc (**9**)		680	497, 720	
NiTPhPyPc (**10**)		671		
ZnTETPc (**18**)		676		
ZnTMPyrPc (**15**)		678		
ZnTPhPyPc (**11**)		678		

[a]Spectra not shown in this thesis.

[b]Note a small shift in the presence of electrolyte compared to Table 3.3.

Fig 4.3b shows that for high CoTPhPyPc concentrations, considerable aggregation of the complex is observed. However, bands due to the reduced Co^{I} species are still evident. Fig 4.3c shows the UV-Visible spectroscopic changes observed upon oxidation of a concentrated solution of CoTPhPyPc at the potential related to couple (**I**). Before oxidation, two bands are observed in the Q band region at 617 and 665 nm, related to the dimeric and monomeric components, respectively. Upon oxidation, the monomer band is enhanced and red shifted to 670 nm Table 4.2. Such behavior is typical[409,415] of metal

based oxidation in cobalt phthalocyanine complexes. Thus the final spectrum in Fig 4.3c is assigned to $Co^{III}TPhPyPc^{-2}$. Electrolysis at 0 V (vs. Ag|AgCl) showed that this species could not be completely reduced back to the starting complex, confirming the lack of complete reversibility observed by cyclic voltammetry. Thus spectroelectrochemistry confirmed the CV assignments.

Controlled potential electrolysis at - 0.6 V (Ag|AgCl), a potential more negative than the first reduction couple (couple **II**, Fig. 4.1(b)) of FeTPhPyPc complex, resulted in spectral changes shown in Fig 4.4a. The spectrum is different from Fig 3.2b in that the peak for aggregate at 636 nm is almost the same height as the monomer at 665 nm. The spectra of FePc complexes are also complicated as is the case with MnPc species. The spectra can be affected by ions in solution such as electrolytes. The peak due to the aggregated species (at 636 nm) decreases with electrolysis time. While the peak due to the monomer increases and shifts to 670 nm, Table 4.2. The observed spectral changes can be assigned to the formation of monomeric species, accompanied by reduction of $Fe^{II}Pc$ to $Fe^{I}Pc$. Reduction of $Fe^{II}Pc$ to $Fe^{I}Pc$ has not been fully documented. The lack of decrease in the Q-band, upon reduction of FePc species is not surprising since metal based reduction is not expected to drastically affect the π system of the MPc macrocycle. Thus reduction results in the formation of the $Fe^{I}TPhPyPc^{2-}$ species, confirming the CV assignment.

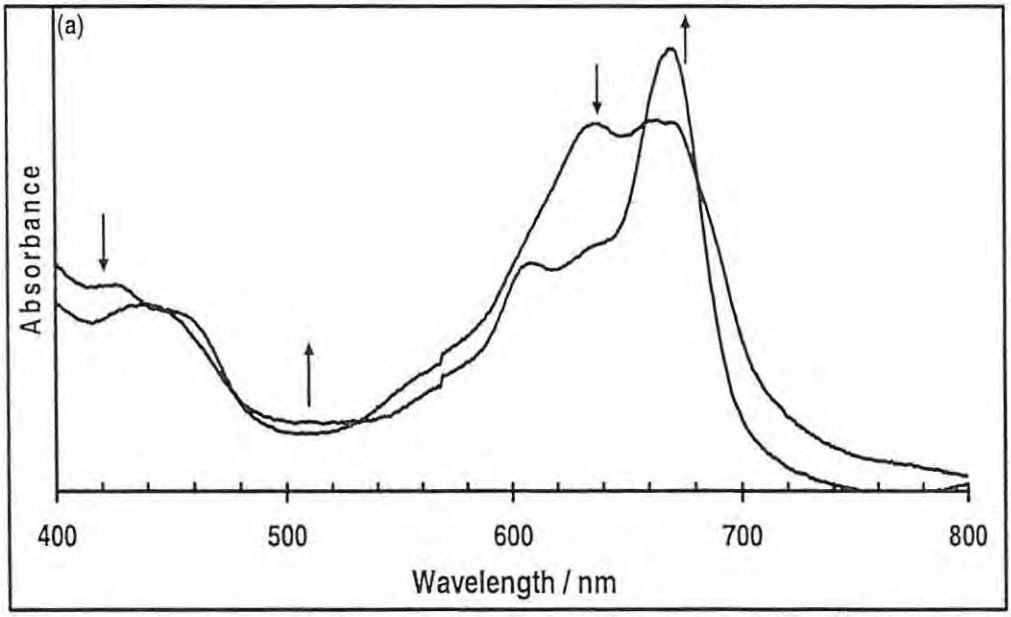

Fig 4.4a: Spectroscopic changes during controlled potential electrolysis (OTTLE) of complex FeTPhPyPc (**8**) in DMF containing 0.1 M TEAP. Applied potential: - 0.6 V (vs. Ag|AgCl). Concentration: ~ 1 x 10^{-5} M. In all cases the spectra were recorded while continuously applying the specified potential.

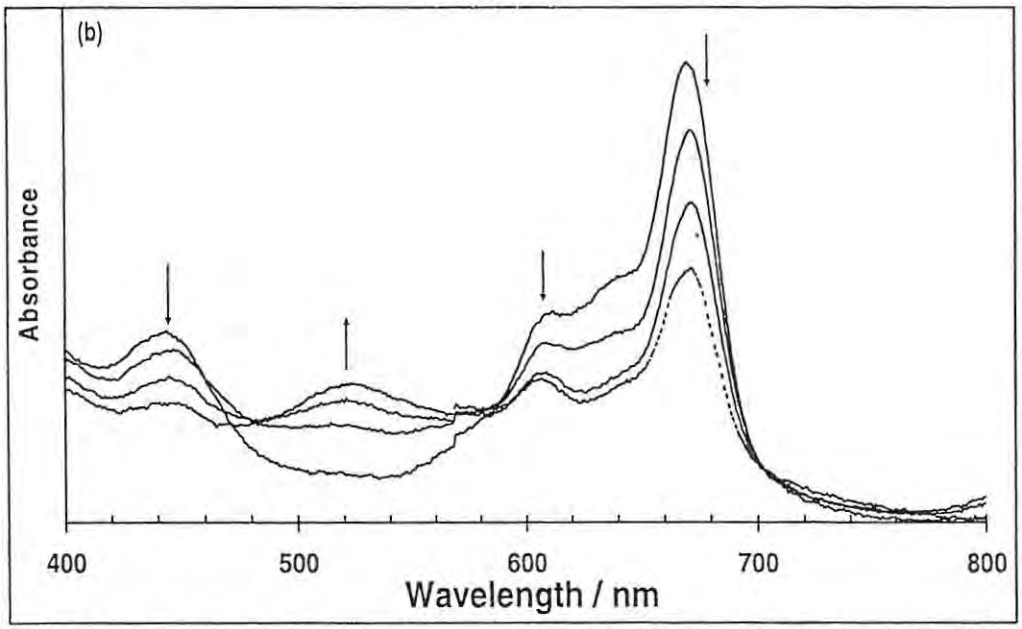

Fig 4.4b: Spectroscopic changes during controlled potential electrolysis (OTTLE) of complex FeTPhPyPc (**8**) in DMF containing 0.1 M TEAP. Applied potential: - 1.0 V. Concentration: ~ 1 x 10^{-5} M. In all cases the spectra were recorded while continuously applying the specified potential.

Further reduction of the Fe species, (following the final reduction in Fig 4.4a), at - 1.0 V (vs. Ag|AgCl) at potentials of couple **III** resulted in spectral changes shown in Fig 4.4b. The first spectrum in 4.4b is same as the last spectrum in 4.4a. A relatively strong peak appeared at 529 nm and a weaker one at around 600 nm, Fig 4.4b. It is known that the first ring reduction in unsubstituted metallophthalocyanine complexes is accompanied by absorption bands between 550 and 650 nm,[415] (spectra not shown). Thus, the new formed species is most likely the $Fe^{I}TPhPyPc^{-3}$ complex confirming CV assignments.

Fig 4.5a shows spectral changes observed during the controlled potential reduction of $Mn^{III}TPhPyPc$ complex (**9**) at - 0.2 V (vs. Ag|AgCl), more negative of the redox potential of couple **I** (Fig 4.1c). The Q band shifts from 720 to 680 nm. This observed spectral change is consistent with the reduction of Mn^{III} in phthalocyanine complex[406] and the formation of the $Mn^{II}TPhPyPc^{-2}$ species. Reduction at potential of couple **II** resulted in only small spectral changes in the bands around 500 nm indicating the formation of the monoanion reduced $Mn^{II}Pc^{-3}$ species[415] (spectra not shown). The first reduction in $Mn^{II}Pc^{-2}$ complexes has been a subject of some controversy, with some reports proposing ring reduction to the $Mn^{II}Pc^{-3}$ species and others suggesting metal reduction to the $Mn^{I}Pc^{-2}$ species.[407] It has been proposed that in non-coordinating solvents reduction to $Mn^{II}Pc^{-3}$ occurs, while in coordinating solvents $Mn^{I}Pc^{-2}$ is formed.[407] DMF, used as a solvent in this work, is a coordinating solvent even though spectroelectrochemistry proves the formation of the $Mn^{II}Pc^{-3}$. It needs to be pointed out that only a small dependence of the reduction potential for the $Mn^{II}Pc^{-2}$ on the nature of solvent has been observed.[407]

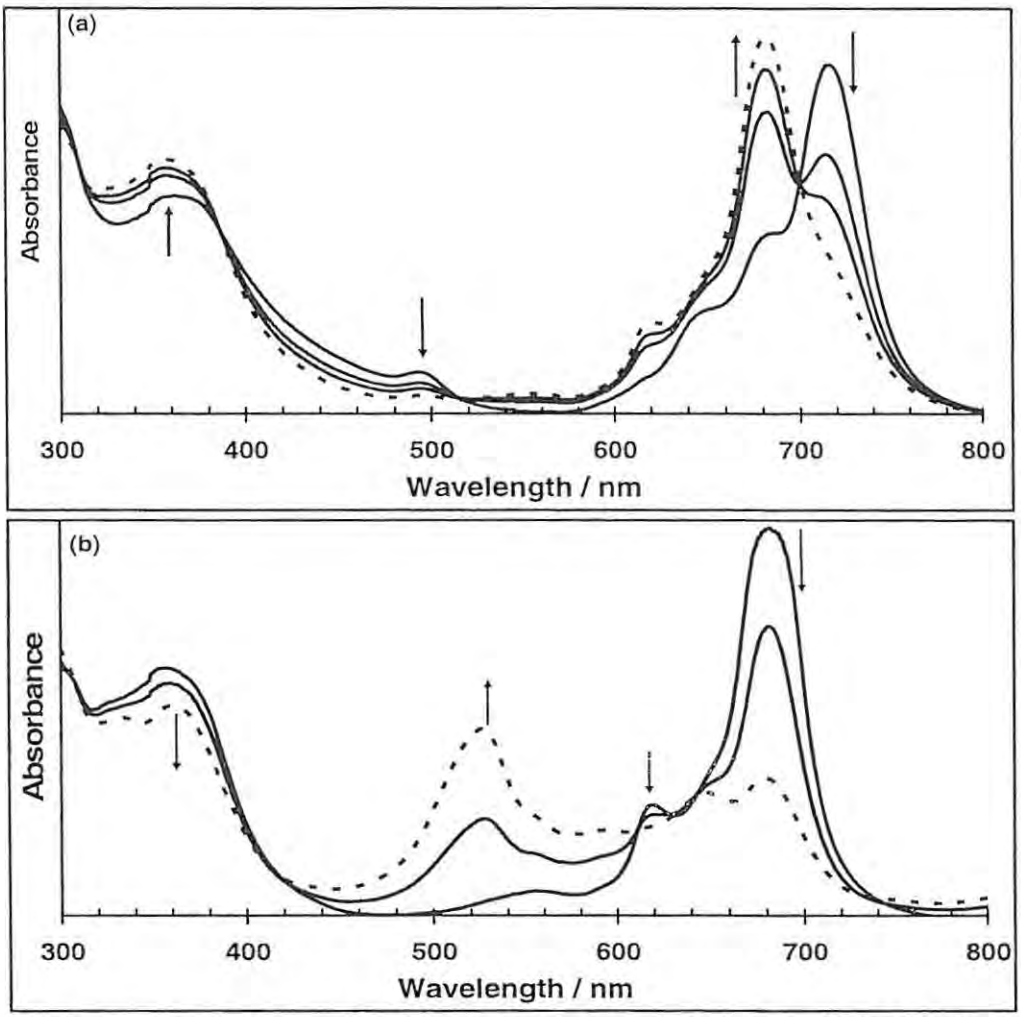

Fig 4.5: Spectroscopic changes during controlled potential electrolysis (OTTLE) of complex MnTPhPyPc (**9**) in DMF containing 0.1 M TEAP. Applied potential for (a) = - 0.2 V and (b) = - 1.3 V (vs. Ag|AgCl). Concentration: ~ 1 x 10^{-5} M. The first spectrum in (b) is similar to the last one in (a). The spectra were recorded while continuously applying the specified potential.

Further reduction at - 1.3 V (vs. Ag|AgCl), the redox potentials of couple **III**, (Fig 4.1c) resulted in a more pronounced modifications of the spectral features as it can be observed in Fig 4.5b. The reduction of $Mn^{II}TPhPyPc^{-2}$ at - 1.3 V resulted in the decrease in the Q band and the formation of new bands at 525 and 595 nm. The lowering in intensity of the Q band is typical behaviour for ring-based reduction in M-Pc complexes and the formation of $Mn^{II}Pc^{-4}$.[415] Thus, results presented in Fig 4.5b clearly confirm the

ring based reduction in the manganese complex and the formation of the $Mn^{II}TPhPyPc^{4-}$ species and confirms the CV results. The reductions were reversible since application of 0 V regenerated the original spectra.

Finally, Fig. 4.6 shows the spectral changes observed on controlled potential reduction of the nickel complex at - 1.0 V (vs. Ag|AgCl). The starting spectrum in Fig 4.6 is different from that in Fig 3.2b (curve iv), due to higher aggregation of the complex expected for concentrations used in this experiment. The spectral changes in Fig 4.6 consisted of the formation of bands which have been reported for $Ni^{II}Pc^{-3}$ species.[415] The low intensity of the new bands, relative to the spectra of the starting species, confirms that they are due to ring reduction.

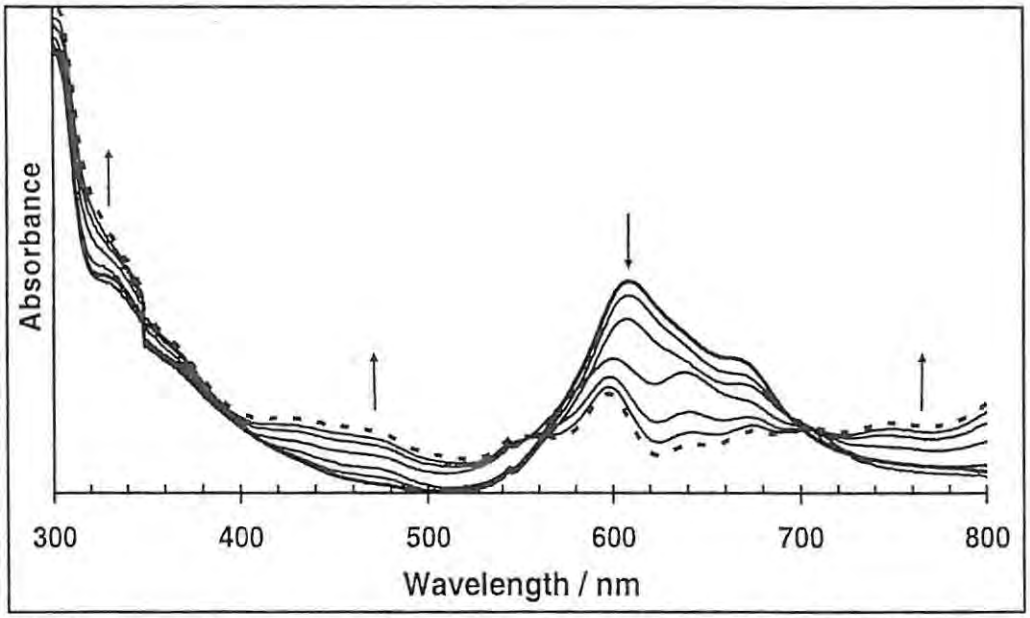

Fig 4.6: Spectroscopic changes during controlled potential electrolysis (OTTLE) of complex NiTPhPyrPc, in DMF containing 0.1 M TEAP. Applied potential: – 1.0 V (vs. Ag|AgCl). Concentration: ~ 1 x 10^{-4} M.

4.2 Mercaptopyrimidin Substituted Metallophthalocyanine Complexes (13-15)

4.2.1 Cyclic voltammetry and square wave voltammetry

Figs 4.7 (a - c) show typical cyclic and Osteryoung square wave voltammograms for complexes **13, 14** and **15** in de-aerated DMF containing 0.1 M $TBABF_4$ at a glassy carbon electrode (GCE). Five redox processes labelled **I-V** are observed in the case of CoTMPyrPc, **13,** (Fig 4.7a). Table 4.3 lists the redox potentials for complexes **13-15**. The quasi-reversible process labelled **IV** (0.47 V) is observed at potentials typical for metal oxidation in $Co^{II}Pc$ complexes in coordinating solvents such as DMF[404] and is thus assigned to $Co^{III}TMPyrPc^{-2}/Co^{II}TMPyrPc^{-2}$ redox process. The oxidation process labelled **V** ($E_{½}$ = 1.00 V) is due to the first ring oxidation and is assigned to $Co^{III}TMPyrPc^{-1}/Co^{III}TMPyrPc^{-2}$ in comparison with literature.[407]

The three redox couples labelled **I-III** observed at $E_{½}$ = - 1.93 V (**I**), - 1.34 V (**II**) and - 0.50 V (**III**) vs. Ag|AgCl are respectively assigned to $Co^{I}TMPyrPc^{-3}/Co^{I}TMPyrPc^{-4}$, $Co^{I}TMPyrPc^{-2}/Co^{I}TMPyrPc^{-3}$ and $Co^{II}TMPyrPc^{-2}/Co^{I}TMPyrPc^{-2}$ in comparison with literature.[407] The assignments were also confirmed using spectroelectrochemistry below. Processes **I-III** exhibited reversible behaviour, whereas **IV** and **V** were quasi-reversible. The anodic to cathodic peak ratios for the redox couples were near unity for **I-III**. Fig 4.7a, also shows the square wave voltammogram (SWV) of CoTMPyrPc obtained under the same conditions as the CV. The peak currents increased linearly with the square root of scan rate for the scan rates ranging from 50 to 500 mVs^{-1}, confirming diffusion-controlled processes.

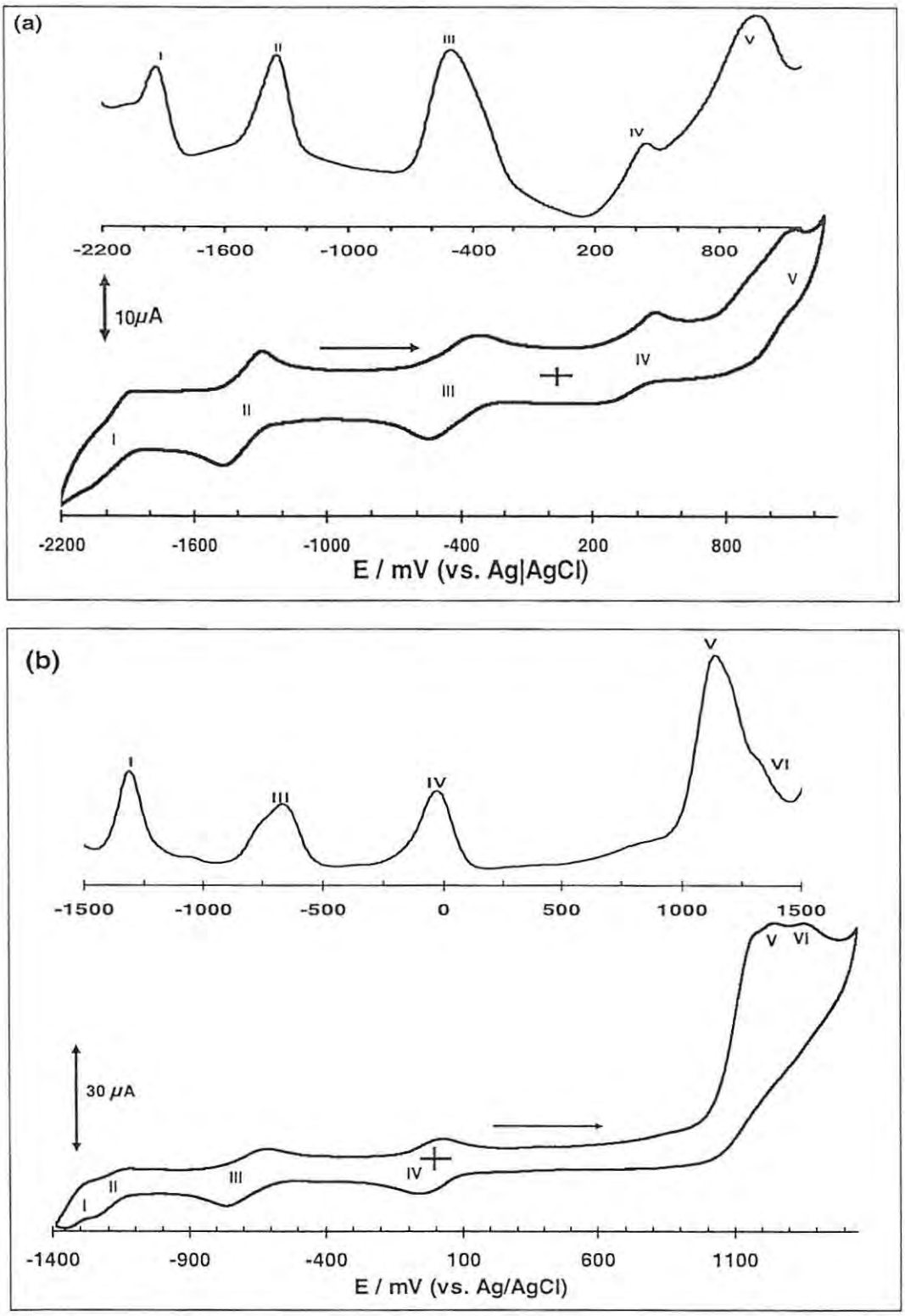

Fig 4.7 (a and b): Cyclic voltammograms of ~ 1.5 mM of (a): CoTMPyrPc (**13**) and (b): MnTMPyrPc (**14**), in DMF containing 0.1 M $TBABF_4$. Scan rate: 100 mVs^{-1}. The curve on top of the CV is the corresponding square wave voltammograms. Electrode: GCE

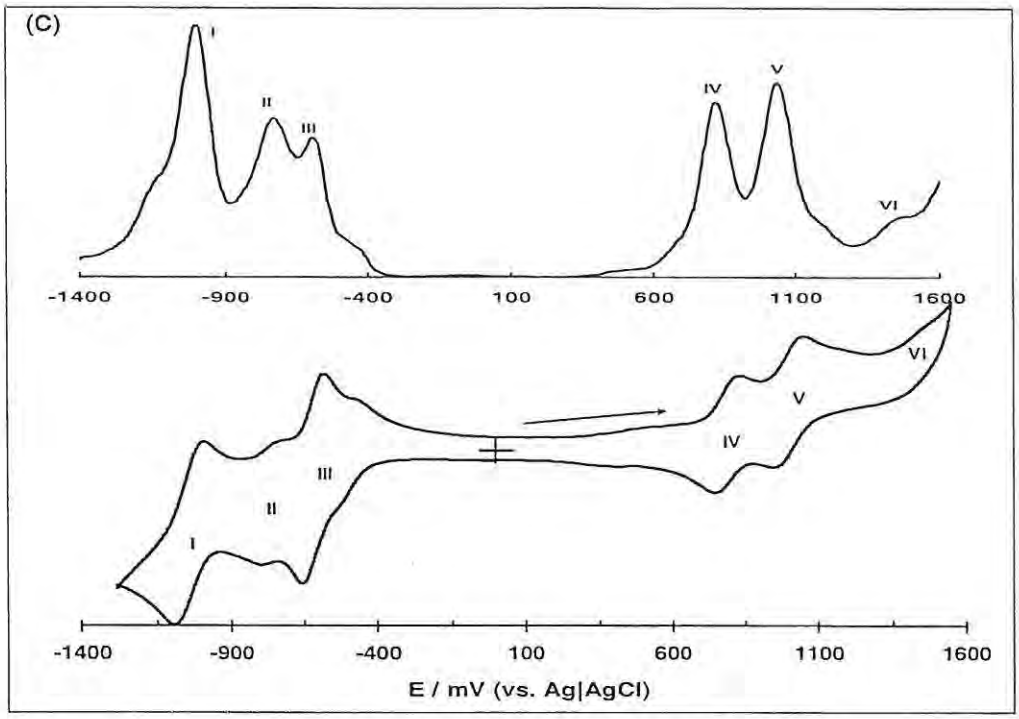

Fig 4.7c: Cyclic voltammograms of ~ 1.5 mM of ZnTMPyrPc (**15**) in DMF containing 0.1 M $TBABF_4$. Scan rate: 100 mVs^{-1}. The curves on top of the CVs are the corresponding square wave voltammograms. Electrode: GCE.

The CV and SWV curves of the manganese complex are represented in Fig. 4.7b. The couples labelled **I** and **II** are observed as separate but with very close potential values in the CV but are seen as a single process in the SWV. The spectrum of MnTMPyrPc, Fig 3.8b showed the presence of Mn^{III}-O-Mn^{III}, Mn^{II}-O-Mn^{II}, Mn^{II} and Mn^{III} species. Under CV and OSWV conditions, N_2 was bubbled hence the predominant species is Mn^{II} (Fig 3.9a) with small amounts of the Mn^{III}-O-Mn^{III}, and insignificant amounts of Mn^{III}. The MnPc μ-oxo dimer is known to undergo a four electron reduction process at potentials more positive than the potentials of couple **I** and **II**. Thus the couples in Fig 4.7b are due to Mn^{II}Pc species and not Mn^{III}-O-Mn^{III} (Table 4.3). In comparison with literature,[407] couples **III** ($E_{½}$ = - 0.68 V) and **IV** ($E_{½}$ = - 0.06 V) are assigned to $Mn^{II}TMPyrPc^{-2}$/$Mn^{II}TMPyrPc^{-3}$ and $Mn^{III}TMPyrPc^{-2}$/$Mn^{II}TMPyrPc^{-2}$ respectively.[407] Process **I** may be

assigned to $Mn^{II}Pc^{-4}/Mn^{II}Pc^{-3}$, the next ring reduction. Spectroelectrochemistry of **14** was complicated by the presence of more than one starting species, hence was not employed for the confirmation of CV assignments.

The large irreversible redox processes labelled **V** (at 1.27 V) and **VI** (at 1.38 V) cannot be definitely assigned at the moment. However ring-based oxidation of substituted MnPc species corresponding to the $Mn^{III}Pc^{-1}/Mn^{III}Pc^{-2}$ couple, have been observed around 1.0 V vs saturated calomel electrode (SCE) and at about 1.6 V vs. SCE for the $Mn^{III}Pc^{0}/Mn^{III}Pc^{-1}$ couple.[407] It is thus likely that redox process in the region of **V** and **VI** are due to ring-based oxidations in MnTMPyrPc species. It is also important to note that peaks due to mercaptopyrimidyl substituent were also observed in this region of processes **V** and **VI**.

Zinc Pc complexes are not known to show any redox activity at the central metal. Thus only ring-based processes are observed (Fig 4.7c). See also Table 4.3. As indicated above in the case of MnTMPyrPc, the process labelled **VI** at 1.55 V (vs. Ag|AgCl) may also be due to the mercaptopyrimidyl substituent.

Table 4.3: Summary of redox potentials of MTMPyrPc in DMF containing $TBABF_4$. Potentials versus Ag|AgCl. Half-wave potentials ($E_{½}$) reported unless otherwise stated.

Complex	$M^{III}Pc^{0}$/ $M^{III}Pc^{-1}$	$M^{III}Pc^{-1}$/ $M^{III}Pc^{-2}$	$M^{III}Pc^{-2}$/ $M^{II}Pc^{-2}$	$(M^{II}Pc^{-2}$/ $M^{I}Pc^{-2})^{c}$	$(M^{I}Pc^{-2}$/ $M^{I}Pc^{-3})^{c}$	$M^{I}Pc^{-3}$/ $M^{I}Pc^{-4}$
CoTMPyrPc (**13**)		1.00 (**V**)	0.47 (**IV**)	-0.50 (**III**)	-1.34 (**II**)	-1.93 (**I**)
MnTMPyrPc[a] (**14**)			-0.06 (**IV**)	-0.68 (**III**) ($Mn^{II}Pc^{-3}$/ $Mn^{II}Pc^{-2}$)	-1.30 (**I**) ($Mn^{II}Pc^{-4}$/ $Mn^{II}Pc^{-3}$)	

Complex	$Zn^{II}Pc^{0}$ /Zn^{II} Pc^{-1}	$Zn^{II}Pc^{-1}$ /$Zn^{II}Pc^{-2}$	$Zn^{II}Pc^{-2}$ /$Zn^{II}Pc^{-3}$	$Zn^{II}Pc^{-3}$ /$Zn^{II}Pc^{-4}$	$Zn^{II}Pc^{-4}$ /$Zn^{II}Pc^{-5}$
ZnTMPyrPc[b] (**15**)	1.01 (**V**)	0.79 (**IV**)	-0.62 (**III**)	-0.76 (**II**)	-1.01 (**I**)

[a] Couples **V** and **VI** left out since could not be assigned definitely.

[b]Only ring-based processes.

[c]For complex **13** only.

4.2.2 Spectroelectrochemistry

Spectroelectrochemistry was used to confirm some of the assignments in the CVs. The experiments were performed using optically transparent thin layer electrochemical (OTTLE) cell. The solution contained ~1 x 10^{-4} M of the metal complex, (e.g. CoTMPyrPc) in DMF + 0.1 M $TBABF_4$ as electrolyte. At these high concentrations, the complex is aggregated, hence the first trace in Fig 4.8a shows considerable broadness compared to Fig 3.8a (curve i). Fig 4.8a shows the UV-Visible spectral changes during a controlled potential reduction of $Co^{II}TMPyrPc^{-2}$ complex (**13**) at - 0.6 V vs. Ag|AgCl corresponding to the redox process labelled **III** in the CV (Fig 4.7a). The Q band at 671 nm decreased in intensity while new bands at 709 and 478 nm appear as the reduction

process continued. These changes are similar to $Co^{I}TPhPyPc$ formation in Fig 4.3a, Table 4.2, for complex **7**.

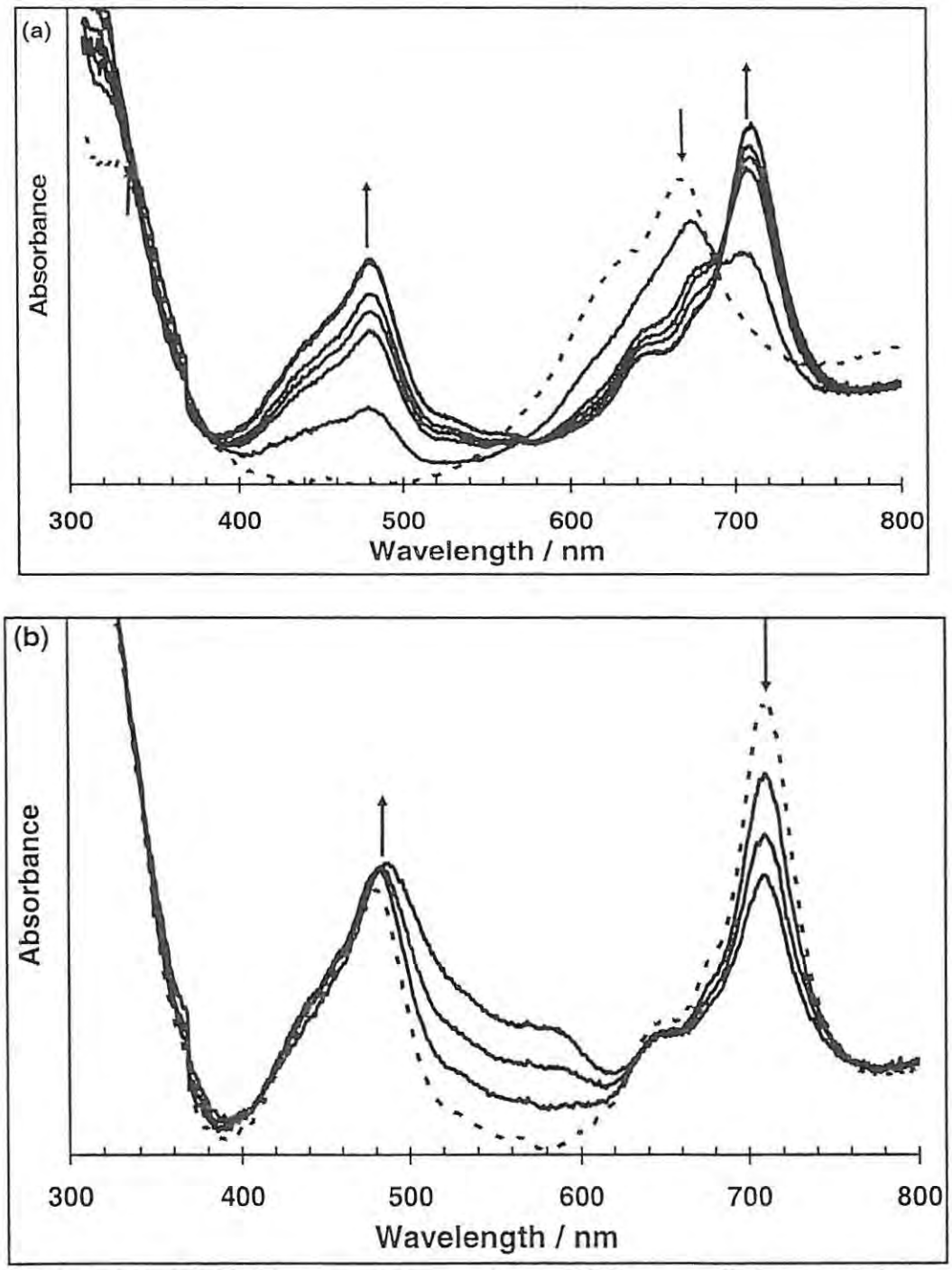

Fig 4.8 (a and b): UV-Visible spectral changes observed during controlled potential electrolysis (OTTLE) of 1.5 mM CoTMPyrPc in DMF containing 0.1 M $TBABF_4$. Applied potential: (a) = - 0.6 V, (b) = - 1.4 V (vs. Ag|AgCl). The first trace in (b) is same as the last trace in (a). The spectra were recorded while continuously applying the specified potential.

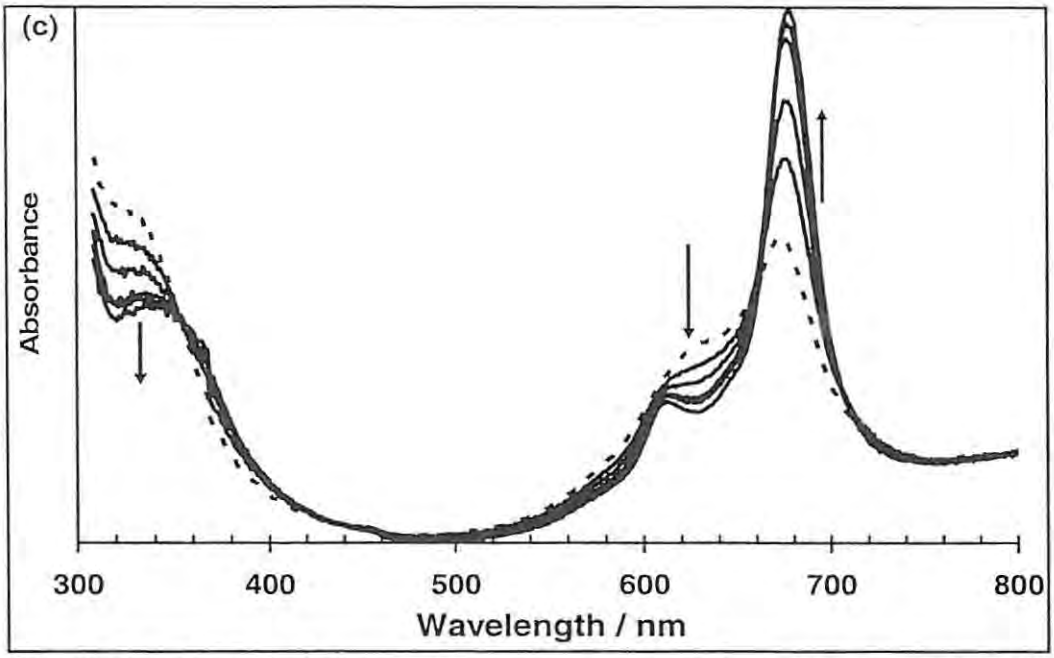

Fig 4.8c: UV-Visible spectral changes observed during controlled potential electrolysis (OTTLE) of 1.5 mM CoTMPyrPc (**13**) in DMF containing 0.1 M $TBABF_4$. Applied potential: + 0.6 V vs. Ag|AgCl. The first trace was obtained by applying 0 V following the formation of the last trace in (b). The spectra were recorded while continuously applying the specified potential

As discussed for $Co^{I}TPhPyPc^{-2}$, the band at 478 nm is typical[409] of the formation of the $Co^{I}TMPyrPc^{-2}$ species, confirming the CV assignment of couple **III** to Co^{II}/Co^{I} process. There was an evolution of a new envelope of bands around 585 nm upon further reduction of the $Co^{I}TMPyrPc^{-2}$ species at potentials of couple **II**, Fig 4.8b. The spectral changes in Fig 4.8b are typical of ring-based reduction in phthalocyanine complexes.[415] This confirms the earlier assignment of the process labelled **II** to $Co^{I}TMPyrPc^{-2}/Co^{I}TMPyrPc^{-3}$. Fig 4.8c shows the spectral changes observed when potentials corresponding to process **IV** were applied to solutions of $Co^{II}TMPyrPc^{-2}$. The first trace in Fig 4.8c was obtained by applying 0 V following the formation of the last trace in Fig 4.8b. This resulted in the formation of the Q band of $Co^{II}TMPyrPc$ at 671 nm with less aggregation compared to Fig 4.8a. There was a shift in wavelength of the Q band from 671 to 676 nm as the electrolysis progressed. This is typical[409] of a metal-based oxidation

in cobalt Pc complexes. The spectrum in Fig 4.8c is therefore assigned $Co^{III}TMPyrPc^{-2}$, confirming CV assignments. It was possible to regenerate the starting $Co^{II}TMPyrPc^{-2}$ complex when a zero potential was applied to the solution after either reduction or oxidation. However, the spectra revealed that while over 95% of the starting material was regenerated from the reduced species only about 86% could be regenerated from the oxidized species. This observation is in agreement with the shape of the CV wave labelled **IV** which is less reversible compared to couple **III**.

4.3 Amino Substituted Phthalocyanine Complexes (19 and 20)

4.3.1 Cyclic and square wave voltammetry

The electrochemical behaviour of the $(OH)Cr^{III}TAPc$ (**19**) monomer was studied in DMF containing 0.1 M $TBABF_4$ using cyclic voltammetry or Osteryoung square wave voltammetry. Fig 4.9 shows the CV and OSWV of $Cr^{III}TAPc$ on GCE. Five processes (**I** – **V**) were observed at the following potentials: 0.44 (**III** E_p), 0.60 (**II** $E_{1/2}$), 1.00 (**I** $E_{1/2}$), - 0.5 V (**IV'**,E_p), - 0.81 (**IV**, $E_{1/2}$) and - 1.35 (**V**, $E_{1/2}$), V vs. Ag|AgCl. Table 4.4 also lists the peak potentials and assignments (except for **IV'**). Most processes are not reversible in Fig 4.9. This behaviour is typical for MTAPc complexes.[283,348,416,417] The first reduction in $Cr^{III}Pc$ complexes is known to occur at the central metal to give $Cr^{II}Pc$ complexes,[407] thus redox process **IV** at - 0.81 V in Fig 4.9 is assigned to $Cr^{III}TAPc/Cr^{II}TAPc$. Available electrochemical data shows that the potentials for redox process **IV** varies over a wide range (- 0.87 to + 0.52 V vs. saturated calomel electrode (SCE)).[407,418]

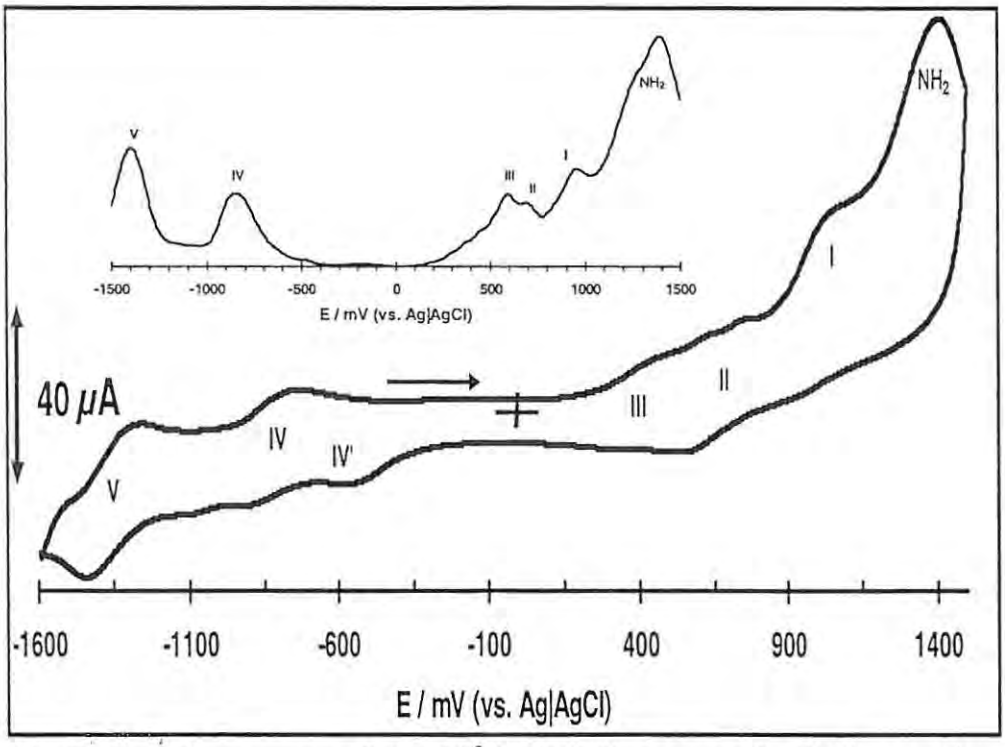

Fig 4.9: Cyclic voltammogram of 3 x 10^{-3} M CrTAPc complex in DMF containing 0.1 M $TBABF_4$. Scan rate: 100 mVs^{-1}. Insert: OSWV. Electrode: GCE.

In comparison with reported data,[407] process **V** (at - 1.35 V) is assigned to the ring-based reduction ($Cr^{II}TAPc^{-2}/Cr^{II}TAPc^{-3}$). The assignments are confirmed below using spectroelectrochemistry. The origins of the process labelled **IV'** in the CV in Fig 4.9 are not known. This peak is not clearly observable using OSWV. But since MTAPc complexes are known to readily aggregate,[419] it is likely that peaks due to both the monomer and the aggregates will be present at the high concentrations involved in cyclic voltammetry.

Table 4.4. Redox potentials (V vs Ag|AgCl) of the CrTAPc and MnTAPc in DMF containing 0.1 M $TBABF_4$.

Process	Assignment/ Potential ($E_{½}$, V) (CrTAPc)	Assignment/ Potential ($E_{½}$, V) (MnTAPc)
NH_2	Amino group **1.40**	Amino group **0.93**
I	$Cr^{IV}TAPc^{0}/Cr^{IV}TAPc^{-1}$ **1.00**	-
II	$Cr^{IV}TAPc^{-1}/Cr^{IV}TAPc^{-2}$ **0.60**	$Mn^{IV}TAPc^{-1}/Mn^{IV}TAPc^{-2}$ **0.75V**
III	$Cr^{IV}TAPc^{-2}/Cr^{III}TAPc^{-2}$ **0.44(E_p)**	$Mn^{IV}TAPc^{-2}/Mn^{III}TAPc^{-2}$ **0.58V**
IV	$Cr^{III}TAPc^{-2}/Cr^{II}TAPc^{-2}$ **- 0.81**	$Mn^{III}TAPc^{-2}/Mn^{II}TAPc^{-2}$ **- 0.30V**
V	$Cr^{II}TAPc^{-3}/Cr^{II}TAPc^{-2}$ **- 1.35**	$Mn^{II}TAPc^{-3}/Mn^{II}TAPc^{-2}$ **- 0.98V**

The irreversible oxidation process labelled **III** (at 0.44 V) is due to metal oxidation hence is assigned to the $Cr^{IV}TAPc^{-2}/Cr^{III}TAPc^{-2}$ process. $Cr^{IV}Pc$ complexes have not been reported, spectroelectrochemistry was used to confirm the present assignment as will be shown later. The oxidation process labelled **II** (0.60 V) in Fig 4.9 is in the range for ring oxidation in $Cr^{III}Pc$ complexes,[407] hence is assigned to $Cr^{IV}TAPc^{-1}/Cr^{IV}TAPc^{-2}$. The oxidation process labelled **I** is then assigned to the second ring oxidation to give $Cr^{IV}TAPc^{0}/Cr^{IV}TAPc^{-1}$. The irreversible process at 1.4 V (Fig 4.9) is due to the oxidation of the amino group attached to the peripheral position of the phthalocyanine ring. The potential for the amino group in MTAPc vary with the nature of the central metal, being observed at 0.625 V for CoTAPc[407] and 1.15 V in FeTAPc.[414]

Literature reported that the CV of $Mn^{II}Pc$ microcrystals show the reduction of this complex to a $Mn^{I}Pc$ species and oxidation to a $Mn^{III}Pc$ species.[420] Reduction of $M^{III}Pc$ to a $Mn^{II}Pc$ species and further reduction to either $Mn^{I}Pc$ or $Mn^{II}Pc^{-3}$ have been reported[410,421-424] as discussed above. As has been shown in Chapter 3, the oxidation state of the Mn species is + 3, giving $Mn^{III}TAPc^{-2}$ species. Fig 4.10a shows that three couples were observed for $Mn^{III}TAPc$ on scanning from - 1.6 to + 1.2 V versus Ag|AgCl. A relatively weak peak (labelled **III**) was observed at 0.58 V versus Ag|AgCl, this peak is more easily seen from the square wave voltammogram. This peak is at a potential too low for a ring based process and is tentatively assigned to a metal-based oxidation ($Mn^{IV}Pc^{-2}/Mn^{III}/Pc^{-2}$) process.

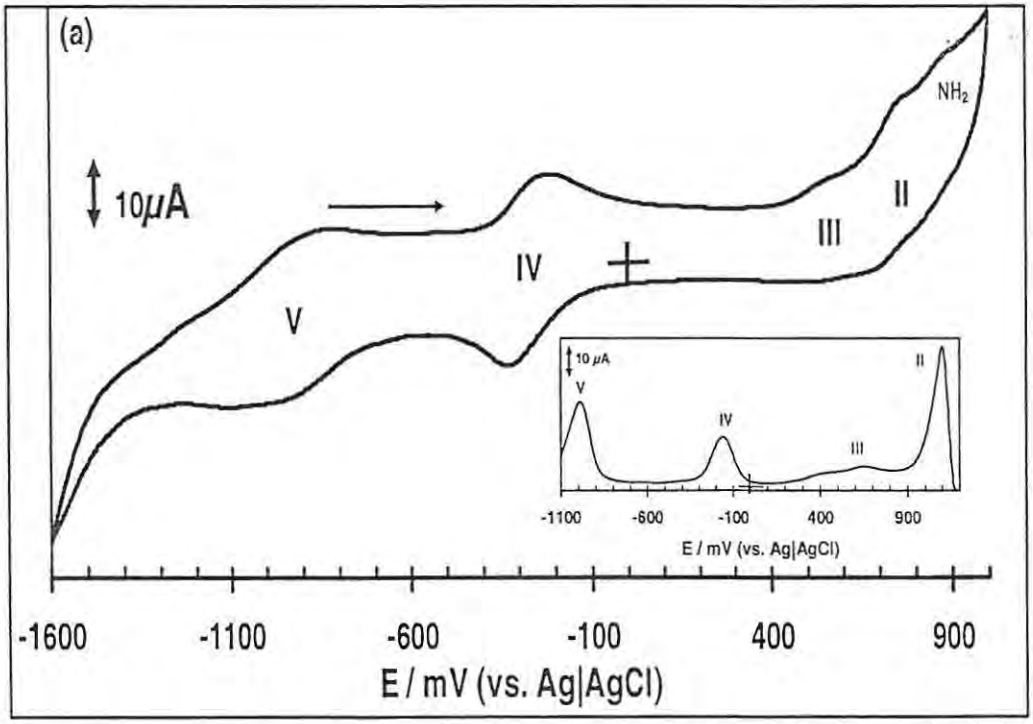

Fig 4.10a: Cyclic voltammogram of MnTAPc in DMF containing 0.1 M $TBABF_4$. Scanning range: - 1.6 to 1.2 V vs. Ag|AgCl. Scan rate: 100 mVs^{-1}. Electrode: GCE. Insert shows the Osteryoung square wave voltammetry.

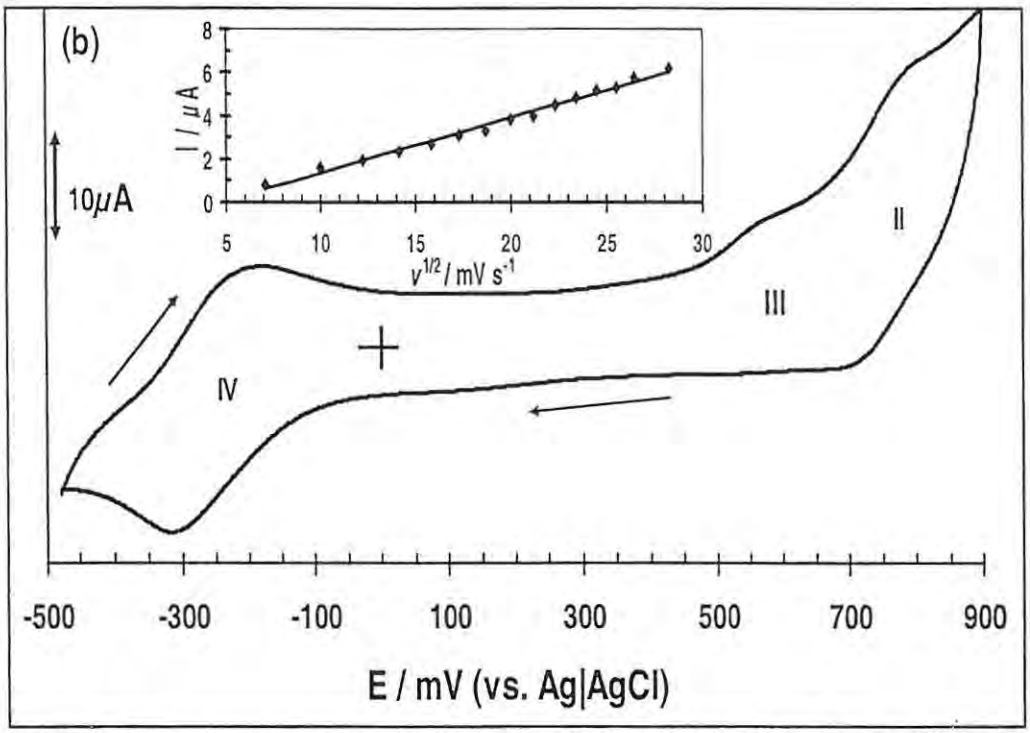

Fig 4.10b: Cyclic voltammograms of MnTAPc in DMF containing 0.01 M $TBABF_4$. Scanning range: - 0.5 to 0.9 V vs. Ag|AgCl. Scan rate: 100 mVs^{-1}. Electrode: GCE. Insert: plot of square root of scan rate versus current for couple **II**.

The three more couples observed are observed at $E_{1/2}$ = 0.75 V (**II**), - 0.30 V (**IV**) and - 0.98 V (**V**) vs. Ag|AgCl, Table 4.4. In addition to these, another irreversible redox process is observed at 0.93 V (labelled $\mathbf{NH_2}$). As stated above and based on literature report,[407,417] the potential for the later process is within the oxidation potential for amino groups in tetraamino Pcs, thus process at + 0.93 V is assigned to the oxidation of the amino substituent. Couple **II** is in the range for ring oxidation in MPc complexes[407] and is assigned to $Mn^{IV}Pc^{-1}/Mn^{IV}Pc^{-2}$. Couple **IV** is in the range for Mn^{III}/Mn^{II} reduction in $Mn^{III}Pc$ complexes[425] and couple **V** at $E_{1/2}$ = - 0.98 V versus Ag|AgCl is due to ring reduction and the formation of $Mn^{II}Pc^{-3}$ species. The redox couples showed large peak separations in some cases, indicating sluggishness of the electrochemical processes. However, when the potential window for the cyclic voltammogram was shortened to - 0.5

to 0.9 V (instead of - 1.6 to 1.2 V), the reversibility of the couples is improved and the peak separation of ~ 100 mV (ΔE = 90 mV for ferrocene/ferrocenium couple) could be obtained, Fig 4.10b, hence showing an improvement in the electrode kinetics. Plots of the square root of current (corrected for background) versus scan rate were linear, Fig 4.10b (insert), suggesting a diffusion controlled process. Spectroelectrochemistry was employed for the confirmation of cyclic voltammetry assignments.

4.3.2 Spectroelectrochemistry

Spectroelectrochemical studies, using the OTTLE cell were employed to provide further information on the nature of the redox processes observed in Figs 4.9 and 4.10. The experiments were performed by recording each spectral trace following application of the appropriate potential for a known time period. Fig 4.11a shows the UV-Visible spectral changes observed during a controlled potential reduction of CrTAPc at potentials of process **IV**. It is clearly seen that the Q-band at 735 nm (dotted trace), Fig 4.11a, blue shifted to 720 nm with a slight increase in intensity.

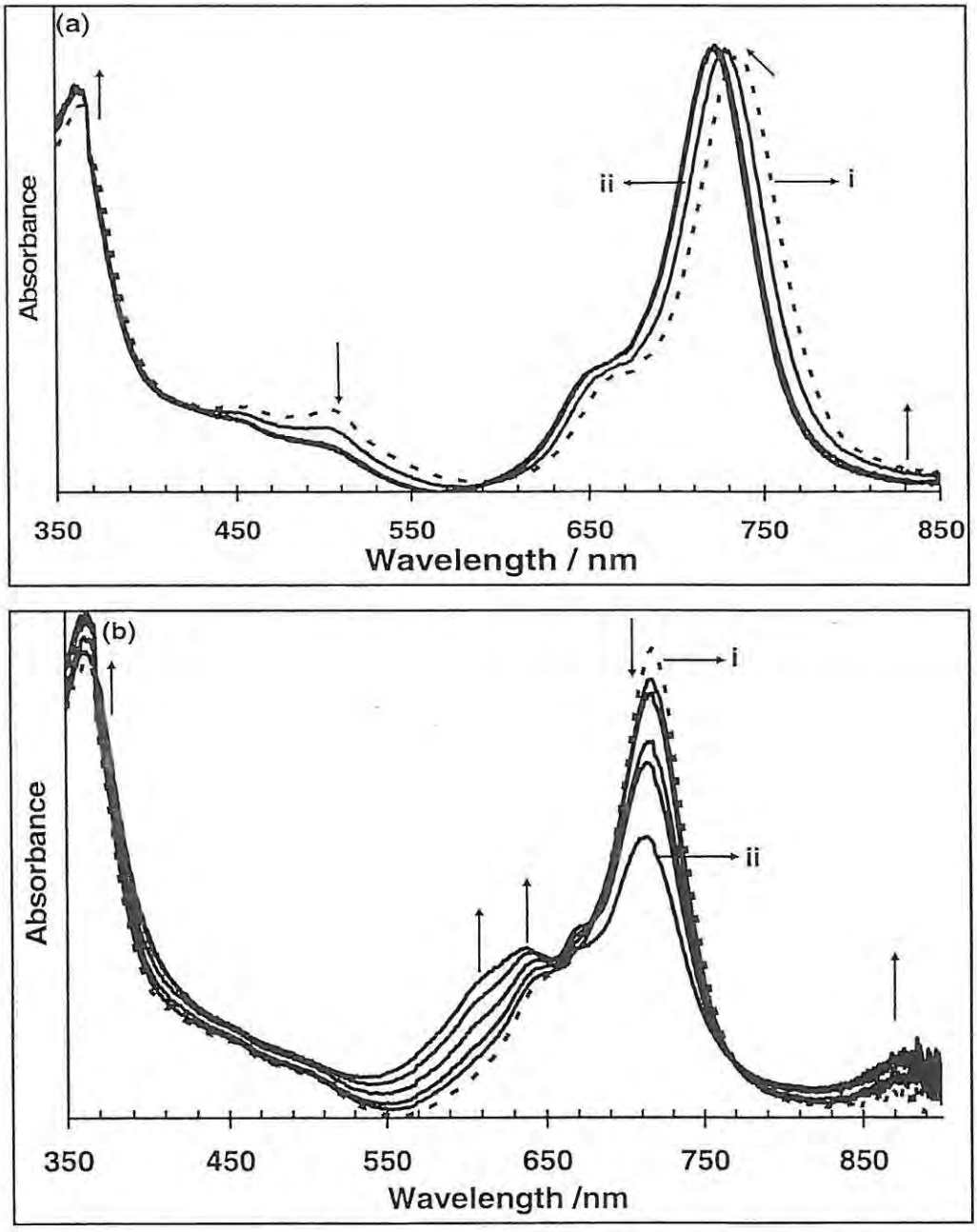

Fig 4.11(a and b): UV-Visible spectral changes observed using the OTTLE cell during (a): reduction of $Cr^{III}TAPc$ at the potential of process **IV** (- 0.9 V) in Fig 4.9, (i): 0 s, (ii): 60 s. (b): reduction at the potential of process **V** (- 1.4 V) in Fig 4.9, (i): 0 s, (ii): 45 s. Electrolyte: DMF containing 0.1 M $TBABF_4$. The first trace in (b) is same as the last trace in (a).

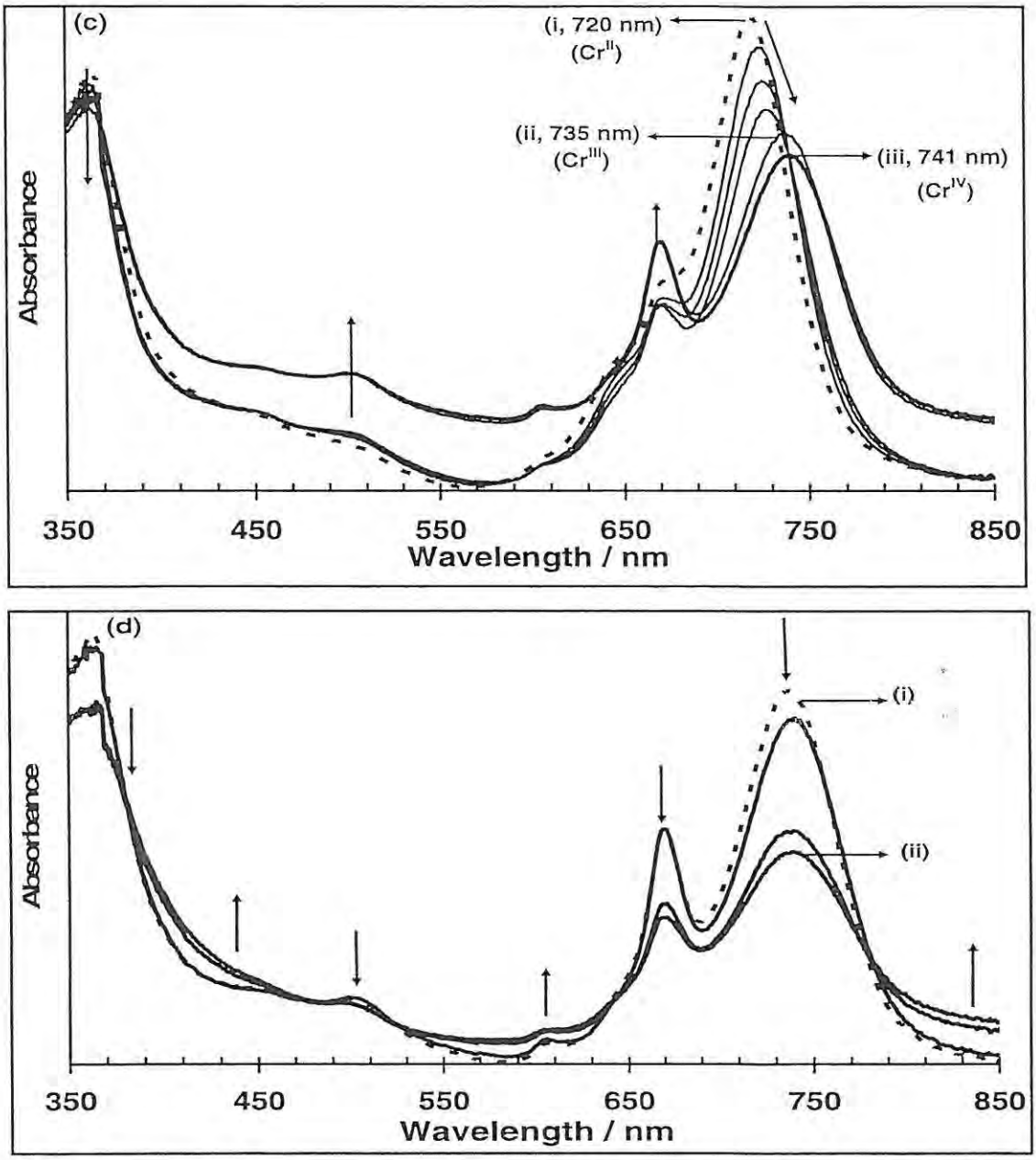

Fig 4.11 (c and d): UV-Visible spectral changes observed using the OTTLE cell during (c): oxidation of Cr^{III}TAPc at potentials of process **III,** + 0.6 V. (i) 0 s, (iii): 45 s. (d): oxidation at the potential of process **II**, + 0.8 V. (i) 0 s, (ii): 80 s Electrolyte: DMF containing 0.1 M $TBABF_4$. The spectra were recorded while continuously applying the specified potential. The first trace in (c) was obtained by applying 0 V to the last trace in (b), generating Cr^{II}. The first trace in (d) is same as the last trace in (c).

This shift is also accompanied by the lowering in intensity of the charge transfer (CT) band at 500 nm, which is associated with Cr^{III}Pc species. The lowering in intensity

(and final disappearance) of the bands in this region, suggest the reduction of $Cr^{III}Pc$ species, and confirm our earlier assignment of the redox process (**IV**) in Fig 4.9 to $Cr^{III}TAPc^{-2}/Cr^{II}TAPc^{-2}$. It was possible to regenerate the starting species by about 92% when a zero potential was applied to the reduced species, showing that the reduction of CrTAPc complex was reversible within these potentials. Fig 4.11b shows the spectral changes for reduction of complex **19** at potentials of process **V** in Fig 4.9. The first trace in Fig 4.11b is same as the last trace in Fig 4.11a. There was a steady decrease in intensity of the Q-band with time and the formation of new bands at 606 and 633 nm. The decrease in intensity of the Q-band is very typical of a ring-based reduction in metallophthalocyanine complexes.[415] Also the appearance of two absorption bands in the 500 to 600 nm region has been observed for other ring-reduced phthalocyanine monoanion species.[415] Hence the spectral changes in Fig 4.11b clearly confirm a ring based reduction of the CrTAPc complex and the formation of $Cr^{II}TAPc^{-2}/Cr^{II}TAPc^{-3}$ species, confirming the assignment of process **V** in Table 4.4.

Following reduction in Fig 4.11b, the Cr^{II} species at 720 nm was re-generated by application of 0 V, giving the first spectrum in Fig 4.11c. The spectral changes, in Fig 4.11c, upon application of potentials corresponding to process **III** (+ 0.6 V, Fig 4.9), show the formation of Cr^{III} species (735 nm) and finally its oxidation and the formation of Cr^{IV}, (741 nm), Table 4.2. The spectral changes in Fig 4.11c are typical behavior for the metal-based oxidation processes,[407] and confirms the assignment of this process to $Cr^{IV}TAPc^{-2}/Cr^{III}TAPc^{-2}$. Oxidation at potentials of process **II**, following oxidation at potentials of **III** resulted in spectral changes shown in Fig 4.11d. The first spectrum in Fig 4.11d was the last spectrum in Fig 4.11c. The spectral changes shown in Fig 4.11d

consist of a decrease in the Q band intensity and the increase in the intensity of the absorption feature near 600 nm. This is typical behavior for ring-based oxidation in phthalocyanine complexes,[415] where the Q band decreases in intensity and new broad and weak bands are observed. Spectral changes in Fig 4.11d confirm that the oxidation process labelled **II** is due to ring-oxidation and formation of $Cr^{IV}TAPc^{-1}/Cr^{IV}TAPc^{-2}$.

As discussed in Chapter 3, the MnPc complex with Mn in the + 2 or + 3 oxidation state have distinct absorption spectra which can be used in differentiating between the two oxidation states.[409] The $Mn^{II}Pc$ complex has an absorption spectrum shifted to shorter wavelengths compared to the corresponding $(X)Mn^{III}Pc$ species[409,425] and a relatively strong band near 520 nm[409] for the latter. Fig 4.12 shows the electronic absorption spectral changes observed during reduction of MnTAPc in DMF at potentials of couple **IV**.

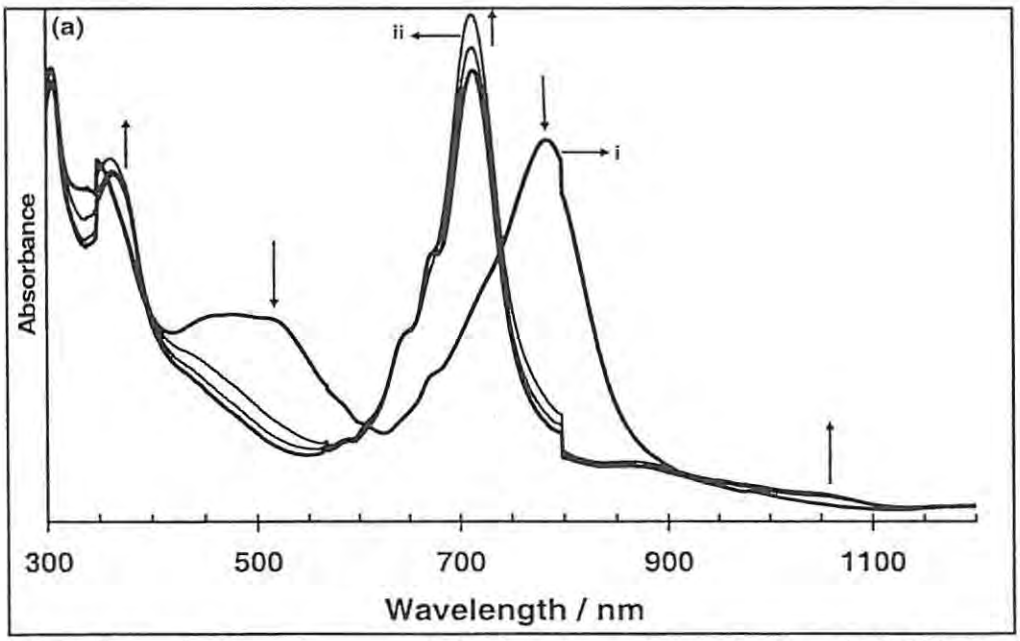

Fig 4.12a: Electronic absorption spectral changes observed on reduction of MnTAPc in DMF containing 0.1 M $TBABF_4$ at potentials of first reduction (couple **IV** in Fig 4.10a). (i) before, (ii) 240 s after application of potential.

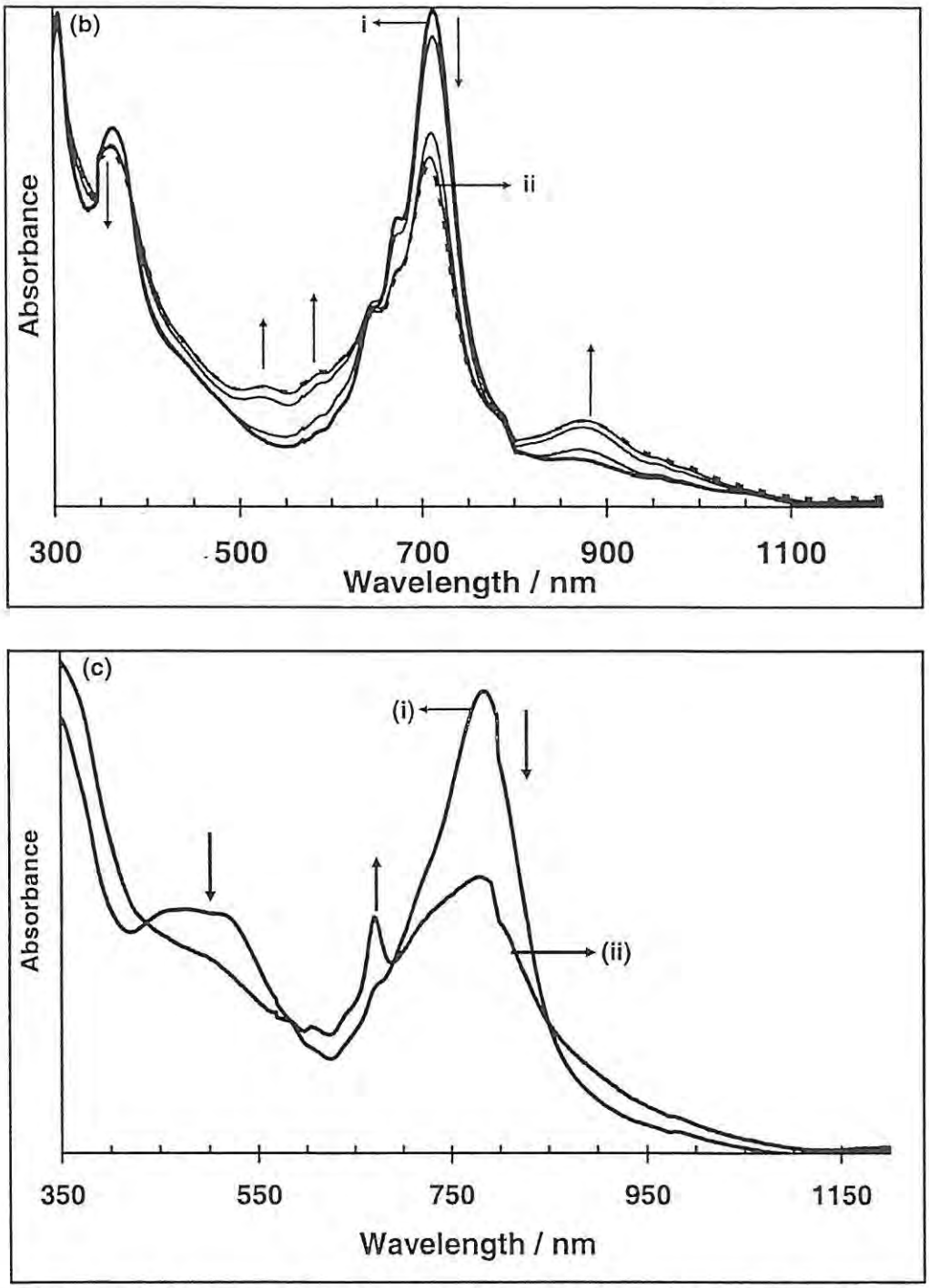

Fig 4.12 (b and c): Electronic absorption spectral changes observed on reduction of MnTAPc in DMF containing $TBABF_4$ at potentials of (b): second reduction (couple **V**, - 1.0 V, in Fig 4.10a); the first spectrum is the same as the last one in (a), (i): before, (ii): 600 s after application of potential. (c): spectral changes for oxidation at potentials of peak **III** (+ 0.6 V): (i) before, (ii) 60 s after application of potential.

On reduction at potentials of couple **IV**, the Q band shifted to shorter wavelength (from 780 nm of the $(OH)Mn^{III}TAPc^{-2}$ species to 710 nm, Table 4.2) and the band near 500 nm disappeared, Fig 4.12a, confirming the formation of $Mn^{II}TAPc^{-2}$ complex from the $(OH)Mn^{III}TAPc^{-2}$ species. Further reduction at potentials of couple **V** in Fig 4.10a, resulted in spectral changes shown in Fig 4.12b. In Fig 4.12 (a and b), the isosbestic points were not resolved, probably due to changes in axial ligation during reduction. The lowering in the intensity of the Q band and the formation of bands in the 500–600 nm region is consistent with the ring based reduction,[415] and the formation of $Mn^{II}Pc^{-3}$. As already discussed above, formation of both $Mn^{II}Pc^{-3}$ and $Mn^{I}Pc^{-2}$ species on reduction of MnPc complexes has been reported by several workers.[410,422] Oxidation of $Mn^{III}Pc$ species to the $Mn^{IV}Pc$ species is known to result in the shift of the Q band to shorter wavelength values.[411] The shift of the Q band with change in oxidation state was shown to be as follows: $Mn^{III}Pc > Mn^{II}Pc > Mn^{IV}Pc$.[411] Oxidation of the $(OH)Mn^{III}TAPc^{-2}$ at potentials of couple **III** resulted in the shift of the Q band to shorter wavelengths (667 nm, Table 4.2) compared to $(OH)Mn^{III}TAPc^{-2}$ and the $Mn^{II}Pc$ species, Fig 4.12c. This shift is, herein, associated to the formation of $Mn^{IV}TAPc$ species. Thus, for the MnTAPc complex, the shift in the Q band with change in oxidation state is as follows: $(OH)Mn^{III}TAPc^{-2}$ (780 nm) > $Mn^{II}Pc$ (710 nm) > $Mn^{IV}Pc$ (667 nm), Table 4.2.

4.4 Thiophene Substituted Metallophthalocyanine Complexes

4.4.1 Cyclic and square wave voltammetry

Figs 4.13 (a-f) show the CVs for complexes **16** (CoTETPc), **17** (MnTETPc) and **18** (ZnTETPc) using different potential windows. Table 4.5 lists the peak potentials. Fig 4.13 also shows the square wave voltammograms for the complexes. A wide potential window was employed in order to interrogate the redox processes including the thiophene oxidation, Table 4.5a. However, less reversibility is observed (Fig 4.13a, c and e) under a wide potential window due to possible decompositions under such extreme conditions. The couples were more reversible when the potential window was narrower, - 1000 to + 1000 mV (Fig 4.13b, d and f) and the potentials are listed in Table 4.5b. Using a wide potential window (- 1300 to + 1500 mV) the CV and OSWV of CoTETPc, (**16**), in DMF containing 0.1 M $TBABF_4$ are shown in Fig 4.13a. Seven redox processes attributable to the central metal, the Pc ring and the thiophene groups can be identified. While for the narrower window, four redox processes are observed in Fig 4.13b for complex **16**. Slight differences in potential were observed for the different potential ranges and the assignments are listed in Table 4.5. As already stated, in a coordinating solvent like DMF, the first oxidation process occurs at the central metal[407] in CoPc complexes. The following discussion of potentials is based on the short range potential values, Table 4.5b. The process labelled **IV** (at 0.41 V vs. Ag|AgCl, Table 4.5) is in the range[407] for the oxidation of the central metal in CoPc complexes and is thus assigned to $Co^{III}TETPc/Co^{II}TETPc$.

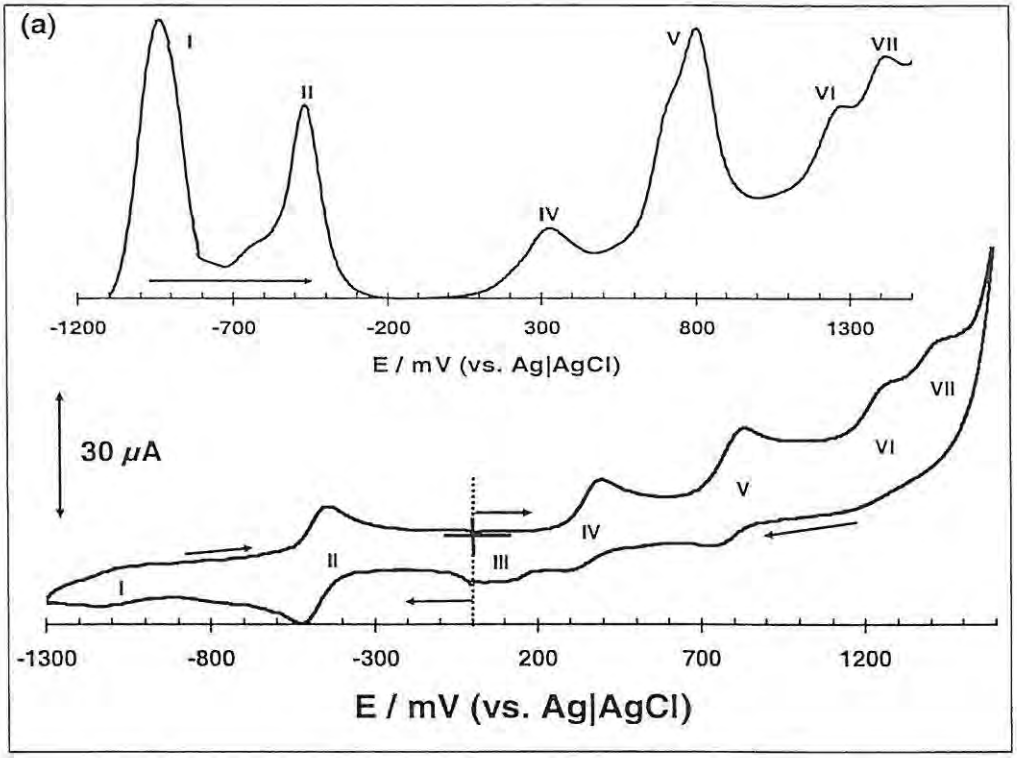

Fig 4.13a: Cyclic voltammograms and OSWV of 5 mM CoTETPc; in DMF containing 0.1 M $TBABF_4$: wide potential windows. Scan rate = 100 mVs^{-1}.

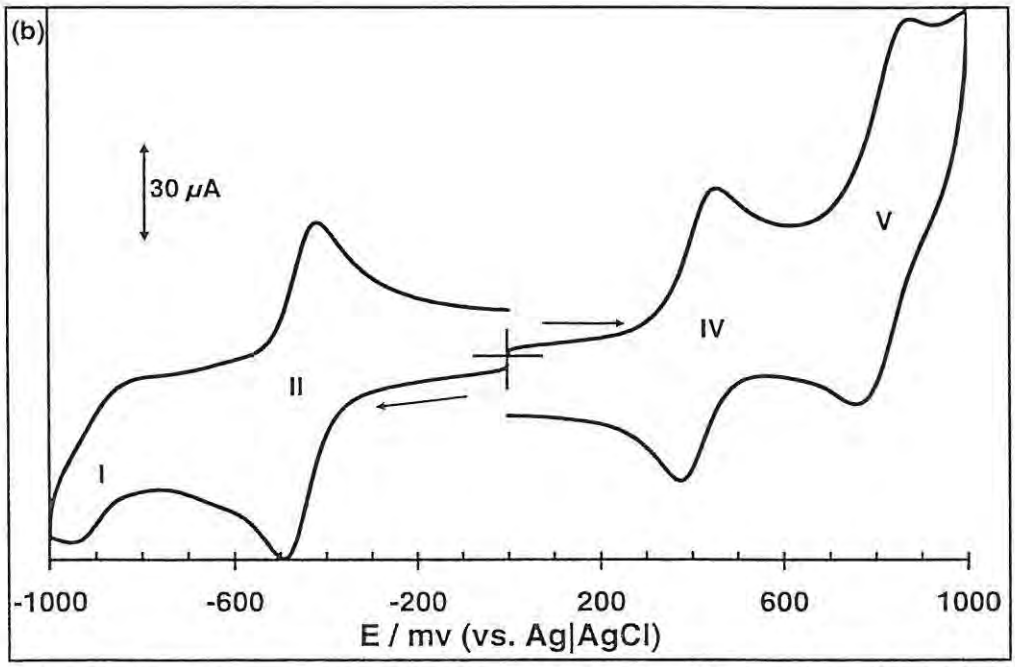

Fig 4.13b: Cyclic voltammograms of 5 mM CoTETPc; in DMF containing 0.1 M $TBABF_4$: narrow potential windows. Scan rate = 100 mVs^{-1}.

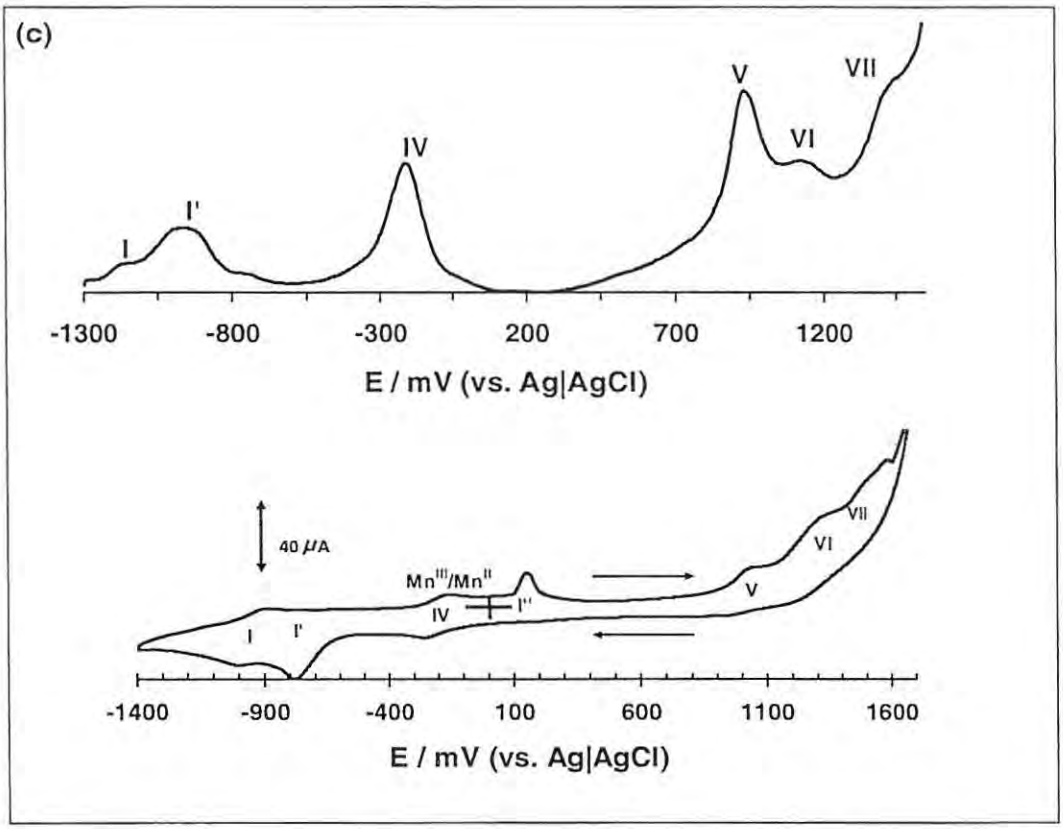

Fig 4.13c: Cyclic voltammograms and OSWV of 5 mM MnTETPc; in DMF containing 0.1 M $TBABF_4$: wide potential windows. Scan rate = 100 mVs^{-1}.

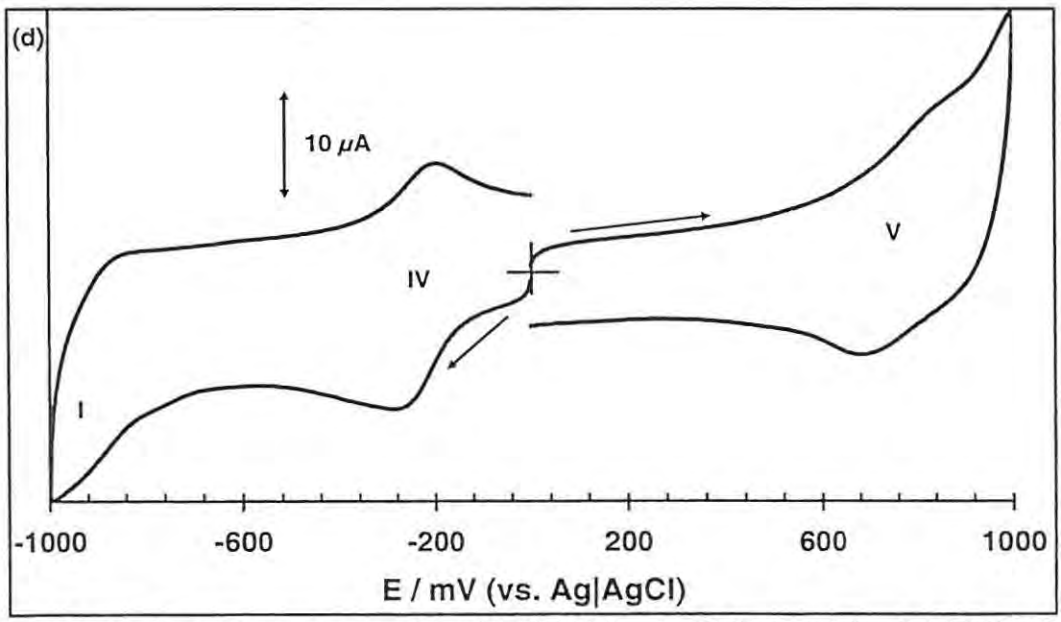

Fig 4.13d: Cyclic voltammograms of 5 mM MnTETPc; in DMF containing 0.1 M $TBABF_4$: narrow potential windows. Scan rate = 100 mVs^{-1}.

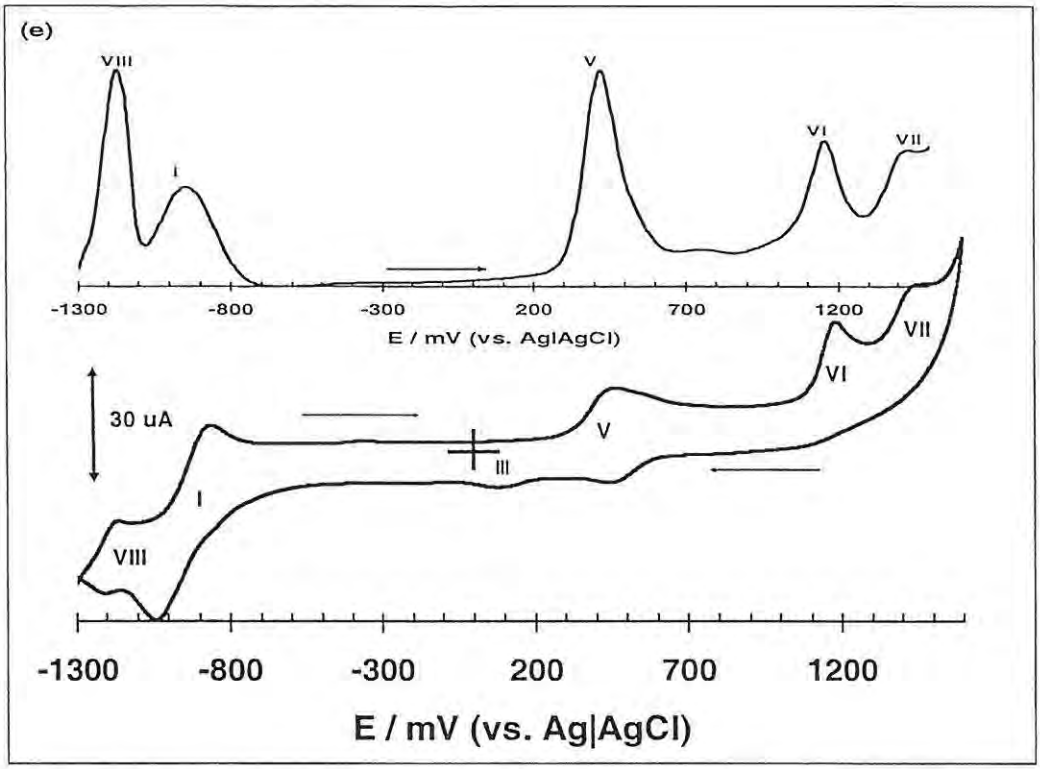

Fig 4.13e: Cyclic voltammograms and OSWV of 5 mM ZnTETPc; in DMF containing 0.1 M $TBABF_4$: wide potential windows. Scan rate = 100 mVs^{-1}.

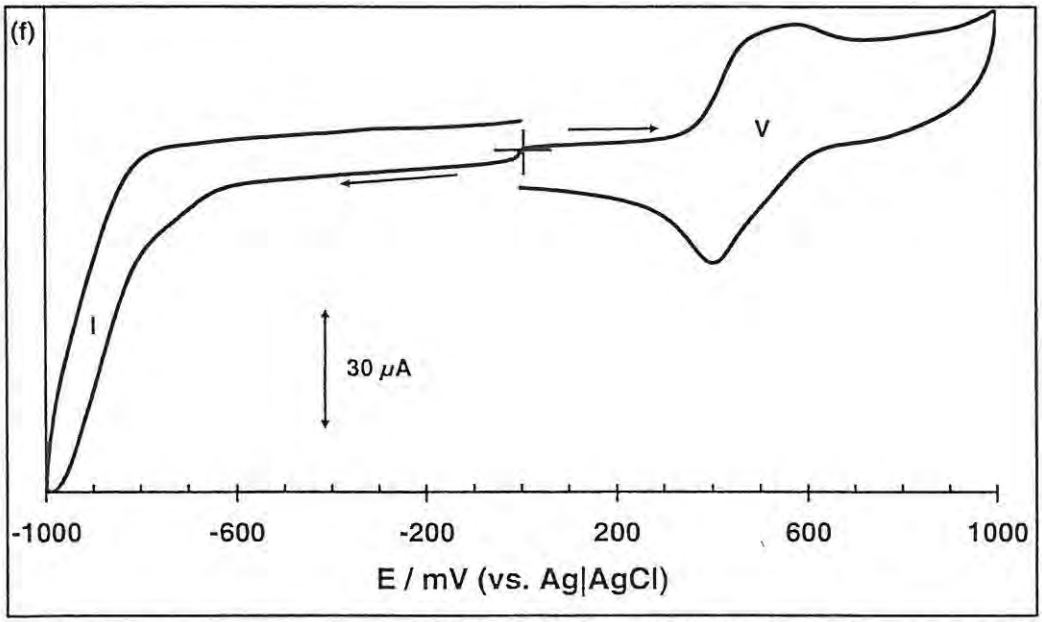

Fig 4.13f: Cyclic voltammograms and OSWV of 5 mM ZnTETPc; in DMF containing 0.1 M $TBABF_4$: narrow potential windows. Scan rate = 100 mVs^{-1}.

This couple was reversible under narrow potential window conditions, Fig 4.13b, in that the ratio of the anodic to cathodic peak currents were unity and cathodic to anodic peak separation was 90 mV (peak separation for the ferrocinium/ferrocene couple was 90 mV). The redox couple labelled **II** at - 0.46 V vs Ag|AgCl, Table 4.5b, may thus be assigned to metal reduction ($Co^{II}TETPc/Co^{I}TETPc$), since it is in the potential range for this couple.[407] The remaining redox processes are assigned (in comparison with literature) as follows: $Co^{I}TETPc^{-2}/Co^{I}TETPc^{-3}$ (couple **I**, - 0.90 V), $Co^{III}TETPc^{-1}/Co^{III}TETPc^{-2}$ and (couple **V**, 0.81 V). The next oxidation process (**VI**) at 1.22 V (Table 4.5a) observed when a wider potential window is employed, Fig 4.13a, is assigned to $Co^{III}TETPc^{0}/Co^{III}TETPc^{-1}$. $Co^{III}Pc^{0}$ species has been reported[407] in non-aqueous media. Couples **II, III** and **V** were reversible in Fig 4.13b. The electrode processes were found to be diffusion controlled as demonstrated by the linearity of a plot of peak current vs. square root of scan rate, for scan rate ranging from 50-600 mVs^{-1}.

The oxidation of the thiophene group can be observed at 1.46 V vs. Ag|AgCl (labelled **VII** in Fig 4.13a), Table 4.5a. Zotti *et al.*[426] reported an irreversible reduction wave for bithiophene in acetonitrile at ~ 0.2 V vs. SCE. A similar wave was assigned to the reduced form of electropolymerized oligothiophene by Audebert *et al.*[427] The broad wave at 0.08 V vs. Ag|AgCl (labelled **III,** Fig 4.13a), is thus tentatively assigned to the reduction of the thiophene, Table 4.5a. It can be seen, in Fig 4.13b, that the wave related to the reduction of the oxidized thiophene group did not appear when the potential window was not extended to the oxidation potential of the thiophene substituent in Fig 4.13a. This observation further confirms earlier claim that the wave at 0.08 V vs.

Ag|AgCl (labelled **III**) in Fig 4.13a is related to the reduction of the oxidized thiophene group.

Table 4.5a: Long range redox potentials $E_{1/2}$ ($E_{1/2} = (E_{pa}+E_{pc})/2$, where E_{pa} and E_{pc} are the anodic and cathodic peak potential values, respectively) or E_{pa} (V vs.Ag|AgCl) for CoTETPc, MnTETPc and ZnTETPc complexes measured in DMF containing 0.1M $TBABF_4$. Scan rate = 100 mVs^{-1}. Potentials in Volts vs. Ag|AgCl

Complex	Thiophene oxidation (VII)	$M^{III}Pc^{0}/M^{III}Pc^{-1}$ ($M^{II}Pc^{0}/M^{II}Pc^{-1}$ for Zn complex) (VI)	$M^{III}Pc^{-1}/M^{III}Pc^{-2}$ ($M^{II}Pc^{-1}$ / $M^{II}Pc^{-2}$ for Zn complex)(V)	$M^{III}Pc^{-2}$ / $M^{II}Pc^{-2}$ (IV)	Thiophene reduction (III)	$M^{II}Pc^{-2}$/ $M^{I}Pc^{-2}$ (II)	$M^{I}Pc^{-2}/M^{I}Pc^{-3}$($M^{II}Pc^{-2}/M^{II}Pc^{-3}$ for Zn complex) (I)	M^{II}-Pc^{-3}/ M^{II}-Pc^{-4} (VIII)
CoTETPc	1.46	1.22	0.78	0.35	0.08	- 0.48	-1.16	-
MnTETPc	1.56	1.28	1.00	-0.23	-	(a)	(a)	-
ZnTETPc	1.46	1.20	0.45	-	0.07	-	-0.96	-1.20

(a) Pre-adsorption phenomena observed.

Table 4.5b: Short range redox potentials $E_{1/2}$ ($E_{1/2} = (E_{pa}+E_{pc})/2$, where E_{pa} and E_{pc} are the anodic and cathodic peak potential values, respectively) or E_{pa} (V vs. Ag|AgCl) for CoTETPc, MnTETPc and ZnTETPc complexes measured in DMF containing 0.1M $TBABF_4$. Scan rate = 100 mVs^{-1}. Potentials in Volts vs. Ag|AgCl

Complex	$M^{III}Pc^{-1}/M^{III}Pc^{-2}$ ($M^{II}Pc^{-1}/M^{II}Pc^{-2}$ for Zn complex) (V)	$M^{III}Pc^{-2}/M^{II}Pc^{-2}$ (IV)	$M^{II}Pc^{-2}/M^{I}Pc^{-2}$ (II)	$M^{II}Pc^{-2}/M^{II}Pc^{-3}$ ($M^{I}Pc^{-2}/M^{I}Pc^{-3}$ for Co complex) (I)
CoTETPc	0.81	0.41	- 0.46	-0.90
MnTETPc	0.75	-0.21	-	-0.95
ZnTETPc	0.47	-	-	-0.99

Figs 4.13(c and d) show the CV (and OSWV, in Fig 4.13c) of MnTETPc (**17**) in DMF containing 0.1 M $TBABF_4$. Table 4.5b shows the data obtained from Fig 4.13d with narrower window (- 1000 to + 1000 mV), hence more reversible and less complicated processes. The first reduction in $Mn^{III}Pc$ complexes occurs at the central metal[407] to give $Mn^{II}Pc$ species. Thus, couple **IV** observed at - 0.21 V is assigned to $Mn^{III}TETPc/ Mn^{II}TETPc$. As already discussed, the first reduction in $Mn^{II}Pc^{-2}$ complexes has been a subject of some controversy, with some reports proposing ring reduction to the $Mn^{II}Pc^{-3}$ species and others suggesting metal reduction to the $Mn^{I}Pc^{-2}$ species.[427] The formation of the $Mn^{II}Pc^{-3}$ has also been shown earlier in the case of pyrrole and amino substituted MnPcs in this work and is further confirmed below using spectroelectrochemistry. Thus the redox process (**I**) at - 0.95 V in Fig 4.13d is due to ring reduction and formation of $Mn^{II}Pc^{-3}$ species. Process **V** (+ 0.75 V) in Fig 4.13d is in the range for ring oxidation in MPc complexes and is assigned to $Mn^{III}TETPc^{-1}/Mn^{III}TETPc^{-2}$. The next oxidation process **VI** (1.28 V, Table 4.5a), is observed only when a wider window is employed, Fig 4.13c, and is assigned to $Mn^{III}TETPc^{0}/Mn^{III}TETPc^{-1}$.

Under wide potential window conditions (- 1400 to + 1600 mV, Fig 4.13c, two redox processes are observed around 900 mV labelled **I** and **I'**. These processes show typical behaviour for the formation of adsorbed species,[428] which is characterized by sharp peaks in the cyclic voltammograms. It is known[428] that the adsorption of a product of the electrode reaction results in the formation of a sharp pre-wave peak (**I'**, Fig 4.13c), preceding the more regular peak (**I**, Fig 4.13c), the latter being due to the diffusion of the electroactive species from solution to the electrode. The diffusing component is most likely due to the $Mn^{II}Pc^{-2}/Mn^{II}Pc^{-3}$ couple, in comparison with electrochemical behaviour of the other MnPc complexes examined in this work. The sharp peak labelled as **I''** in Fig 4.13c is then assigned to the desorption of the adsorbed species. The adsorption behaviour observed for the Mn complex was not observed for the Zn or Co complexes. When a narrow potential window was employed, the pre-wave behaviour was not observed showing that extreme potentials results in products which adsorb onto the electrode surfaces. The thiophene reduction which was observed as a broad peak at 0.08 V for the Co complex is only observed as an increase in background in this potential region for the Mn complex, Fig 4.13c. Thiophene oxidation was observed at 1.56 V for Mn complex.

Figs 4.13 (e and f) show the redox behavior of ZnTETPc (**18**) in DMF containing 0.1 M $TBABF_4$. Using a wide potential window (- 1300 to + 1600 mV), Fig 4.13e, five redox processes, (**I, V-VIII**) and a weak wave (**III**) at 0.06 V vs. Ag|AgCl can be readily seen in the cyclic voltammogram. Two couples at - 0.99 V (**I**) and 0.47 V (**V**) are observed using a narrow potential window (- 1000 to + 1000 mV). Since Zn^{II} metal is redox inactive, all the redox processes are centred on the Pc ring and the thiophene.

Processes **I** and **V** are assigned as indicated in Table 4.5. The couples are quasi-reversible. Following the discussion above, processes **III** (0.06 V) and **VII** (1.46 V), Fig 4.5a, are due to thiophene reduction and oxidation, respectively observed in the wider potential window, in Fig 4.13e. Peak separations in couples **VIII** (- 1.20 V) and **V** (0.45 V) are 79 mV and 45 mV respectively in Fig 4.13e. The relatively small peak separation of 45 mV for couple V suggests oxidation of a surface confined species, again showing that wider potential window results in the formation of products which adsorb onto the electrode as was observed in the case of the Mn complex. In Fig 4.13e, the peak separation for couple **I** was ~ 200 mV suggesting quasi-reversibility, while cathodic to anodic peak current ratios (i_{pc}/i_{pa}) for couples **I** and **VIII** were unity. As explained above in the case of CoTETPc, thiophene reduction is not expected when using a narrow potential window.

4.4.2 Spectroelectrochemistry

Spectroelectrochemical experiments, using the OTTLE cell, were employed to confirm some of the CV assignments for the MnTETPc complex. Fig 4.14a shows the electronic absorption spectral changes observed upon a controlled potential reduction of MnTETPc at - 0.4 V corresponding to the couple **IV** assigned to Mn^{III}/Mn^{II} process. The bands at 500 nm and 723 nm are characteristic of $Mn^{III}Pc$ complexes. Upon reduction, the Q band at 723 nm decreased in intensity, and a new band was formed at 682 nm, Table 4.2. The formation of $Mn^{II}Pc$ is characterized by the shift of the Q band to lower wavelength values (by ~ 40 nm as indicated earlier in the case of pyrrole substituted

MnPc), thus the formation of the 682 nm band suggests the formation of the $Mn^{II}TETPc$ from $Mn^{III}TETPc$

Fig 4.14b, shows further spectral changes observed on application of the potentials of process **I** (- 1.0 V Fig 4.13b). The spectral changes are typical[412] of ring reduction in MPc complexes with two bands in the 500 to 600 nm region and the decrease in the Q band. Thus the $Mn^{II}TETPc^{-2}$ complex is reduced $Mn^{II}TETPc^{-3}$ species at potentials of processes **I** considering only short range. The UV-Visible absorption maxima (λ_{max}) relating to the central metals for the various MPc complexes are summarized in Table 4.2. Electrode modification using some of the synthesized complexes is discussed next in Chapter Five.

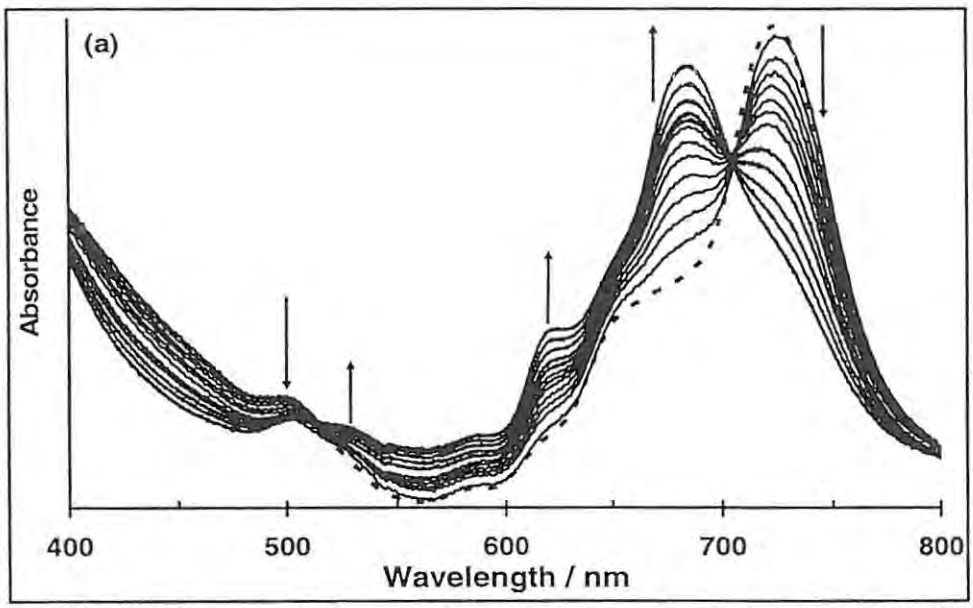

Fig 4.14a: UV-Visible spectral changes observed during controlled potential (OTTLE cell) reduction of ~3.0 mM MnTETPc, in DMF containing 0.1 M $TBABF_4$. Applied potential = - 0.5 V vs. Ag|AgCl

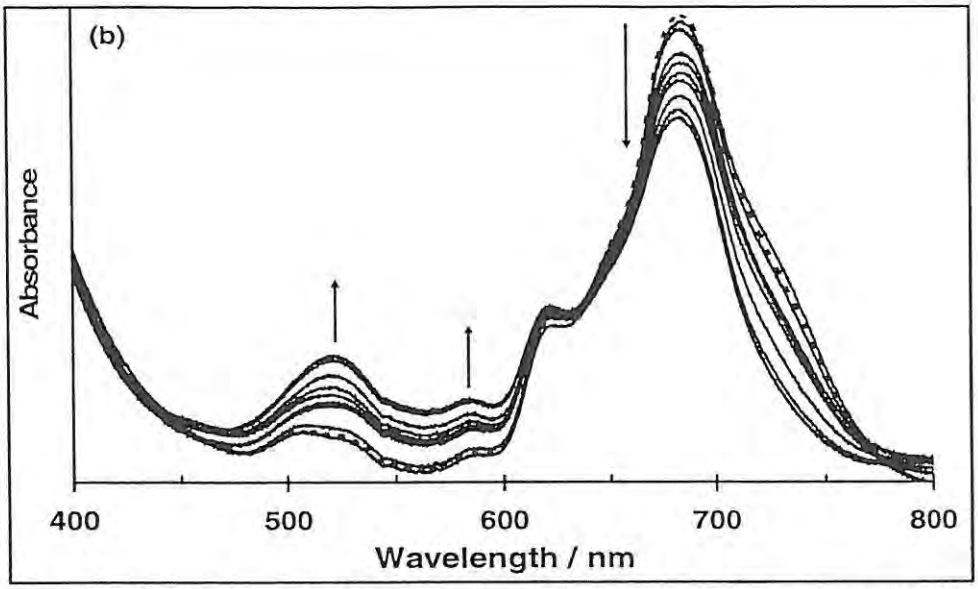

Fig 4.14b: UV-Visible spectral changes observed during controlled potential (OTTLE cell) reduction of ~3.0 mM MnTETPc, in DMF containing 0.1 M $TBABF_4$. Applied potential for = -1.1 V vs. Ag|AgCl

Chapter Five

Electrode Modification

This chapter is concerned with the methods employed to attach the metallophthalocyanine complexes studied in this thesis on electrode surfaces. The following methods were used to immobilize the complexes: Electropolymerization; drop-dry and chemisorption by self-assembly. The spectral and electrochemical properties of the immobilized species, on different electrode substrates, will be discussed in this chapter. First, the electropolymerization will be discussed, followed by the drop-dry method and finally the self-assembled monolayer (SAM) formation.

5.1 Pyrrole Substituted Metallophthalocyanines (7-12)

Glassy carbon and ITO electrodes were employed for the polymerization. The ITO modified electrodes were employed for spectral studies. The polymerization of only CoTPhPyPc (**7**), NiTPhPyPc (**10**) and CoTPOPyPc (**12**) are presented as representatives for the rest of the pyrrole substituted MPcs. Electropolymerization was also observed for the rest of the pyrrole substituted complexes, FeTPhPyPc (**8**), MnTPhPyPc (**9**), and ZnTPhPyPc (**11**). Electropolymerization of the pyrrole-substituted phthalocyanines was difficult to achieve in DMF. Indeed, no formation of thin films was visible on the surface of the electrodes, probably because of the high solubility of the oligomer (intermediates) in DMF, as it was previously reported in the case some pyrrole-substituted complexes.[413] Only dichloromethane (DCM) showed promising utility, thus DCM was used to perform the electrochemical polymerization of the prepared complexes.

5.1.1 Electropolymerization of Cobalt-tetra-4-(pyrrol-1-yl)phenoxyphthalocyanine (CoTPhPyPc, 7)

Fig 5.1 shows the cyclic voltammogram of CoTPhPyPc (7) in DCM + 0.1 M $TBABF_4$ solution, at a glassy carbon electrode. The CV indicates that the complex exhibits in the potential range, - 1.4 to 1.2 V vs. Ag|AgCl, the previously discussed redox processes shown in DMF (see Fig 4.1) and assigned to metal oxidation and the formation of $Co^{III}TPhPyPc^{-2}$ species at 0.70 V (**I**) and metal reduction followed by ring reduction leading to the formation of $Co^{I}TPhPyPc^{-2}$ and $Co^{I}TPhPyPc^{-3}$ at - 0.4 V (**II**) and - 1.1 V

(III) vs. Ag|AgCl, respectively. However, in DCM (Fig 5.1), the peaks were less resolved compared to DMF, Fig 4.1a.

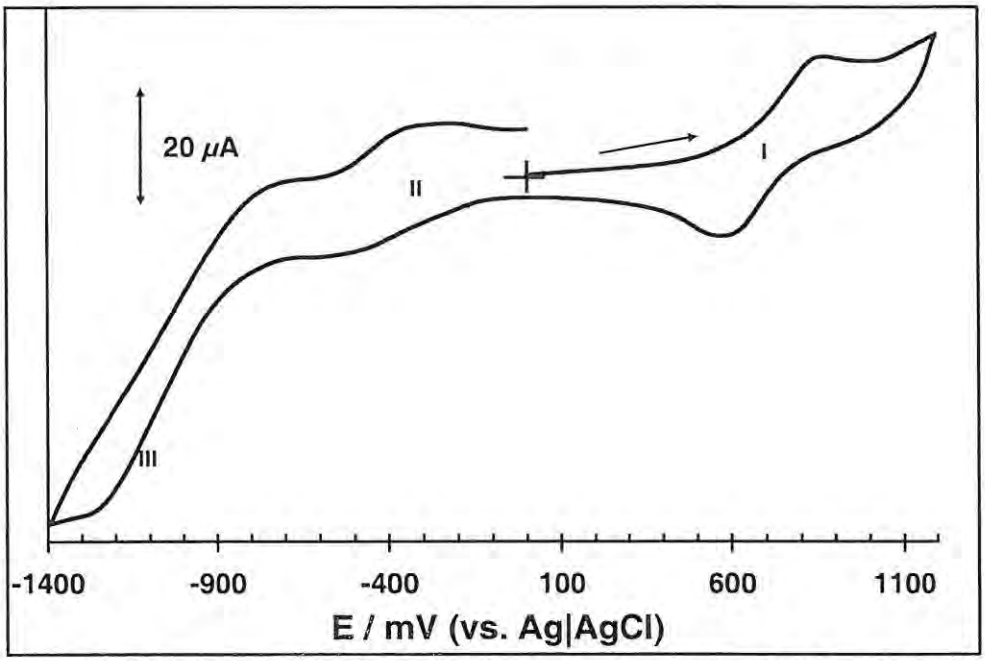

Fig. 5.1: Cyclic voltammogram of CoTPhPyPc (7) in DCM containing 0.1 M $TEABF_4$. Scan rate = 200 mVs^{-1}, concentration = 3 x 10^{-3} M, electrode = GCE.

Fig 5.2 shows the evolution of the cyclic voltammograms of CoTPhPyPc during repeated potential scans from - 0.6 V vs. Ag|AgCl to 1.2 V vs. Ag|AgCl. The continuous increase in the amplitude of the cyclic voltammetric peaks for the previously described systems related to $Co^{III}TPhPyPc^{-2}/Co^{II}TPhPyPc^{-2}$ (couple **I,** Fig 5.2) and $Co^{II}TPhPyPc^{-2}/Co^{I}TPhPyPc^{-2}$ (couple **II,** Fig 5.2) processes indicates that a film was formed on the electrode as a consequence of electrochemical polymerization of the attached pyrrole groups due to their irreversible electrochemical oxidation. In addition, after 5 potential scans, a new peak appears around 0.4 V vs. Ag|AgCl. A similar peak (referred to as "prepeak") at the onset of polymer matrix oxidation has been observed for numerous types of functionalized electroactive polymer films.[429-434] The intensity of the peak

around 0.4 V increases with the number of scans and its potential shifts gradually to more positive values.

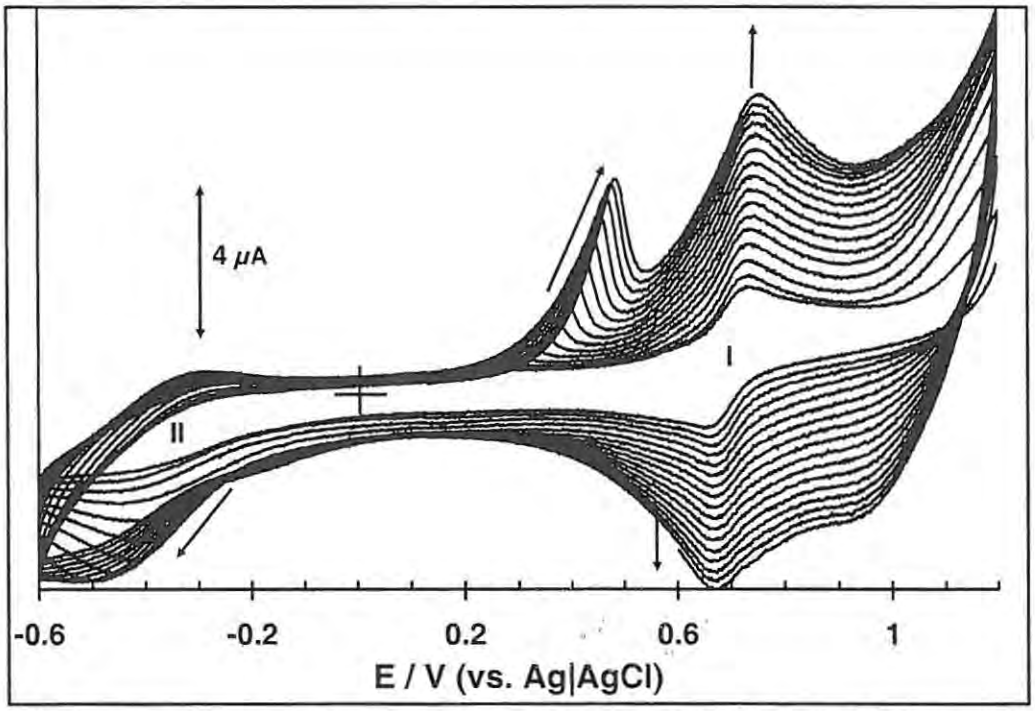

Fig 5.2: Evolution of the cyclic voltammograms of complex CoTPhPyPc in DCM containing 0.1 M $TEABF_4$ during repetitive cycling (only 15 scans are shown). Scan rate = 200 mVs^{-1}, concentration = ~1.5 x 10^{-3} M, electrode = GCE.

This new anodic process depicts the electroactivity of the polymer matrix formed during the electropolymerizing scans, as it has been previously reported with other pyrrole-substituted complexes.[402,435] Note that the number of the electropolymerizing scans controls the amount of the deposited complex and thus the surface density of the obtained film.[405,435] Several attempts at electropolymerizing the complex by scanning the potential electrode through wider ranges, by varying either the anodic or the cathodic limits, did not favour the expected typical evolution for the electropolymerization of the complex shown in Fig. 5.2. After seven consecutive scans, the peak current related to the Co^{II}/Co^{I} couple decreased gradually until no current signal was observed as the cycling

continued. However, the peak currents related to the polymer pre-peak and the Co^{III}/Co^{II} progressively increased as the scanning continued until up to 120 electropolymerization scans.

After a period of scanning, the electrode is transferred after rinsing in DCM to a DCM + 0.1 M $TBABF_4$ solution (without monomeric CoTPhPyPc in solution). In addition to the new polymer peak, the cyclic voltammogram of this electrode (Fig 5.3) exhibits the electrochemical responses previously described for the complex in solution. This indicates that a polymeric phthalocyanine film, noted as *poly*-CoTPhPyPc, was formed on the electrode. The two well-defined pairs of peak, which can be attributed to the $Co^{III}TPhPyPc^{-2}/Co^{II}TPhPyPc^{-2}$ (**I**) and $Co^{II}TPhPyPc^{-2}/Co^{I}TPhPyPc^{-2}$ (**II**) redox processes, are observed at nearly the same potential as for the monomer redox systems in solution. The additional anodic peak (prepeak) assigned to the polymer matrix electroactivity (as previously discussed) appears only upon scanning the electrode potential through values more negative than - 0.2 V vs. Ag|AgCl.

No prepeak was observed when the initial potential was more negative the – 0.2 V. However when the second sweep was allowed to start from potentials more neative than – 0.2 V, (such - 0.6 V vs. Ag|AgCl in Fig 5.3), the polymer prepeak became very apparent. This observation has been referred to a 'memory effect' where the response of the film depends on its preceding treatment[432,436] The term 'memory effect' was first proposed by Odin and Nechtchein[436] for the modification of the oxidation wave of polypyrrole, polyaniline (and related polymers) after an extended exposure to a high negative potential. The first scan is different from the second and subsequent scans in that there was no polymer peak observed during the first scan. However, upon reversal, and

at a switching potential of – 0.6 V, the polymer peak became evident. This may be due to the activation of the polymer peak at a more negative potential.

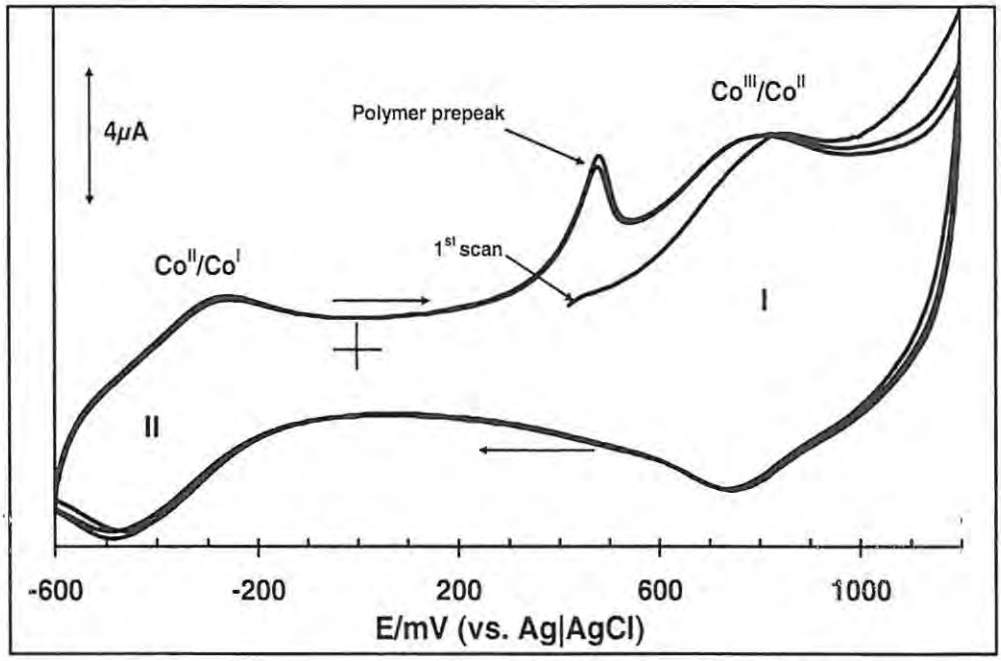

Fig. 5.3: Cyclic voltammograms of poly(Co-TPhPyrPc) film (prepared as indicated in Fig 5.2) after its transfer to a fresh DCM containing 0.1 M $TEABF_4$ solution. . Scan rate = 200 mVs^{-1}, concentration = ~1 x 10^{-4} M, electrode = GCE.

It should be noted that the obtained cyclic voltammograms, as shown in Fig. 5.3, are very stable upon repeated potential scans, i.e. after the first scan. A plot of scan rate vs. current for the modified electrodes in blank electrolyte solution was linear. The polymer surface coverage was estimated by integrating the area under the Co^{III}/Co^{II} wave and the results are in the range of monolayer coverage as indicated in Table 5.1.

Table 5.1: Total surface coverage of the polymer modified electrodes using complexes **7**, **10** and **12.**

Complex	No of scans	Surface coverage (moles cm^{-2})
CoTPhPyPc (7)	20	1.97×10^{-10}
	30	2.81×10^{-10}
	60	3.91×10^{-10}
	120	5.18×10^{-10}
CoTPOPyPc (**12**)	20	2.04×10^{-10}
	40	3.23×10^{-10}
	60	3.98×10^{-10}
	80	4.58×10^{-10}
	100	4.92×10^{-10}
NiTPhPyPc (**10**)	10	1.21×10^{-10}
	20	2.01×10^{-10}
	30	1.98×10^{-10}
	40	1.38×10^{-10}

Spectral characterization of Poly-CoTPhPyPc on ITO

The electropolymerization of CoTPhPyPc (**7**) complex was further studied on optically transparent indium tin oxide (ITO) electrodes. Fig 5.4 shows the typical CVs obtained during a continuous scan of 1.5 mM of complex **7** in DCM + 0.1 M $TBABF_4$ on ITO electrode, and these are similar to Fig 5.3. Indeed, *poly*-CoTPhPyPc films were obtained on ITO electrodes and this allows the monitoring of their growth by the changes observed in the UV-Visible spectra. The spectra were recorded by placing the dry *poly*-CoTPhPyPc-ITO electrodes in the light path of the spectrometer.

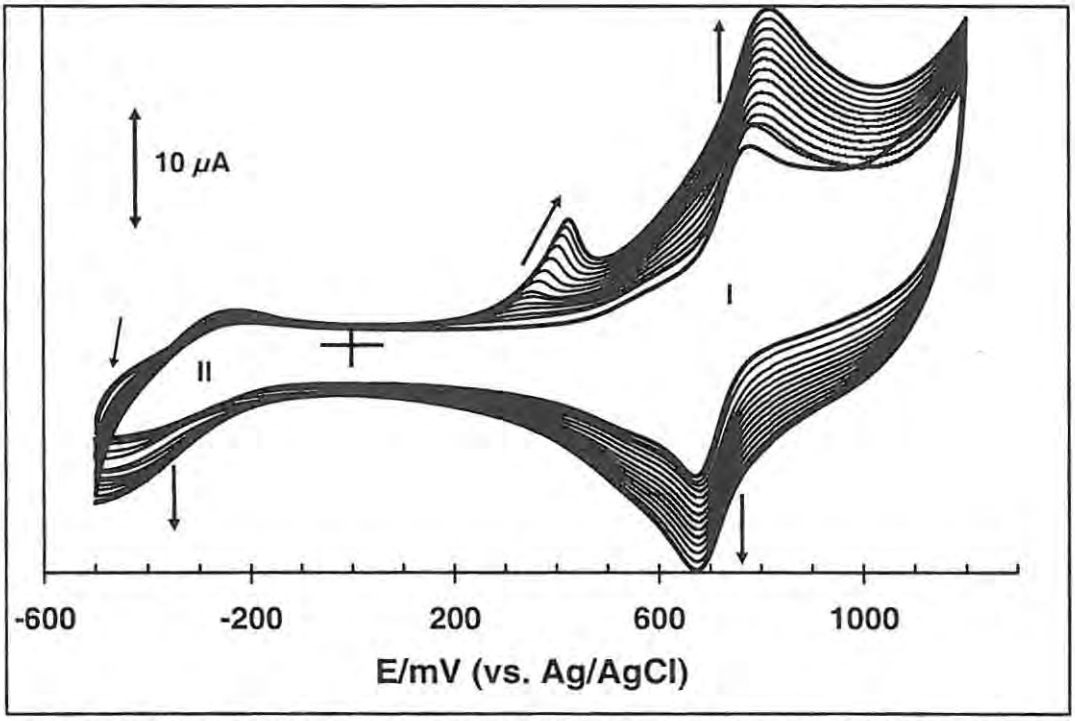

Fig 5.4: Evolution of the CVs of 1.5 mM CoTPhPyPc in DCM containing 0.1 M $TBABF_4$ during repetitive cycling. Scan rate: 200 mVs^{-1}. Electrode: ITO

Typical spectra for three films of polymeric CoTPhPyPc (7) prepared by 30, 60 and 120 electropolymerizing scans are shown in Fig 5.5. The curve labelled (*) corresponds to the absorption spectra of CoTPhPyPc monomer in DCM solution and shows bands at 600 and 680 nm. The UV-Visible spectra obtained for the polymer films are similar to monomer species, but exhibit a notorious broadening of the bands along with a red shift. Such a considerable broadening of UV-Visible bands have been previously reported in the case of electropolymerized metalloporphyrin and phthalocyanine films[283,399,437] and explained in terms of stacking and high aggregation of the complexes on the electrode surface. The intensity of the absorption bands increased with the number of electropolymerizing scans, indicating that the electroformation process of the film progresses during the cycling of the potential. The similarity of the

polymer and monomer spectra indicates that the Pc conjugated-π system has remained intact upon electropolymerization.

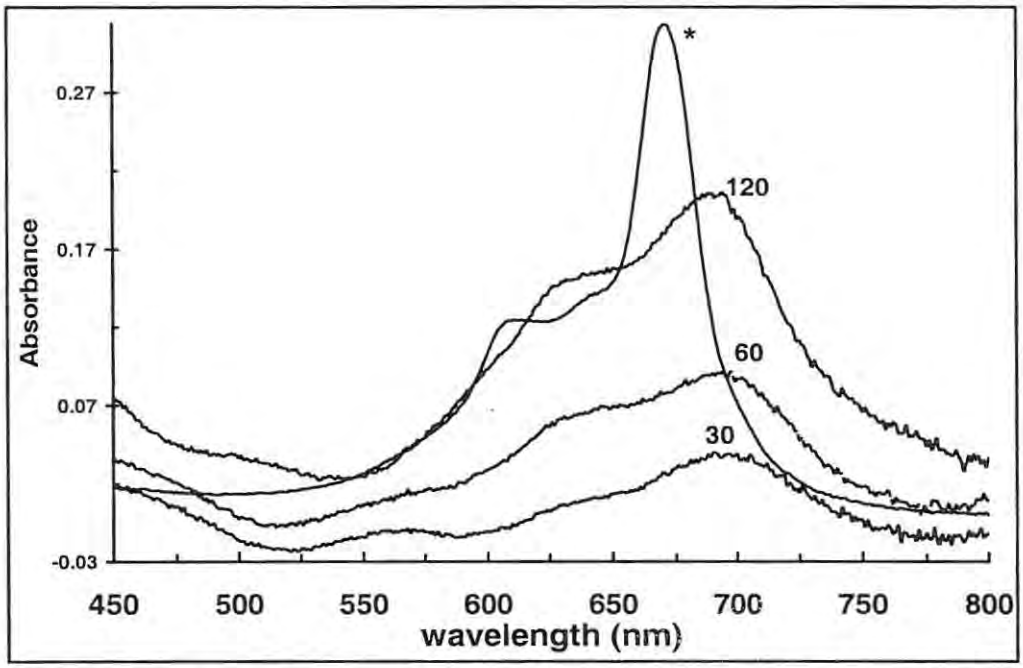

Fig. 5.5: Absorption spectra of *poly*-CoTPhPyPc films on ITO electrodes prepared with 30, 60 and 120 electropolymerizing scans as indicated in Fig. 5.4. The curve labelled (*) corresponds to CoTPhPyPc monomer adsorbed by dipping ITO in DCM solution of complex **7**.

5.1.2 Electropolymerization of Cobalt-tetra-5-(pyrrol-1-yl)pentoxyphthalocyanine (CoTPOPyPc, 12)

As stated earlier, the electropolymerisation of N-substituted pyrrole functionalised MPcs are easier to achieve in DCM than in DMF. Fig 5.6 shows the voltammogram evolutions during a repetitive cycling of CoTPOPyPc (**12**) in a DCM solution containing 0.1 M $TBABF_4$. The continuous increase in both the anodic and cathodic waves shows that there is the formation of polymeric films on the electrode. The increase in the irreversible anodic wave around 0.2 V (vs. Ag|AgCl) (Fig 5.6a) relates to the polymer

formation emanating from polymerization of the attached pyrrole ring[405] as observed above in the case of CoTPhPyPc (7). The couple at ~ 0.6 V is associated with Co^{III}/Co^{II} oxidation observed as **I** in Fig 4.2 for the monomer in DMF.

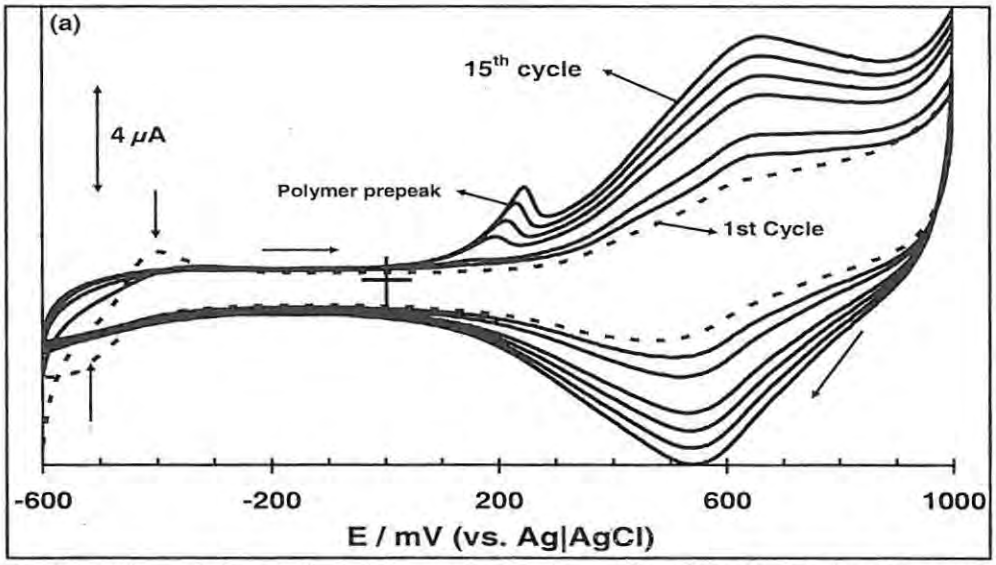

Fig 5.6a: Evolution of the cyclic voltammograms of complex CoTPOPyPc in DCM containing 0.1 M $TEABF_4$ during repetitive cycles for the first 15 scans. Scan rate = 200 mVs^{-1}, concentration = ~ 0.9 mM, electrode = GCE.

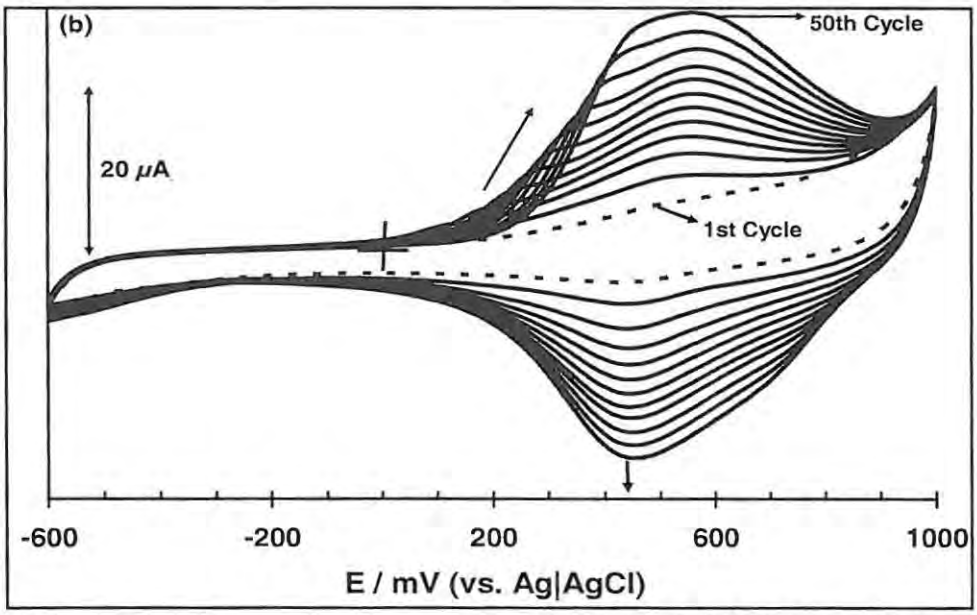

Fig 5.6b: Evolution of the cyclic voltammograms of complex CoTPOPyPc in DCM containing 0.1 M $TEABF_4$ during repetitive cycles for 50 scans showing the overlap of the polmer prepeak with the Co^{III}/Co^{II} redox process.. Scan rate = 200 mVs^{-1}, concentration = ~ 0.9 mM, electrode = GCE.

Upon continuous scanning, it can be seen that the wave ascribed to the polymer shifted to a more positive potentials until it overlaps with the process due to the central metal (Fig. 5.6b). Considering the consistency, (i.e. no shift), of the peak potential for the central metal redox process as a function of electropolymerisation scan number, the shift in the wave due to the polymer may have resulted from the reorganisation of the *poly*-CoTPOPyPc.[438] The growth mode of Pc thin films is said to depend on various conditions including molecular structures, central metal, substrate materials (i.e. the electrode material) and the deposition rate.[173] This change in orientation is possibly allowed since the insulating pentoxy group is flexible enough to accommodate such a change as the electropolymerisation proceeds, as opposed to the voltammograms observed in the case of the more rigid phenoxy spacer in CoTPhPyPc (7). It was possible to control the surface concentration with the electropolymerization scan number.

Fig 5.7 shows the cyclic voltammograms obtained when the *poly*-CoTPOPyPc modified GCE is transferred into a blank solution of DCM + 0.1 M $TBABF_4$. The numbers indicate the voltammetric scan numbers employed to obtain the respective polymer films. The voltammetric response of *poly*-CoTPOPyPc film on repeated cycling in a blank DCM solution (i.e. without MPc monomer) is shown in Fig. 5.7b. It can be seen that the voltammogramms in Fig 5.7 are similar to the CV obtained during polymerization. The films can be cycled repetitively in the anodic direction more than 50 times with a less than 10% loss of electroactivity. The surface coverage of the complex at different scan numbers on the modified GCE show an increase with number of scans as summarized in Table 5.1

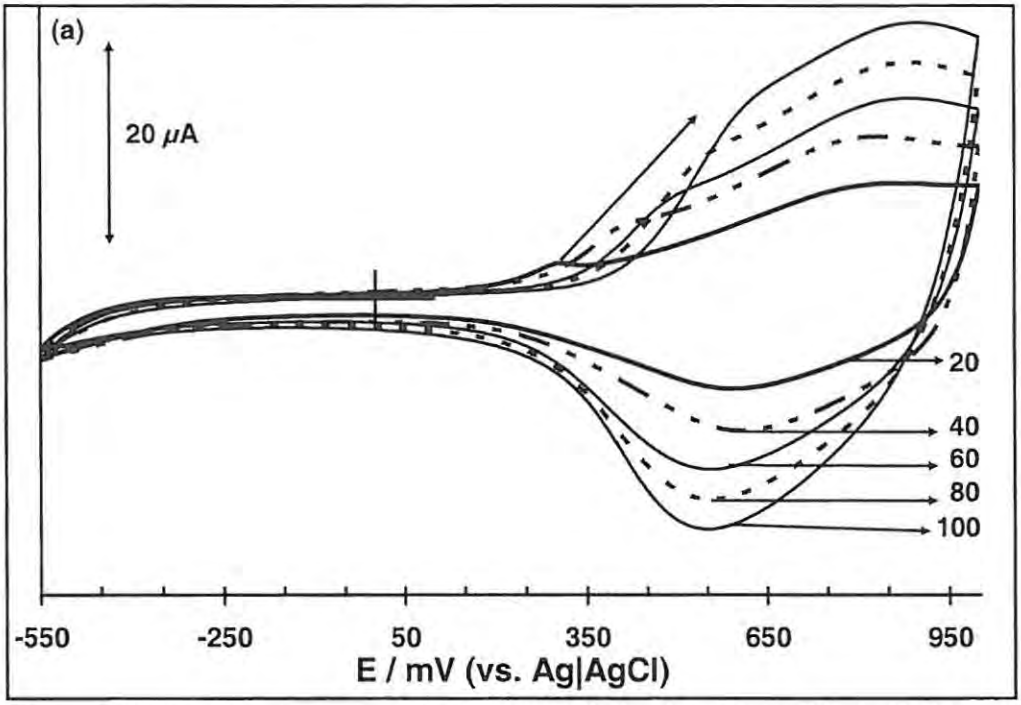

Fig 5.7a: Voltammetric responses of *poly*-CoTPOPyPc electrode in blank DCM + 0.1 M $TBABF_4$ solution for different scan numbers. The number shows the polymerization scan numbers. Scan rate: 100 mVs^{-1}.

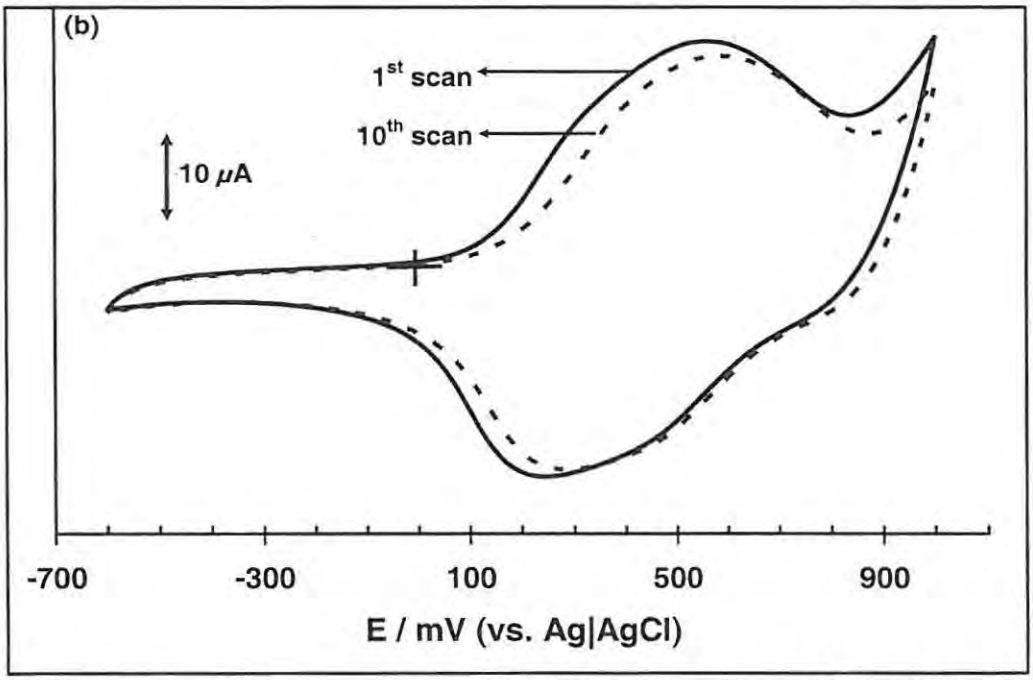

Fig 5.7b: Voltammetric responses of *poly*-CoTPOPyPc electrode in blank DCM + 0.1 M $TBABF_4$ solution upon repetitive cycling. Scan rate: 100 mVs^{-1}.

5.1.3 Electropolymerization Nickel-tetra-4-(pyrrol-1-yl)phenoxyphthalocyanine (NiTPhPyPc, 10)

Fig 5.8 shows typical cyclic voltammograms observed during film growth in the monomer solution of 1.5 mM NiTPhPyPc in DCM containing 0.1 M $TBABF_4$. The growth was only observed, and more obvious, when the anodic switching potential was above 1.1 V, hence 1.2 V vs. Ag|AgCl was used as the oxidation potential in agreement with the previous results using CoTPhPyPc (**7**). The couple observed at ~ 0.78 V in Fig 5.8 was not observed for complex **10** in DMF (Fig 4.1d) and was not observed in the first scan in Fig 5.8 thus suggesting that it is a consequence of polymer formation.

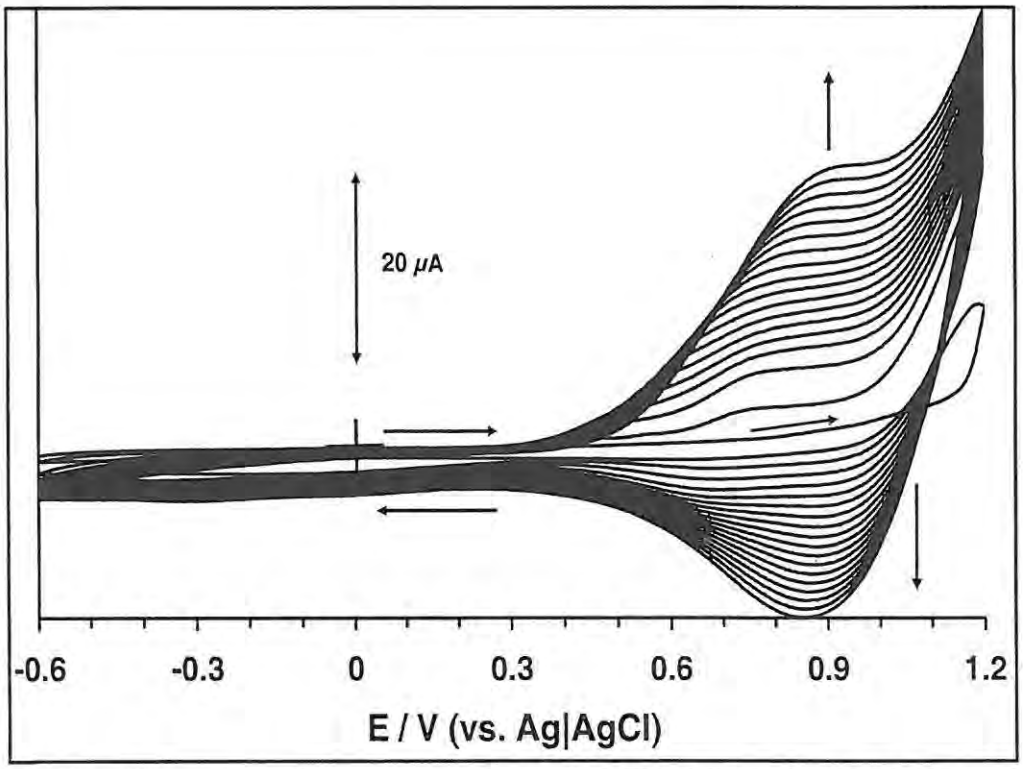

Fig 5.8: Repetitive cyclic voltammograms of 1.5 mM NiTPhPyPc in 0.1 M $TBABF_4$ + DCM. Scan rate: 200 mVs^{-1}. Horizontal arrows show the direction of scan.

As it is shown in Fig 5.8, there is a noticeable difference between the first scan and the subsequent scans. The direction of the scan was reversed at a potential just before the pyrrole oxidation peak. This 'early' potential switch resulted in a loop. This is an observation occurring where a surface phase is formed by a nucleation and growth mechanism as reported by Asavapiriyanont *et al.*[439] in the case of polypyrrole formation on platinium electrode, and it indicates that the oxidation of the pyrrole attached to the Pc ring occurs more readily on the polymer than on unmodified GCE, i.e., the formation of polymer involves a nucleation step.[439-442] The shift of the polymer peak to more positive potentials on cycling suggests an increase in the electrical resistance of the polymer film and that an overpotential is needed to overcome the resistance[443] A progressive change from light green to dark green, as the film thickens, was seen on the electrode surface depending on the sweep number.

Fig. 5.9 shows the cyclic voltammograms for *poly*-NiTPhPyPc obtained form 10, 20 and 30 cyclic scans. It can be seen that above 20 electropolymerisation cycles, the polymer film tends to lose conductivity. When the scan number was increased to 40 cycles, a further decrease in peak current was observed. Thus, the optimum sweep number of 20 scans gave the best result (in terms of conductivity) for a monomer solution of 1.5 mM of the NiTPhPyPc complex, and was employed for subsequent studies. The polymer is denoted as [*poly*-NiTPhPyPc]$_{20}$. The estimated surface coverage for each cycle scan number shows an increase until 20 scans then a decrease as indicated in Table 5.1. The surface coverage was in the order of ~ 10^{-10} moles cm^{-2}, hence a monolayer coverage.

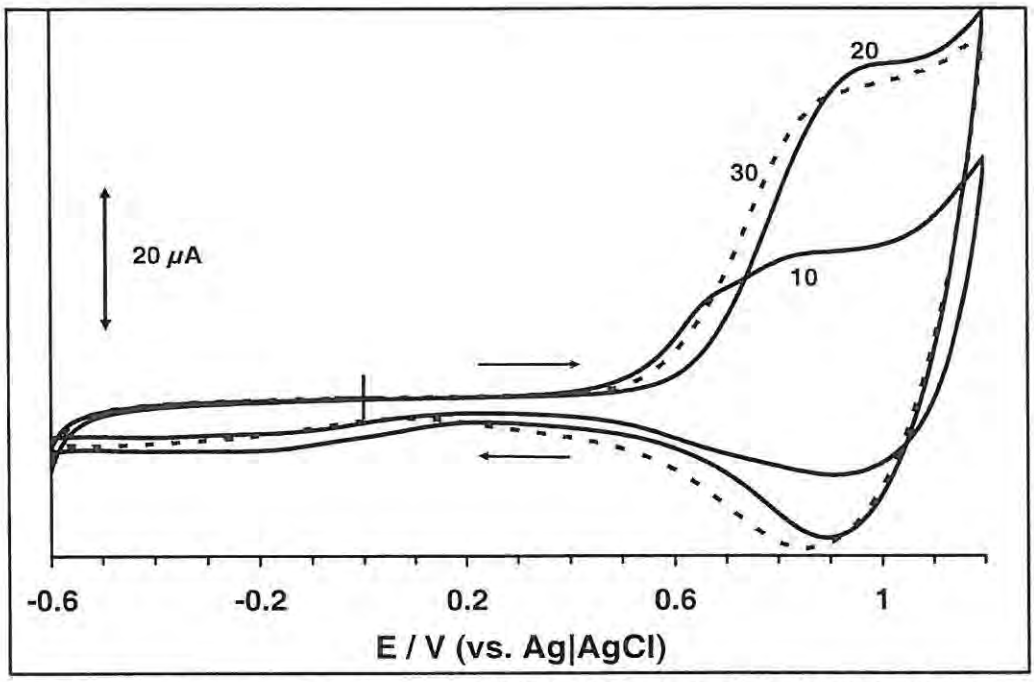

Fig 5.9: Cyclic voltammograms of *poly*-NiTPhPyPc-GCE electrode in 0.1 M $TBABF_4$ + DCM. Scan rate: 200 mVs^{-1}. The numbers indicate the scan numbers used to obtain the films.

Fig 5.10 shows the evolution of the cyclic voltammograms obtained during a repetitive cycling of [*poly*-NiTPhPyPc]$_{20}$ electrode in 0.1 M NaOH solution between - 0.1 and + 1.1 V vs. Ag|AgCl. The progressive increase of the anodic and cathodic waves between 0.1 and 0.4 V, vs. Ag|AgCl, is indicative of the transformation of *poly*-NiTPhPyPc to *poly*-Ni(OH)TPhPyPc as suggested by literature[444,445] in the case of nickel tetraaminophthalocyanine (NiTAPc) and NiTSPc. The voltammogram in Fig. 5.10 is similar to those previously reported for NiTAPc complex[443,444] except that in the present study, the wave corresponding to the organic moiety of the macrocycle of the Pc appears to be significantly involved in the transformation process.

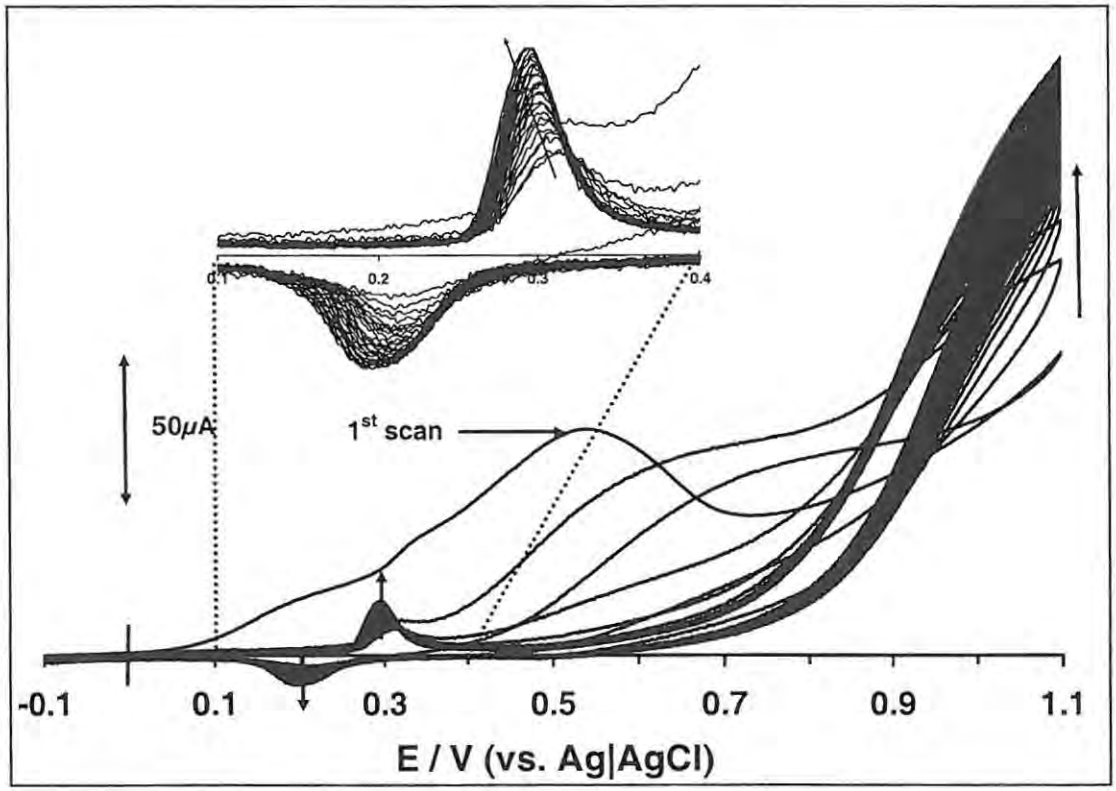

Fig 5.10: Repetitive cyclic voltammograms of *poly*-$[NiTPhPyPc]_{20}$ in 0.1 M NaOH for the transformation of *poly*-$[NiTPhPyPc]_{20}$ to *poly*-Ni(OH)TPhPyPc. Scan rate: 200 mVs^{-1}. Insert: Expansion of the 0.1 to 0.4 V area.

Indeed, during the first scan, a large anodic current was observed at E ~ + 0.5 V showing that a transformation of the *poly*-NiTPhPyPc film was occurring. As soon as the second scan was performed, the intensity of the peak at ~ + 0.5 V became significantly smaller and shifted to more positive potentials, showing the end of the irreversible transformation of the film. In addition, a new well-defined couple of voltammetric peaks appears centred around 0.25 V, which grows continuously until a steady state is reached. The shape of the final cyclic voltammogram is very similar to those obtained with electroformed nickel macrocyclic-based films in alkaline aqueous solution, which are also similar to those of $Ni(OH)_2$ electrode.[446,447] This tends to show that during the electrochemical treatment of *poly*-NiTPhPyPc in alkaline aqueous media, the nickel

phthalocyanine incorporated into the polymeric film behaves in a similar manner to nickel hydroxide electrode and this can be explained by the changes in the axial occupation of the Ni sites as a consequence of the formation of the O-Ni-O oxo bridges in alkaline aqueous solution. The increase and shift of the waves related to the $Ni(OH)_2$-like redox process stabilized after 37 scans, thus all tranformations could be attained, at most, between 35 and 40 cyclic scans. Fig 5.11 shows the cyclic voltammogram of *poly*-Ni(OH)TPhPyPc in blank 0.1 M NaOH solution. The well-defined couple between 160 and 320 mV vs. Ag|AgCl indicates that O-Ni-O oxo bridges have formed. [443,444]

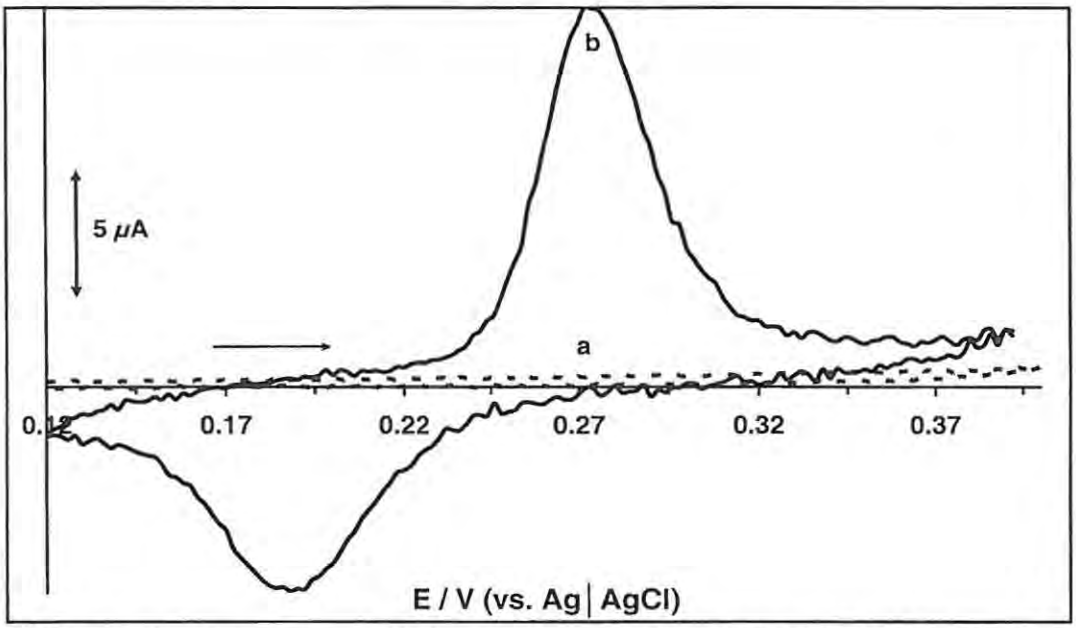

Fig 5.11: Cyclic voltammograms of (a) unmodified and (b) *poly*-Ni(OH)TPhPyPc VC electrode in 0.1 M NaOH solution. Scan rate: 200 mVs^{-1}.

The proposed mechanism, (based on references 441 and 442), for the electrotransformation of *poly*-NiTPhPyPc to *poly*-Ni(OH)TPhPyPc is shown in Scheme 5.1. The initial insertion of the hydroxyl group between the nickel and the GCE at the *poly*-NiTPhPyPc-electrode interface may be responsible for the huge current observed in

the first scan as reported in literature complex[444,445] After this first scan, the subsequent scans afford the continuity of the O-Ni-O link in the presence of the OH^- in the electrolyte solution, hence the increase in the current signal associated with the nickel hydroxide-like electrode in the CV (Fig 5.10 insert). Thus the role of the OH^- group is to furnish the oxygen required for the O-Ni-O linkage in the polymer.

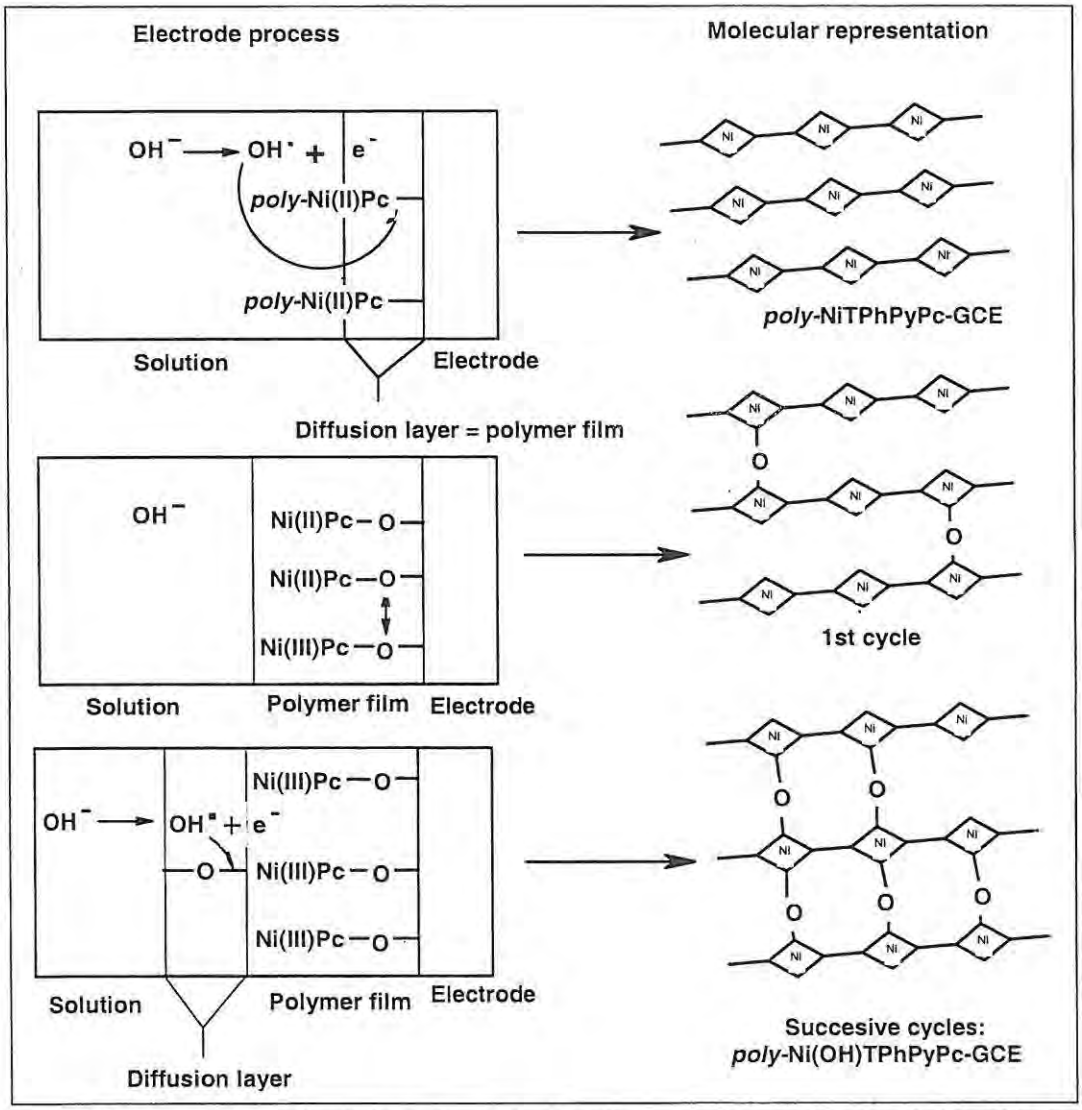

Scheme 5.1: Proposed mechanistic pathway for the electrotransformation of *poly*-NiTPhPyPc to *poly*-Ni(OH)TPhPyPc.[444,445]

Spectral characterization of Poly-NiTPhPyPc and poly-Ni(OH)TPhPyPc

UV-Visible spectral studies were conducted to record the spectral changes on the thin films of the polymer on ITO (dry film). The results were correlated with those obtained from GCE for different electropolymerization scan numbers. Fig 5.12a shows the spectra of four different polymer films on ITO electrodes. The numbers indicated on the curves represent the respective electropolymerisation scan numbers employed to obtain the polymer films.

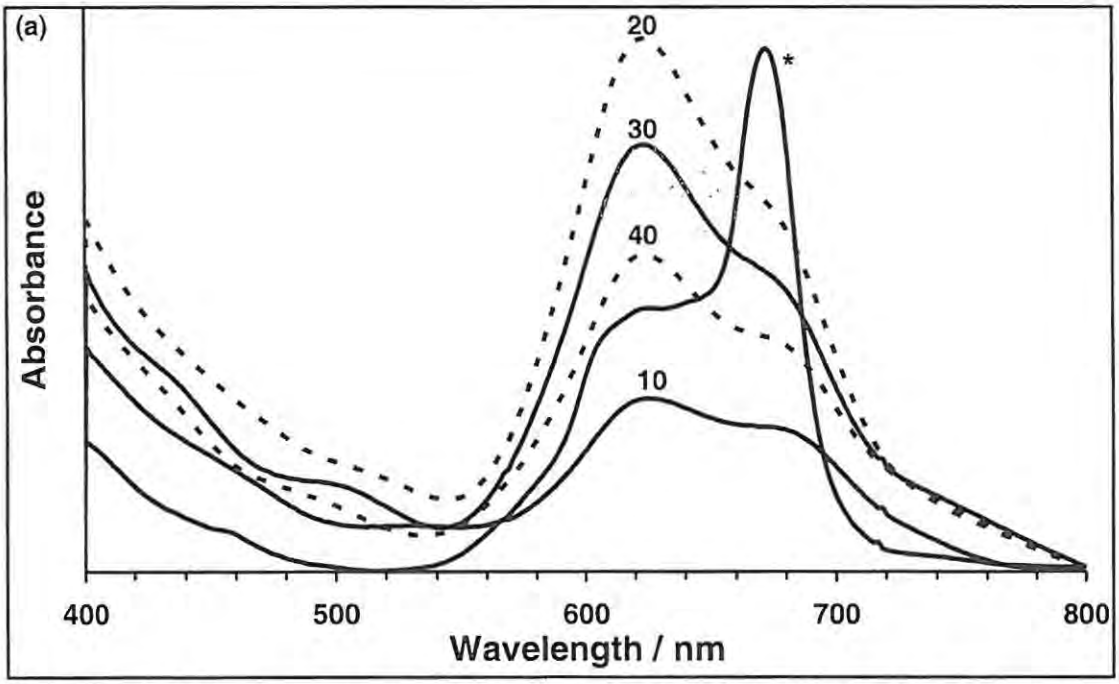

Fig 5.12a: UV-Visible spectra of *poly*-[NiTPyPhPy]$_n$-ITO electrode (dry film). The numbers show the scan numbers used to obtain the polymers. (*): UV-Visible spectrum of freshly adsorbed monomer on ITO (by placing the ITO in a solution of monomer and allowing it to dry).

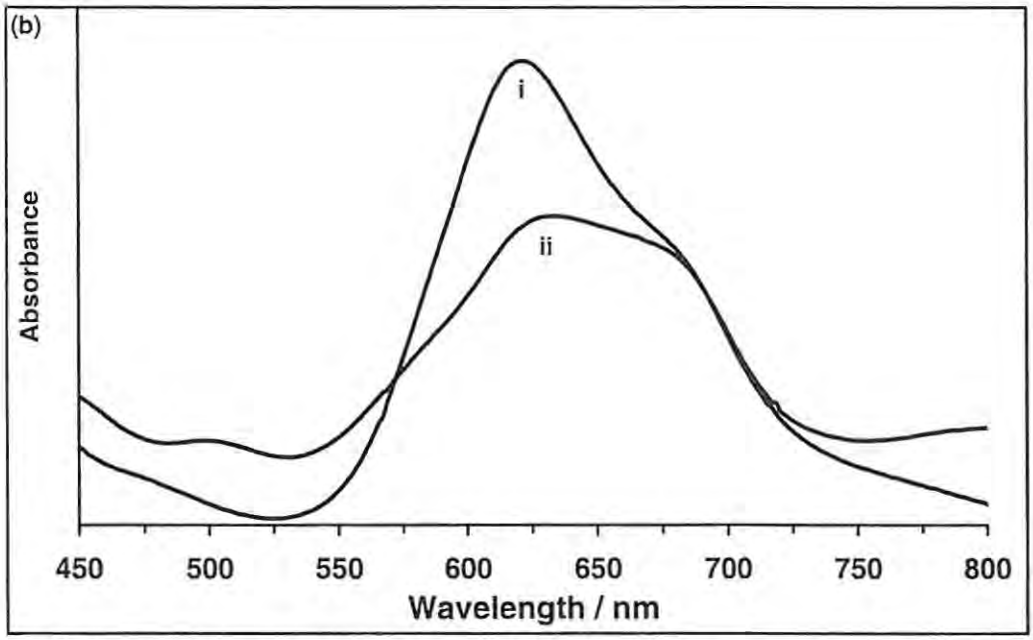

Fig 5.12b: UV-Visible spectra of (i), *poly*-[NiTPhPyPc]$_{20}$ before electrotransformation and (ii), *poly*-Ni(OH)TPhPyPc on ITO electrode (dry film).

The spectra corresponding to 10 and 20 cyclic scans show a progressive increase in π conjugation as the polymer density increased and there is a decrease in peak height after 20 scans confirming the observation for GCE (Fig 5.9). The increase in absorbance (up to 20 scans) could also be a result of stacking of the monomeric species. The relative increase in the absorbance of the high-energy band, (at 621 nm), compared to the low-energy band at 671 nm shows that the polymer formed is a product of the dimeric species formed from the monomer as the voltammetric cycling is continued. It has been shown earlier that the dimeric species of the NiTPhPyPc predominates at higher concentrations of the complex **10** (see Fig 3.2b, trace IV, Chapter Three). It has been shown,[150,448,449] that oligomers are formed and play an important role during the growth of poly pyrrole and poly thiophene. Electropolymerization is known to occur simultaneously with the formation of dispersed or dissolved oligomers in the monomer solution in which the electrolysis is taking place. Since polymers formed from small oligomers are expected to

have more cross-linked structures than those formed from strictly monomer solutions[450] it not surprising that as more oligomers are formed and dispersed in the solution, some non-conducting cross-linked oligomers may be trapped into the polymer film. It seems that as the cycling number is increased more oligomers of different lengths are formed. These oligomers are probably trapped in the polymer films hence reducing the π-conjugation of the "effective" polymer. This process may increase the cross-linking and lead to loss of conductivity as electropolymerization progresses, thus explaining the decrease in peak currents and absorbances of the polymer formed from cycles above 20. The loss of conductivity could also be due to a different type of polymer which is less conducting.

The electropolymerization was also affected by the concentration of the monomer solutions. At higher concentrations, the maximum conducting state of the polymer or oligomer is soon attained followed by a rather early loss of conductivity. The observation may be due to faster cross-linking of polymers as more non-conducting oligomers are expected to form at higher concentrations. The conducting state of the oligomer (or polymer) seems to occur above five electropolymerization cycles. This assumption was reached from the fact that there was no noticeable change in the voltammograms and UV-Visible spectra when the electrodes were transferred into blank $TBABF_4$ solution after five cycles. It could also imply that there was not enough polymer film on the electrode surface, after five cycles that can be observed by UV-Visible spectrophotometric measurement.

The UV-Visible spectrum of *poly*-Ni(OH)TPhPyPc on ITO is shown in Fig. 5.12b. The high energy absorption peak (at 623 nm) for *poly*-Ni(OH)TPhPyPc is of about the same intensity as the low energy peak (at 671 nm). Whereas for the *poly*-

$[NiTPhPyPc]_{20}$ on ITO, the high energy peak is more intense than the low energy peak. The band at 500 nm may be related to complexes containing oxo bridges formed between the individual Ni(III) species on the ITO as suggested by Hahn *et al.*[451] using UV-Visible reflectance spectroscopy.

5.2 Tetraamino Metallophthalocyanine Complexes (19 and 20)

For the MTAPc complexes, electropolymerization was achieved in DMF since the complexes were not soluble in DCM. As indicated above in the case of the pyrrole substituted MPcs the electropolymerization were performed on GCE and ITO electrodes.

5.2.1 Electropolymerization of Chromium tetraamino-phthalocyanine (CrTAPc, 19)

It is known that repetitive cyclic voltammetry scanning of solutions containing MTAPc in DMF results in the polymerization of the species onto electrode.[348,452] Polymerization of CrTAPc was achieved by scanning in the potential range - 0.6 to + 1.3 V (vs. Ag|AgCl). Repeated cycling of the monomer in this potential range resulted in the deposition of an electroactive polymer on the GCE surface. Fig 5.13 shows the evolution of voltammograms during the electropolymerization. There was a general increase in currents with scanning, except for the currents in the 700 mV region which decreased.

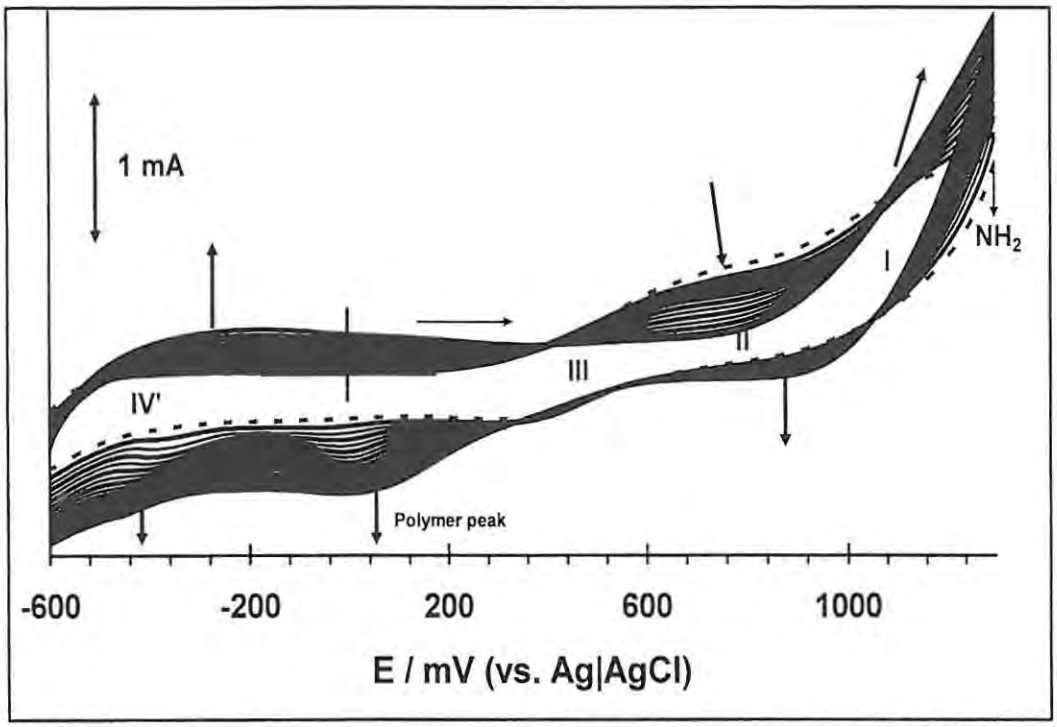

Fig 5.13: Evolution of cyclic voltammograms during electropolymerization of CrTAPc in DMF containing 0.1 M $TBABF_4$ on GCE. Scan rate: 200 mVs^{-1}.

The oxidation of the amino group is believed to generate free radicals, which initiate the electropolymerization process. It was possible to control the surface concentration of the polymer by varying the electropolymerisation scan number. In this study, scan numbers: 20, 40, 60, 80 and 100 (hereinafter referred to as [*poly*-CrTAPc]$_x$, where x = number of scans), were used and the conductivities of the polymer films were examined as a function of the Faradaic currents of the cathodic and/or anodic waves in the blank electrolyte solutions (either TBABF4 in DMF, or pH 7.3 and pH 4.3 buffers).

Fig 5.14 shows the CV for modified electrodes in a blank pH 4.3 acetate buffer solution. The numbers represent the number of repetitive cycles employed during the electrosynthesis of the polymer. An interesting feature is the colour of the *poly*-CrTAPc modified electrode surface. The surface of the electrode was green when the

polymerisation scan number was 20 ([poly-CrTAPc]$_{20}$). With [poly-CrTAPc]40, [*poly*-CrTAPc]$_{60}$ and [poly-CrTAPc]$_{80}$ the electrode surfaces changed gradually from green to light blue. Since there was an increase in conductivity going from [poly-CrTAPc]$_{20}$ to [poly-CrTAPc]$_{40}$, the colour change could simply be a result of increasing surface density of the polymer on the electrode.

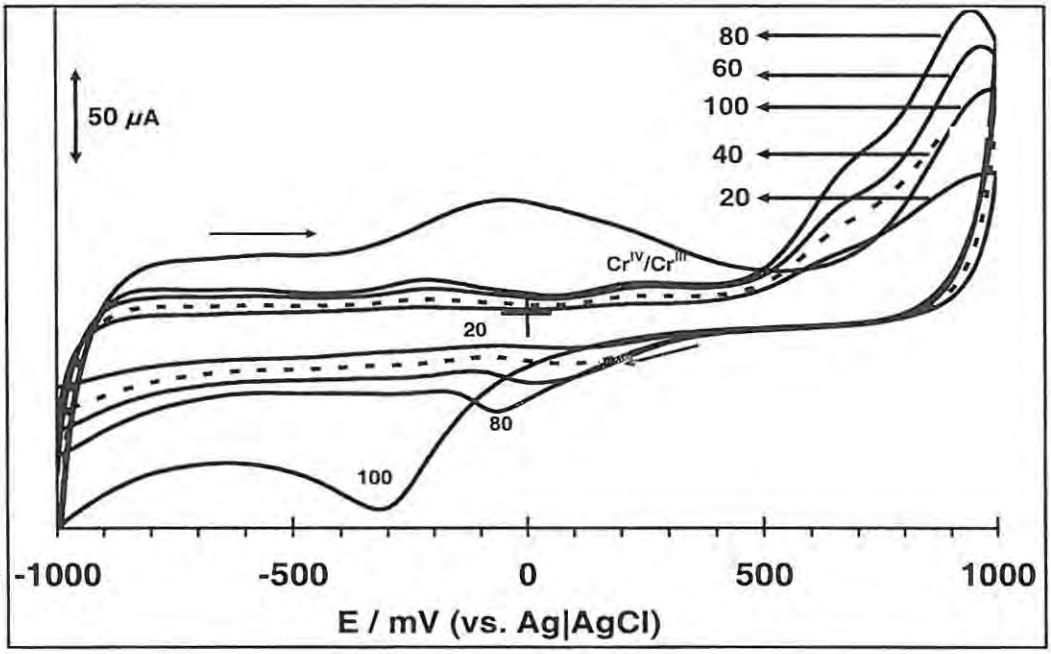

Fig. 5.14: Voltammetric profiles of the absorbed CrTAPc polymer on a GCE in a N_2 deaerated pH 4.3 acetate buffer solution. Scan rate: 200 mVs^{-1}. The numbers correspond to the number of repetitive scans used for the respective polymerization.

The reduction peak near 100 mV, after 20 cycles on the reverse scan, shifted to more negative potentials with increase in polymerization scan number in Fig 5.14. Surface coverage on the electrode was calculated from the area under the peaks for the last cycle, after the specified scan numbers, and was found to be of the order of 10^{-10} mol cm^{-2}, typical[283] value for monolayer coverage. Comparing the peaks in Fig 4.9 with the peaks of the polymer in Fig 5.14, it is likely that the peaks near 950 and 675 mV for the polymer, Fig 5.14, are due to ring based oxidation processes of the polymer and the peak

(between 0 and 300 mV) which shifts to negative potentials with scan number is due to the preceding metal based oxidation, $Cr^{IV}TAPc^{-2}/Cr^{III}TAPc^{-2}$. Above a polymerization scan number of 80, there was a steady decrease in current in the 400–1000 mV range, which was accompanied by a dramatic change of electrode surface colour from light blue to deep blue. This shows that the optimum polymerization scan number is around 80 within the limits of experimental conditions employed in this work. The decrease in current between 400 and 1000 mV (Fig 5.14) shows that after the optimum polymerization scans, the *poly*-CrTAPc modified electrode becomes less conducting (resistant to further polymerization of the active surface). Electropolymerization was also performed on indium tin oxide (ITO) coated glass electrodes. The evolution of the voltammograms was similar to that observed for the GCE as can be seen in Fig 5.15.

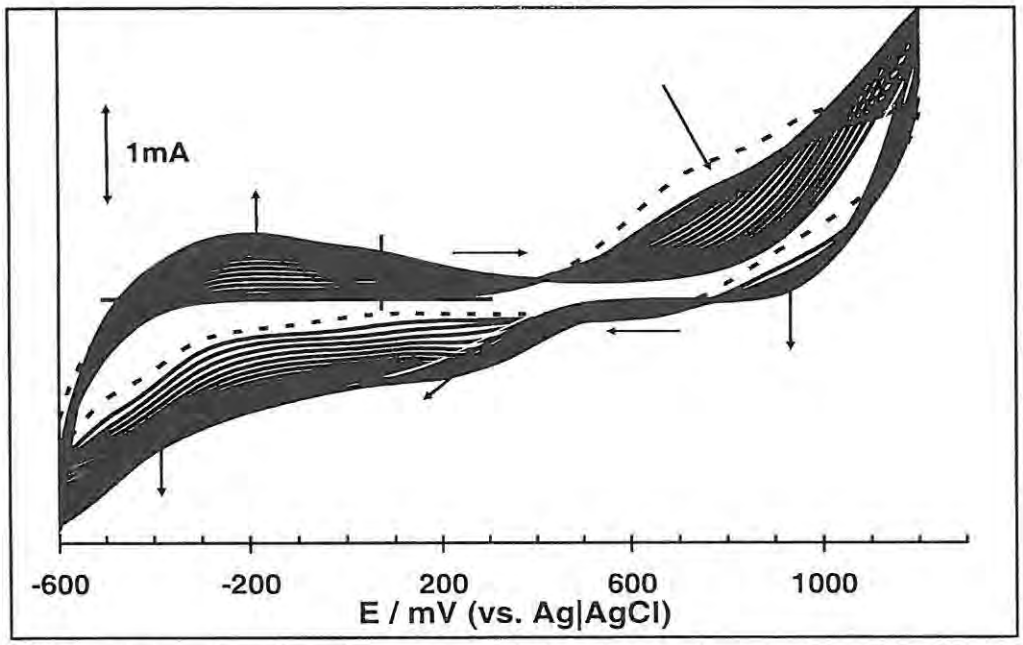

Fig 5.15: Evolution of cyclic voltammograms during electropolymerization of CrTAPcin DMF containing 0.1 M $TBABF_4$ on ITO. Scan rate: 200 mVs^{-1}.

Spectral Characterization of Poly-CrTAPc on ITO

Fig 5.16 shows the spectra for the monomer on ITO and the increase in the intensity of the absorption bands with increase in polymerization scans on ITO. Very broad spectra were observed for the polymers compared to the adsorbed monomer (Fig 5.16 (*)). The monomer was adsorbed onto the ITO by dipping the ITO electrode in the CrTAPc solution, and drying in air. The peak broadening of the polymer spectra has been attributed to the aggregation of the phthalocyanine polymer on the ITO.[283]

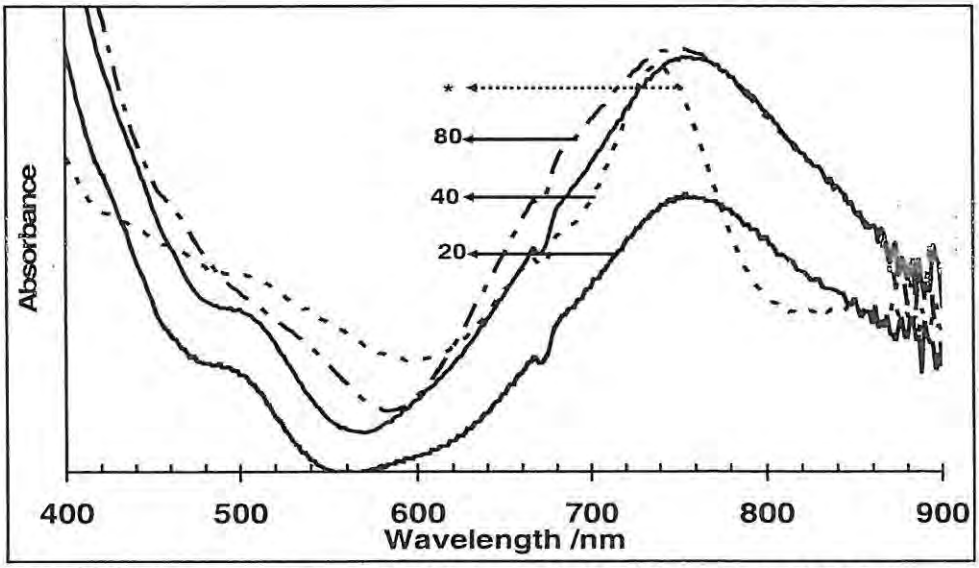

Fig 5.16: UV-Visible spectra of [*poly*-CrTAPc]$_{20}$; [*poly*-CrTAPc]$_{40}$; [*poly*-CrTAPc]$_{80}$ on ITO. (*) monomeric CrTAPc (adsorbed by dipping the ITO electrode in the CoTAPc solution, and dying in air). The spectra are recorded in pH 4.3 buffer.

The films grown by different electropolymerization scan numbers can also be showed by examining their surface morphology (Figure not shown). It was easy to see the surface structure of the films increase progressively with a more uniform and finely networked pattern as the electropolymerization scan number increased from 20 to 60. The observation confirmed that there was progressive aggregation or stacking of the *poly*-

CrTAPc on the electrode surface with scan number as suggested by the increase in the absorbance of the UV-Visible spectra of the polymers

5.2.2 Electropolymerization Manganese tetraamino-phthalocyanine (MnTAPc, 20)

Fig 5.17 shows that repetitive scanning of MnTAPc solution in DMF results in a gradual increase in the Faradaic current for both the oxidation and reduction processes. The CV peaks are similar to those observed for the monomer in Fig 4.10a except that the peak at - 1.37 V, (labelled **VI**), is more easily observed here on repetitive scanning.

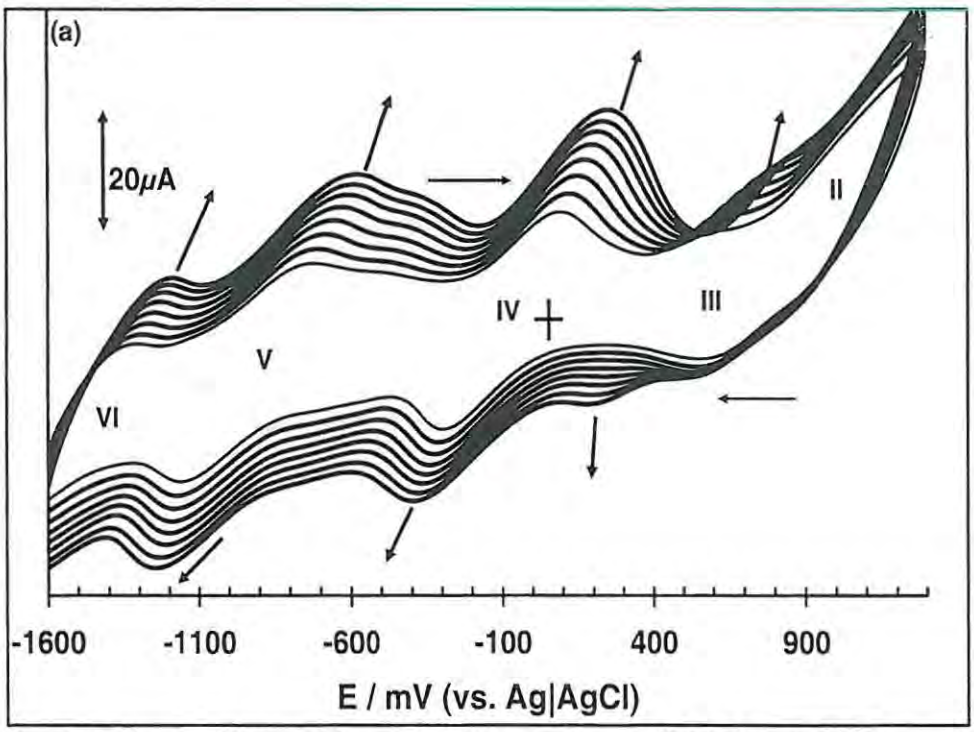

Fig 5.17a: Evolution (on GCE) of the cyclic voltammograms of MnTAPc in DMF containing 0.1 M $TBABF_4$ during repetitive cycles and the formation of *poly*-MnTAPc. Long range scan: - 1.6 to + 1.2 V vs. Ag|AgCl (only eight scans are shown). Scan rate: 200 mVs^{-1}.

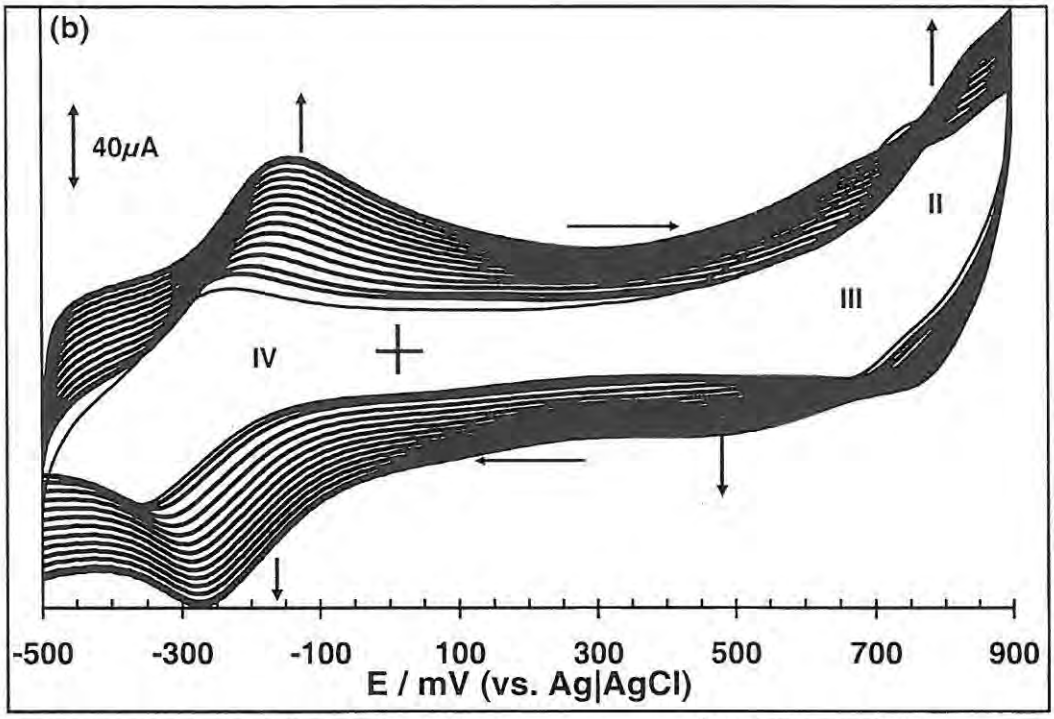

Fig 5.17b: Evolution (on GCE) of the cyclic voltammograms of MnTAPc in DMF containing 0.1 M $TBABF_4$ during repetitive cycles and the formation of *poly*-MnTAPc. Short range scan: - 0.6 to + 0.9 V vs. Ag|AgCl. Scan rate: 200 mVs^{-1}.

As seen in Fig 5.18 (a and b), the first scan is different from the subsequent scans suggesting that different species (the polymer) is formed on the electrode. The increase in currents on repetitive scanning is also attributable to the polymeric species deposited onto the electrode. The anodic to cathodic peak separations of the polymer couples are wider than for the monomer. This behaviour suggests an increased electrical resistance and the resistance to mass transport as the surface concentration of the polymer increases and this becomes a major obstacle to fast growth.[139] The polymer formed was clearly visible on the electrode as a blue surface. It was found that after 110 cyclic voltammetry cycles there was no observable increase in the current attributed to the polymer, suggesting the complete electropolymerization, i.e. no further adsorption of the polymer onto the electrode. The couples shifted to more positive values with cycling. Fig 5.17b shows the

effect of short-range polymerisation (scanning range: from - 0.50 to 0.90 V), as opposed to long range polymerisation (scanning from - 1.8 to 1.2 V in Fig 5.17a). As discussed in Chapter Four, cyclic voltammograms recorded using a wide window results in less reversible couples than observed for narrower scan windows. Polymerizing in the narrow potential window resulted in improvement in the sharpness of the peaks, Fig 5.17b, and a much smaller increase in anodic to cathodic peak separations of the couples on polymerization, compared to the increase in peak separation in the larger potential window. Thus, for a wide potential window there is apparent loss of conductivity and electroactivity, but the condition improves for a narrower potential window. This observation has been suggested to be due to oxidation reactions which lead to a loss of conjugation in the case of poly pyrrole, when scanning within a long potential range.[411] There is less cross-linking and fewer structural defects at a smaller potential window. At high reducing or oxidizing potentials, side reactions can lead to products which attack the polymer. The cyclic voltammetry behaviour of the polymer film formed within a narrow potential window was more reproducible compared to the wider range one. Hence, the electrode film formed from the former was used in all subsequent studies. Different polymerization scan numbers were done but catalytic properties of the electrodes were examined with the films obtained from 20 scans (denoted [*poly*-MnTAPc]$_{20}$). The surface coverage was in the order of 10^{-10} mol cm^{-2} expected for monolayer coverage on the electrode surface. The plot of current versus scan rate was linear for the polymer as expected for surface adsorbed species.

5.2.2.1 pH Study of the Redox Processes of Poly-MnTAPc

The cyclic voltammograms of the electrode (GCE) coated with the polymer, $[_{poly}$-MnTAPc$]_{110}$ cycled in the blank electrolyte (DMF + $TBABF_4$ and at different pHs in aqueous media) solutions are shown in Fig 5.18. Surface coverage on the electrode was calculated from the area under the peaks obtained from cyclic voltammetry when the coated electrode was placed in the blank $TBABF_4$ + DMF (Fig 5.18a) and pH 4 buffer solution (Fig 5.18b), and cycled until no further increase in current was obtained (using 110 scans). The surface coverage was of the order of 10^{-10} mol cm^{-2}.

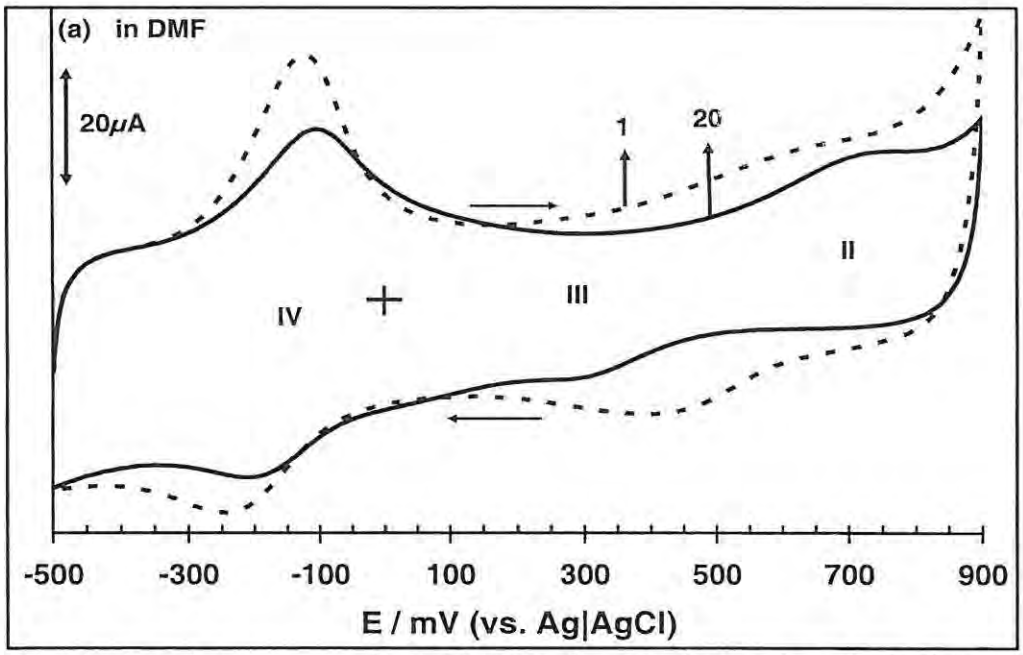

Fig 5.18a: Cyclic voltammograms of *poly*-MnTAPc film, after its transfer to fresh DMF + 0.1 M $TBABF_4$ and then continuously scanned. Scan rate: 100 mVs^{-1}. Electrode: GCE. The peaks are labelled for the 20^{th} scan.

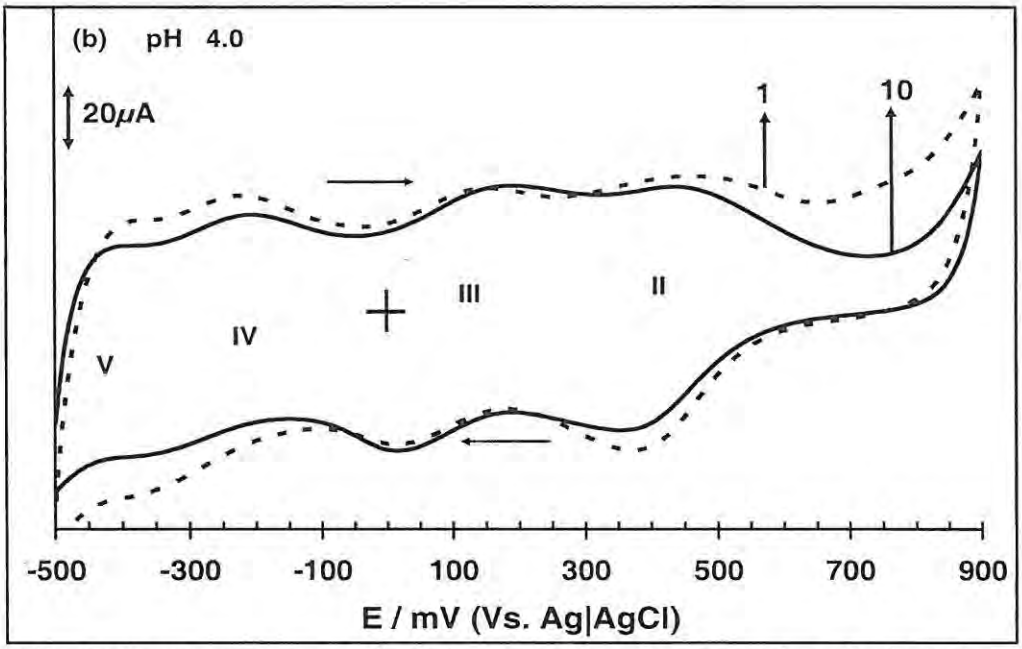

Fig 5.18b: Cyclic voltammograms of *poly*-MnTAPc film, after its transfer to fresh pH 4 and then continuously scanned. Scan rate: 100 mVs^{-1}. Electrode: GCE. The peaks are labelled for the 10^{th} scan.

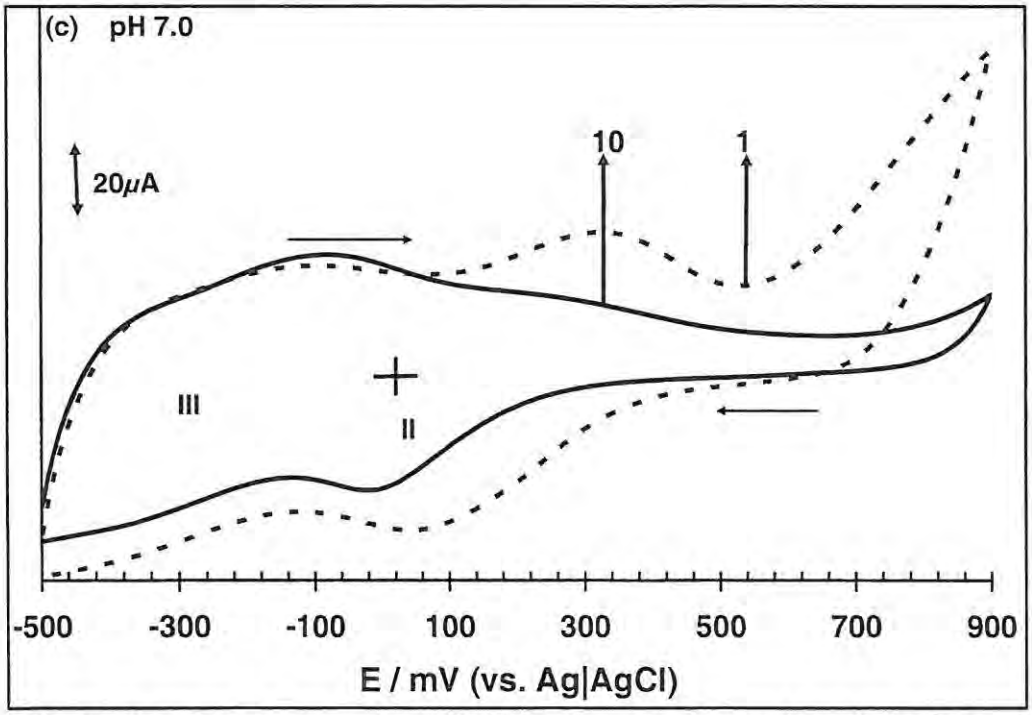

Fig 5.18c: Cyclic voltammograms of *poly*-MnTAPc film, after its transfer to fresh pH 7 and then continuously scanned. Scan rate: 100 mVs^{-1}. Electrode: GCE. The peaks are labelled for the 10^{th} scan.

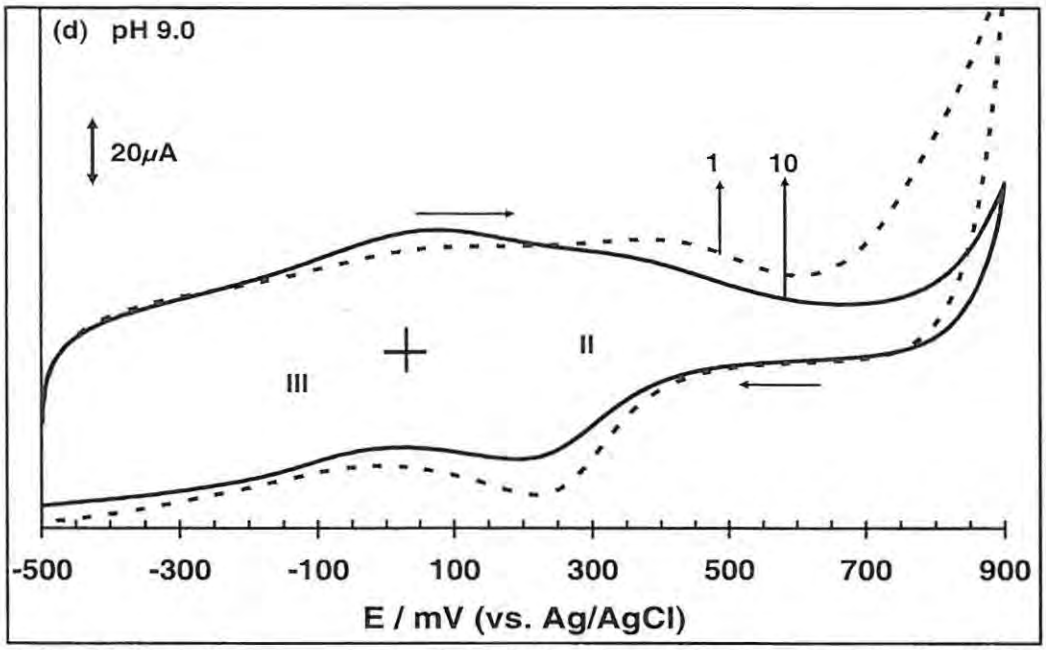

Fig 5.18d: Cyclic voltammograms of *poly*-MnTAPc film, after its transfer to fresh pH 9 buffer solutions, and then continuously scanned. Scan rate: 100 mVs^{-1}. Electrode: GCE. The peaks are labelled for the 10^{th} scan.

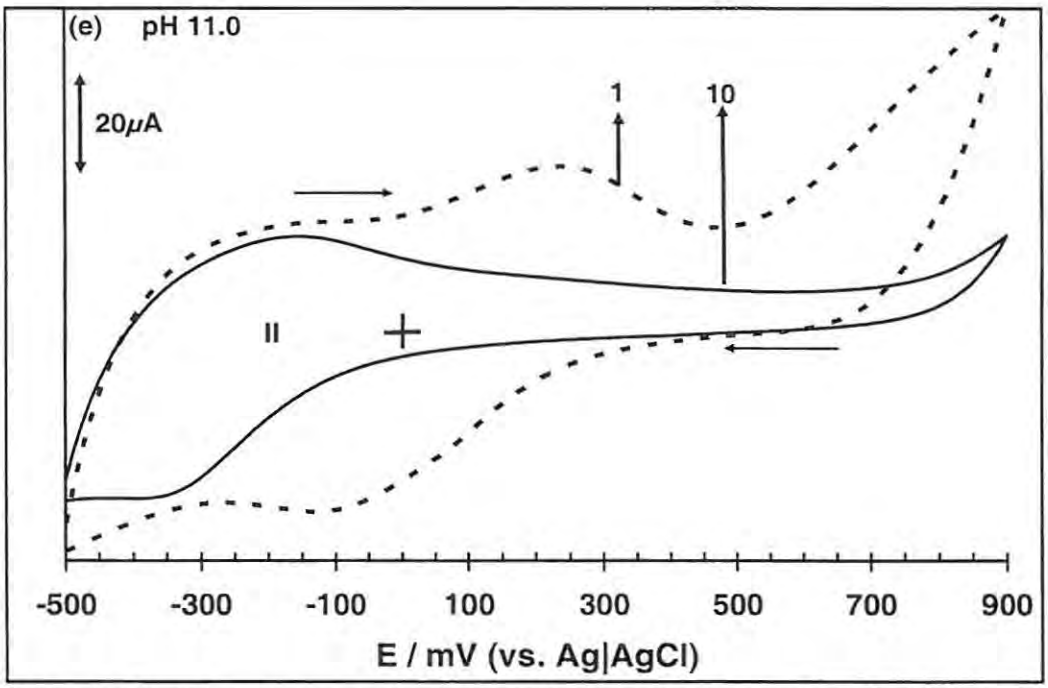

Fig 5.18e: Cyclic voltammograms of *poly*-MnTAPc film, after its transfer to fresh pH 11 buffer solutions, and then continuously scanned. Scan rate: 100 mVs^{-1}. Electrode: GCE. The peak labelling for the 10^{th} scan.

The potentials of polypyrrole polymer are known to shift to more negative potentials with increase in pH.[453] Four couples are observed in Fig 5.19b, and the potentials of the stabilized peaks or couples are $E_{1/2}$ = 0.42 (**II**, $Mn^{IV}Pc^{2-}/Mn^{III}Pc^{2-}$), - 0.07 (**III**, $Mn^{III}Pc^{2-}/Mn^{II}Pc^{2-}$) and - 0.27 V (**IV**, $Mn^{II}Pc^{2-}/Mn^{II}Pc^{3-}$). The last reduction couple at - 0.46 V (**V**) is most likely due to further reduction of the ring and the formation of a Pc^{4-} species. Fig 5.18 also shows that the couples shift to more negative potentials with increase in pH (only pHs 4, 7, 9 and 11 shown). In all cases, there is a decrease in current with scan number, but the current soon stabilizes with a reduction in intensity of about 20% (for couple **III**). For some pHs, (e.g. pH 7 and 11), a shift in peak potential to more negative values with cycling for each pH was observed, until only couple **III** and/or **II** remains, since the other peaks are beyond the scan range. For pH 11, only couple **II** is observed, but is shifted to negative potentials (Fig 5.18e). The shift to the negative potential with increase in pH suggests that OH^- is involved during the redox process. As the pH increases, the couple(s) becomes more irreversible. The peak becomes less reversible with cycling at each pH. The best reversibility is observed in acid media (Fig. 5.18b), suggesting that the H^+ ions assist in the electron transfer associated with the couples. However, as will be shown below, the dependence of potential on pH at low pH was not significant.

It is now accepted that anions become inserted into the phthalocyanine film to maintain charge neutrality during oxidation of the film.[454] It is expected that smaller anions will allow oxidation better than larger anions. Fig. 5.19 shows the effect of anions: Cl^- and NO_3^- on the film. Cl^- being a smaller anion shows marginally more resolved peaks than the larger NO_3^- anion. There is no significant shift in the peak

potential with change in the nature of the anion. The solution was not buffered for Fig. 5.19, but the pH of the bulk solution will be around 7. Comparing the voltammogram obtained at pH 7, Fig. 5.18c, with those in the presence of Cl^- and NO_3^- (Fig. 5.19a and b) shows that the peaks in the presence of anions are shifted to more positive potentials. This shows that the presence of the smaller OH^- in solutions allows for better oxidation than Cl^- and NO_3^-.

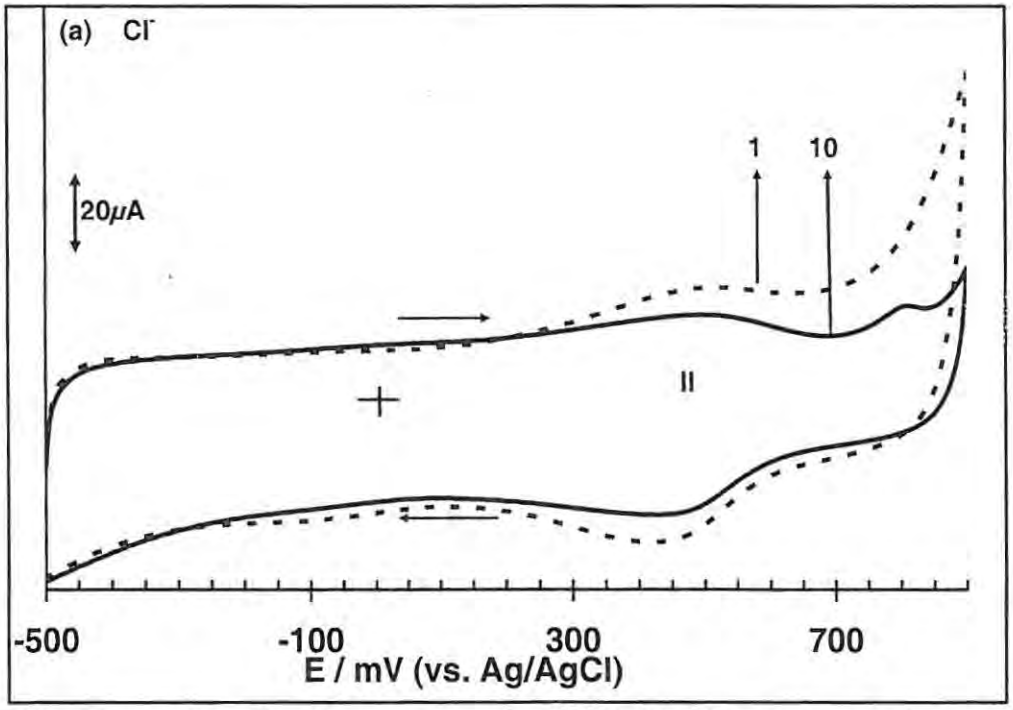

Fig 5.19a: Changes in cyclic voltammograms of *poly*-MnTAPc film, after its transfer to a solution containing 0.1 M KCl. Electrode: GCE.

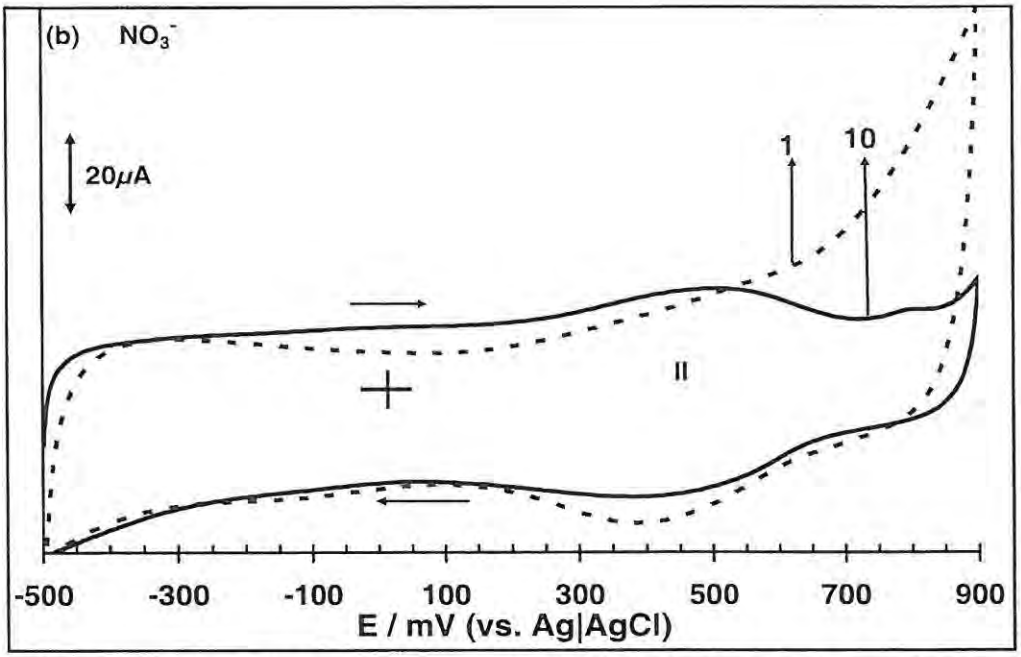

Fig 5.19b: Changes in cyclic voltammograms of *poly*-MnTAPc film, after its transfer to a solution containing 0.1 M KNO_3. Electrode: GCE.

The voltammetric response (couple **II**) of the polymer in different pHs is plotted against pH in Fig. 5.20. At low pH (2–6), the response was basically independent of pH. At high pH (7–12), a 140 mV/pH slope was obtained indicating the involvement of a hydroxyl group during the electron transfer. It seems that the counterion content in the polymer films remains unchanged in acidic media and is progressively lost as the solution pH increases from neutral to more alkaline media. These observations suggest the involvement of protons and hydroxyl groups in the doping and de-doping of the polymer films and that protonation is highly difficult in alkaline media as suggested in literature report.[453]

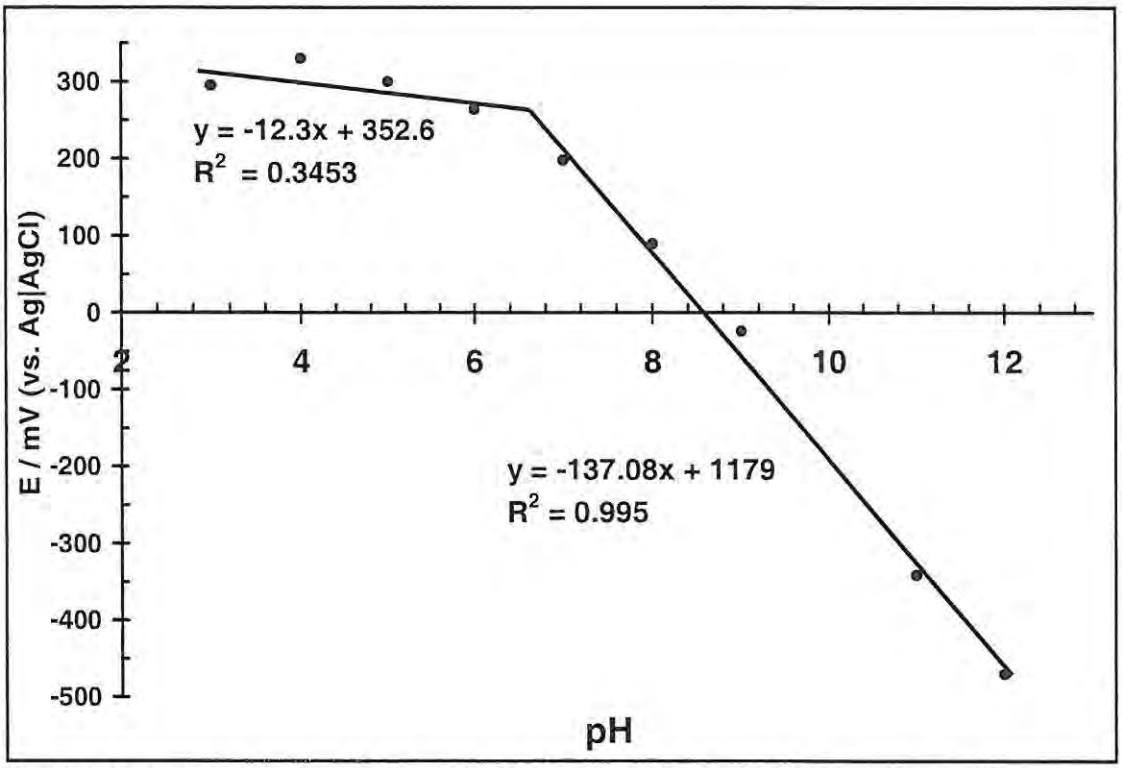

Fig 5.20: Variation of peak potential with pH for couple **II** of poly-MnTAPc (Fig 5.18).

5.2.2.2 Spectral Characterization of Poly-MnTAPc film

Electropolymerization was also carried out on ITO, and the cyclic voltammetry changes were similar to those observed on GCE. It is known that electropolymerization of the MTAPc complexes on various metallic surfaces leads to films of similar properties. The spectrum poly-MnTAPc coated on an ITO surface was compared with that of the monomer on ITO. A very broad spectrum was obtained for the polymer (Fig 5.21, curve a) compared to that of the corresponding monomer (Fig 5.21, curve b). The broadness may be attributed to the aggregation of the phthalocyanine polymer molecules on the ITO electrode,[283] as discussed above for the other polymers.

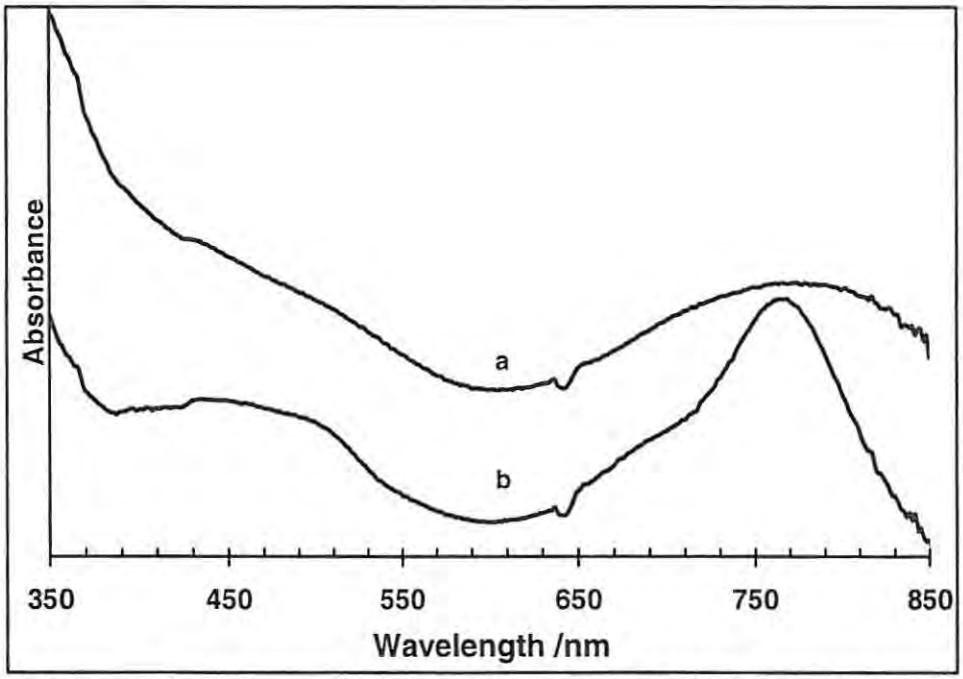

Fig 5.21: Electronic absorption spectra of (a) polymer ([poly-MnTAPc]$_{20}$) and (b) monomeric (MnTAPc) on ITO, formed by dipping the ITO in monomer solution and allowing to dry in air.

5.3 Mercaptoyrimidin Substituted Metallo-phthalocyanine (MTMPyrPc) (13-15)

5.3.1 Electropolymerization

MnTMPyrPc (**14**) is given as example for the polymerization of the mercaptopyrimidin substituted Pcs. Fig. 5.22 shows a series of cyclic voltammograms (CVs) recorded during the formation of polymeric MnTMPyrPc (hereinafter referred to as *poly*-MnTMPyrPc) on GCE from DCM solutions. The first scan in Fig 5.22 is similar to Fig 4.7b in DMF in that high intensity peaks are observed at potentials higher than 1.1 V. These peaks are associated with the mercaptopyrimidyl substituent and/or ring

oxidation of the Pc. Process **IV** (~ 70 mV) observed in Fig 4.7b can be seen during the first scan in Fig 5.22. The electropolymerization required high overpotentials to occur. This could be due to a high potential needed for the oxidation of the pyrimidyl group. The growth of new peaks can be taken as a measure of polymer growth on the electrode surface.[139,140] As can be seen in Fig 5.22, the currents due to the new peaks increased with the number of scans indicating that the polymer film was growing. The slight increase in the peak separation with scan number suggests that the polymer film got increasingly less conductive as the surface concentration of the deposited species increased. This behavior results from the increased electrical resistance and the resistance to mass transport through the film as the film thickness increases which becomes a major obstacle to fast growth.[140] After 50 repetitive cycles, the electrode was thoroughly rinsed with purified DCM followed by washing with methanol and de-ionized water. The electrochemical behavior of the *poly*-MnTMPyrPc electrode was studied in phosphate buffer solution, pH 2-10.

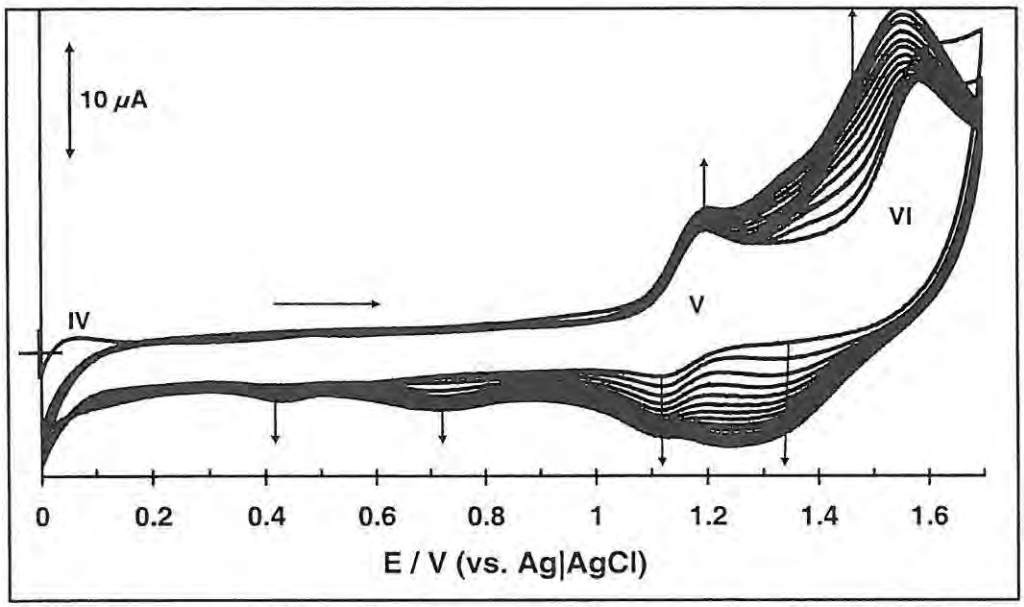

Fig 5.22: Repetitive cyclic voltammetry at a glassy carbon electrode, of 1.5 mM MnTMPyrPc in DCM containing 0.1 M $TBABF_4$. Scan rate: 200 mVs^{-1}. Electrode: GCE.

5.3.2 The Effect of pH on the Poly-Mn^{III}TMPyrPc/ Mn^{II}TMPyrPc Redox Couples

It is vital to understand the basic electrode reactions and evaluate the redox potentials as well as the site of electron transfer of the electrode modified with the polymer films. This is a necessary step in search of electrochemical applications in which this newly synthesized MPc derivatives can be used.[455] Fig 5.23 shows some typical CVs for the *poly*-MnTMPyrPc modified GCE in aqueous solutions ranging from pH 2-7. The peaks of the *poly*-MnTMPyrPc are in the range for Mn^{III}/Mn^{II} couple. This couple was observed at - 0.06 V in DMF but shifted in aqueous media in the case of the adsorbed species. The CV curves show that there is loss of reversibility with increase in pH as was observed in the case of *poly*-MnTAPc. This shows that the electron transfer process is highly favored in proton reach environments. In fact no cathodic wave was observed for CVs performed in phosphate buffer solutions above pH 8. It can be seen that the electrode process changed from reversible to quasi-reversible and finally to irreversible as the media changed from highly acidic to more alkaline. The anodic peaks seem to be less responsive to pH going from acidic to basic media (Fig 5.23).

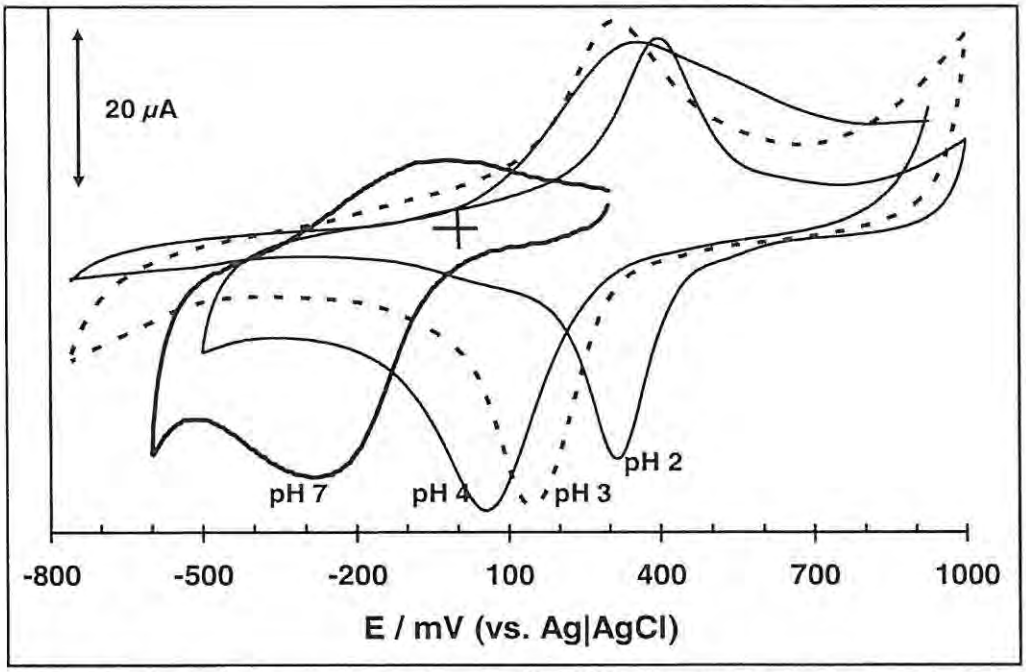

Fig 5.23: Cyclic voltammograms of *poly*-MnTMPyrPc in aqueous phosphate buffer solutions. The respective pHs are as indicated on the curves. Scan rate: 100 mVs^{-1}.

In highly acid solutions, the anodic and cathodic peaks are closer together meaning that oxidation and reduction are easier under these pH conditions, Fig. 5.23. The decrease in reversibility with increase in pH is also demonstrated by Fig. 5.24 (curve a). It has been suggested that the lowering of pH increases the electroactivity of polypyrroles owing to a more open swollen film structure.[453] As discussed above, as the pH increases, the couple becomes more irreversible, suggesting that the H^+ ions assist in the electron transfer associated with the couples. The cathodic peak potential (E_{pc}) vs. pH plot exhibits a linear relationship with slope of - 162 mV/pH, for pH ≤ 4 and slope of - 31 mV/pH, for pH between 4 and 7, Fig. 5.24 (curve b). The slope of the curve at pH < 4 suggest that some of the aza-nitrogen of the Pc ring and/or the pyrimidin units of the polymer film become protonated when the electrode is immersed in acidic solutions and the linear dependence of E_{pc} vs. pH in acidic to neutral solutions may have resulted from

the ionic exchange of the H^+. It seems logical therefore, to conclude that the charge balance is predominantly controlled by the availability of positively charged species and as observed in the case of *poly*-MnTAPc, the films are difficult to protonate in alkaline media, hence the involvement of H^+ and hydroxyl groups are implicated in the general electron transfer process.

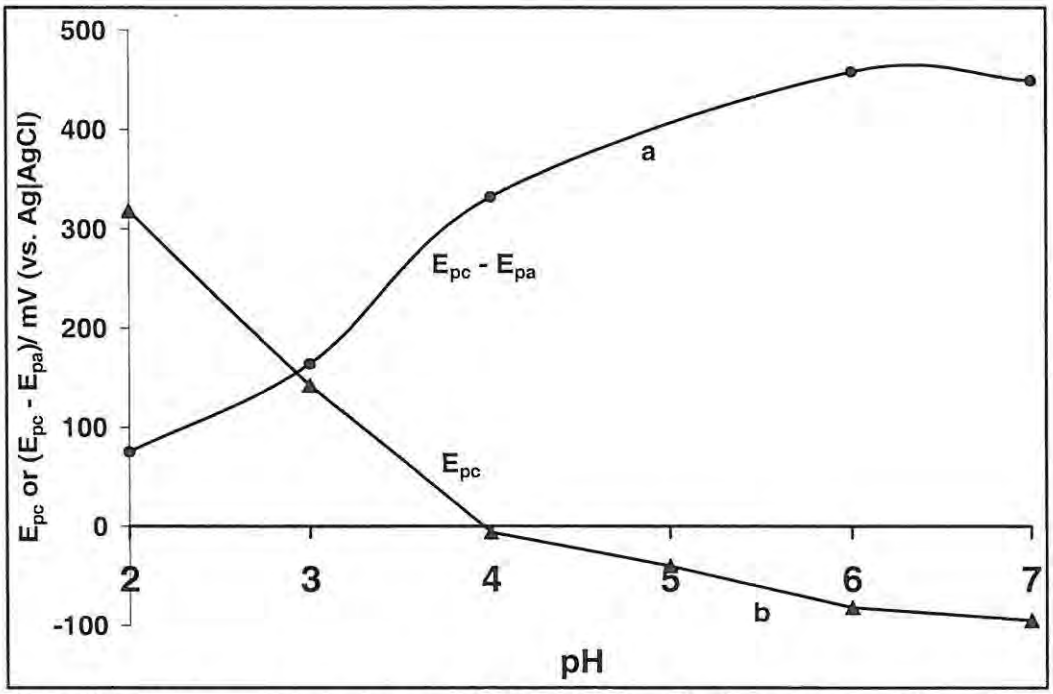

Fig 5.24: Plot of (•): peak separation vs. pH (a) and (▲): cathodic peak potential vs. pH (b) for *poly*-MnTMPyrPc in aqueous phosphate buffer solution. Data obtained from Fig 5.23.

5.4 Thiophene Substituted Metallophthalocyanine Complexes (16-18)

Attempts to electropolymerize all the MTETPc complexes (M= Co, Mn or Zn), (for use in cysteine detection), failed hence the GCE was modified by the drop dry method described in the experimental section. Only CoTETPc is given as an example.

The others did not show any catalytic activity toward L-cysteine hence are not discussed. Electropolymerization of thiophene complexes is known to be possible using thiophenes with no substituents on the 2 and 5 positions of the ring. The polymer is mainly coupled at the 2 and 5 positions.[456] The introduction of the Pc ring close to the coupling position may have produced a blocking of the polymerization process. It is also possible that the radicals formed during electrooxidation of the thiophene groups are too unstable to participate in further coupling so that no polymers are formed.

Fig 5.25a shows the CV of the adsorbed CoTETPc on GCE in pH 4 phosphate buffer. Although the waves are not well resolved, it can be seen from Fig 5.25a (curve ii) that the CoTETPc complex is attached to the GCE when compared with the bare GCE in the same electrolyte solution (curve i).

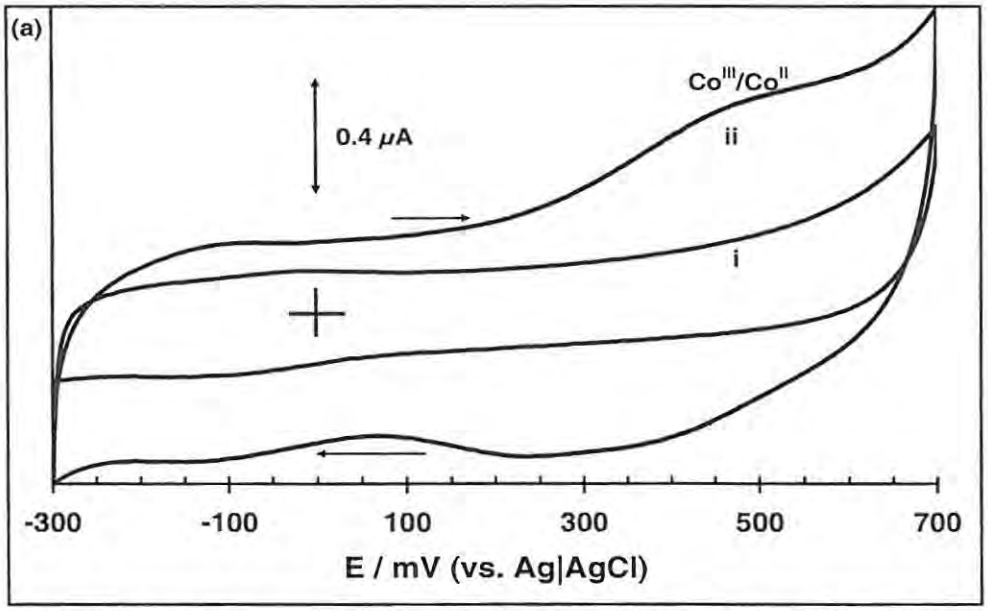

Fig 5.25a: Cyclic voltammograms of bare glassy carbon electrode (i) and CoTETPc modified GCE (ii) in pH 4.0 phosphate buffer. Scan rate = 100 mVs^{-1}.

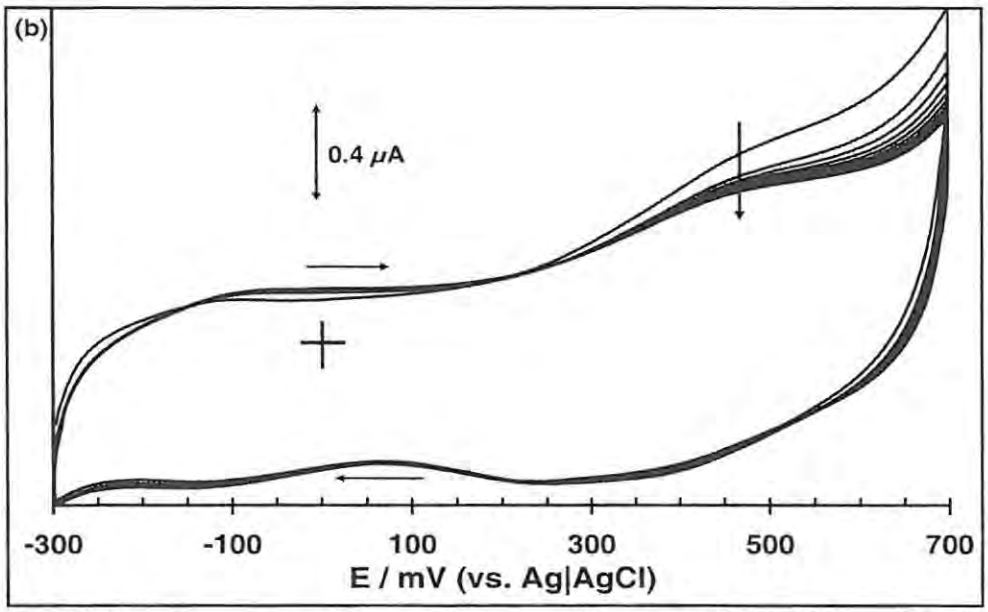

Fig 5.25b: Cyclic voltammograms of repetitive scans, (30 scans), of CoTETPc modified GCE in pH 4.0 phosphate buffer. Scan rate = 100 mVs^{-1}.

The broad couple around ~ 0.4 V vs. Ag|AgCl (Fig. 5.25a) is due to the $Co^{III}Pc^{-2}/Co^{II}Pc^{-2}$ process in comparison with Fig 4.13a. Before catalytic studies, successive cyclic voltammograms were recorded in buffer until steady currents were obtained, Fig. 5.25b. The observed feature of the CV in Fig 5.25b shows that the electrode process of the CoTETPc-modified GCE is unaffected by repeated cycling when compared to the CV in Fig 5.25a. For comparative purposes, a similar approach was used to deposit CoTMPyrPc on GCE and the electrodes were used for catalytic investigations discussed later in Chapter Six.

5.5 Self-Assembled Monolayer Formation

As examples, sulfur containing complexes (**13** and **16**) and amino complex (**19**) were employed for SAM formation. Both sulfur and nitrogen are known[2,74,96,151-160] for their affinity for gold.

5.5.1 CoTMPyrPc (13)

Figure 5.26 is a typical CV of bare gold electrode in 0.01 M KOH (curve i). A well defined gold reduction peak due to the stripping of gold oxide is easily seen at 0.08 V vs. Ag|AgCl. The area under the cathodic peak is proportional to the amount of gold oxide formed in the anodic scan. The oxide removal peak represents the total pinhole area available for an undisturbed penetration of ions present in the working solution.[457] Figure 5.26a, (curve ii) shows the CV obtained from CoTMPyrPc-SAM electrode in 0.01 M KOH. It is evident that the broad gold oxidation peak as well as the reduction peak in Fig 5.26a (curve i) are inhibited by the CoTMPyrPc-SAM. This indicates that the gold surface is isolated from the aqueous solution, the oxygen source for the gold oxide formation. The choice of self-assembling solvent depends on many factors such as solubility. The best solvent was chosen for each complex for SAM formation. CoTMPyrPc-SAM was prepared from THF.

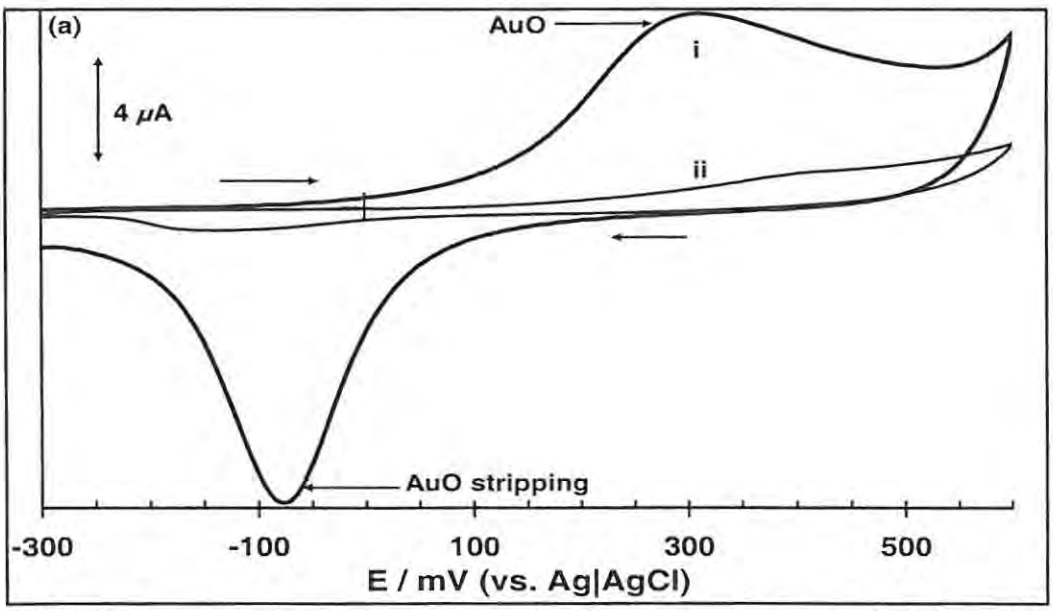

Fig 5.26a: Cyclic voltammograms of gold electrode before (i) and after CoTMPyrPc/gold-SAM formation (ii) in 0.05 M KOH. Scan rate = 100 mVs^{-1}.

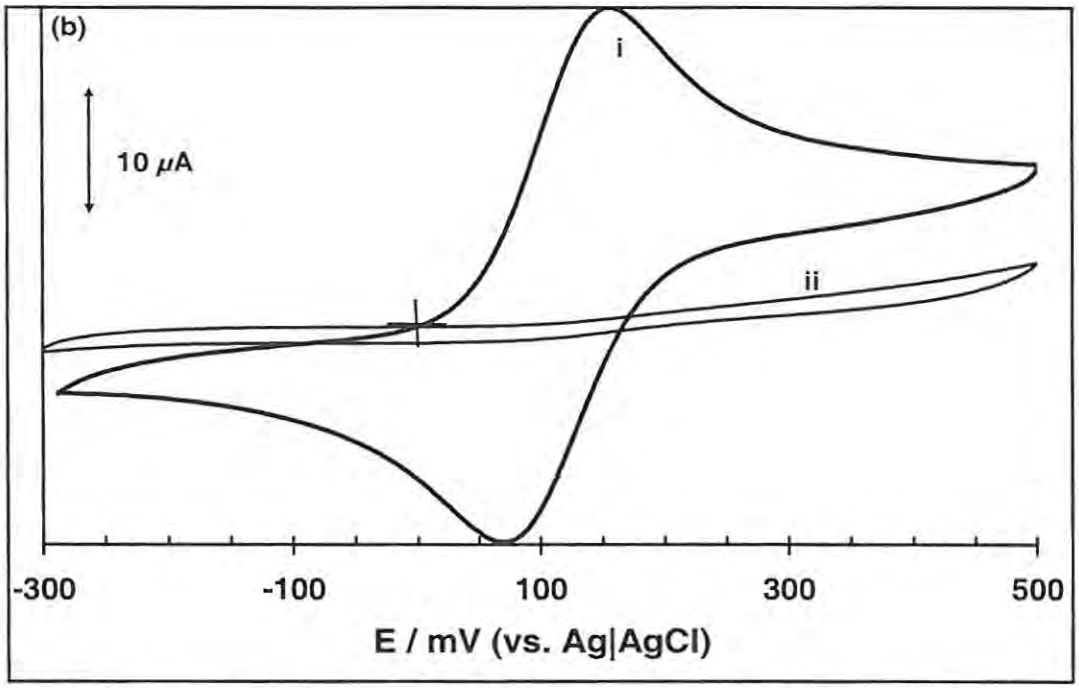

Fig 5.26b: Cyclic voltammograms of gold electrode before (i) and after CoTMPyrPc/gold-SAM formation (ii) in 1 mM $K_4Fe(CN)_6$ in 0.1 M KCl. Scan rate = 100 mVs^{-1}.

The ion barrier factor[402,458] was obtained by comparing the total charges produced under the peak due to the reduction of gold oxide at the bare gold, (Q_{Bare}), (Fig. 5.26a, curve i) and the CoTMPyrPc-SAM modified electrode, (Q_{SAM}), (Fig 5.26a, curve ii), using Equation 5.1:

$$\Gamma_{ibf} = 1 - Q_{SAM} / Q_{Bare} \qquad 5.1$$

The total charge, Q (μC) was obtained by integrating the charging currents (μAs^{-1}) under the cathodic wave. The charge, Q, for the bare gold was 16.1 μC while that of the CoTMPyrPc-SAM (Q_{Bare}) was 0.35 μC. The ion barrier factor, Γ_{ibf}, obtained from equation (5) above was close to unity indicating an effective barrier to ion and solvent permeability afforded by the CoTMPyrPc-SAM. The information obtained from the data

treatment suggests that about 2 % of the gold surface is accessible to the solvent, hence not covered by the SAM.

The monolayer defect and packing arrangement of SAM can be probed using the interfacial capacitance, C_s.[402,457,459] The lower the C_s value, the less defects there are in the SAM. From the charging current I_{cc} (Amps) obtained from the non-Faradaic region of the voltammogram, (-250 to -300 mV), in Figure 5.27a, the C_s (μFcm^{-2}) can be obtained using Equation 5.2 below:

$$C_s = I_{cc} / A\upsilon \qquad 5.2$$

Where υ is the scan rate (Vs^{-1}) and A, is the electrode area. The C_s value obtained for bare gold electrode was ~31 μFcm^{-2} while that for CoTMPyrPc-SAM was 1.4 μFcm^{-2}. In comparison with literature,[162] this implies that the SAM is relatively defect-free with low permeability of the electrolyte ions. Table 5.1 summarizes the Γ_{ibf} and C_s for the complexes examined.

The level of pinhole in monolayer films was determined using either $Fe(NH_4)(SO_4)_2$ in 1 mM $HClO_4$ solution or 1 mM $K_4Fe(CN)_6$ in 0.1 M KCl. The results obtained from both were similar, hence only $K_4Fe(CN)_6$ data are presented here. Fig 5.26b (curve i) shows the CV of 1.0 mM $K_4Fe(CN)_6$ in 0.1 M KCl on a bare gold electrode. It can be clearly seen that the electron transfer process in curve a (Fig 5.27b) has been seriously inhibited by the CoTMPyrPc-SAM. The low current obtained in the SAM modified electrode is indicative of a well-packed SAM, thus asserting the results obtained from the ion barrier / permeability probe test conducted earlier in KOH and Equations 5.1 and 5.2 above.

5.5.2 CoTETPc and CrTAPc

Figs 5.27 and 5.28 show the cyclic voltammograms obtained for the surface characterization of CoTETPc-SAM and CrTAPc-SAM, respectively. The CoTETPc-SAM was prepared from a 1.0 mM CoTETPc in THF while the CrTAPc was prepared from 2 mM CrTAPc in ethanol. A similar electrode pre-treatment was used for all SAM preparations as described in the experimental section. The Γ_{ibf} value for CoTETPc-SAM was near unity showing effective barrier to ion and solvent permeability. The C_s for CoTETPc was less than that obtained for CoTMPyrPc (Table 5.2) showing the former to be more defect-free. The Γ_{ibf} and C_s for CrTAPc-SAM could not be obtained as the film tends to dissolve in alkaline medium hence no reproducible voltammogram was obtained for the modified electrode under this condition.

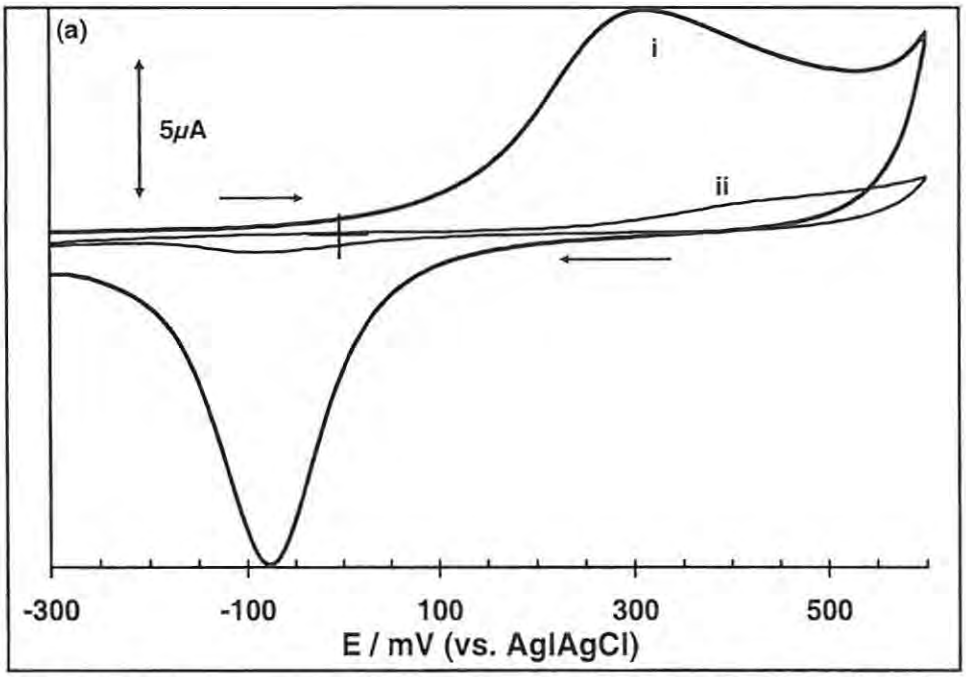

Fig 5.27a: Cyclic voltammograms of gold electrode before (i) and after CoTETPc/gold-SAM formation (ii) in 0.05 M KOH. Scan rate = 100 mVs^{-1}.

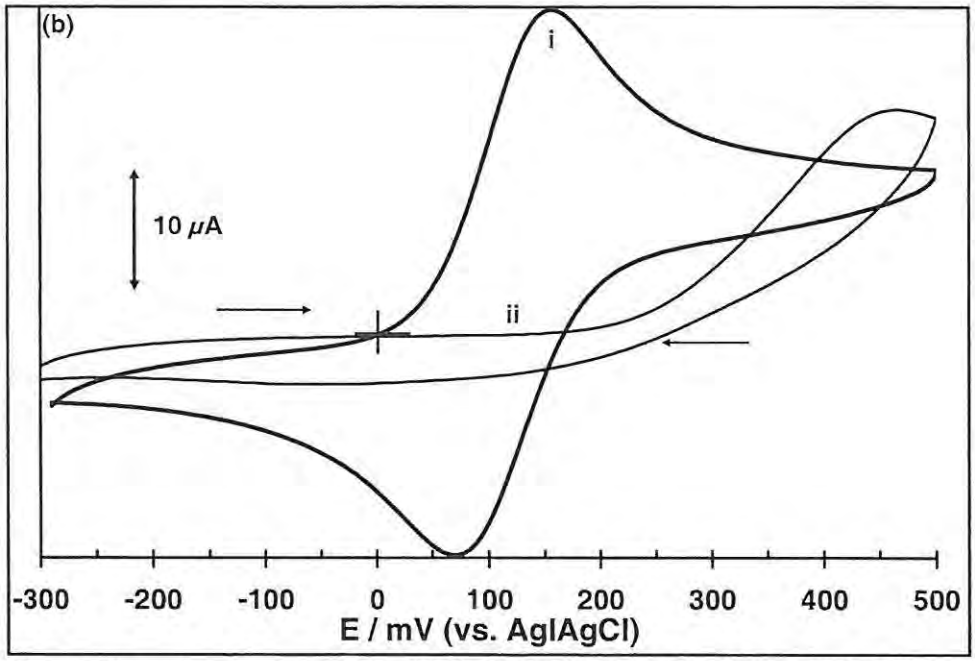

Fig 5.27b: Cyclic voltammograms of gold electrode before (i) and after CoTETPc/gold-SAM formation (ii) in 1 mM $K_4Fe(CN)_6$ in 0.1M KCl. Scan rate = 100 mVs^{-1}.

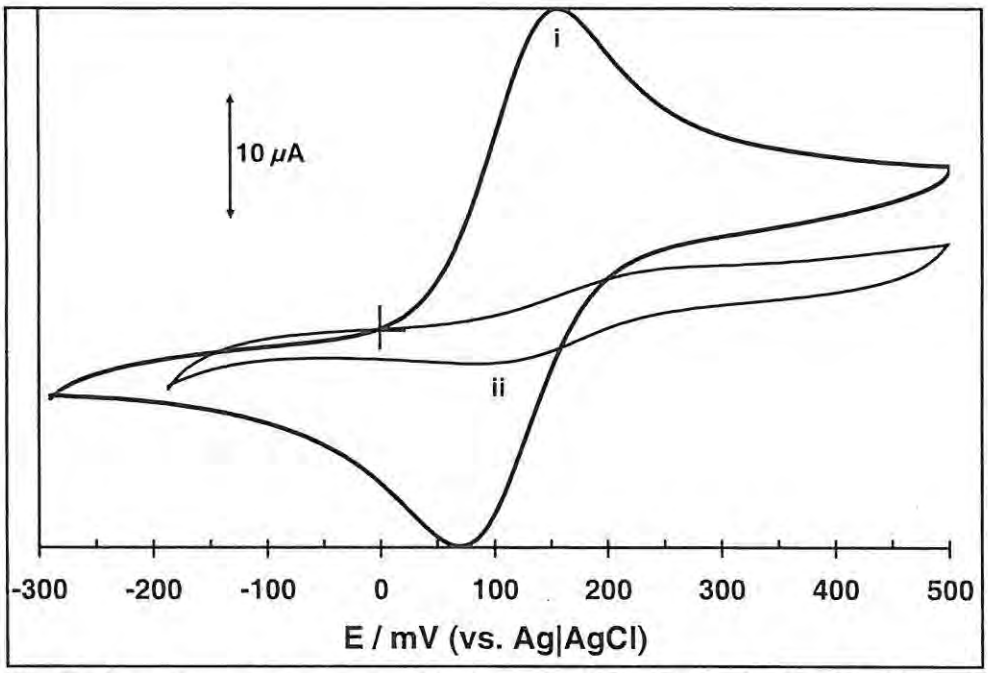

Fig 5.28: Cyclic voltammograms of gold electrode before (i) and after CrTAPc/gold-SAM formation (ii) in 1 mM $K_4Fe(CN)_6$ in 0.1 M KCl. Scan rate = 100 mVs^{-1}.

Table 5.2: Summary of ion-barrier factor (Γ_{ibf}) and interfacial capacitance (C_s) of the MPc-SAM on gold studied in this work. Scan rate = 100 mVs^{-1}.

MPc-SAM	Γ_{ibf}	C_s (μFcm^{-2})
Bare gold	-	31.0
CoTMPyrPc (13)	0.982	1.44
CoTETPc (16)	0.985	0.67

Conclusions:

The electrochemical deposition of polymer films of N-pyrrole funtionalized metallophthalocyanine complexes (**7-12**) have been demonstrated in this work. DCM proved to be the most suitable solvent for the effective electrosyntheses of films containing N-pyrrole substituted metallophthalocyanine as well as mercaptopyrimidine metallophthalocyanine (**13-15**) polymers. The inability to electropolymerize the thiophene substituted MPcs (**16-18**) is attributable to the steric hindrance due to the blocking of the polymerization process as a result of the introduction of the Pc ring close to the coupling position since the thiophene polymer is mainly coupled at the 2 and 5 positions. It is also possible that the radicals formed during electrooxidation of the thiophene groups are too unstable to participate in further coupling so that no polymers are formed. Electrochemical investigation of the *poly*-NiTPyPhPc reveals that the polymer could be electrotransformed to a stable *poly*-Ni(OH)TPhPyPc film in NaOH solution to afford a $Ni(OH)_2$-like electrode with interconnected O-Ni-O oxo bridges.

The electropolymerization of chromium and manganese tetraaminophthalocyanine (CrTAPc and MnTAPc) complexes was achieved in DMF. The

conductivities of the electroformed polymers are governed by several factors including the potential window used during the electropolymerization, the reductive and oxidative potential limits to which the polymer modified electrodes were subjected, the concentration of the monomer solution used for the electrosynthesis. The redox processes of the polymer films were pH dependent. In some cases where electropolymerization was not feasible, drop-dry methods were used to attach a monolayer of the chosen MPcs on the electrodes. The electrocatalytic applications of some of the polymer and monolayer-modified electrodes will be investigated in the chapter that follows (chapter 6).

The sulfur (i.e. the thiophene and mercaptopyrimidine functionalized MPcs) and amino group containing complexes synthesized in the work have been shown to form SAM on gold electrode. The MPc-SAM formation was achieved in THF (in the case of CoTETPc-SAM and CoTMPyrPc-SAM) while ethanol was used as the deposition solvent in the case of CrTAPc.

Chapter Six

Electrocatalytic Properties

This section dwells on the electrocatalytic applications of some of the metallophthalocyanine complexes synthesized in this work. The electrocatalytic properties are examined on the electrodes modified with the complexes. The modes of attaching the various MPc complexes have been fully described in the preceding chapter.

6.1 Electrocatalytic Oxidation of Amino Acids (L-cysteine and Glycine)

6.1.1 L-Cysteine

6.1.1.1 Pyrrole Substituted CoPc (7)

The catalysis for L-cysteine was found to be best on electrodes modified with CoPc derivatives, hence only these are reported for this application. Complex **7** (CoTPhPyPc) showed activity toward L-cysteine while CoTPOPyPc (**12**) did not. Most conventional electrodes are characterized by slow electron transfer reactions leading to the electrooxidation of thiols at very high overpotentials and poor detection limits.[331,333] In order to further characterize the electrochemical properties of the films, obtained from the synthesized cobalt phthalocyanine complexes, the capability of the obtained modified electrodes to act as electrocatalysts towards the oxidation of L-cysteine was checked in aqueous solution. This reaction has been reported by several authors[333,460] with cobalt phthalocyanine modified electrodes, and has been used as a good test for assessing the activity of the complexes examined in this work. Fig 6.1 shows the CVs of 5 mM L-cysteine on a bare GCE (curve i) and on the electropolymerized *poly*-CoTPhPyPc film (curve ii) in aqueous pH 4.0 phosphate buffer solution.

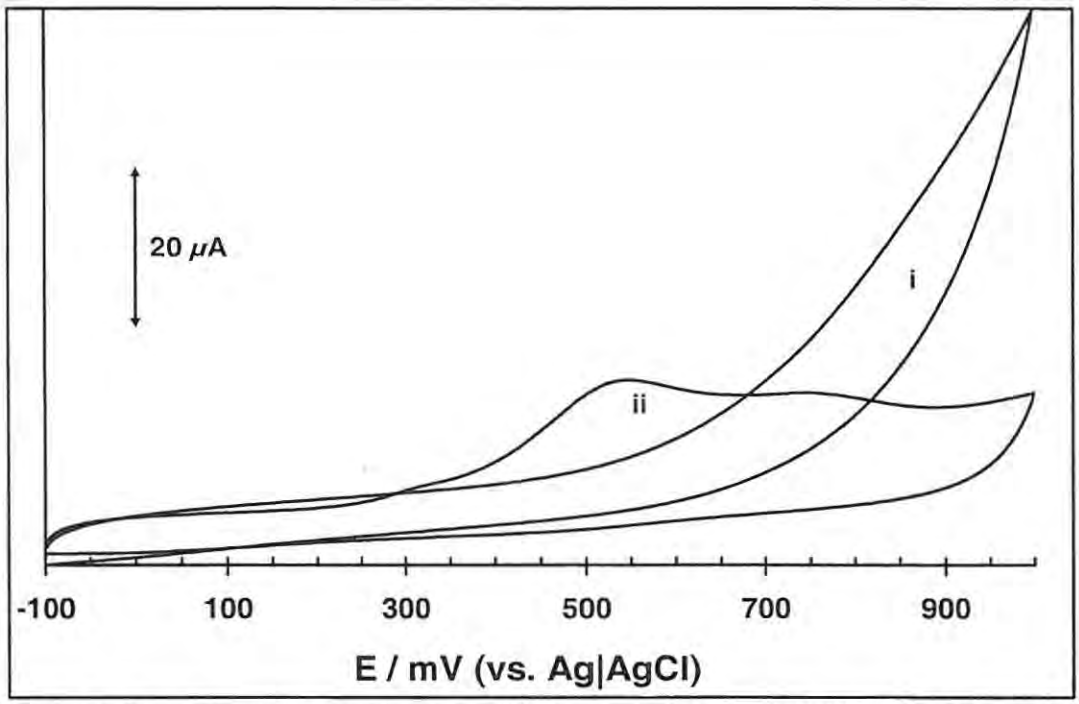

Fig 6.1: Cyclic voltammograms of a bare GCE (curve i) and a *poly*-CoTPhPyPc film modified GCE (curve ii) (film was prepared as indicated in Fig 5.2) in aqueous solution (phosphate buffer, pH = 4) containing 5 x 10^{-3} M of L-cysteine. Scan rate = 100 mVs^{-1}, electrode = GCE.

It appears from these data that the use of the modified electrode gave rise to an irreversible oxidation peak at 0.54 V (vs. Ag|AgCl). This is related to the mediated oxidation of L-cysteine by the electropolymerized CoTPhPyPc. It is important to note that no comparable electrochemical activity over this potential range was seen for the film itself in absence of L-cysteine or with uncoated electrode. Peaks due to *poly*-CoTPhPyPc alone which were observed in Fig 5.3 are not seen in the large current scale in Fig 6.1. This is the case with most of the adsorbed MPcs discussed in this chapter. This observation is consistent with that reported for cobalt phthalocyanine supported electrodes. [331,333,460,461] Although these results are preliminary, they show that the developed electropolymerized film can be useful in designing new catalysts for the activation of thiols. The catalytic behaviour of $Co^{II}Pc$ complexes is associated with the redox activity of the central metal. The potential at which a catalytic current is observed

is closely related to the Co^{III}/Co^{II} or Co^{II}/Co^{I} couples in CoPc complexes.[462] This shows that the CoPc derivative is functioning as a redox mediator for cysteine electrooxidation, according to the mechanism proposed in literature for acid media,[293] equations 6.1-6.4:

$$RSH + PcCo(II) \rightleftharpoons PcCo(II)—SR + H^{+} \quad 6.1$$

$$PcCo(II)—SR \rightleftharpoons PcCo(III)—SR + e^{-} \quad 6.2$$

$$PcCo(III)—SR \rightleftharpoons PcCo(II) + RS^{\cdot} \quad 6.3$$

$$2\ RS^{\cdot} \rightleftharpoons RSSR \quad 6.4$$

where RSH is L-cysteine and RSSR is cystine. The interaction of cysteine with CoPc derivatives, prior to electron transfer, has been reported before.[293] The potentials at which L-cysteine oxidation occurs are listed in Table 6.1.

Table 6.1: Summary of peak potential (E_p) for the electroassisted reactions of the analytes at the modified electrodes using the MPc complexes[a] studied in this work

MPc	Electrode	Analyte (pH)[b]	Analyte E_p/V vs. Ag|AgCl	Corresponding MPc $E_{1/2}$/V vs. Ag|AgCl[c]	Source of MPc $E_{1/2}$
CoTPhPyPc, **7**	*Poly*-MPc-GCE	L-cys (4)	+ 0.54	+ 0.75 ($Co^{III/II}$)	Fig 5.3
CoTMPyrPc, **13**	DD-MPc-GCE	L-cys (4)	+ 0.16	+ 0.09 ($Co^{III/II}$)	Fig 6.6
CoTETPc , **16**	DD-MPC-GCE	L-cys (4)	+ 0.39	+ 0.37 ($Cr^{III/II}$)	Fig 5.26
NiTPhPyPc, **10**	*Poly*-MPc(OH)-GCE	Ph (11)	+ 0.26	+ 0.25 ($Ni^{III/II}$)	Fig 5.11
NiTPhPyPc, **10**	*Poly*-MPc(OH)-GCE	*p*CPh (11)	+ 0.35	+ 0.25 ($Ni^{III/II}$)	Fig 5.11
NiTPhPyPc, **10**	*Poly*-MPc(OH)-GCE	*p*NPh (11)	+ 0.76	+ 0.25 ($Ni^{III/II}$)	Fig 5.11
CrTAPc, **19**	*Poly*-MPc-GCE	NO_2^- (7.3)	+ 0.80	+ 0.68 (Cr^{IV}/Pc^{-1})	Fig 5.14
CrTAPc, **19**	*Poly*-MPc-GCE	NO (4)	+ 0.68	+ 0.68 (Cr^{IV}/Pc^{-1})	Fig 5.14
MnTAPc, **20**	*Poly*-MPc-GCE	Gly (4)	- 0.61	- 0.25 ($Mn^{III/II}$)	Fig 5.19
CoTPhPyPc, **7**	*Poly*-MPc-GCE	O_2 (DCM)	- 0.80	- 0.45 ($Co^{II/I}$)	Fig 5.3
CrTAPc, **19**	*Poly*-MPc-GCE	O_2 (DCM)	- 1.04	- 0.94 ($Cr^{III/II}$)	Fig 6.16
MnTAPc, **20**	*Poly*-MPc-GCE	O_2 (DCM)	- 1.04	- 0.25 ($Mn^{III/II}$)	Fig 6.18
MnTMPyrPc,**14**	*Poly*-MPc-GCE	O_2 (DCM)	- 0.59	- 0.30 ($Mn^{III/II}$)	Fig 5.24 (at pH 7)

[a]CoTPOPyPc (**12**) did not show any catalytic activity towards L-cysteine, hence not represented in the table.

[b]Oxygen reduction in DCM containing 0.1 M $TBABF_4$.

[c]The potentials are for adsorbed (by polymerization or drop-dry) MPc complexes.

Poly-MPc-GCE = polymer electrode obtained by electropolymerization of the MPc film onto GCE; DD-MPc-GCE = monomer electrode obtained by Drop-dry method;

Poly-MPc(OH)-GCE = polymer electrode obtained from electrotransformation of *poly*-NiTPhPyPc to Ni(OH)TPhPyPc-GCE.; L-cys = L-cysteine; Ph = phenol, pCPh = 4-chlorophenol; *p*NPh = 4-nitrophenol; Gly = glycine

6.1.1.2 Thiophene Substituted CoPc

Fig 6.2(c) shows the CV of CoTETPc (**16**) monomer modified GCE electrode (by drop dry method, Section 5.4) in the presence of 1mM L-cysteine in pH 4.0 phosphate buffer solution. A well-defined peak due to L-cysteine oxidation can be seen at 0.39V vs. Ag|AgCl, on GCE modified with CoTETPc. The dip in current observed on the return is typical of CoPc catalyzed oxidation of cysteine.[293,463]

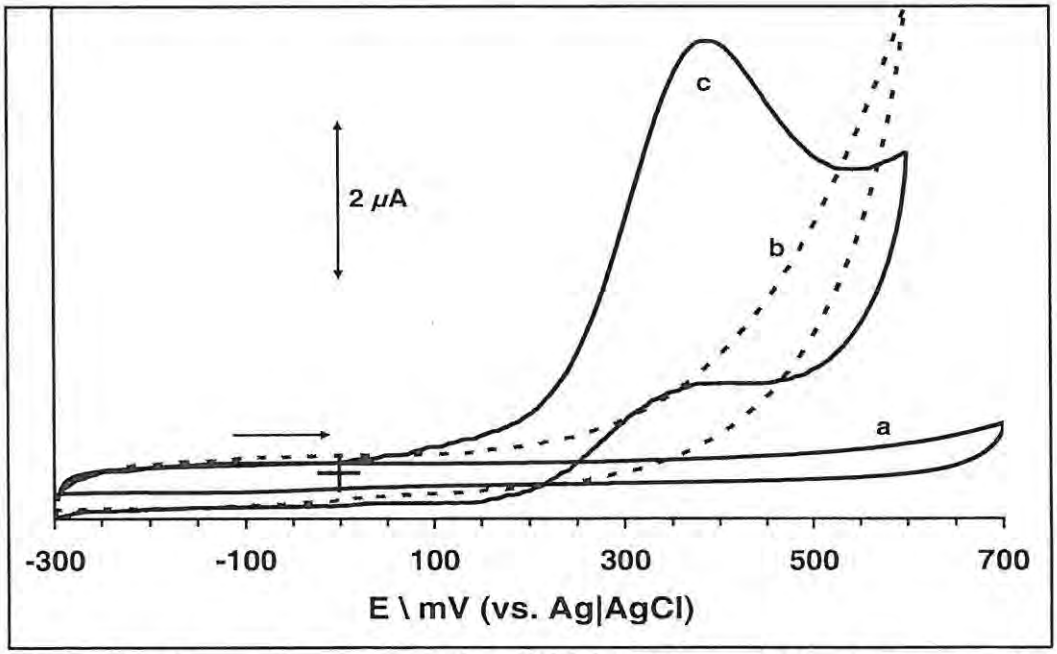

Fig 6.2: Cyclic voltammetric responses of bare GCE, (a) without and (b) in the presence of 1 mM L-cysteine. (c) CoTETPc modified GCE in the presence of 1 mM L-cysteine in pH 4.0 phosphate buffer. Scan rate = 100 mVs^{-1}.

It can be seen that no wave related to L-cysteine was observed for the bare GCE within the potential window under consideration, Fig 6.2b. The rate of electron transfer of the L-cysteine at the electrode/solution interface is significantly mediated by the Co^{III}TETPc/Co^{II}TETPc such that a less negative potential (0.39 V vs. Ag|AgCl), compared to *poly*-CoTPhPyPc above and other CoPc species[293] is required for the oxidation of L-cysteine in pH 4.0.

Stability of the modified electrode

The modified electrode was subjected to thermal annealing in that it was repeatedly scanned in the blank buffer solution after heating in the oven and before immersing it into the solution containing L-cysteine. Fig 6.3a shows the results obtained from repetitive CV of the CoTETPc-GCE in a 1 mM solution of L-cysteine in pH 4.0 phosphate buffered solution.

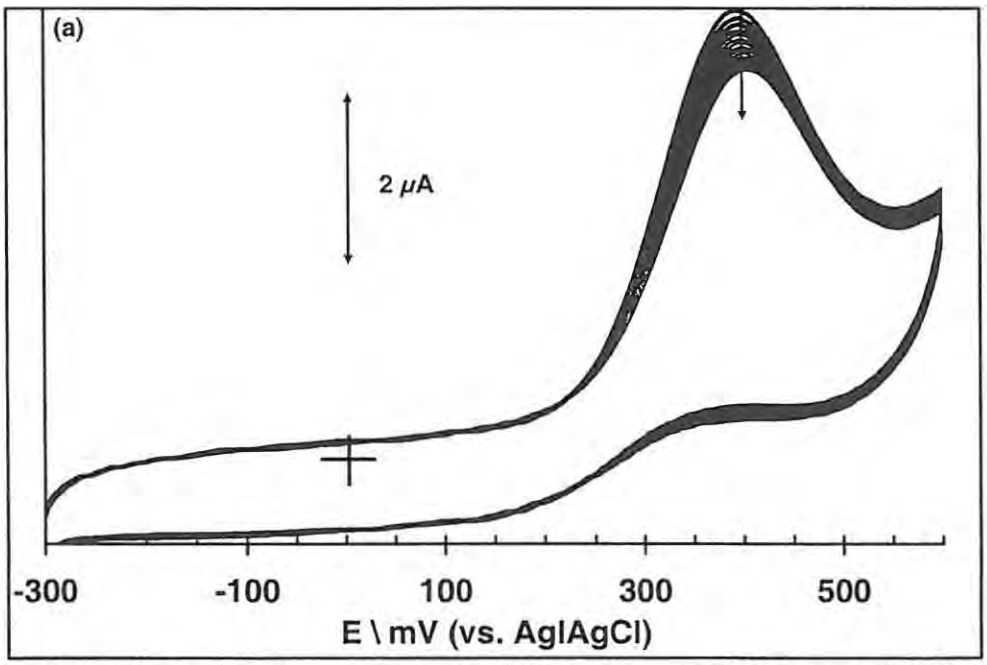

Fig 6.3a: Repetitive cyclic voltammogram of 1 mM L-cysteine at CoTETPc modified GCE in pH 4.0 phosphate buffer solution: 30 repetitive CV cycles. Scan rate 100 mVs^{-1}.

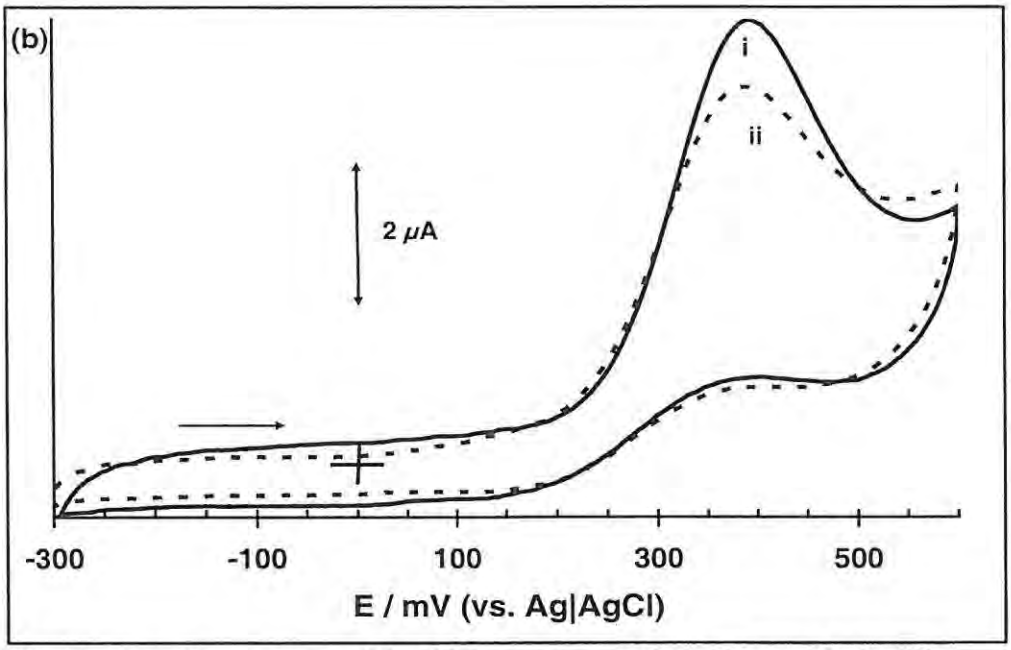

Fig 6.3b: Cyclic voltammogram of 1 mM L-cysteine at CoTETPc modified GCE in pH 4.0 phosphate buffer solution: (i) first scan before cycling as in (Fig 6.3a) and (ii) after 30 repetitive scans in 1 mM L-cysteine solution followed by rinsing and transferring into a fresh 1 mM solution of L-cysteine. Scan rate 100 mVs^{-1}.

The loss in catalytic current after 30 repetitive scans may be attributed to the poisoning of the modified electrode by the oxidation product of L-cysteine (cystine). However, when the electrode was rinsed with a generous amount of pH 4.0 phosphate buffer solution the voltammetric response of the electrode showed a measure of recovery in that the current signal was 94% of the first scan before the repetitive scan was done, Fig 6.3b.

Fig 6.4 shows an increase in current with increase in cysteine concentration, giving a linear plot (Fig 6.4, insert), with detection limit of 3.1 μM.

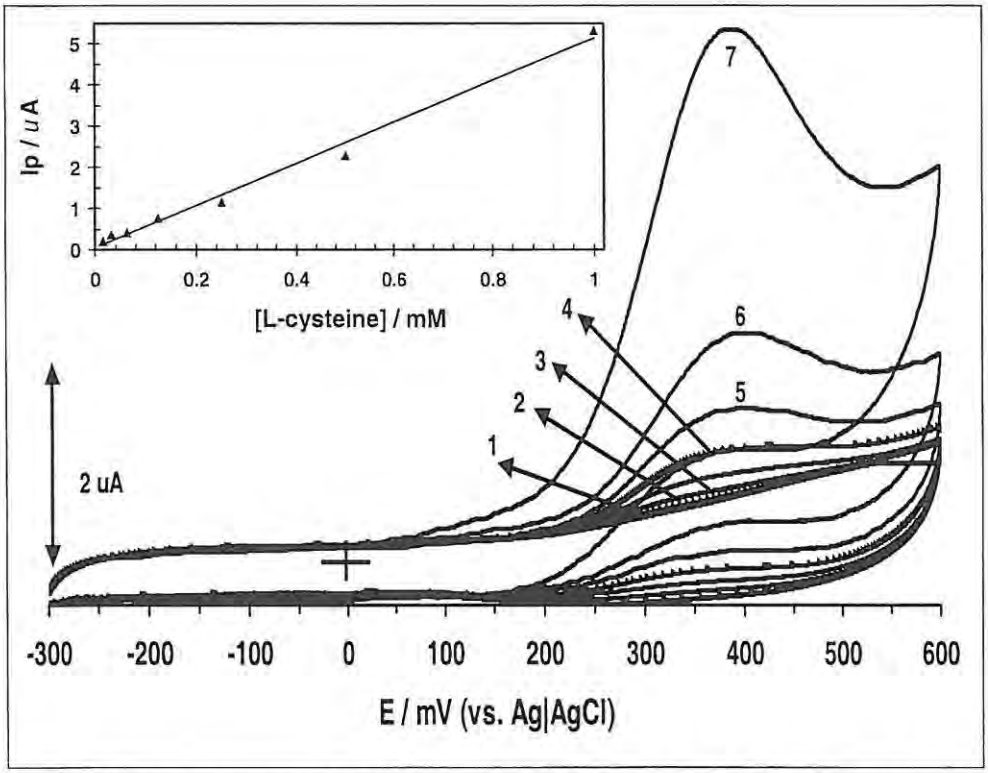

Fig 6.4: Cyclic voltammetry of CoTETPc modified GCE in the presence of varying concentrations of L-cysteine: 0.0015 (2), 0.0625 (3), 0.125 (4), 0.25 (5), 0.5 (6) and 1 mM (7). Curve 1 is the CV for CoTETPc modified GCE in the absence of L-cysteine. Scan rate 100 mVs^{-1}. Inset shows the plot of peak current vs. concentration of L-cysteine. pH = 4.0.

When the modified electrode was kept in either pH 4.0 or pH 7.0 phosphate buffered solution for 8 days and re-used again for analyses of L-cysteine, it was observed that there was no difference in the behavior of the electrode as compared to the results obtained before storage. This suggests that the electrode can be used repeatedly provided it is properly stored. The electrode was also stable after analysis of different concentrations of cysteine as in Fig. 6.4. No significant loss of current (Fig 6.5) was obtained in all cases after rinsing the modified electrode in deionised water and transferring it to a fresh 0.1 mM L-cysteine solution. This is a very important

observation since the main limitation for application of electrodes for analysis is its poisoning by oxidation products.

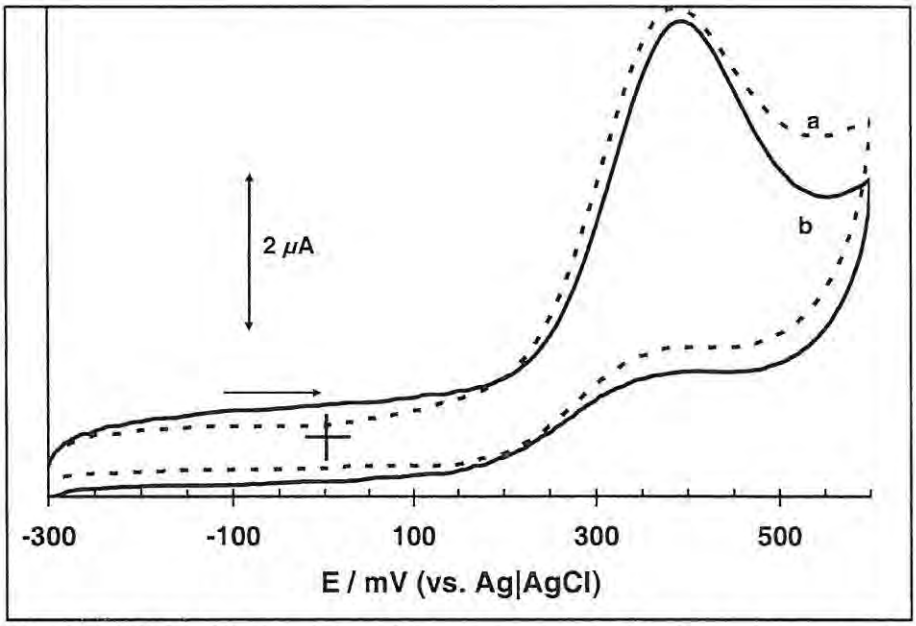

Fig 6.5: CV of CoTETPc-GCE in 0.1 mM L-cysteine in pH 4 buffer solution. (i): immediately after the electrode fabrication, (b): 8 days after use as in (i) and stored in a pH 7.0 phosphate buffer solution. No difference was observed when the electrode was stored in pH 4.0 solution. Scan rate: 100 mVs^{-1}.

6.1.1.3 Mercaptopyrimidin Substituted CoPc

CoTMPyrPc (**13**) was employed for L-cysteine determination and the electrode for this purpose was modified by drop dry method. The aim was to compare the activity of CoTETPc dicussed in 6.1.2, with that of another CoPc monomer. Thus CoTMPyrPc (**13**) was chosen and was adsorbed on the electrode by drop-dry in a similar manner to CoTETPc. Fig 6.6 (curve i) shows the CV of 0.025 mM L-cysteine on bare GCE. It can be seen that the catalytic current attributable to L-cysteine oxidation is enhanced in the CoTMPyrPc modified GCE (Fig 6.6, curve ii). The Co^{III}/Co^{II} redox process (at ~ 0.09 V) is weak but observable on the scale used.

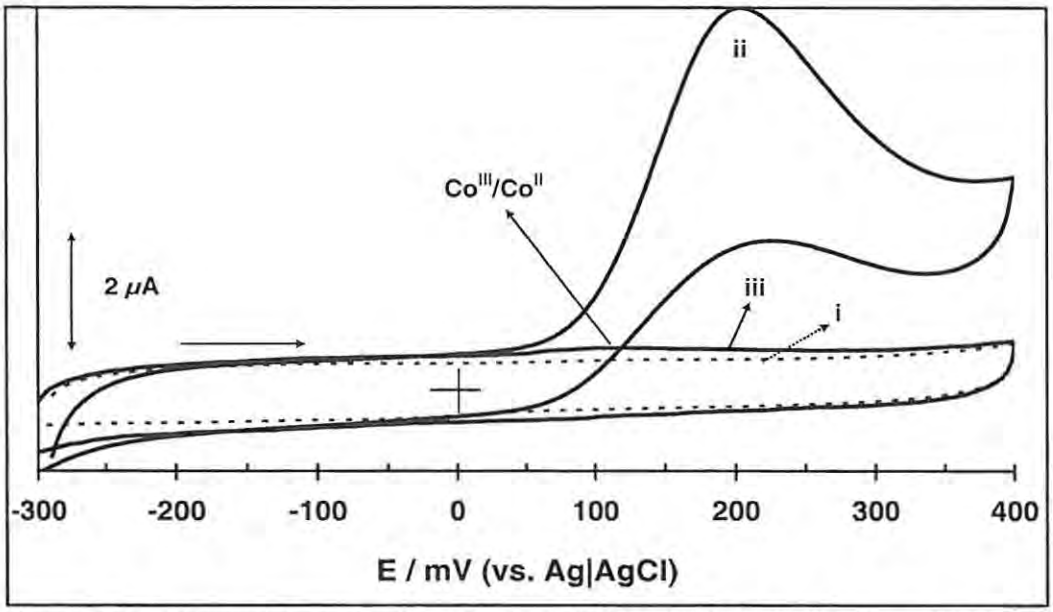

Fig 6.6: Cyclic voltammetric responses of (i), bare GCE and (ii), CoTMPyrPc modified GCE in the presence of 0.025 mM L-cysteine in pH 4.0 phosphate buffer. Curve (iii) is the CV of the CoTMPyrPc modified GCE in blank pH 4.0. Scan rate = 50 mVs^{-1}.

Fig 6.7 shows the voltammetric responses of the CoTMPyrPc modified GCE in the presence of varying concentrations of L-cysteine. The curves suggest that peak potential increases with concentration of the analyte. The catalytic currents for the oxidation of L-cysteine on GCE modified with CoTMPyrPc increased linearly with L-cysteine concentration with a correlation of 0.995. The detection limit attained in this study using complex **13** was 0.5 μM. A comparison of the L-cysteine oxidation potentials (Table 6.1) for the three complexes (**7**, **13** and **16**) reveals that the adsorbed mercptopyrimidin substituted cobalt Pc (**13**) is by far a better catalyst for the examined analyte, as judged by lowering of L-cysteine overpotential. The L-cysteine oxidation potential for the *poly*-CoTPhPyPc-GCE was 0.54 V (vs. Ag|AgCl) while the adsorbed CoTETPc and CoTMPyrPc catalytically oxidized L-cysteine at relatively lower potentials of 0.39 V and 0.16 V (vs. Ag|AgCl) respectively, Table 6.1.

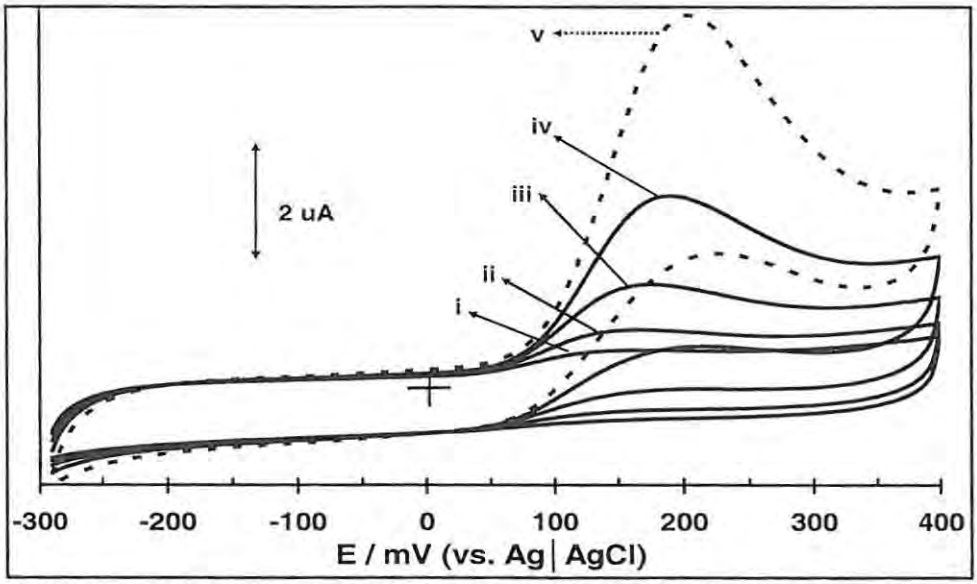

Fig 6.7: Cyclic voltammetry of CoTMPyrPc modified GCE in the presence of varying concentrations of L-cysteine. Concentration / μM: (i) = 1.5 (ii) = 3.1, (iii) = 6.25, (iv) = 12.5, (v) = 25.0. Scan rate = 50 mVs^{-1}.

It seems that the presence of thio groups on the ring substituents (complexes **13** and **16**) lowers the oxidation potential of L-cysteine more thereby improving the catalytic response of the electrodes towards L-cysteine. Alternatively, it could be that a better catalytic activity is observed on **13** and **16** due to the drop-dry method of electrode modification as opposed to the electropolymerization in the case of complex **7**.

6.1.2 Glycine Reduction on MnTAPc-Modified Electrode

Fig 6.8 (curve a) shows that a very small current was observed for the reduction of 5.0mM glycine on bare GCE. When *poly*-MnTAPc modified GCE was employed a large increase in currents was observed, after correcting for the currents due to adsorbed *poly*-MnTAPc. That is, the cathodic current increased over the background due to the catalytic reduction of glycine. The increase of current with increase in glycine concentration is shown by Fig 6.8 (curves b–d). The increase in current with

concentration of glycine was linear at concentrations lower than 5 mM (insert in Fig 6.24). The deviation from linearity at higher concentrations is often observed in analysis and is associated with the competition of the analyte molecules for the electrode surface. The electrode was used for analysis after allowing for the stabilization of the current in the buffer alone, since as has been shown above, (in Chapter Five, Fig 5.18), there is a decrease in current on cycling. The catalytic behaviour for reduction of glycine decreased with increasing pH suggesting that the protonated form of glycine is the most active. Also as discussed in Chapter Five (Fig 5.10), the redox potential of the polymer shifted to more negative values with increase in pH, which could result in the lowering of catalytic behaviour at high pH.

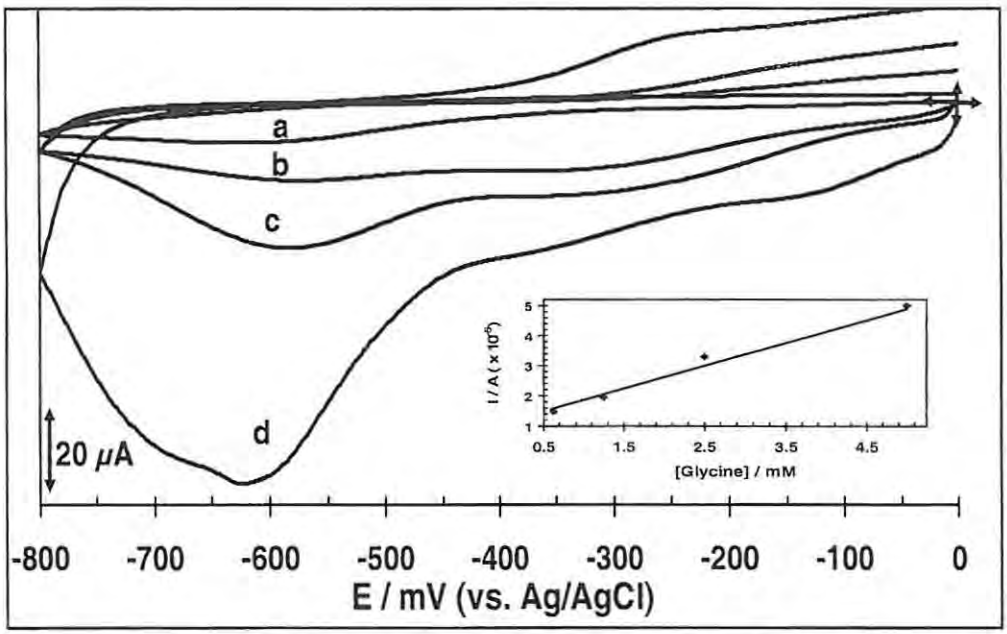

Fig 6.8: Detection of glycine on bare GCE and *poly*-MnTAPc-GCE. Glycine concentration / mM: (a) = 5, (b) = 0.55, (c) = 1.0 and (d) = 5 mM. pH = 4; scan rate: 50 mVs^{-1}. Insert: variation of peak current with concentration of glycine.

The electrode was found to be stable for the detection of glycine, since there was no significant decrease in currents with scan number. The glycine peak shifted by 80 mV

per pH unit, consistent with a one-electron process. On the basis of the voltammetric results described above, it appeared likely that amperometric detection of glycine in acidic media might be carried out at the MnTAPc-modified GC electrodes.

6.2 Phenol and its Derivatives on NiTPhPyPc

6.2.1 Electrocatalytic Oxidation of p-Chlorophenol

Fig 6.9 shows the cyclic voltammograms of 0.7mM *p*-chlorophenol (*p*-CPh) in 0.1M NaOH solution at unmodified GCE (curve a), *poly*-Ni(OH)TPhPyPc (curve b) and *poly*-$[NiTPhPyPc]_{20}$ (curve c) electrodes.

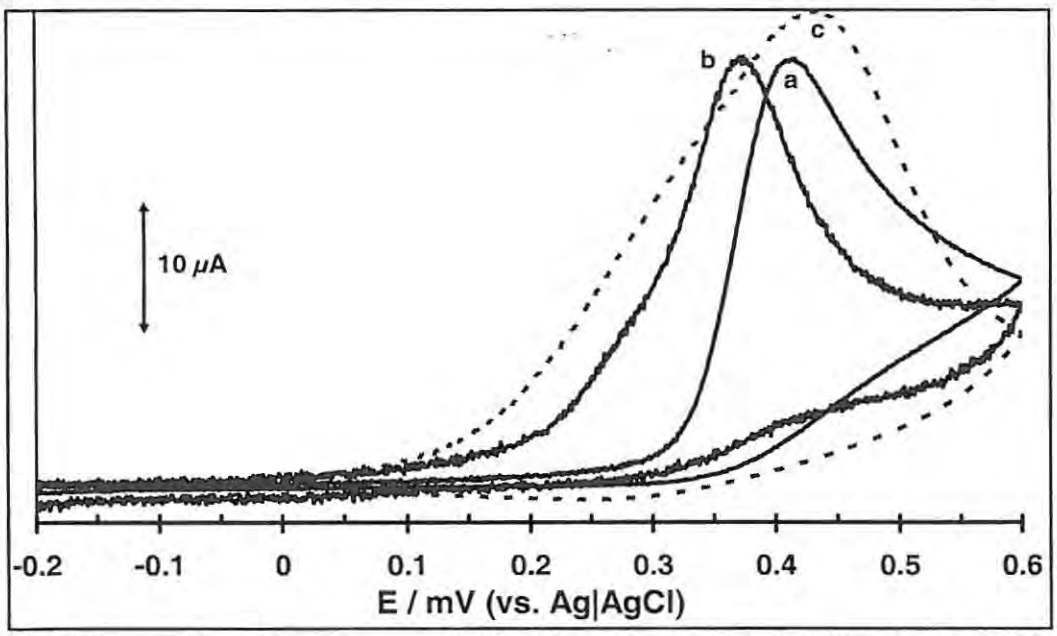

Fig 6.9: First cyclic voltammogram of 0.7 mM p-chlorophenol, (p-CPh), in 0.1 M NaOH solution. (a): unmodified GCE, (b) *poly*-Ni(OH)TPhPyPc and (c) *poly*-$[NiTPhPyPc]_{20}$ modified GCE. Scan rate: 100 mVs^{-1}.

It can be seen (Fig 6.9, curve b) that the Ni(OH)TPhPyPc electrode showed a better catalytic behavior toward oxidation of p-CPh compared to the unmodified GCE

and *poly*-[NiTPhPyPc]$_{20}$ electrodes in that there is a shift in the peak potential to a less positive value. The huge and broad current seen in the case of *poly*-[NiTPhPyPc]$_{20}$ might be due to both the electrode processes emanating from the transformation of the polymer film as seen in the first scan in Fig 5.10 during the electrotransformation of *poly*-[NiTPhPyPc]$_{20}$ to *poly*-Ni(OH)TPhPyPc and the actual oxidation wave of the *p*-CPh.

Fig 6.10(a-c) represent the voltammograms obtained during repetitive scan of the various electrodes in the presence 0.7 mM *p*-CPh. The *poly*-Ni(OH)TPhPyPc-GCE, (Fig 6.10c), showed a better stability and resistance to passivation than the *poly*-[NiTPhPyPc]$_{20}$-GCE, (Fig 6.9b), and unmodified GCEs (Fig 6.10a).

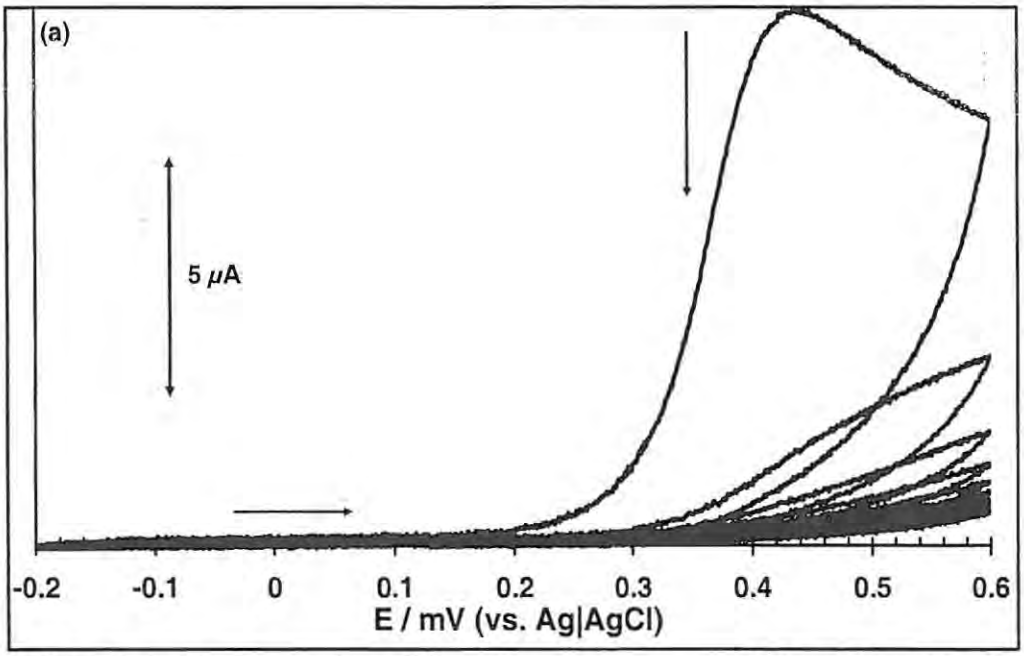

Fig 6.10a: Repetitive successive cyclic voltammogram scans (15) of 0.7 mM p-CPh at unmodified GCE in 0.1 M NaOH solution. Scan rate 200 mVs^{-1}.

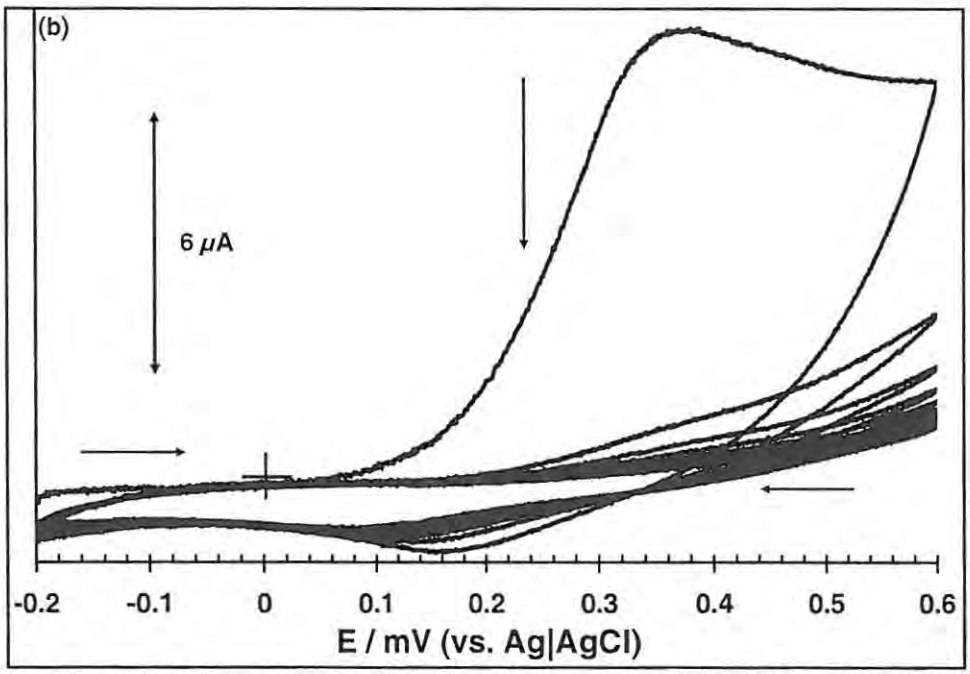

Fig 6.10b: Repetitive successive cyclic voltammogram scans (15) of 0.7 mM p-CPh at *poly*-$[NiTPhPyPc]_{20}$ modified GCE in 0.1 M NaOH solution. Scan rate: 200 mVs^{-1}.

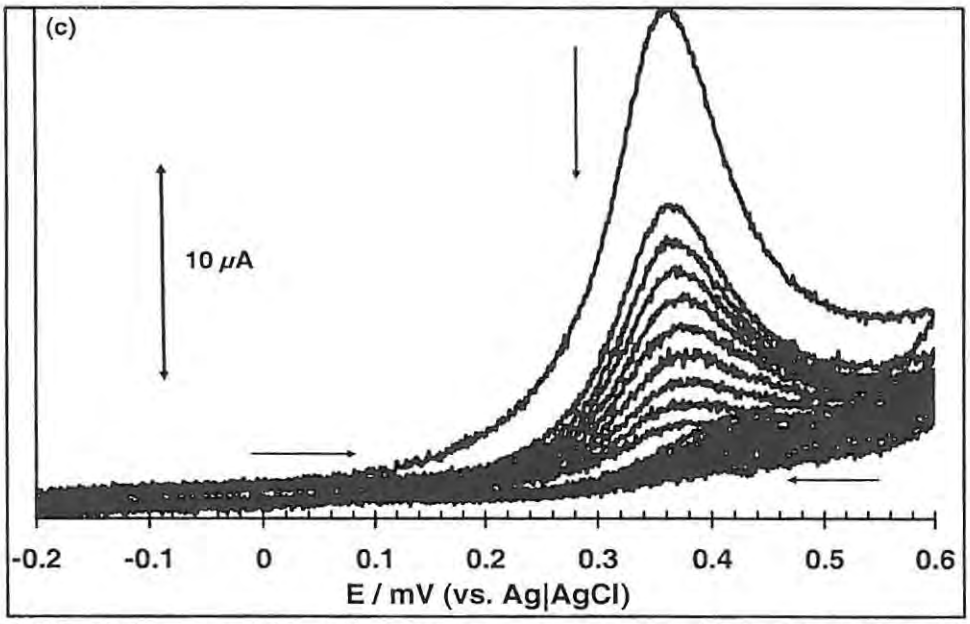

Fig 6.10c: Repetitive successive cyclic voltammogram scans (15) of 0.7 mM p-CPh at *poly*-Ni(OH)TPhPyPc modified GCE in 0.1 M NaOH solution. Scan rate: 200 mVs^{-1}.

Fig 6.11 shows the voltammograms obtained in the presence of 0.7 mM p-CPh solution after the passivated electrodes (15 CV cycles in p-CPh) were rinsed in water,

then immediately used in a fresh p-CPh solution with no recovery time allowed. 'Recovery' here refers to the time (in 0.1 M NaOH) between repetitive cycling (15 cycles), followed by rinsing in water and cycling in fresh *p*-CPh. It is evident that the *poly*-Ni(OH)TPhPyPc (curve c) showed excellent recovery by just rinsing in water, hence was not severely passivated by oxidation products of *p*-CPh. The solutions were de-aerated with a stream of argon before every run in order to homogenize the p-CPh in solution. There was no effect on the currents on bubbling argon through the solution. There is a complete loss of activity of both the unmodified GCE and *poly*-$[NiTPhPyPc]_{20}$ electrodes (curves a and b in Fig 6.11).

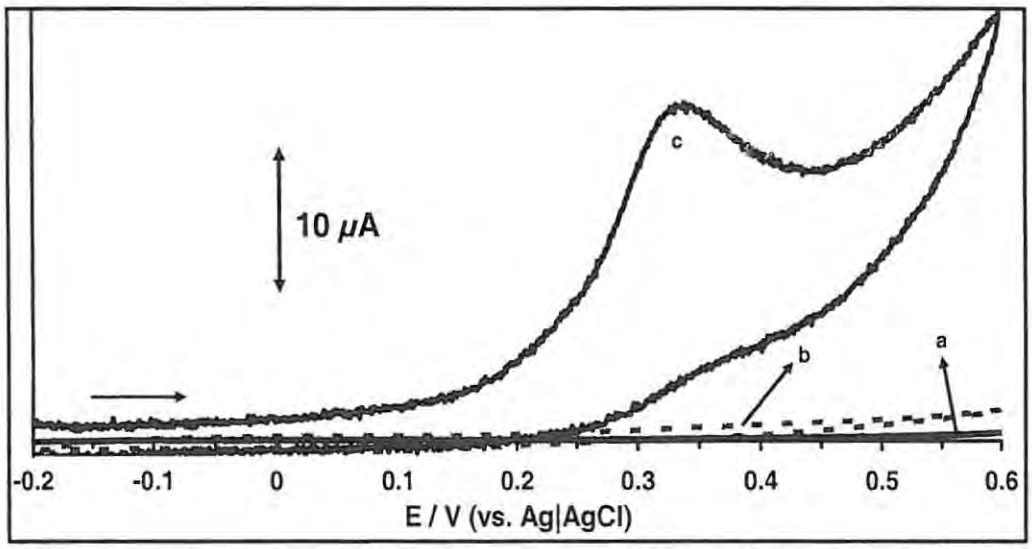

Fig 6.11: Cyclic voltammograms of 0.7 mM p-CPh in 0.1 M NaOH at passivated electrodes (15 cycles in p-CPh then rinsed in water, but no recovery time allowed). (a) unmodified, (b) *poly*-NiTPhPyPc and (c) *poly*-Ni(OH)TPhPyPc modified GCE. Scan rate: 100 mVs^{-1}.

Evaluation of effects of recovery time on electrode activity was made between the unmodified GCE and the *poly*-Ni(OH)TPhPyPc modified electrode (and not *poly*-$[NiTPhPyPc]_{20}$), since as has been pointed out earlier, more than one electrode process is likely involved on cycling *poly*-NiTPhPyPc in p-CPh solution. Fig 6.12 shows the effect

of time on the recovery of the electrodes. Curve c, (Fig 6.12), represents the first scan of *poly*-Ni(OH)TPhPyPc in the presence of 0.7 mM p-CPh. The electrode was then subjected to passivation and recovery (for 30 mins and 5 hrs in electrolyte) as explained earlier. Curves d and e show voltammograms of 0.7 mM p-CPh after 30 mins and 5hr recovery times were respectively allowed. The electrode recovered appreciably after 5 hrs as can be seen in curve e (Fig 6.12). There was no change (Fig 6.12, curve b) in the voltammograms for the passivated unmodified electrode after a 5-hour recovery time, implying an irreversible surface blocking of the electrode by the products of *p*-CPh oxidation.

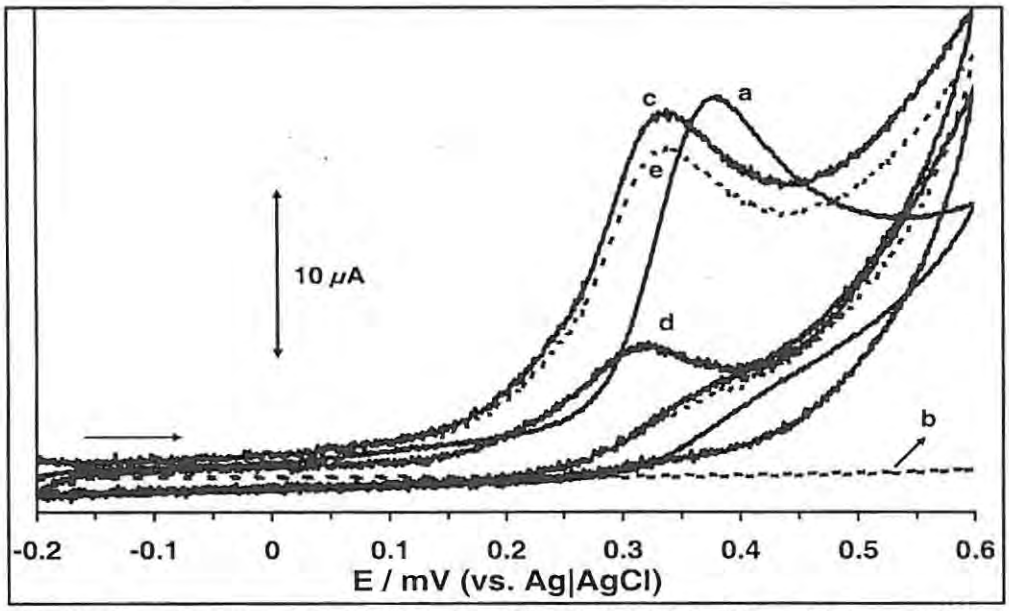

Fig 6.12: Cyclic voltammograms of 0.7 mM p-CPh in 0.1 M NaOH at (a) unmodified (before passivation); (b) unmodified (after passivation and 5 hrs recovery); (c) *poly*-Ni(OH)TPhPyPc (before passivation); (d) *poly*-Ni(OH)TPhPyPc-(after passivation and 30 mins recovery) and (e), *poly*-Ni(OH)TPhPyPc modified GCE after passivation and 5 hrs recovery). Scan rate: 100 mVs^{-1}.

Poly-NiTSPc has been used for modification of glassy carbon electrode[82] and has been shown to fare well in the electrooxidation of chlorophenols. The report[82] indicated that the electrode surface became blocked in the long term. The integrity of the *poly*-

Ni(OH)TPhPyPc modified electrode was compared to the performance of *poly*-NiTSPc modified GCE. Both electrodes *poly*-Ni(OH)TPhPyPc and *poly*-NiTSPc modified GCE were subjected to constant potential electrolysis at 0.4 V (near the peak potential for the oxidation of p-CPh) in the presence of 0.7 mM p-CPh for 60 mins and the electrodes were rinsed with Millipore water and then transferred to a fresh solution containing 0.7 mM p-CPh. Fig 6.13a shows cyclic voltammograms of 0.7 mM p-CPh in 0.1 M NaOH at *poly*-NiTSPc before (curve i) and after (curve ii) controlled potential application. Curve (iii) is the cyclic voltammograms of *poly*-NiTSPc in blank 0.1 M NaOH solution.

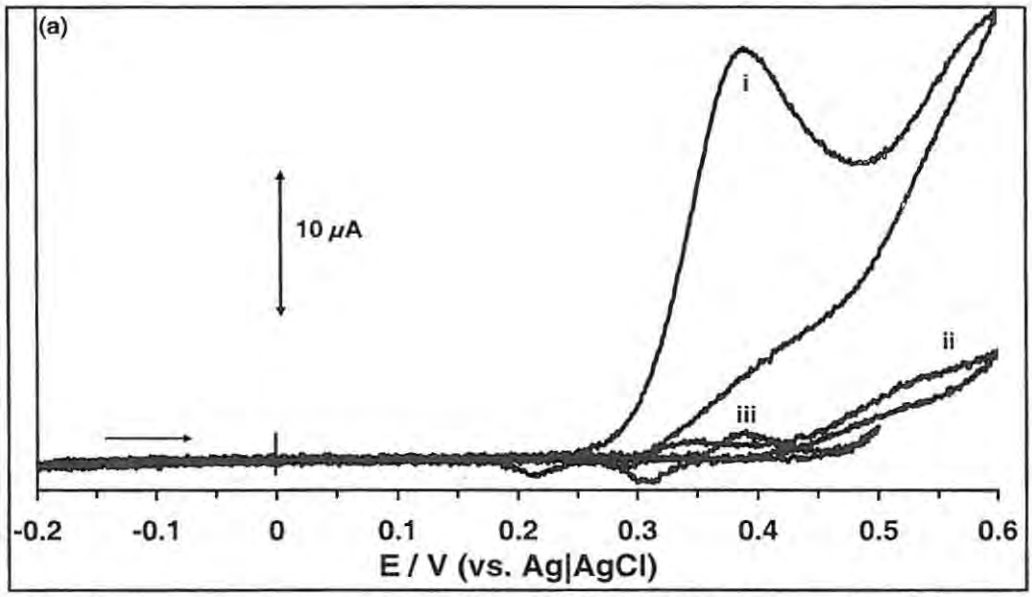

Fig 6.13a: Cyclic voltammograms of 0.7 mM p-CPh in 0.1 M NaOH at *poly*-NiTSPc modified GCE (i) before electrolysis and (ii) after controlled potential electrolysis at 0.4V for 60 mins. (iii) is the cyclic voltammograms of *poly*-NiTSPc in blank 0.1 M NaOH solution. Scan rate: 100 mVs^{-1}.

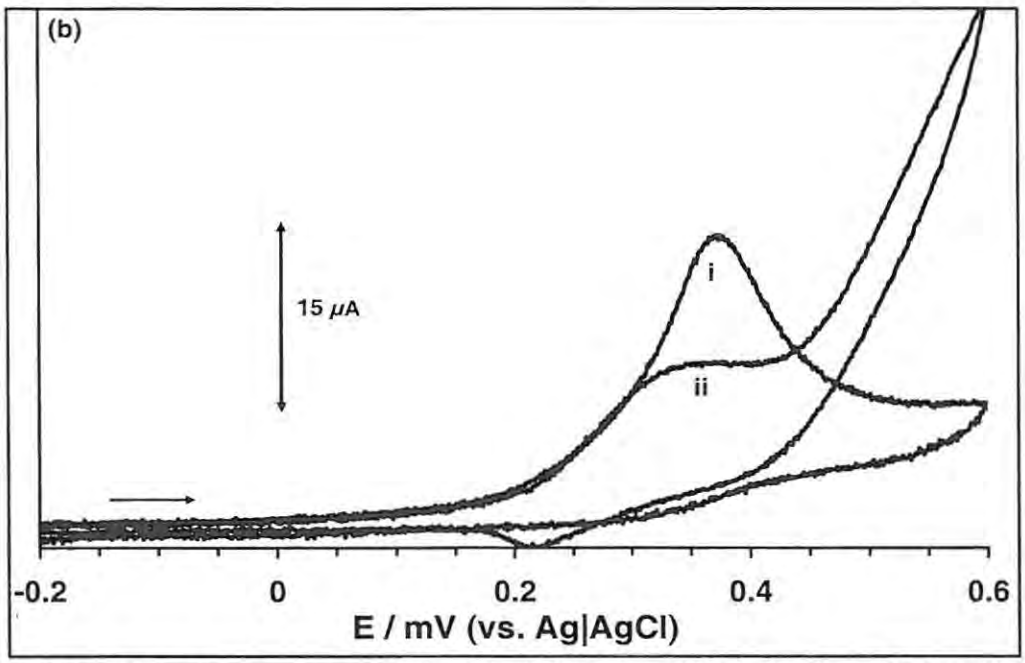

Fig 6.13b: Cyclic voltammograms of 0.7 mM p-CPh in 0.1 M NaOH at *Poly*-Ni(OH)TPhPyPc-GCE (i) before electrolysis and (ii) after controlled potential electrolysis at 0.4 V for 60 mins. Scan rate: 100 mVs^{-1}.

Fig 6.13b demonstrates the superiority of *poly*-Ni(OH)TPhPyPc over *poly*-NiTSPc for the modification of GCE for prevention of electrode fouling with respect to phenols. While the *poly*-Ni(OH)TPhPyPc modified GCE shows 65% (see curve ii, Fig 6.13b) activity with respect to the first scan (before electrode passivation, curve i), the *poly*-NiTSPc modified GCE showed only about 4.3% response (compared to before electrode passivation) as shown in Fig 6.13a (curves i and ii). It seems that the polyphenol formed on the *poly*-Ni(OH)TPhPyPc is more porous than on the *poly*-NiTSPc thereby allowing the passage of the p-CPh through the polymer channel as suggested in literature.[82] Also the porosity of the polyphenol on the electrode may be due to the size and structure of the ring substituent, phenoxypyrrole, which is larger than the SO_3^- of the NiTSPc complex. Since polyphenol films are known to be thick and nonporous,[459,464,465] the more complex nature of the *poly*-Ni(OH)TPhPyPc than the *poly*-NiTSPc may

contribute to a lowered degree of polymerization as well as formation of irregular polymer structure of the polyphenol on the electrode thereby making the electrode more difficult to deactivate.[82] It is worth mentioning that the *poly*-Ni(OH)TPhPyPc electrode surface remained green, (to the naked eye), after the constant potential electrolysis and after several cycles in fresh p-CPh solution while the thin film of the polyphenol tar could be visibly seen on the *poly*-NiTSPc-GCE passivated electrode, further confirming that the electrode, (*poly*-Ni(OH)TPhPyPc-GCE), is deactivated more slowly than the NiTSPc modified electrode.

6.2.2 Electrocatalytic Oxidation of Phenol

Fig 6.14a shows the first cyclic voltammograms of 0.7 mM phenol (Ph) in 0.1 M NaOH at unmodified GCE (curve i) and *poly*-Ni(OH)TPhPyPc modified GCE (curve iii). As was the case with *p*-CPh, there is a shift of the peak potential to a less positive potential suggesting a catalytic influence of the *poly*-Ni(OH)TPhPyPc electrode compared to the unmodified electrode. When the electrodes were subjected to passivation followed by recovery process, the unmodified electrode experienced surface blockage earlier than the modified electrode for the oxidation of 0.7 mM phenol. As was the case with *p*-CPh, the unmodified GCE reached a complete surface blockage, which could not be recovered, as can be seen from Fig 6.14a (curves i and ii), while the *poly*-NiT(OH)PhPyPc showed recovery of 92% after 5 hrs, Fig 6.14a (curve (iii) and (iv)).

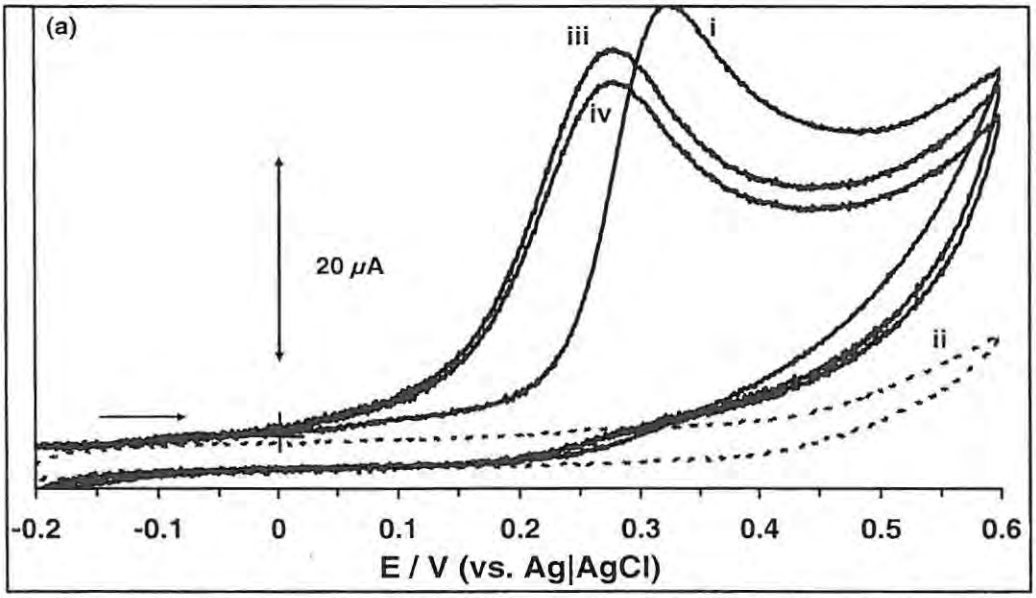

Fig 6.14a: Cyclic voltammograms of 0.7 mM Ph (in 0.1 M NaOH) at (i), unmodified GCE; (iii) *poly*-Ni(OH)TPhPyPc (before passivation), (ii) Unmodified GCE after passivation, and 5 hrs recovery time; (iv) *poly*Ni(OH)TPhPyPc modified GCE after passivation and 5 hrs recovery. Scan rate: 100 mVs^{-1}.

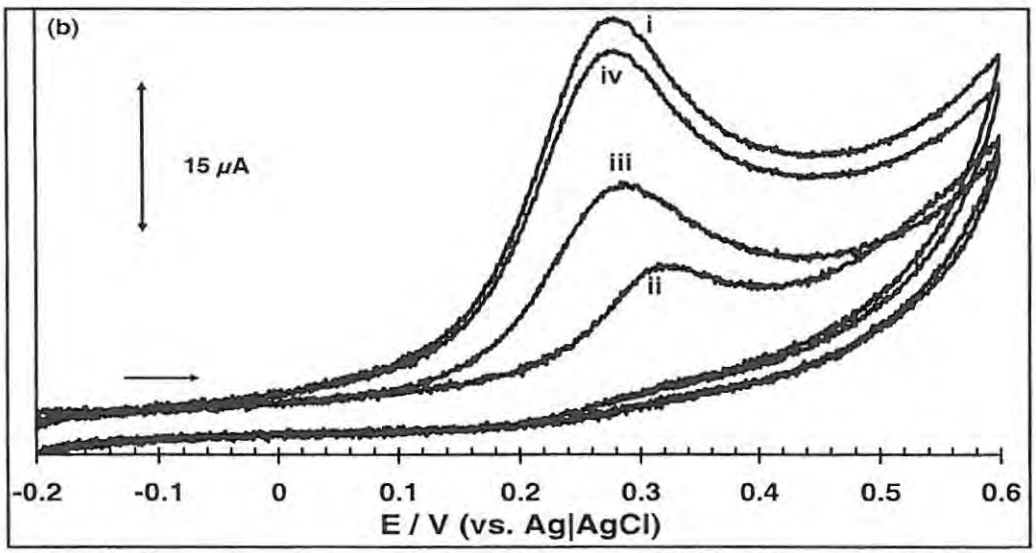

Fig 6.14b: Cyclic voltammograms of 0.7 mM Ph (in 0.1 M NaOH) at *poly*-Ni(OH)TPhPyPc modified GCE (i) before passivation; (ii) after passivation, and no recovery time, and (iii) after passivation and recovery for 30mins and (iv) after passivation and recovery for 5 hrs. Scan rate: 100 mVs^{-1}.

Fig 6.14b shows the effect of recovery time of the electrodes towards the oxidation of phenol. It can be seen that the activity of the electrode increases with recovery time until it gains over 92% of its activity (relative to the first scan before

passivation) after 5 hrs. This observation is quite interesting for a preparative scale application of the *poly*-Ni(OH)TPhPyPc modified electrode for electrooxidation of phenols. The lack of recovery in the case of the unmodified GCE after passivation, shows the superiority of *poly*-Ni(OH)TPhPyPc over the unmodified electrode

6.2.3 Electrocatalytic Oxidation of p- Nitrophenol

The electrodes were also used for the electrooxidation of para nitrophenol (p-NPh) in 0.1 M NaOH. Fig 6.15 shows the voltammograms obtained for 4.5 mM p-NPh at unmodified (curve i) and passivated, (unmodified), GCE (curve ii). Unlike in the case of phenol and *p*-CPh, it can be seen that the extent of passivation is less pronounced for the p-NPh for a similar number of repetitive CV scan cycles.

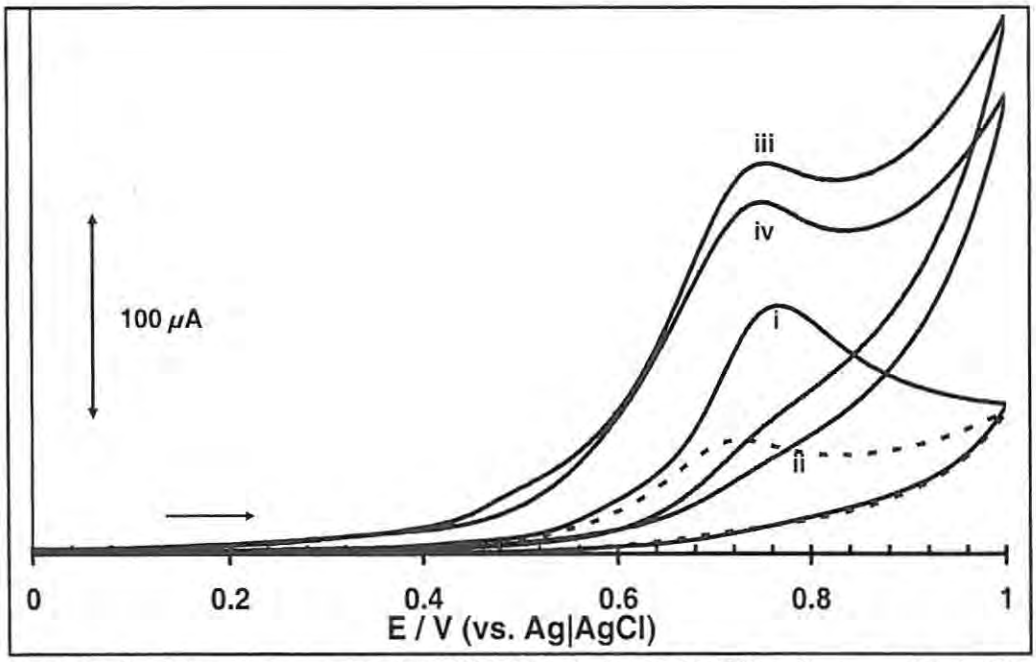

Fig 6.15: Cyclic voltammograms of 4.5 mM p-NPh in 0.1 M NaOH at (i), unmodified GCE, (ii) unmodified GCE, after passivation and rinsing in water, no recovery time allowed (iii) *poly*-Ni(OH)TPhPyPc-GCE before passivation, and (iv) *poly*-Ni(OH)TPhPyPc-GCE after passivation and rinsing in water, no recovery time allowed. Scan rate: 100 mVs^{-1}.

A comparison with the *poly*-Ni(OH)TPhPyPc modified GCE, showed a better integrity than the unmodified electrode in that about 90% of the activity of the modified electrode was recovered after passivation for the former (Fig 6.15 (curves iii and iv). On the other hand only 46% recovery was observed in the case of the unmodified electrode.

The differences in the extent of passivation of the modified electrodes by the oxidation products of the different phenols could be a result of a combination between the polyphenol structure and *poly*-NiPc film structure. As stated earlier poly-chlorophenol looks different on *poly*-NiTSPc and on *poly*-Ni(OH)TPhPyPc. Thus, there are probably two effects: phenol substitution and the initial native NiPc polymer structure. The relative stabilities of resonance structures formed following the formation of the phenoxy radicals will be influenced by the substituents, resulting in a variety of coupling products, which deactivate the electrode to different extents.

6.3 Electrocatalytic Reduction of Oxygen

Even though metallophthalocyanines are known to exhibit versatile electrocatalytic properties,[282,292,378] the electrocatalytic properties of CrPc has not been fully investigated. This report presents the first example of electrocatalytic reduction of oxygen at CoTPhPyPc-GCE, CrTAPc-GCE, MnTAPc-GCE and MnTMPyrPc-GCE in organic medium (dichloromethane). The electrocatalytic reduction of oxygen on cobalt tetraaminophthalocyanine (CoTAPc) has been investigated by Tse and coworkers[347] in aqueous media. Their results showed that the polymerized CoTAPc fared better than monomeric CoTAPc adsorbed onto GCE. The reduction of dioxygen on [*poly*-

CrTAPc]$_{20}$ modified GCE, (obtained as described in Fig 5.13), is shown in Figs 6.16 and 6.17. Fig 6.17 shows the CV of [*poly*-CrTAPc]$_{20}$ in deaerated DCM + 0.1 M $TBABF_4$.

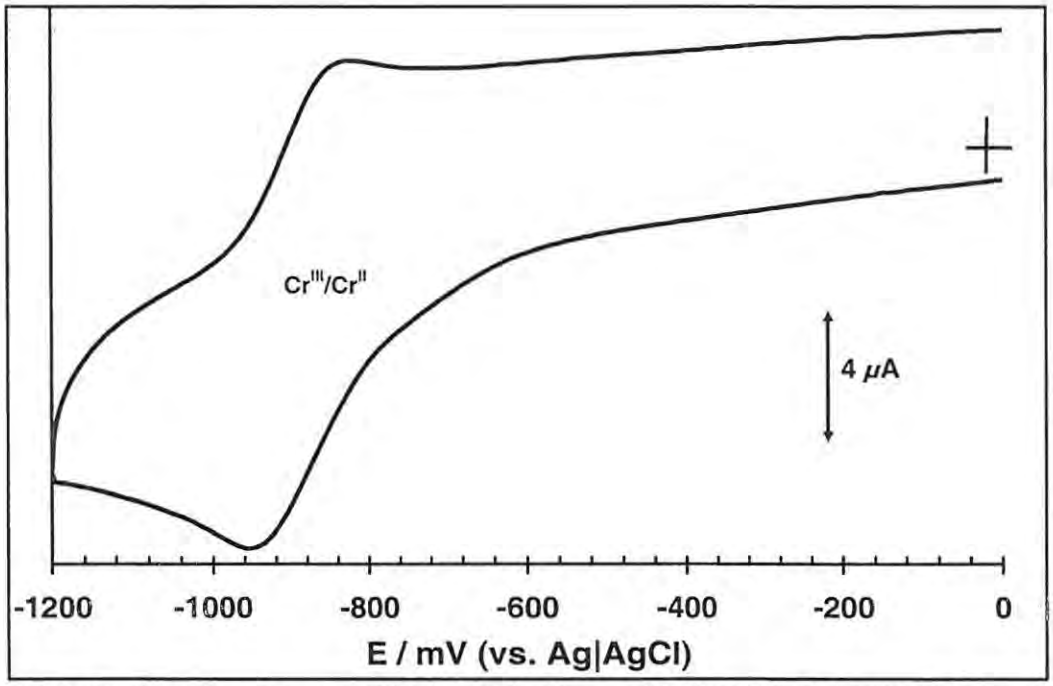

Fig 6.16: Cyclic voltammogram of [*poly*-CrTAPc]$_{20}$ modified GCE in 0.1 M $TBABF_4$ + DCM solution. The electrode was prepared in 0.1 M $TBABF_4$ + DMF and transferred into the DCN solution after thorough rinsing in DMF and DCM. Scan rate: 100 mVs^{-1}.

The assignment of the redox couples are shown in Fig 6.16. It shows a reversible couple of peaks centred at -0.87 V (vs. Ag|AgCl) which can be related to the Cr^{III}/Cr^{II} redox process of the phthalocyanine, by reference to the behaviour of the monomer complex in DMF + 0.1 M $TBABF_4$ (Fig 4.9). When the electrode was transferred into an oxygen-rich DCM + 0.1 M $TBABF_4$, a huge catalytic current (Fig 6.17a, curve ii) that almost obscures the CV signal of the redox couple due to the polymer alone (Fig 6.17a, curve i) was observed.

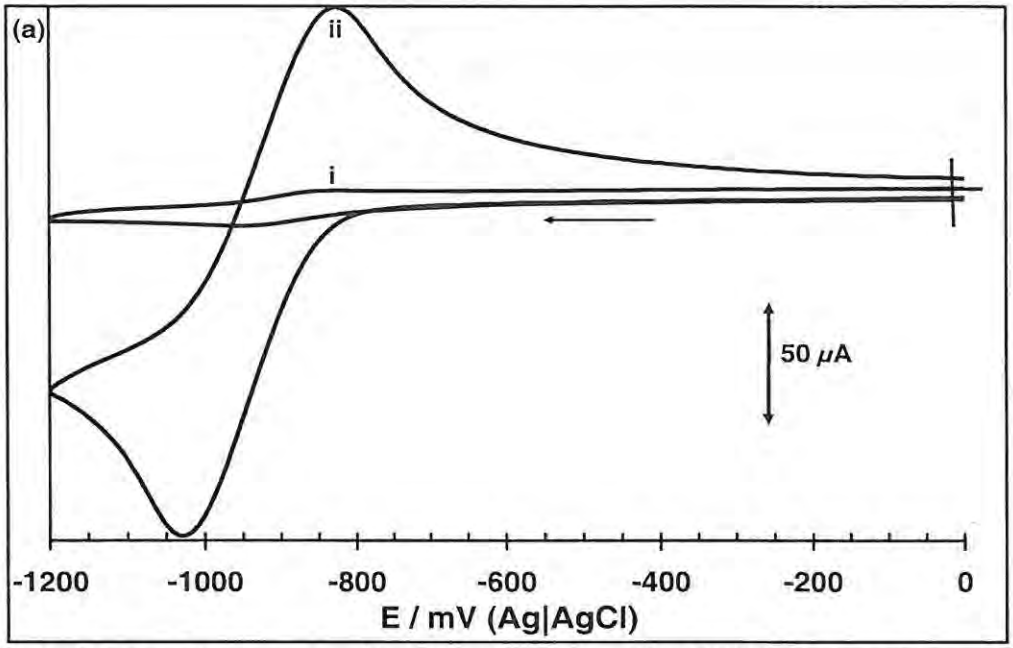

Fig 6.17a: Cyclic voltammogram of [*poly*-CrTAPc]$_{20}$ modified GCE in (a, curve i) oxygen-free; curve ii, molecular oxygen saturated DCM + 0.1 M $TBABF_4$ solution. Scan rate: (a): 100 mVs^{-1}. Curve i is same as the CV shown in Fig 6.16.

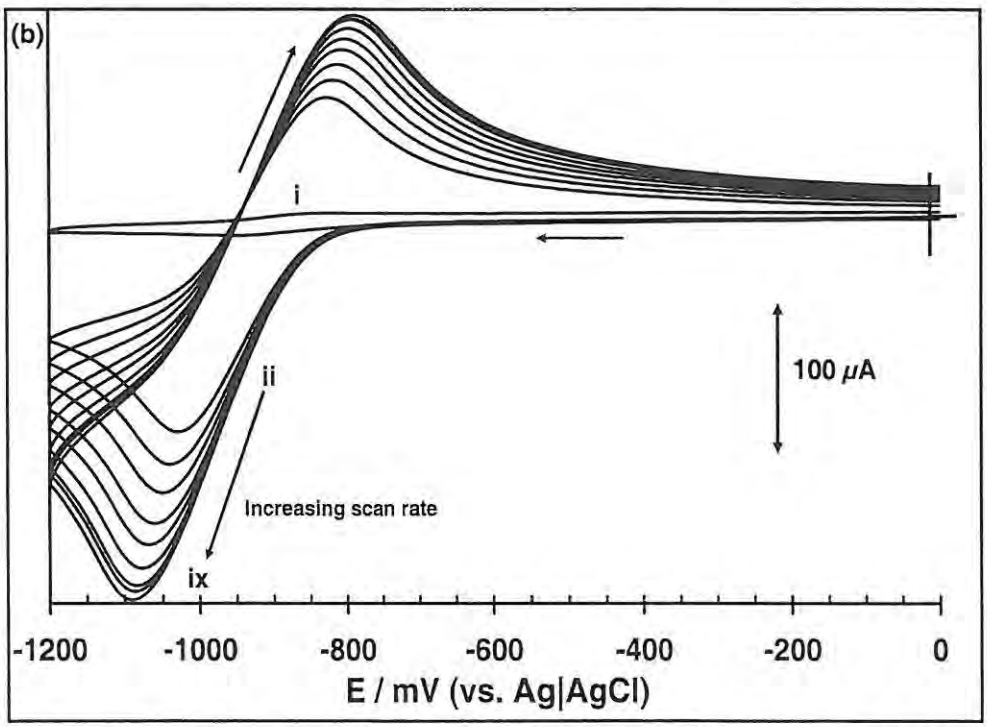

Fig 6.17b: Cyclic voltammogram of [*poly*-CrTAPc]$_{20}$ modified GCE in (curve i) oxygen-free; curve ii, molecular oxygen saturated DCM + 0.1 M $TBABF_4$ solution showing the effect of scan rate on the voltammetric response of the electrodes in oxygen saturated solution. Scan rate: (b): 50, 100, 150, 200, 250, 300, 350, 400 and 450 mVs^{-1}. Curve I is same as the CV shown in Fig 6.16.

The catalytic current related to oxygen reduction in Fig 6.17 reveals an effective enhancement in the current intensity when compared to the voltammetric curve obtained in oxygen-free DCM electrolyte solution, Fig 6.17 (curve i). This may be due to the binding of dioxygen to Cr^{III}TAPc to afford the adduct Cr^{III}-O_2 followed by the four-electron reduction of molecular oxygen to water. The peak on the reverse scan can be relate to the regeneration of the trivalent chromium (Cr^{III}) as suggested in literature for manganese porphyrin analogue.[466] Fig 6.17b shows a stable and reproducible quasi-reversible redox response in the potential range under investigation. The CVs (ii → ix) represent the voltammetric signals obtained from varying scan rates. A plot of the peak currents vs. square root of scan rate was linear suggesting that the electrode process is diffusion controlled.

Electroassisted activation of molecular oxygen by manganese porphyrins and phthalocyanine polymers has been reported.[466] In the presence of benzoic anhydride as an "activator" electrocatalytic reduction of oxygen occurs. Fig 6.18 shows the CV of *poly*-MnTAPc modified GCE in blank electrolyte solution.

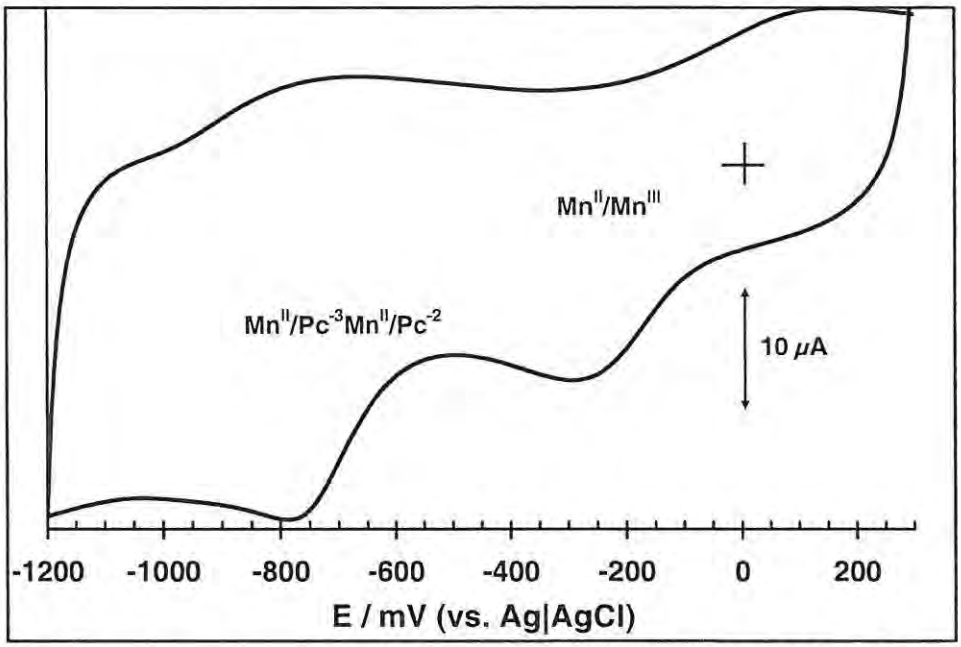

Fig 6.18: Cyclic voltammogram of [*poly*-MnTAPc]$_{20}$ modified GCE in 0.1 M $TBABF_4$ + DCM solution. The electrode was prepared in 0.1 M $TBABF_4$ +DMF and transferred into the DCM solution after thorough rinsing in DMF and DCM. Scan rate: 100 mVs^{-1}.

Even though complete polymerization occurred at 110 scans, 20 scans were used (denoted [*poly*-MnTAPc]$_{20}$) since for catalysis in this chapter, all electropolymerized films were obtained from 20 CV scans. The redox process related to $Mn^{II}Pc^{-3}/Mn^{II}Pc^{-2}$ can be seen around - 0.77 V (vs. Ag|AgCl), based on the assignment for a monomeric MnTAPc in DMF by CV and spectroelectrochemistry in Chapter Four. The enhanced current signals at - 0.9 V and - 1.04 V (vs. Ag|AgCl) (Fig 6.19, curve iii), in the presence of oxygen, suggest that the oxygen reduction process proceeds via a 2 x 2 electron transfer mechanism.[348] The peak potential at - 0.9 V may be due to the first reduction of molecular oxygen to H_2O_2 followed by another two-electron reduction of H_2O_2 to water. It can be seen that the voltammograms labelled (ii) and (iii) are similar except that the first wave shifted to - 0.86 V in curve (ii) compared to - 0.9 V in curve (iii). The CV scans were recorded at 60 seconds interval to monitor the effect of time on the possible coordination of the molecular oxygen to the Mn^{II}.

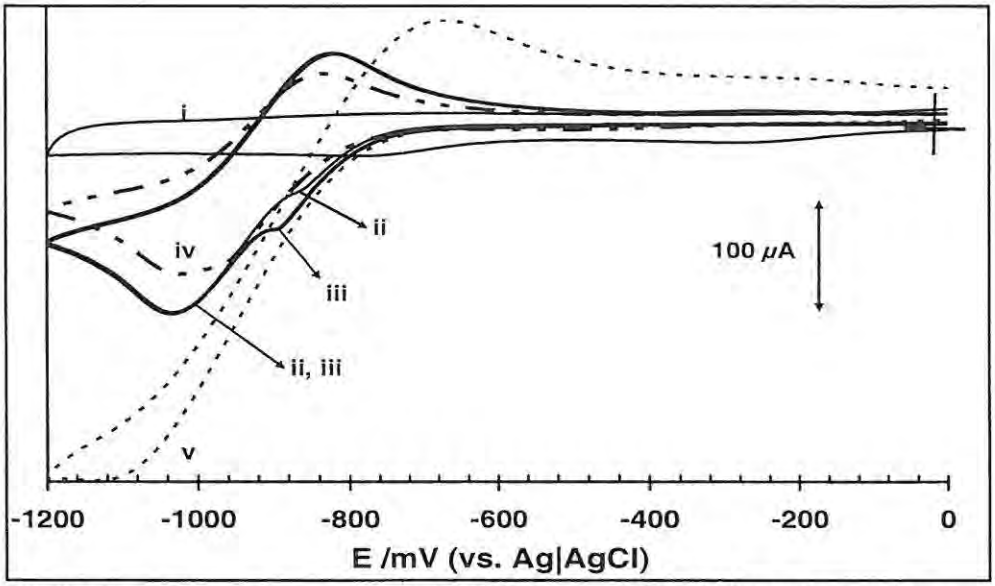

Fig 6.19: Cyclic voltammogram of [*poly*-MnTAPc]$_{20}$ modified GCE in (curve i) oxygen-free; curve ii, molecular oxygen saturated DCM + 0.1 M $TBABF_4$ solution. Curves iii and iv represent the CVs obtained two and three minutes, respectively, after ii was recorded; v: in the presence of benzoic anhydride. Scan rate: (a): 100 mVs^{-1}.

Note that while the peak potential at - 0.86 V shifted to - 0.9 V (accompanied be an enhanced current signal), on the second scan, the peak potential and peak current of the CVs remained unaffected at - 1.04 V (vs. Ag|AgCl).

The origin of the peak on the reverse scan (in both Fig 6.17 and 6.19) is not immediately certain since the reduction of oxygen is expected to be irreversible. It may be associated to the regeneration of the trivalent manganese (Mn^{III}) species.[466] Curve iv (Fig 6.19) shows that the peak currents related to $O_2 \rightarrow H_2O_2$, (at - 0.9 V), and $H_2O_2 \rightarrow H_2O$ (at - 1.04 V), merged as a single peak with time with a concomitant decrease in intensity. This may be due to the direct conversion of the molecular oxygen to water and decrease in the concentration of available reducible molecular oxygen as time went by. However the effect of an activator (benzoic anhydride) can be seen in the voltammetric response depicted in curve v (Fig 6.19). A huge increase related to the cleaving of the

O-O bond once the oxygen is coordinated to and activated by Mn centre, as has been reported before[463] is noticed. The O-O cleaving if facilitated by the anhydride.[466]

Fig 6.20 shows the cyclic voltammogramof *poly*-MnTMPyrPc under argon (curve i) and in the presence of dissolved oxygen (curve ii). It appears that in presence of molecular oxygen, the CV of the *poly*-MnTMPyrPc is subjected to a degree of modification.

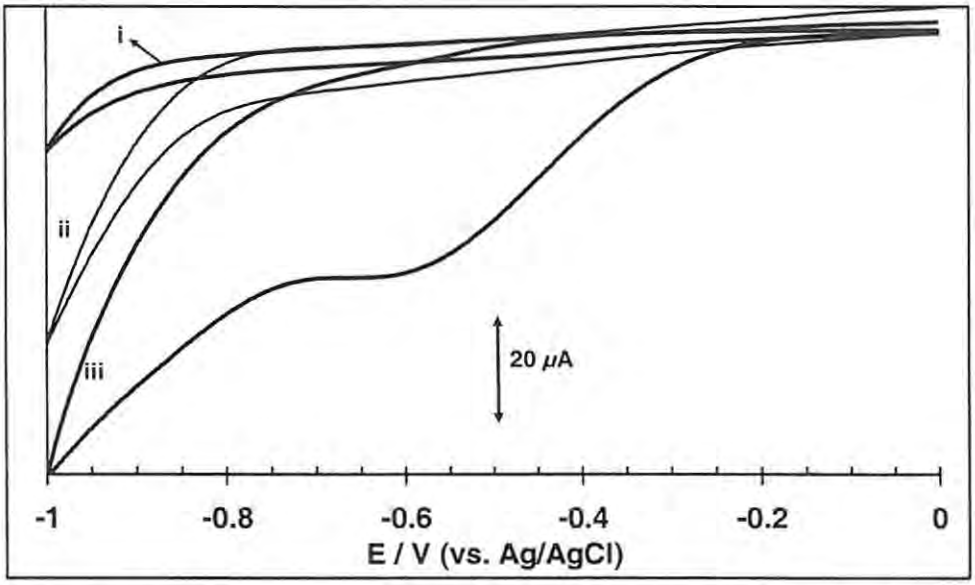

Fig 6.20: Cyclic voltammogram of *poly*-MnTMPyrPc modified GCE in (curve i) oxygen-free; curve ii, molecular oxygen saturated DCM + 0.1 M $TBABF_4$ solution. iii, in the presence of benzoic anhydride. Scan rate: (a): 100 mVs^{-1}.

Such modification of the cyclic voltammogram was previously reported in the literature with related manganese catalysts in various conditions, dissolved or immobilised on solid supports and in organic solvents.[466] The authors suggested that, in a first step, oxygen binds to Mn^{II} leading to a formulated Mn^{III}-superoxide adduct that accepts a second electron to form a doubly reduced superoxo intermediate. Curve iii (Fig. 6.20) shows the cyclic voltammogram of *poly*-MnTMPyrPc film in DCM + 0.1 M $TBABF_4$ solution containing benzoic anhydride (activator), upon addition of molecular

oxygen. As stated earlier, the anhydride function is to cleave the O-O bond once the oxygen is coordinated to and activated by Mn center.[466] A large enhancement of the Mn^{III}/Mn^{II} reduction current peak is clearly observed. By reference to previously reported studies of porphyrins and Schiff base complexes, the modification of the cyclic voltammogram can be explained by the occurrence of the expected formation of the high-valent manganese-oxo $[Mn^{V}=O]^{+}$ intermediate, followed by its reduction and the steady state electrocatalytic regeneration of Mn^{III} form.[466]

It should be noted that the direct reduction of molecular oxygen does not take place in the potential range investigated in this study, and that the presence of benzoic anhydride does not induce any electrochemical interference. A similar modification of the CV was observed for the *poly*-CoTPhPyPc modified GCE. Fig 6.21 (curve i) shows the CV of the *poly*-CoTPhPyPc electrode in oxygen-free DCM + 0.1 M $TBABF_4$ solution.

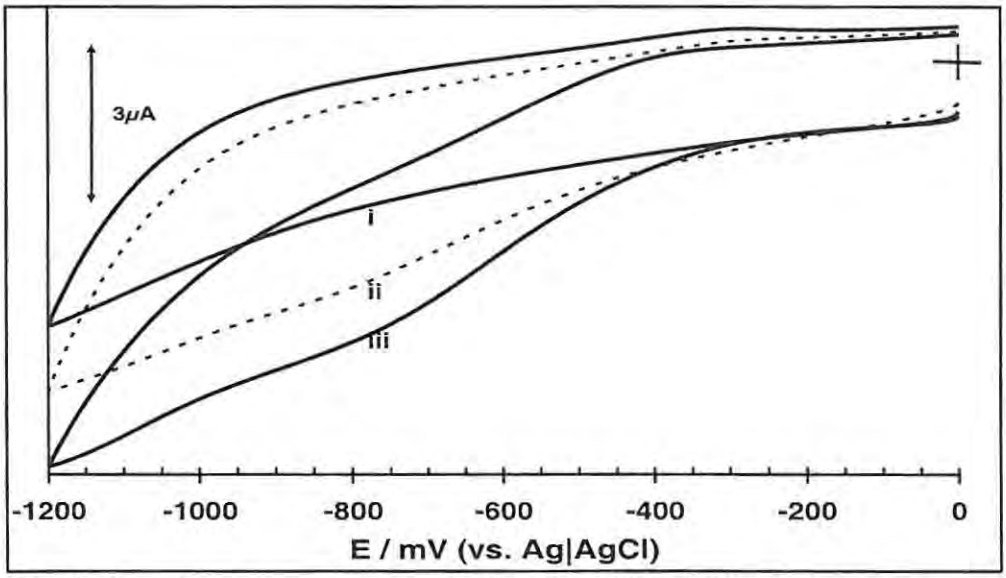

Fig 6.21: Cyclic voltammogram of *poly*-CoTPhPyPc modified GCE in (curve i) oxygen-free; curve ii, molecular oxygen saturated DCM + 0.1 M $TBABF_4$ solution. iii, in the presence of benzoic anhydride. Scan rate: (a): 100 mVs^{-1}.

It can be seen that the shoulder on the reverse scan of curve **I** (at ~ -0.4 V) is reduced in intensity upon addition of molecular oxygen to the electrolyte solution

accompanied by an increase in the current signal on the cathodic segment of the curve. A reference to the CV of the monomeric CoTPhPyPc in DCM + 0.1 M $TBABF_4$ solution (Fig 5.1) would suggest that the Co^{I} centre is the active site responsible for the oxygen reduction since the catalytic current in Fig 6.21 (curve ii and iii) are in the region of the central metal (Co^{I}/Co^{II}) redox process of the monomer solution.

As noted by Tse et al,[348] the reduction process occurred at potentials too negative to be used in fuel cell applications. However, the intrinsic capacity of the MPc complexes examined in this work to reduce oxygen has been demonstrated.

6.4 Electrocatalytic Oxidation of Nitric Oxide and Nitrite

6.4.1 Nitric Oxide (NO)

The electrochemical properties of *poly*-CrTAPc towards oxidation of nitric oxide (NO) and nitrite were pursued in this work. CrTAPc was chosen since as stated above, electrocatalytic behaviour of CrPc complexes has not been fully explored. Under pH 4.3 conditions, nitrite disproportionates, mainly, to NO, and the catalytic currents are due to NO. Hence the quantitative measurement of the NO is recorded as a function of the concentration of the nitrite added into the solution. Fig 6.22 shows the electrocatalytic behaviour of the *poly*-CrTAPc modified GCE towards NO oxidation. A large increase in currents was observed on *poly*-CrTAPc modified GCE.

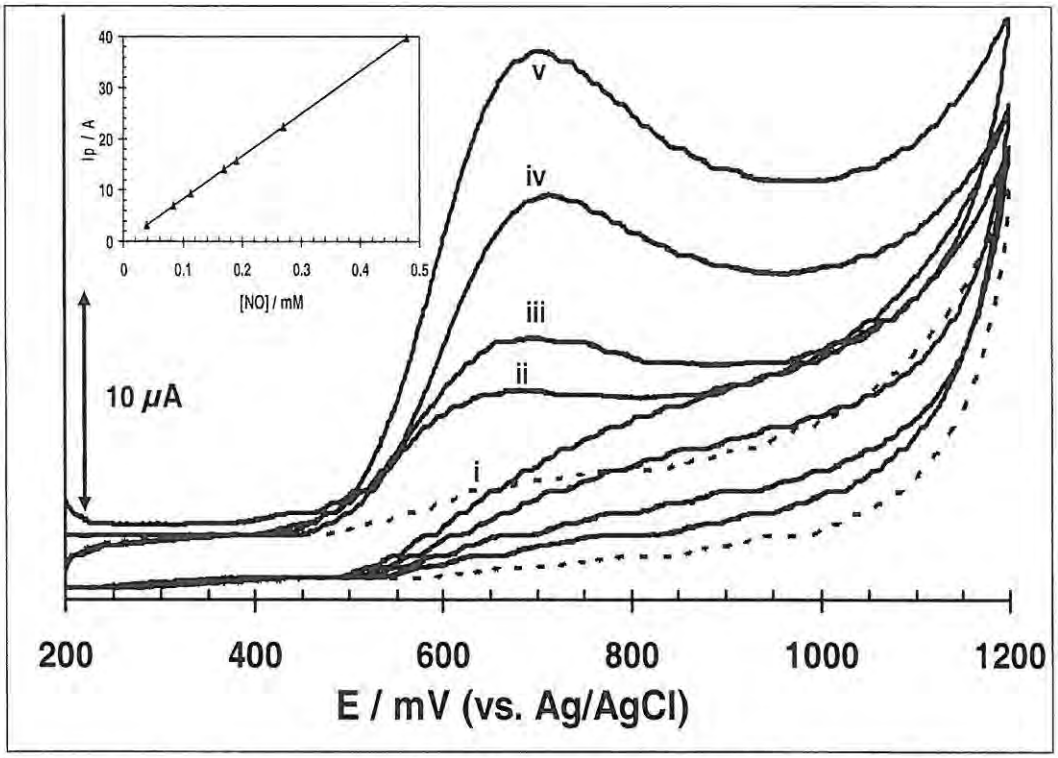

Fig 6.22: Voltammetric response for NO at an unmodified GCE (i) and [*poly*-CrTAPc]$_{20}$ electrode (ii to v). Concentrations of nitrite / μM: (i) = 38; (ii) = 20; (iii) = 38; (iv) = 84; (v) = 110. Scan rate = 100 mVs^{-1}. pH 4.3 buffer. Insert shows the plot of peak current vs. concentration of nitrite.

The catalytic peak for NO was observed at 0.68 V, vs. Ag|AgCl. All catalytic studies were carried out using [*poly*-CrTAPc]$_{20}$ modified electrode. It is important to mention that the catalytic currents for the oxidation of the NO occurred at potentials where ring-based process occurs, suggesting the involvement of $Cr^{IV}TAPc^{-1}$/ $Cr^{IV}TAPc^{-2}$ redox process (**II**) in Fig 4.9. Catalytic oxidation of NO mediated by ring-based redox processes has been described.[379] The catalytic currents varied linearly with nitrite concentration as shown in Fig 6.22, for concentrations ranging from 5 x 10^{-6} to 5.0 x 10^{-4} M.

6.4.2 Nitrite

Dissolving a known amount of $NaNO_2$ in pH 7.3 phosphate buffer solution generated the nitrite ion. At this pH, the disproprtionation of nitrite to NO is insignificant hence the species being catalyzed is the oxidation of nitrite. Fig 6.23 represents the cyclic voltammograms for a *poly*-CrTAPc/GCE catalyst-based electroxidation of NO_2^-.

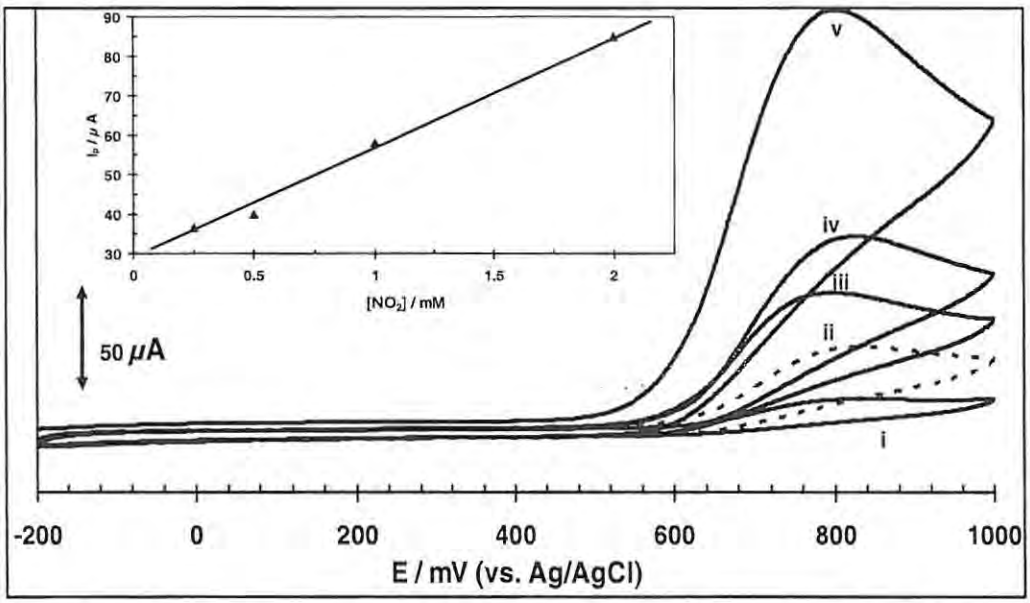

Fig 6.23: Cyclic voltammetric response of NO_2^- on unmodified GCE (i) and $[poly\text{-CrTAPc}]_{50}$ (ii to v) for varying concentrations of NO_2^- in N_2 deaerated pH 7.3 phosphate buffer solution. Concentrations of NO_2^- / mM: (i) = 0.025; (ii) = 0.025; (iii) = 0.05; (iv) = 0.1; (v) 0.2. Scan rate: 100 mVs^{-1}. Insert shows the plot of peak current vs. concentration of NO_2^-.

Redox peaks corresponding to oxidation and reduction of the *poly*-CrTAPc on GCE in the blank pH 7.3 solution were not clearly observed at the scale employed in Fig 6.23. However, when the electrode was transferred into a pH 7.3 solution containing 2.5 x 10^{-5} M NO_2^-, an enhancement of anodic currents attributable to the catalytic oxidation of nitrite was observed, Fig 6.23 (ii to v). It has been suggested[388] that nitrite ion interacts with cobalt (II) tetrasulfophthalocyanine in aqueous solutions forming a 5-coordinate

intermediate by its replacement of one of the axially bound water molecules. This point might be helpful in understanding the interaction of the nitrite ion with the *poly*-CrTAPc film on the electrode. Again the position of the catalytic peak suggests the involvement of the $Cr^{IV}TAPc^{-1}/Cr^{IV}TAPc^{-2}$ couple in the catalytic process. Table 6.1 shows a summary of the results obtained from the electrocatalytic studies carried out in this thesis.

Fig 6.24a shows that nitrite electrooxidation is a diffusion-controlled process. Also, the chemical irreversibility of the nitrite electrocatalytic oxidation is confirmed from the peak potential, E_p, shift with log of scan rate (Fig 6.24b). The presence of two linear regions in the E_p vs. log v plot suggests the chemical reactions coupled with electrochemical steps are involved in the electrocatalytic oxidation of nitrite.[274] The shape of the plot of peak current versus potential in Fig 6.24c is typical of a catalytic process.[274]

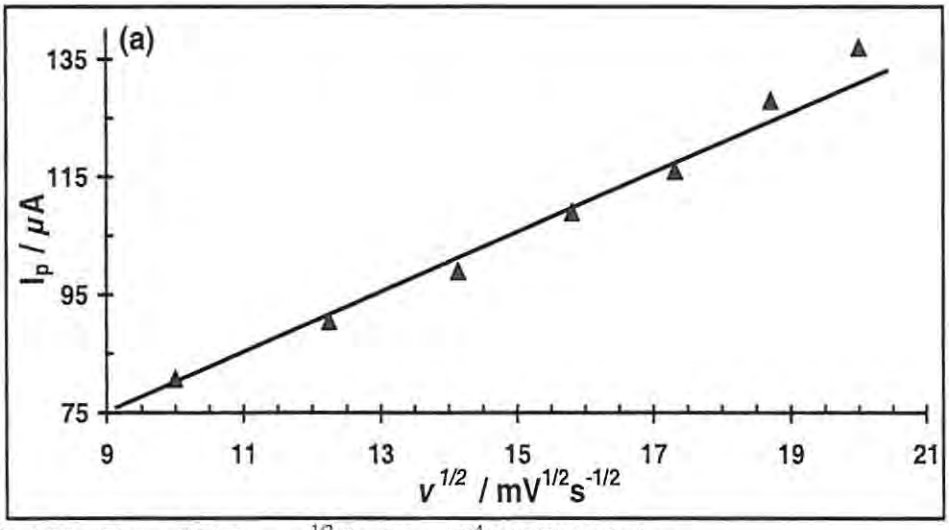

Fig 6.24a: Plots of (a) Ip vs. $v^{1/2}$ for 1.4 x 10^{-4} M NO_2^- solution.

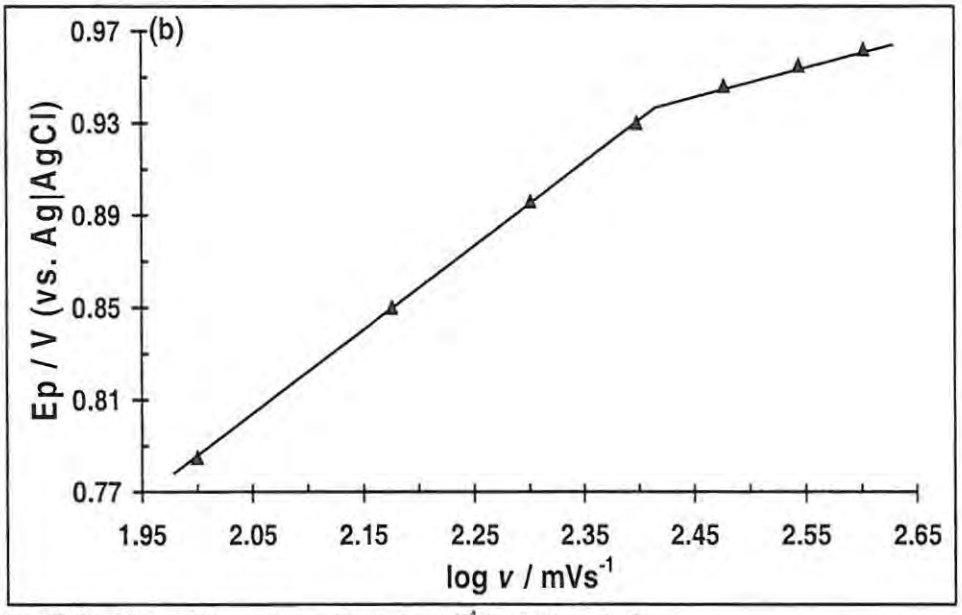

Fig 6.24b: Plots of E_p vs. log v for 1.4 x 10^{-4} M NO_2^- solution.

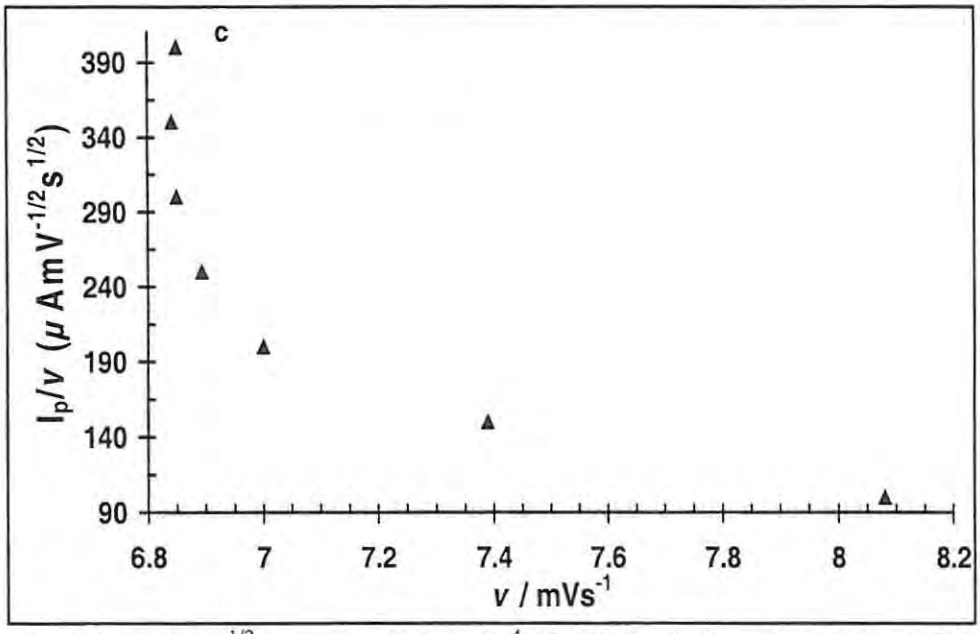

Fig 6.24c: Plots of $I_p v^{1/2}$ vs. v for 1.4 x 10^{-4} M NO_2^- solution. I_p and E_p refer to the catalytic currents and oxidation potential for NO_2^-, respectively.

Chapter Seven

Conclusions

For the first time, the syntheses, characterization and electrocatalytic activity of a new family of pyrrole, thiophene and mercaptopyrimidin substituted metallophthalocyanine complexes has been reported. The results show that thermal annealing of the adsorbed cobalt complexes (CoTETPc (**16**) and CoTMPyrPc (**14**)), can afford reproducible, stable and dependable modified electrodes. Moreover, the material has proven effective for decreasing the overpotentials associated with electrochemical oxidation of L-cysteine, in acidic medium, (pH 4.0), compared to unsubstituted CoPc. The detection limit was in the micromolar range at millimeter-sized electrode. This suggests that the catalysts could be used for better detection limits when used to modify micrometer-sized electrode, e.g. ultramicroelectrodes, depending on the strategic intent. The complexes are therefore promising electrocatalysts for the oxidation of L-cysteine and related thiols. Another interesting feature highlighted in this work is the capability of the sulfur containing MPcs (MTETPc (**16-18**) and MTMPyrPc (**13-15**)) to form self-assembled monolayer films on gold electrodes. Although their catalytic activities were not investigated in the work the promising results obtained from the monomers adsorbed on GCE demonstrates the potential candidacy of these complexes as sensors when immobilized on GCE or gold surfaces.

This report has shown, (in the case of the pyrrole substituted MPc), that *poly*-NiTPhPyPc can be electrotransformed to *poly*-Ni(OH)TPhPyPc to afford a more stable electrode towards the electrooxidation of phenol and its derivatives. *Poly*-Ni(OH)TPhPyPc, showed good anti-fouling ability than the unmodified and *poly*-NiTSPc modified electrodes in the presence of phenols and its derivatives. This result is a

contribution to the quest for suitable electrodes for the development of electrochemical methods for environmental monitoring and pollution control.

The electrochemical behavior of MnPc complexes is still not fully understood. This work is a contribution towards the characterization of the various oxidation states of MnPc using spectroelectrochemistry. The formation of Mn^{II} and Mn^{IV} (in the case of MnTAPc) species on reduction and oxidation, respectively, is presented in this work from spectroelectrochemical data coupled with cyclic voltammetry. This work has also shown that the polymeric MnTAPc complex adsorbed onto a GCE results in a stable surface which can be used for analysis. The behaviour of *poly*-MnTAPc under different pH conditions shows that more reversible couples are observed at low pH. The dependence of potential on pH shows the involvement of hydroxyl groups accompanying the redox processes of the polymer. The polymer shows catalytic activity towards the reduction of glycine and oxygen with reasonable degrees of stability. This is an important observation since the practical applications of many MPc complexes for analysis has been limited by their loss of catalytic activity with time.

The characterization of CrTAPc complex has been performed on both the monomer and the polymerized film. The potential use of the CrTAPc complex for amperometric detection of nitrite has been shown in this study. The $Cr^{IV}TAPc^{-1}$ species is implicated as responsible for the electrocatalytic oxidation of nitrite and NO. The comparison of the efficiencies of the various film thicknesses towards the electroactivity of the electrogenerated *poly*-CrTAPc shows that an increase in the surface concentration of the polymer (as a function of scan number e.g. above 80 scans) results in a decrease in the electroactivity, and hence, in the electrocatalytic performance. The possibility of

casting an electropolymerizable film of this complex makes it particularly interesting for further investigations for possible application in photochromic devices and multidimensional arrays for sensor applications owing to the multiple oxidation states of the central metal.

References:

1. D.B. Hibbert, *Introduction to Electrochemistry*, Macmillan, London, 1993.
2. A.E. Kaifer and M. Gomez-Kaifer, *Supramolecular Electrochemistry*, Willey, VCH, New York, 1999.
3. A.J. Bard and L.R. Faulkner, *Electrochemical Methods: Fundamentals and Applications,* John Willey & Sons, 1996.
4. D.G. Davis, in D. Dolphin (Ed), *Physical Chemistry: The porphyrins*, Part A, vol III. Academic Press, NY, 1978, Ch. 4.
5. J.E.B. Randles, *Trans. Faraday Soc.*, 1948, 44, 327.
6. R.S. Nicholson and I Shain, *Anal. Chem.*, 1964, 36, 1351.
7. A. Sevćik, *Coll. Czech. Chem. Comm.*, 1958, 13, 349.
8. R. Greef, R. Peat, L.M. Peter, D. Pletcher and J Robinson, *Instrumental Methods in Electrochemistry*, Ellis Series in Physical Chemistry, T.J. Kemp (Ed), Ellis Horwood Ltd, Chichester, 1985, ch 6.
9. J. Wang, *Analytical Chemistry*, VCH publishers, New York, 1994.
10. J. Wang, D.B.Luo, P.A.M. Farias and J.S. Mahmoud, *Anal. Chem.*, 1985, 57, 158.
11. W.R. Heineman and W.B. Jensen, in S.T. Stock and M.V. Orna (Eds), Electrochemistry,Past and Present, ACS Symposium Series, **390**, American Chemical Society, Washinton DC, 1989, Chapter 30.]
12. T. Kuwana, R.K. Darlington and D.W. Leedy, *Anal. Chem.*, 1964, 36, 2023.
13. W.R Heineman, F.M. Hawkridge and H.N. Blount, in *Electroanalytical Chemistry*, A.J. Bard (Ed), vol 13 Marcel Dekker, Inc., New York, 1984. Pp 1-114.

14. D.E. Stilwell and S.M.Park, *J. Electrochem. Soc.*, 1982, **129**,1501.

15. J.W. Strojek and T. Kuwana, *J. Electroanal. Chem.*, 1968, **16**, 471.

16. S.M. Ahmed, *J. Phys. Chem.*, 1969, **73**, 3546.

17. C. Iwakura, M. Inai and T. Vemura, *Electrochim. Acta.,* 1981, **26**, 579.

18. M.A. Butler and D.S. Ginley, *J Electrochem. Soc.,* 1978, **125**, 228.

19. H.A. Laitenen, C.A. Vincent and T.M. Bednarski, *J. Electrochem. Soc.*, 1968, **115**, 1024.

20. A. Nanthakumar and N.R. Armstrong, in H.O. Finklea (Ed), *Semiconductor Electrodes: Studies in Physical and Theoretical Chemistry*, vol. 55, Elsevier, Amsterdam, 1988, Ch. 4.

21. J. Stotter, S. Haymond, J.K. Zak, Y. Show, Z. Cvackova and G.M. Swain, *The Electrochem Soc. Interface*, 2003, **12**, 1.

22. C. Donley, D. Dunphy, D. Paine, C. Carter, K. Nebesny, P. Lee, D. Alloway and N.R. Amstrong, *Langmuir*, 2002, **18**, 450.

23. H.L. Landrum, R.T. Salmon and E.M. Hawkridge, *J. Am Chem. Soc.,* 1997, **99**, 3154.

24. M.L. Stegemiller, W.R. Heineman, T.H. Ridgway, C.J. Seliskar, S.A. Bryan, T. Hubber and R.L. Sell, *Environ. Sci. and Technol.*, 2002, **37**, 123.

25. W.R. Heineman, *Anal.l Chem.*, 1978, **50**, 50.

26. R. Cieslinski and N.R. Amstrong, *Anal. Chem.*, 1979, **51**, 565.

27. P.A. Christenson and A. Hamnet, *Techniques and Mechanisms in Electrochemistry*, 1st ed, Blackie Academic and Professional, London, 1994.

28. W.R. Heineman and P.T. Kissinger: in *Laboratory Techniques in Electrochemistry*, 2nd ed, Eds P.T.Kissinger and W.R. Heineman, Marcel Deccer Inc. New York, 1996.

29. M. Krejčik, M. Deněk and F. Hartl, *J. Electroanal. Chem.*, 1991, **317**, 179.

30. S. Besnes, A. Ltaief, K. Reybier, L. Ponsonner, N. Jaffrezic, J, Davenas and H.B. Ouada, *Synthetic Metals*, 2003, **138**, 197.

31. R.W. Murray, W.R. Heineman and G.W. O'Dom, *Anal. Chem.*, 1967, **39**, 1666.

32. M. Petek, T.E. Neal and R.W Murray, *Anal. Chem.*, 1971, **43**, 1069.

33. W.J. Blaedel and S.L. Boyer, *Anal. Chem.*, 1973, **45**, 258.

34. D. Lexa, J.M. Saveant and J. Zickler, *J. Am. Chem. Soc*, 1977, **99**, 2786.

35. A.J. Bard and L.R. Faulkner, *Electrochemical Methods. Fundamentals and Applications,* John Willey and Sons, Inc., New York, 1980.

36. H.B. Mark Jr. and B.S. Pons, *Anal. Chem.*, 1966, **38**, 119.

37. D.R. Tallant and D.H. Evans, *Anal. Chem.*, 1969, **41**, 835.

38. A.J. Bard and L.R. Faulkner, *Electrochemical Methods: Fundamentals and Applications*, 2nd ed. John Willey & Sons New York, 2001.

39. J. Wang, *Analytical Electrochemistry*, 2nd Ed., Willey, VCH, New York, 2000.

40. J.O'M. Bockris, B.E. Conway and E. Yeager (eds), *Comprehensive Treaties of Electrochemistry,* vol. 1, Plenum Press, New York, 1980.

41. A.T. Hubbard and F.C. Anson, in *Electroanalytical Chemistry*, A.J. Bard (Ed) vol. 4. Marcel Dekker Inc. New York, 1970, Pp 129-214.

42. W.R. Heineman, B.J. Norris and J.F. Goelz, *Anal. Chem.*, 1975, **47**, 79.

43. T.P. De Angelis and W.R Heineman, *J. Chem. Educ.*, 1976, **53**, 594.

44. E.A. Blubaugh, A.W. Yacynych and W.R. Heineman, *Anal. Chem.*, 1979, **51**, 561.

45. J.L. Owens and G. Dryhurst, *J. Electroanal. Chem.*, 1977, **80**, 171.

46. M.Z. Wrona, J.L. Owens and G. Dryhurst, *J. Electroanal. Chem.*, 1982, **132**, 323.

47. P.T. Kissinger and C.N. Reilley, *Anal. Chem.*, 1970, **42**, 12.

48. R.W. Murray, *Electroanalytical Chemistry, A Series of Advances*, A.J. Bard (Ed.), Vol. 13, Marcel Dekker, Inc., New York, pp 191-368.

49. B.E. Firth, L.L. Miller, M. Mitani, T. Rogers, J. Lennox and R.W. Murray, *J. Am. Chem. Soc.*, 1976, **98**, 8271.

50. J.C. Lennox and R.W. Murray, *J. Electroanal. Chem* 1977, **78**, 395.

51. C.A. Koval and F.C. Anson, *Anal. Chem.*, 1978, **50**, 223.

52. J.F Evans and T. Kuwana, *Anal. Chem.*, 1977, **49**, 1632.

53. F. Marken, A. Neudeck and A.M. Bond, in *Electroanalytical Methods: Guide to Experiments and Applications*, F. Scholz (Ed), Springer, Berlin, 2002, pp 51-97

54. P.N. Barllet and J.M. Cooper, *J. Electroanal. Chem.*, 1993, **362**, 1

55. E. Laviron, *J. Electroanal. Chem.* 1974, **52**, 355.

56. S. Srinivasan and E Gileadi, *Electrochim. Acta*, 1966, **11**, 321.

57. A.P. Brown and F.C. Anson, *Anal. Chem.*, 1977, **49**, 1589.

58. E.A.M.F. Dahmen, *Electroanalysis: Theory and Applications in Aqueous and Non-aqueous media and in Automated Chemical Control*, Elsevier Science Pub, New York, 1986, Ch. 1.

59. P.L. Bailey, *Analysis with Ion-selective Electrodes*, Heyden, London, 1980.

60. J.E. Frew and H.A.O. Hill, *Anal. Chem.*, 1987, **59**, 933A.

61. G.S. Calabrese and K.M. O'Connell, in E. Steckhan (Ed) *Electrochemistry II, Topics in Current Chem.*, vol. 143, Springer, Berlin Heidelberg, p 49.

62. M.W. Espenscheid, A.R. Ghatak-Roy, R.B.I.I.I. Moore, R.M. Penner, M.N. Szentirmay and C.R. Martin, *J. Chem. Soc., Faraday Trans.*, 1986, **82**, 1051.

63. A. Merz, in E. Steckhan (Ed), *Topics in Current Chem.*, vol. 152, Springer-Varleg, Berlin Heidelberg, 1990, p 51.

64. J.P. Collman, M. Marrocco, P. Denisevich, C. Koval and F.C. Anson, *J. Electroanal. Chem.*, 1979, **101**, 117.

65. J.P. Collman, P. Denisevich, Y. Konai, M. Marrocco, C. Koval and F.C. Anson, *J. Am. Chem. Soc.*, 1980, **102**, 602.

66. N.M. Rowley and R.J. Mortimer, *Science Progress*, 2002, **85**, 243.

67. K. Shinbo, K. Kato, F. Kaneko, K. Onishi, R.C. Advincula and X. Fan, *Molecular Crystals and Liquid Crystals*, 2003, **407**, 1.

68. M.D. Ward (Ed), *Comprehensive Coordination Chemistry II, From Biology to Nanotechnology: Application of Coordination Chemistry*, Elsevier, Amstardam, vol. 9, 2003.

69. S. Radhakrishnan and S.D. Deshpande, *Sensors*, 2002, **2**, 185.

70. M. Matsuda, N. Hanasaki, S. Ikeda, H. Tajima, T. Naito and T. Inabe, *J. Phys. IV France*, 2004, **114**, 541.

71. Z. Bao, A.J. Lovinger and A. Dodabalapur, *Appl. Phys. Lett*,, 1996, **69**, 3066.

72. Z. Bao, A.J. Lovinger and B. Janelle, *J. Am. Chem. Soc.*, 1998, **120**, 207.

73. B.R. Eggins, *Biosensors: An Introduction*, John Willey and Sons, West Chichester, 1996, ch 3.

74. A.J. Bard, *J. Chem. Educ.*, 1983, **60**, 303.

75. R.W. Murray, *Accts., Chem. Res.* 1980, **13**, 135.

76. R.W. Murray, *Electroanal. Chem.*, 1983, **13**, 1.

77. M.S. Wrighton, *Inorg. Chem.*, 1985, **4**, 269.

78. R.W. Murray, A.G. Ewing and R.A. Durst, *Anal, Chem.*, 1987, **59**, 379A.

79. G. Inzelt, *J. Electroanal. Chem.*, 1994, **18**, 89.

80. A.J. Bard, *J. Electroanal. Chem.*, 1962, **2**, 117

81. P. Guo, T.-W. Hui, K.-C. Wong and K.-K. Shiu, *J. Electroanal. Chem.*, 2001, **498**, 142.

82. M.S. Ureta-Zanartu, C. Berrios, J. Zagal, C. Gutierrez and J.F. Marco, *J. Electranal. Chem.*, 2003, **553**, 147

83. G.P. Evans, in *Advances in Electrochemical Sciences and Engineering* H. Gerischer, C.W. Tobias (Eds) Vol.1 VCH, Weinheim, (1990) ch. 1.

84. R. de Saja, J. Souto, M.L. Rodriguez-Mendez and J.A. de Saja, *Mater. Sci. Eng.*, 1999, **8-9**, 565.

85. A. Chyla, J. Sworakowski, A. Szczurek, E. Brynda and S. Nespurek, *Mol. Cryst. Liquid Crys.* 1993, **230**, 1.

86. J. Alvarez, J. Souto, M.L. Rodriguez-Mendez and J.A. de Saja, *Sens. Actuators B*, 1999, **48**, 339.

87. K.R. Rickwood, D.R. Lovett, B. Lukas and J. Silver, *J. Mater. Chem.*, 1995, **5**, 725.

88. M. Bouvet, A. Leroy, J. Simon, F. Toumilhac, G. Guillaud, P. Lessnick, A. Maillard, S. Spirkovitch, M. Debliquy, A. de Haan and A. Decroly, *Sens. Actuators B*, 2001, **72**, 86.

89. M. Bouvet, G. Guillaud, A. Leroy, A. Maillard, S. Spirkovitch and F.-G. Tournilhac, *Sensors and Actuators B: Chemical*, 2001, **73**, 63.

90. L.L. Miller and M.R. Van De Mark, *J. Am. Chem. Soc.*, 1978, **100**, 3223.

91. J.B. Kerr, L.L. Miller and M.R. Van De Mark, *J. Am. Chem. Soc.*, 1980, **102**, 3383.

92. M.F. Dautartas, J.F. Evans, T. Kuwana, *Anal. Chem.* 1978, 51, 104.

93. N. Oyama and F.C. Anson, *J. Am. Chem. Soc.*, 1979, **101**, 739.

94. A.H Schroeder and F.B. Kaufman, *J. Electroanal. Chem.*, 1980, **133**, 209.

95. F.B. Kaufman, A.H. Schroeder, E.M. Engler, S.R. Kraimer and J.Q. Chambers, *J. Am. Chem. Soc.*, 1980, **102**, 483

96. M.J. Cook, *Pure Appl. Chem.*, 2002, **71**, 2145.

97. M.J. Cook and A. JafariFini, *J. Mater. Chem.*, 1997, **7**, 5.

98. P. Daun and R.W. Murray, *J. Phys. Chem.* 1981, **85**, 389.

99. G.J. Samuels and T.J. Meyer, *J. Am. Chem. Soc.*, 1981, **103**, 307.

100. J. Facci and R.W. Murray, *J. Electroanal. Chem.* 1981, **124**, 339.

101. A. Merz and A.J. Bard, *J. Am. Chem. Soc.*, 1978, **100**, 3222.

102. P.J. Peerce and A.J. Bard, *J. Electroanal. Chem.*, 1980, **114**, 89.

103. K. Itaya and A.J. Bard, *Anal. Chem.*, 1978, **100**, 1478.

104. D.R. Rolison, M. Umana, P. Burgmayer, R.W. Murray, *Inorg. Chem.* 1981, **20**, 2996.

105. M.B. Gilbert and D.J. Curran, *Anal. Chem.*, 1986, **56**, 1028.

106. J. Wang, T. Golden, K. Varughese and I. El-Rayes, *Anal. Chem.*, 1989, **61**, 509.

107. T.J. Mafatle and T. Nyokong,, *J. Electroanal. Chem.*, 1996, **408**, 213.

108. J. Oni P. Westbroek and T. Nyokong, *Electrochem. Commun.*, 2001, **3**, 524.

109. J. Oni and T. Nyokong, *Anal. Chim. Acta*, 2001, **432**, 9.

110. R. Nowak, F.A. Schultz, M. Umana, H. Abruna and R.W. Murray, *J. Electroanal. Chem.*, 1978, **94**, 219.

111. P. Daun and R.W. Murray, *J. Electroanal. Chem.*, 1979, **103**, 289.

112. M.F. Dautartas and J.F. Evans, *J. Electroanal. Chem.*, 1981, **109**, 301.

113. J. Facci, R.W. Murray, *Anal. Chem.*, 1980, **54**, 772.

114. M.-C. Pham, P.-C. Lacaze and J.-E. Dubois, *J. Electroanal. Chem.*, 1979, **99**, 331

115. A. Volkov, G. Tourillon, P.C. Lacaze and J.-E. Dubois, *J. Electroanal. Chem.*, 1980, **115**, 279.

116. A.F. Diaz and J.A. Logan, *J. Electroanal. Chem.*, 1980, **111**, 111.

117. A.F. Diaz, J.I. Castillo, J.A. Logan and W.-Y. Lee, *J. Electroanal. Chem.*, 1981, 129, 115.

118. E.M. Genies, G. Bidan and A.F. Diaz, *J. Electroanal. Chem.*, 1983, **149**, 101.

119. R.M. Penner and C.R. Martin, *J. Electrochem. Soc.*, 1986, **133**, 300.

120. K.K. Kanazawa, A.F. Diaz, R.H. Geiss, W.D. Gill, J.F. Kwak, J.A. Logan, J.F. Rabolt and G.B. Street, *J. Chem. Soc.* 1979, 854.

121. H.D. Abruna, P. Denisevich, M. Umana, T.J. Meyer and R.W. Murray, *J. Am. Chem. Soc.*, 1981, **103**, 1.

122. P. Denisevich, H.D. Abruna, C.R. Leidner, T.J. Meyer and R.W. Murray, *Inorg. Chem.*, 1982, **21**, 2153.

123. K.W. Willman and R.W. Murray, *J. Electroanal. Chem.*, 1982, **133**, 211

124. B.F.Y.Yan Hin, C.R. Lower, *Sens. Actuators B*, 1992, **7**, 339.

125. G. Bidan, *Sens. Actuators* B: 1992, **6**, 45.

126. G. Harsãnyi, *Sensors in Biomedical Applications. Fundamentals, Technology and Applications*, Techonic Publishing Co. Inc. Lanchester, 2000, ch 2.

127. L. Duic, Z. Mandic and S. Kovac, *Electrochim. Acta*, 1995, **40**, 1681.

128. D. Orata and D.A. Buttry, *J. Am. Chem. Soc.*, 1987, **109**, 3574.

129. H. Yang, D.O. Wipt and A.J. Bard, J. *Electroanal. Chem.*, 1992, **331**, 913.

130. N. Kuramoto, J.C. Michaelson, A.J. McEvoy and M. Gratzel, *J. Chem. Soc. Chem. Commun.*, 1990, 1478.

131. S.N. Hoier and S.-M. Park, J. *Electrochem. Soc.*, 1993, **140**, 2454.

132. S. Prumeanu, E. Csahok, V. Kertesz and G. Ingelt, *Electrochim. Acta*, 1998, **43**, 2305.

133. S.A. Chen and G.W. Hwang, *J. Am. Chem. Soc.*, 1994, **104**, 7939.

134. H. Ding and *S.-M. Park, J. Electrochem. Soc.*, 2003, **150**, E33.

135. S.-M. Park, in *Handbook of Organic Conductive Molecules and Polymers*, Vol. 3, H.S. Nalwa (Ed), John Willey & Sons, Chichester 1997.

136. A.S. Ribeiro, D.A. Machado, P. Faria dos Santos Filho and M.-A. De Paoli, *J. Electroanal. Chem.*, 2004, **567**, 243.

137. R.M. Penner and C.R. Martin, *J.Electrochem. Soc.*, 1986, **133**, 310.

138. R.M. Penner and C.R. Martin, *J. Electrochem. Soc.*, 1986, **133**. 2206.

139. H.S. Sharma and S.-M. Park, *J. Electrochem. Soc.*, 2004, **151**, E61.

140. D.E. Stilwell and S.-M. Park, *J. Electrochem. Soc.*, 1988, **135**, 2254.

141. E.W. Paul, A.J. Ricco and M.S. Wrighton, *J. Phys. Chem.* 1985, **89**, 1441.

142. Y.-B. Shim and S.-M. Park, *J. Electrochem. Soc.*, 1997, **144**, 3027.

143. H.J. Lee, S.-Y. Cui and S.-M. Park, *J. Electrochem. Soc.*, 2001, **148**, D139.

144. E.M. Genies, G. Bidan and A.F. Diaz, *J. Electroanal. Chem.* 1983, **152**, 101.

145. C.K. Baker and J.R. Reynolds, *J. Electroanal. Chem.*, 1988, **251**, 307.

146. A.F. Diaz, J. Crowley, J. Bargon, G.P. Gardini and J.B. Torrance, *J. Electroanal. Chem.*, 1981, **121**, 355.

147. R.J. Waltman and J. Bargon, *Tetrahedron*, 1984, **40**, 3963.

148. M.A. Dayton, J.C. Brown, K.J.Stutts and R.M. Wightman, *Anal. Chem.*, 1980, **52**, 946.

149. K.L. Brown and H.A. Mottola, *Langmuir*, 1998, **14**, 3411.

150. R. John and G.G. Wallace, *J. Electroanal. Chem.*, 1991, **306**, 157.

151. C.R. Martin and C.A. Foss Jr, in *Laboratory Techniques in Electroanalytical Chemistry*, 2nd ed., P.T. Kissinger and W.R. Heineman, (Eds), Marcel Dekker Inc., New York, 1996.

152. C.M. Elliot and R.W. Murray, *Anal. Chem.*, 1976, **48**, 1247.

153. R.F. Lane and A.T. Hubbard, *J. Phys. Chem.*, 1973, **77**, 1401.

154. T.R.E. Simpson, D.A. Russell, I. Chambrier, M.J. Cook, A.B. Horn and S.C. Thorpe, *Sens. Actuators* B, 1995, **29**, 353.

155. T.R.E. Simpson. M.J. Cook, M.C. Petty, S.C. Thorpe and D.A. Russell, *Analyst*, 1996, **121**, 1501.

156. T.R.E. Simpson, D. J. Revell, M.J. Cook and D.A. Russell, *Langmuir*, 1997, **13**, 461.

157. M.P. Somashekarappa, J. Keshavayya and S. Sampath, *Pure Appl. Chem.*, 2002, **74**, 1609.

158. K. Ozoemena, P. westbroek and T. Nyokong, *Electrochem. Commun.*, 2001, **3**, 529.

159. K. Ozoemena, P. Westbroek and T. Nyokong, *Electroanalysis,* 2003, **14**, 1762.

160. K. Ozoemena and T. Nyokong, *Electrochim. Acta,* 2002, **47**, 4035.

161. I. Chamber, M.J. Cook and D.A Russell, *Synthesis*, 1995, **10**, 1283.

162. H.O. Finklea, in *Electroanalytical Chemistry,* A.J Bard and I. Rubinstein (Eds.), Marcel Dekker, New York, Vol. 19, 1996.

163. R.L. Garrell, J.E. Chadwick, D.L. Severance, N.A. McDonald and D.C. Myles, *J. Am. Chem. Soc.,* 1995, **117**, 1563.

164. B. Zeng, Y. Yang and F. Zhao, *Electroanalysis,* 2003, **15**, 1054.

165. J.R. de Sousa, A..A. Batista, I.C.N. Diogenes, G.F.S. Andrade, M.L.A. Temperini, L.G.F. Lopes and I.. d-S. Moreira, *J. Electroanal. Chem.,* 2003, **543**, 93.

166. J. Chen, J. Su, W. Wang, M.A. Reed, *Physica E, Low-dimensional Systems and Nanostructures,* 2003, **16**, 17

167. B. Liedberg and P. Tengvall *Langmuir*, 1995, **11**, 3821.

168. S. Besbes, A. Ltaief, K. Reybier, L. Ponsonnet, N. Jaffrezic, J. Davenas and H.B. Ouada, *Synthetic Metals*, 2003, **138**, 197

169. X. Huang, Y. Liu, S. Wang, S. Zhou and D. Zhu, *Chem. Eur. J.*, 2002, **8**, 4179.

170. N. Muskal and D. Mandler, *Current Separations*, 2000, **19**, 49.

171. M.S. El-Deab and T. Ahsaka, *Electrochem. Commun.*, 2003, **5**, 214.

172. D.-S. Kong, L.-J. Wan, M.-J. Han, G.-B. Pan, S.-B. Lei, C.-L. Bai and S.-H. Chen, *Electrochim. Acta*, 2002, **48**, 303.

173. Y. Naitoh, T. Matsumoto, K.-I. Sugiura, Y. Sakata and T. Kawai, *Surf. Sci.*, 2001, **487**, L534.

174. J. Lipkowski, P.N. Ross (Eds.), *Adsorption of Molecules at Metal Electrodes*. VCH Publishers, New York, 1992.

175. H. Striegler, P. Skoluda and D.M. Kolb, *J. Electroanal. Chem.*, 1999, **471**, 9.

176. M.S. Zei and G. Ertl, *Phys. Chem. Chem. Phys.*, 2000, **2**, 3855.

177. B.M. Ocko, I.K. Robinson, M. Weinert, R.J. Randler and D.M. Kolb, *Phys. Rev. Lett.*, 1999, **83**, 780.

178. A.T. Fiory, *Proceedings of RTP 2000, Eight International Conference on Advanced Thermal Processing of Semiconductors* (Gaitherburg, Md.).pp 15-25.

179. P. Skoluda, M. Hőlzle, J. Lipkowski and D.M. Kolb, *J. Electroanal. Chem.*, 1993, **358**, 343.

180. P.J. Peerce and A.J. Bard, *J. Electroanal. Chem.*, 1980, **112**, 97.

181. J.F. Evans, T. Kuwana, M.T. Henne and G.P. Royer, *J. Electroanal. Chem.*, 1977, 80, 409.

182. C. DeGrand and L.L. Miller, *J. Am. Chem. Soc.*, 1980, **102**, 5728.

183. C.P. Andrieux and J.-M. Saveant, *J. Electroanal. Chem.* 1978, **93**, 163.

184. I. Rubinstein and A.J. Bard, *J. Am. Chem. Soc.*, 1980, **102**, 6641.

185. R.D. Rocklin and R.W. Murray, *J. Phys. Chem.* 1981, **85**, 2104.

186. C.M. Elliot and C.A. Marrese, *J. Electroanal. Chem.*, 1989, **199**, 395.

187. D.C.-S. Tse and T. Kuwana, *Anal. Chem.*, 1978, **50**, 1315.

188. F.C. Anson, J.M. Saveant, *J. Electroanal. Chem.*, 1983, **134**, 163.

189. W.J. Albery, M.J. Eddowes, H.A.O.Hill and A.R. Hillman, *J. Am. Chem. Soc.*, 1981, **103**, 3904.

190. C. Ueda, D.C. Tse and T. Kuwana, *Anal. Chem.*, 1982, **54**, 850.

191. K.N. Kuo and R.W. Murray, *J. Electroanal. Chem.*, 1982, **131**, 37.

192. A. Braun and J. Tchemiac, *Ber. Disch. Chem. Ges.* 1907, **40**, 2709.

193. R.P. Linstead, *J. Chem. Soc.*, 1934, 1016.

194. J.M. Robertson, *J.Chem. Soc.*, 1935, 615.

195. J.M. Robertson, *J.Chem. Soc.*, 1936, 1195.

196. J.M. Robertson and I. Woodward, *J.Chem. Soc.*, 1936, 219.

197. *Phthalocyanines: Properties and Applications,* C.C. Leznoff and A.B.P. Lever (Eds.) VCH Publishers, New York, Vols. **1-4**, 1989, 1993, 1993, 1996

198. M.S. Fischer, D.H. Templeton, A. Zalkin and M. Calvin, *J. Am. Chem. Soc.*, 1975, **97**, 2676.

199. M. Gouterman, In D. Dolphin (Ed) *The Porphyrins,* Physical Chemistry, Part A, Vol. 3, Academic Press: New York, 1978; pp. 1-165.

200. F.R. Fan and L.R. Faulkner, *J. Am. Chem. Soc.*, 1979, **101**, 4779.

201. T. Nyokong, Z. Gasyna and M.J. Stillman *Inorg. Chem.*, 1987, **26**, 548.

202. T. Nyokong, Z. Gasyna, and M.J. Stillman, *Inorg. Chem.*, 1987, **26**, 1087.

203. E.A. Ough, T. Nyokong, K.A. Creber and M.J. Stillman, *Inorg. Chem.*, 1988, **27**, 2724.

204. E.A. Ough, Z. Gasyna and M.J. Stillman, *Inorg. Chem.*, 1991, **30**, 2301.

205. E.A. Ough and M.J. Stillman, *Inorg. Chem.*, 1994, **33**, 573.

206. J. Mack and M.J. Stillman, *J. Am. Chem. Soc.*, 1994, **116**, 1292

207. T.H. Huang, K.E. Reickhoff and E.M. Voight, *J. Chem. Phys.*, 1982, **77**, 3424.

208. T.H. Huang, K.E. Reickhoff and E.M. Voight, *J. Chem. Phys.*, 1981, **85**, 3322.

209. M. L'Her and A. Pondaven. In: *The Porphyrin Handbook*, K.M. Kadish, K.M. Smith and R. Guilard, (Eds), Academic Press: San Diego, 2003, vol. 16, pp 117-169.

210. K.M. Kadish, in Lippard (Ed), *Progress in Inorganic Chemistry*, Vol. 34, Marcel Dekker, New York, 1986

211. M. Hanack and M. Lang, *Adv. Mat.* 1994, **6**, 819

212. D. Wohrle, G. Schnurpfeil and G. Knothe, *Dyes and Pigments*, 1992, **18**, 91.

213. A. Lützen, S.D. Starnes, D.M. Rudkevich and J. Rebeck Jr, *Tetrahedron Letters*, 2000, **41**, 3777.

214. F. Yilmaz, D. Atilla and V. Ahsen, *Polyhedron*, 2004, **23**, 1931.

215. M. Brewis, M. Helliwell, N.B. McKeown, S. Reynolds and A. Shawcross, *Tetrahydron Letters,* 2001, **42**, 813.

216. M. Brewis, M. Helliwell and N.B. McKeown, *Tetrahedron*, 2003, **59**, 3863.

217. C.-H. Lee and D.K. Ng, *Tetrahedron Lett.*, 2002, **43**, 4211.

218. W.M. Sharman and J.E. Van Lier, *The Porphyrin Handbook*, K.M Kadish, K.M. Smith and R. Guilard (Eds), Academic Press, N.Y., vol. 15, 2003, pp 1-60.

219. P. Yiru, H. Fenghua, L. Zhipeng, C. Naisheng and H. Jinling, *Inorg. Chem. Commun.* 2004, **7**, 967

220. N.B. Mckeown, *Phthalocyanine Materials: Synthesis, Structure and Function*, Cambridge University Press, London, 1998, p 211.

221. M. Ambroz, A. Beeby, A.J. MacRobert, M.S.C. Simpson , R.K. Svensen and D. Phillips, *J. Photochem. Photobiol. B: Biol.,* 1991, 9, 87.

222. E. Hamuryudan, S. Merey and Z.A. Bayir, *Dyes and Pigments,* 2003, **59**, 263.

223. S. Foley, J. Gurnos, R. Luizzi, D.J. McGarvey, M. Perry and T.G. Truscott, *J. Chem. Soc., Perkin Trans.,* 1997, **2**, 1725.

224. G. Torre and A.T. Torres, *J. Prophyrins Phthalocyanines,* 1997, **1**, 221.

225. D. Wöhrle, M. Eskes, K. Shigehara and A. Yamada, *Synthesis*, 1993, 194.

226. X. Ding and H. Xu, *Sens. Actuators* B: 2000, 65, 108.

227. Q. Zhang, D. Huang, Y. Liu, *Synthetic Metals*, 2003, **137**, 989.

228. H. Xu, H. Li and K. Liu, *Dyes and Pigments*, 2001, **49**, 9.

229. X. Ding, H. Xu, L. Zhang, D. Jiang and A. Lu, *Thin Solid Films,* 1999, 340, 271.

230. X. Ding and H. Xu, *Thin Solid Films,* 1999, **338**, 286.

231. K. Sakamoto, T. Kato, E. Ohno-Okumura, M. Wanatab and M.J. Cook, *Dyes and Pigments*, 2005, **64**, 63.

232. O. Oda, S.-I. Ogura and I. Okura, *J. Photochem. and Photobiol. B: Biology,* 2000, **59**, 20.

233. Z. Smetana, E. Mendelson, J. Manor, J.E. van Lier, E. Ben-Hur, S. Salzberg and Z. Malik, *J. Photochem. Photobiol. B: Biology,* 1994, **22**, 37.

234. P. Margaron, R. Langois and J.E. van Lier, *J. Photochem. and Photobiol.* B: 1992, **14,** 187.

235. N. Kobayashi, T. Ishizaki, K. Ishii, and H. Konami, *J. Am. Chem. Soc.*, 1999, **121**, 9096.

236. S. Greenberg, A.B.P. Lever and C.C. Leznoff, *Can. J. Chem.*, 1988, **66**, 1059

237. N. Kobayashi, R. Kondo, S. Nakajima and T. Osa, *J. Am. Chem. Soc.* 1990, 112, 9640.

238. A. Meller and A. Ossko, *Monatsh. Chem.*, 1972, **103**, 150.

239. M.A. Diaz-Garcia and F. Agullo-Lopez, *J. Phys. Chem.*, 1995, **99**, 14988.

240. N. Kobayashi, *Bull. Chem. Soc. Jpn.*, 2002, 79.

241. J.G. Young and W. Onyebuagu, *J. Org. Chem.*, 1990, **55**, 2155.

242. D.M. Drew and C.C. Leznoff, *Syn. Lett.*, 1994, 623.

243. B.N. Acher, G.M. Fohlon, J.A. Parker and J. Keshavayya, *Polyhedron*, 1987, **6**, 1463.

244. N.B. McKeown, in, *The Porphyrin Handbook*, K.M Kadish, K.M. Smith, R. Guilard (Eds), Academic Press, N.Y., vol. 15, 2003, pp 61-124.

245. R. Hagen and T. Bieringer, *Adv. Mater.* 2001, **13**, 1805.

246. S. Priyadarshy, M.J. Therien and D.N. Beratan, *J. Am. Chem. Soc.*, 1996, **118**, 1497.

247. S.M. LeCours, H.W. Guan, S.G. DiMagno, C.H. Wang and M.J. Therien, *J. Am. Chem. Soc.*, 1996, **118**, 1504.

248. M.P. De Filippis, D. Dei, L. Fantetti and G. Roncucci, *Tetrahedron Lett.*, 2000, **41**, 9143.

249. F. Gan, *Chinese Sci. Bull.* 2000, **45**, 572.

250. R. Hagen and T. Bieringer, *Adv. Mater.* 2001, **13**, 1805.

251. J.E. Kuder, *Inorg. Sci.,* 1988, **32**, 51.

252. G.G. Robert, M.C. Petty, S. Baker, M.T. Flowler and N.J. Thomas, *Thin Solid films,* 1985, **132**, 113.

253. M.J. Cook, A,J. Dunn, F.M. Daniel, R.C.O. Hart, R.M. Richardson and S.J. Rose, *Thin Solid films*, 1988, **159**, 83.

254. H. Schultz, H. Lehmann, M. Rein and M. Hannack, *Struct. Bonding,* 1991, **74**, 41.

255. S.B. Brown and T.G. Truscott, *Chem. Br.* 1993, 955.

256. G.T. Byrne, R.P. Linstead and A.R. Lowe, *J. Chem. Soc.,* 1934, 1017.

257. R.P. Linstead and A.R. Lowe, *J. Chem. Soc.,* 1934, 1022.

258. C.E. Dent, R.P. Linstead and A.R. Lowe, *J. Chem. Soc.,* 1934, 1033.

259. J.A. Elvidge and R.P. Linstead, *J. Chem. Soc.,* 1955, 3536.

260. D. Ma, D. Wang, Z. Hong, X. Zhao, X. Jing, F.Wang, *Synthetic Metals*, 1997, **91**, 331.

261. H. Kojima, A.Ozawa, T. Takahashi, M. Nagaoka, T. Homma, T. Nagatomo and O. Omoto, *J. Electrochem. Soc.*, 1997, **144**, 3628

262. K.Y. Law, *Chem. Rev.*, 1993, **93**, 449.

263. J.W. Owens, M.Perry and D.W. Seybert, *Inorg. Chim. Acta*, 1998, **277**, 1.

264. B.C. Sheker, S.Sakthivel, D. Mangalraj, S.A.K. Narayandass and S. Venkatachalam, *Bull. Electrochem.*, 1987, **14,** 422

265. J.P. Collman, J.T. McDevitt, C.R. Leidner, G.T. Yee, J.B. Torrance and W.A. Little, *J. Am. Chem. Soc.*, 1987, **109**, 4606.

266. J. Simon, C.Sirlin, *Pure Appl. Chem.*, 1989, **61**, 1625.

267. D.W. Bruce, D.A. Dunmur, L.S. Santa and M.A. Wali, *J.Mater. Chem.*, 1992, **2**, 363.

268. Y. Liu, K. Shigehara, M.Hara and A. Yamada, *J. Am. Chem. Soc.*, 1991, **113**, 440.

269. B.Z. Zmudzka, A.G. Stickland, J.Z. Beer and E.Ben-Hur, *Photochem. Photobiol.* 1997, **65**, 461.

270. E. Ben-Hur, J. Oetjen and B. Horowitz, *Photochem. Photobiol.*, 1997, **65**, 456.

271. A.N. Vzorov, L.G. Marzilli, R.W. Compaus and D.W. Dixon, *Antiviral Research*, 2003, **59**, 99.

272. M. Ebadi and ABP Lever, *J. Porphyrins Phthalocyanines,* 2003, **7**, 529.

273. S. Griveau, M. Gulppi, F. Bedioui and J. H. Zagal, *Solid State Ionics,* 2004, **169**, 59.

274. C.A. Caro, F. Bedioui and J.H. Zagal, *Electrochim.* Acta, 2002, **47**, 1489.

275. L.J. Ignarro, R.E. Byrns, G.M. Buga, K.S. Wood, G. Chaudhuri, *J. Pharmacol. Exp. Ther.* 1988, **244**, 181.

276. F.J. Fenoy, P. Ferrer, L. Carbonell, M. García-Salom, *Hypertension.* 1995, **25**, 408.

277. L.J. Huffman, D.J. Prugh, L. Millecchia, K.C. Schuller, S. Cantrell and D.W. Porter, *J. Biosci.,* 2003, **28**, 29.

278. J.H. Zagal, *Coord. Chem.*, Rev., 1992, **119**, 89

279. J.L. Hoard, in K.M. Smith (Ed), *Porphyrins and Metalloporphyrins*, Elsevier, Amsterdam, 1975, 317.

280. N.H. Sabelli, C.A. Melendres, J. Phys. Chem., 1982, **86**, 4342.

281. N.H. Sabelli, L.K. Lee and C.A. Melendres, in W.E. O'Grady, P.N. Ross, Jr. and F.G. Wills (eds), *Electrocatalysis*, Electrochem. Soc. Proc. Ser., The Electrochemical Society, Princeton, NJ, 1982, 131.

282. A.B.P. Lever, *J. Porphyrin Phthalocyanines,* 1999, **3**, 488.

283. S. Griveau, G. Pavez, J.H. Zagal and F. Bedioui, *J. Electroanal. Chem.,* 2001, **497**, 75.

284. N. Kobayashi and W.A. Nevin, *Appl. Organomet. Chem.,* 1996, **10**, 579.

285. P. Randin, *Electrochim. Acta,* 1974, **19**, 83.

286. F. Beck, *J. Appl. Electrochem.,* 1977, **7**, 191.

287. R. Jalinsky, *J. Electrochem. Soc.,* 1965, **112**, 526.

288. R. Jalinsky, *Nature*, 1964, **201**, 1212.

289. M. Sekota and T, Nyokong, *Polyhedron* 1997, **16**, 3279.

290. S. Vilakazi and T. Nyokong, *Polyhedron*, 2000, **19**, 229.

291. R.K. Sen, J. Zagal and E. Yeager, *Inorg. Chem.,* 1977, **16**, 3379.

292. M. Thamae and T. Nyokong, *J. Electroanal. Chem.,* 1999, **470**, 126.

293. S. Maree and T. Nyokong, *J. Electroanal. Chem..*, 2000, **429**, 120.

294. J.S. Bett, H.R. Kunz, A.J. Aldykeiwicz Jr, J.M. Fenton, W.F. Bailey and D.V. McGrath, *Electrochim. Acta*, 1998, **43**, 3645.

295. T. Yoshida, K. T. Kamato, M.Tsukamoto, T. Iida, D. Schlettwein, D. Wohrle and M. Kaneko, *J. Electroanal. Chem.*, 1995, **385**, 209.

296. T. Abe, T. Yoshida, S. Tokita, F. Taguchi, H. Imaya and M. Kaneko, *J. Electroanal. Chem.*, 1996, **412**, 125.

297. N. Phougat, P. Vasudevan, Santosh and A.K. Sukka, *J. Power Sources*, 1993, **46**, 61

298. K.J. Balkus, In *Phthalocyanines: Properties and Applications*, C.C. Leznoff and A.B.P. Lever (Eds), VCH Publishers, Inc, New York, vol. .4, 1996, pp 285-306.

299. K.J. Balkus, A.G. Gabrieov, S.L. Bell, F. Bedioui, L.Roue and J. Devynck, *J. Inorg. Chem.*, 1994, **33**, 67.

300. F. Bedioui, L. Roue and J. Devynck, *New J. Chem.*, 1996, **20**, 1235.

301. C. Coutanceau, A. El Hourch, P. Crouigneau and J.M. Lamy, *Electrochim. Acta*, 1995, **40**, 2739.

302. C. De La Fuente, J.A. Acuna, M.D. Vazquez, M.L. Tascon and P. Sanchez Batanero, *Talanta*, 1999, **49**, 441.

303. M. Gulppi, F. Bedioui and J. Zagal, *Electroanalysis*, 2001, **13**, 1136.

304. A. Breborowicz, H. Rodela, L. Martis and D.G. Oreopoulos, *Int. J. Artif. Organs*. 1996, **19**, 268.

305. F. Canestrari, F. Galli, A. Giorgini, M.C. Albertini, P. Galiotta, M. Pascucci and M. Bossu, *Acta Haematol.* 1994, **91**, 187.

306. V. Calabrese, R. Raffaele, E. Cosentino and V. Rizza., *Int. J. Clin. Pharmacol. Res.*, 1994, **14**, 119.

307. J. Mai , P.S. Sorensen, J.C. Hansen, *Biol. Trace Elem. Res.*, 1990, **24**,109.

308. J. Behr, B. Degenkolb, K. Maier, B. Braun, T. Beinert, F. Krombach, C. Vogelmeier and G. Fruhmann, *Eur. Respir. J.*, 1995, **8**, 1286.

309. P. Chevez-Barrios, A.L. Wiseman, E. Rojas, C.N. Ou and M.W. Lieberman, *Exp. Eye Res*. 2000, **71**, 575.

310. S.M. Cohen, K.L. Olin, W.J. Feuer, L. Hjelmeland, C.L. Keen and L.S. Morse, Br, *J. Ophthalmol.*, 1994, **8**, 791.

311. O. Beloqui, J. Prieto, M. Suarez, B. Gil, C.H. Qian, N. Garcia and M.P. Civeira, *J. Interferon Res.* 1993, **13**, 279.

312. P. Dentico, A. Volpe, R. Buongiorno, I. Grattagliano, E. Altomare, G. Tantimonaco, G. Scotto, R. Sacco and O. Schiraldi, *Recent Prog. Med.* 1995, **86**, 290.

313. F. Farinati, R. Cardin, N. De Maria, G. Della Libera, C. Marafin, E. Lecis, P. Burra, A. Floreani, A. Cecchetto and R. Naccarato. *J. Hepatol.*, 1995, **22**, 449.

314. N.A. Ankrah, T. Rikimaru, F.A. Ekuban and M.M. Addae, *J. Int. Med. Res.*, 1994, **22**, 171.

315. O.A. Andreassen, A. Dedeoglu, P. Klivenyi, M.F. Beal and A.I. Bush, *Neuroreport*, 2000, **11**, 2491.

316. S.C. De Rosa, M.D. Zaretsky, J.G. Dubs, M. Roederer, M. Anderson and A. Green, *Eur. J. Clin. Invest.*, 2000, **30**, 915

317. W.A. Lieinman, J.P. Richie, *Biochem. Pharm.*, 2000, **60**, 19.

318. M. Ebadi, S.K. Srinivasan and M.D. Baxi, *Prog. Neurobiol.* 1996, **48**, 1.

319. J.D. Adams Jr and I.N.Odunze, *Free Radic. Biol. Med.* 1991, **10**, 161.

320. M. Cengiz, A. Yuksel and M. Seven, *Pharmacol. Res.* 2000, **41**, 423

321. K. Abe, K. Nakanishi and H.Saito, *Biol. Pharm. Bull.*, 1999, **22**, 1177.

322. E. Ben-Menachem, M. Kyllerman and S. Marklund, *Epilepsy Res.*, 2000, **40**, 33.

323. M.T. Goodman, K. McDuffie, B. Hernandez, L.R. Wilkens, and J. Selhub, *Cancer*, 2000, **89**, 376.

324. E. Bald, E. Kaniowska, G. Chwatko and R. Glowacki, *Talanta*, 2000, **50**, 1233.

325. J.K. Shabert, C. Winslow, J.M. Lacey and D.W. Wilmore. *Nutrition*. 11 1999, **11**, 860.

326. W. Droge, H.P. Eck and S. Mihm, *Immunol. Today*, 1992, **13**, 211.

327. W. Droge, *Pharmacology*, 1993, **46**, 61.

328. P.C. White, N.S. Lawrence, J. Davies and R.G. Compton, *Electroanalysis*, 2002, **14**, 89.

329. A. Napier and J.P. Hart, *Electroanalysis*, 1996, **8** 1006.

330. T.R. Ralph, M.L. Hitchman, J.P. Millington and F.C. Walsh, *J. Electroanal. Chem.*, 1994, **375**, 1.

331. M. Gulppi, S. Griveau, F. Bedioui and J.H. Zagal, *Electrochim. Acta*. 2001, **46**, 3397

332. M. Sekota and T. Nyokong, *J. Porphyrins Phthalocyanines*, 1999, **3**, 477.

333. X. Qi, R.P. Baldwin, H.W. Li and T.F. Guarr, *Electroanalysis*, 1991, **3**, 119.

334. C. Coutanceau, P.Crouigneau, J.M. Leger and C. Lamy, *J. Electroanal. Chem.*, 1994, **379**, 389.

335. K.I. Ozoemena, *PhD Thesis*, Rhodes University, 2002.

336. F. Damrau, *J. Am Geriatr. Soc.*, 1962, **10**, 426

337. H.M. Feinblatt and J.C. Gant, *J. Maine Med. Assoc.*, 1958, **49**, 99.

338. M.R. Tarasevich, A. Sadkowski and E. Yeager, In *Comphrehensive Treaties of Electrochemistry*, B.E. Conway, J. O'M Bockris, E. Yeager, S.U.M. Khan, R.E. White (Eds), vol 7, Plenum Press, New York, 1983, ch 6.

339. J. Zagal, R.K. Sen and E. Yeager, *J. Electroanal. Chem.*, 1977, **83**, 207.

340. J.P. Randin, *Electrochim. Acta*, 1974, **19**, 83.

341. A. Kozawa, V.E. Zillion and R.J. Brodd, *J. Electrochem. Soc.*, 1970, **117**, 1470.

342. J-C. Moutet and A. Ourari, *Electrochim. Acta*, 1997, **42**, 2525.

343. V. Albin and F. Bedioui, *Electrochem. Commun.*, 2003, **5**, 129.

344. M. Savy, P. Andro, C. Bernard and C. Magner, *Electrochim. Acta*, 1974, **18**, 403.

345. H. Alt, H. Binderand and G. Sandstede, *J. Catal.*, 1973, **28**, 8

346. A.J. Appleby, J. Fleish and M. Savy, *J. Catal,*. 1976, **44**, 281.

347. C.P. Horwitz, S.E. Creager and R,W. Murray, *Inorg. Chem.*, 1990, **29**, 1006.

348. Y.-H. Tse, P. Janda, H. Lam, J. Zhang, W.J, Pietro and A.B.P. Lever, *J. Porphyrins Phthalocyanines*, 1997, **1**, 3.

349. L.J. McDonald andF. Murad, *Proc. Soc. Exp. Biol. Med.* 1996, **211**, 1.

350. T. Michel and O. Feron, *J. Clin. Invest.*, 1997, **100**, 2146.

351. T. Moeslinger, R. Friedl, I. Volf, M. Brunner, E. Koller and P. G. Spieckermann, *Can. J. Physiol. Pharmacol./Rev. Can. Physiol. Pharmacol.* 2000, **78**, 861.

352. D.A. Wink, J.B. Mitchell, *Free Radic. Biol. Med.* 1998, **25**, 434.

353. F. Murad, *Adv. Pharmacol.* 1994, **26**, 19.

354. R.M. Palmer, D.S. Ashton, S. Moncada, *Nature*, 1988, **333**, 664.

355. N. Suzuki, K. Mizuno and Y. Gomi, *Eur. J. Pharmacol.* 1994, **251**, 221.

356. P. Holzer, I. Th. Lippe, A.L. Tabrizi, L. Lénárd, Jr. and L. Barthó, *The J. Pharmacology and Experimental Therapeutics,* 1997, **280**, 154.

357. R. L. Rairigh, T.A. Parker, D.D. Ivy, J.P. Kinsella, I-Da Fan and S.H. Abman, *Circulation Research.* 2001, **88**, 721.

358. K. Matsushita, C.N. Morrell, B. Cambien, S.X. Yang, M. Yamakuchi, C. Bao, M.R. Hara, R.A. Quick, W. Cao, B. O'Rourke, J.M. Lowenstein , J. Pevsner, D.D. Wagner and C.J. Lowenstein, *Cell,* 2003, **115**, 139.

359. X. Ni, E.C. Chan, J.T. Fitter and R. Smith, *J. Clin. Endocrinol Metab.* 1997, **82**, 4171.

360. B.B. Finlay, R.H. See and R.C. Brunham, *Nature Reviews | Microbiology* 2004, **2**, 607.

361. C.G. Mata and L. Lamattina, *Plant Physiol.,* 2001, **126**, 1196.

362. Y. Sakihama, S. Nakamura and H. Yamasaki, *Plant Cell Physiol.*, 2002, **43**, 290.

363. M.V. Beligni and L. Lamattina, *Planta*. 2000, **210**, 215.

364. F. Bedioui, S. Trevin, J. Devynck, F. Lantione, A. Brunet and M.-A. Devynck, *Biosensors Bioelectronics*, 1997, **12**, 205.

365. F. Bedioui, S. Trevin and J. Devynck, *Electroanalysis*, 1996, **8**, 1085.

366. S.R. Smith and H.H. Thorp, *Inorg. Chim. Acta*, 1998, **273**, 316.

367. J. Jin, T. Miwa, L. Mao, H. Tu and L. Jin, *Talanta*, 1999, **48**, 1005.

368. M. Pontie, F. Bedioui, and J. Devynck, *Electroanalysis*, 1999, **11**, 845.

369. T. Malinski, Z. Taha, S. Grunfeld, A. Burewicz and P. Tomboulian, *Anal. Chim. Acta*, 1993, **279**, 135.

370. F. Bedioui, S. Trevin, V. Albin, M.G.G. Vilegas and J. Devynck, *Anal. Chim. Acta*, 1997, **341**, 177.

371. S. Trevin, F. Bedioui and J. Devynck, *J. Electroanal. Chem.*, 1996, **408**, 261.

372. S.L. Vilakazi and T. Nyokong, *J. Electroanal. Chem.*, 2001, **512**, 56.

373. C.-H. Yu and Y.O. Su, *J. Electroanal. Chem.*, 1994, **368**, 323.

374. I. Zilbermann, J. Hayon, T. Katchalski, R. Ydgar, J. Rishpon, A.I. Shames, E. Korin and A. Bettelheim, *Inorg. Chim. Acta*, 2000, **305**, 53.

375. K. Uchida, M. Soma, T. Onishi and K. Tamaru, *J. Chem. Soc. Faraday Trans.*, 1979, **75**, 2839.

376. P. Ascenzi, M. Brunori, G. Pessesi, C. Ercolani and F. Monacelli, *J. Chem. Soc. Dalton Trans.*, 1987, 369

377. S.X. Guo and S.B. Khoo, *Anal. Lett.*, 1999, **32**, 689.

378. I. Zilbermann, J. Hayon, T. Katchalski, O. Raveh, J. Rishpon, A.I. Shames, E. Korin, and A. Bettelheim, *J. Electrochem. Soc.*, 1997, **144**, L228.

379. S.L. Vilakazi, and T. Nyokong, *Polyhedron*, 1998, **17**, 4415.

380. N. Pieira-Rodrigues, V. Albin, M. Koudelka-Hep, V. Auger, A. Pailleret and F. Bedioui, *Electrochem. Commun.*, 2002, **4**, 922.

381. S. Isik, L. Berdondini, J. Oni, A. Blőchl, M. Koudelka-Hep and W. Schuhman, *Biosensors Bioelectronics,* 2005, **20**, 1566.

382. K. Ogura and S. Yamasaki, *J. Appl. Electrochem.*, 1985, **15**, 279.

383. P. MacCarthy, R.W. Klusman and S.W. Cowling, *Anal. Chem.,* 1991, **63**, 301.

384. G.F. Wang, M. Satake and K. Horita, *Talanta*, 1998, **46**, 671.

385. A.A. Ensafi and G.B. Dehaghei, *Fresenius' J. Anal. Chem.*, 1999, **363**, 131.

386. M.J. Moorcroft, J. Davis and R.J. Compton, *Talanta*, 2001, **54**, 785.

387. J.Z. Li, X.Y. Pang and R.Q. Yu, *Anal. Chim. Acta.*, 1994, **297**, 437.

388. N. Chebotareva and T. Nyokong, *J. Appl. Electrochem.*, 1997, **27**, 975.

389. J.N. Younathan, K.S. Wood and T.J. Meyer, *Inorg. Chem.*, 1992, **31**, 3280.

390. N. Chebotareva and T. Nyokong, *J. Coord. Chem.*, 1999, **46**, 433.

391. D. Mimica, J.H. Zagal and F. Bedioui, *J. Electroanal. Chem.* 2001, **497**, 106.

392. J.M. Bollag, C.S. Helling and M.J. Alexander, *J. Agric., Food Chem.* 1986, **16**, 826

393. L.H. Keither and W.A. Tellard, *Environ. Sci. Technol.* 1979, **13**, 416.

394. L.P. Moos, E.J. Kirsch, R.F. Wukasch and C.P.L. Grady, *Water Res.*, 1983, **17**, 1575.

395. C. Saby and J.H.T.Luong, *Electroanalysis,* 1998 **10**, 7

396. M. Gatretrll, D.W. Kirk, *J. Electrochem. Soc.*, 1992, **139**, 2736.

397. J. Manriquez, J.L. Bravo, S. Guitierrez-Granados, S.S. Succar, C. Bied-Charreton, A.A. Ordaz and F. Bedioui, *Anal. Chim. Acta,* 1999, **378**, 159.

398. M.S. Ureta-Zanartu, P. Bustos, C. Berrios, M.C. Diez, M.L. Mora and C. Gutierrez, *Electrochim. Acta*, 2002, **47**, 2399.

399. N. Trombach, O. Hild, D. Schettwein and D. Wöhrle, *J. Mater. Chem.*, 2002, **12**, 879.

400. B.N Achar, G.M. Fohlen, J.A. Parker and J. Keshavayya, *Polyhedron*, 1987, **6**, 1463.

401. F. Hartl and K.M. Daněk, *J. Electroanal. Chem.*, 1991, **317**, 179

402. D. Losic, J.G. Shapter and J.J. Gooding, *Langmuir*, 2001, **17**, 3307.

403. N. Diab and W. Schuhmann, *Electrochim. Acta,* 2001, **47**, 265.

404. F. Bedioui, J. Devynck and C. Bied-Charreton, *Acc. Chem. Res.*, 1995, **28**, 30.

405. S. Cosnier, C. Gondran, R. Wessel, F.P. Montforts and M. Wedel, *J. Electroanal. Chem.*, 2000, **488**, 83.

406. M.N. Golovin, P. Seymour, K. Jayaraj , Y.S. Fu and A.B.P. Lever, *Inorg. Chem.*, 1990, **29**, 1719.

407. A.B.P. Lever, E.R. Milaeva and G. Speier, In *Phthalocyanines: Properties and Applications*, C.C. Leznoff, A.B.P. Lever (eds) VCH Pub. New York, 1993, vol.3, Ch 1.

408. A.B.P. Lever, J.P. Wilshire and S.K. Quan, *Inorg. Chem.*, 1981, **20**, 761.

409. M.J. Stillman, T. Nyokong. In Phthalocyanines: Properties and Applications, vol.1, C.C. Leznoff, A.B.P. Lever (Eds) VCH: New York, 1989, Chap. 3.

410. S. Knecht, K. Dürr, G. Schmid, L.R. Subramanian and M. Hanack, *J. Porphyrins Phthalocyanine*, 1999, **3**, 292.

411. W. Pasiuk-Bronikowska, M. Krajewska and I. Flis-Kabulska, *Polyhedron*, 1998, **18**, 561.

412. J. Limson and T. Nyokong, *Electroanalysis*, 1997, **9**, 255.

413. A.F. Diaz, J. Bargon, in *Handbook of Organic Conducting Polymers*, Ed, T.A. Stokheim, Marcel Dekker, New York, 1986, vol. 1, pp 87-88

414. H.S. Nalwa (Ed) in handbook of conductive molecules and polymers, John Wiley and Sons Ltd, 1997, vol. 2.

415. M.J. Stillman, In *Phthalocyanines: Properties and Applications*, C.C. Leznoff and A.B.P. Lever (Eds) VCH, New York, 1993, vol. 3, ch. 5.

416. K.L. Brown, J. Shaw, M. Ambrose and H.A. Mottola, *Microchem. J.*, 2002, **72**, 285.

417. G. Ramirez, E. Trullund, M. Isaacs, F. Armijo, J. Zagal, J. Costamagna and M.J. Aguiree, *Electroanalysis* , 2002, **14**, 540.

418. C. Alexiou and A.B.P. Lever, *Coord. Chem. Rev.*, 2001, **216-217**, 45.

419. P. Tau, A.O. Ogunsipe, S. Maree, D. Maree and T. Nyokong, *J. Porphyrins Phthalocyanines*, 2003, **7**, 438.

420. Š. Komorsky-Lovríc, *J. Electroanal. Chem.* 1995, **397**, 211.

421. A.B.P. Lever and J.P. Wilshire, *Can. J. Chem.*, 1976, **54**, 2514.

422. A.B.P. Lever, P.C. Minor and J.P. Wilshire, *Inorg. Chem,* 1981, **20,** 2550.

423. D.K. Rittenberg, L. Baars-Hibbe, A. Böhm and J.S. Miller, *J. Mater. Chem.*, 2000, **10**, 241.

424. C.-L. Lin, C.-C. Lee and K.-C. Ho, *J. Electroanal. Chem.*, 1995, **397**, 211.

425. O.V. Dolotova, N.I. Bundina, O.L. Kaliya and E.A. Lukyanets, *J. Porphyrins Phthalocyanines*, 1997, **1**, 355.

426. G. Zotti, S. Cattarin and N. Comisso, *J. Electroanal. Chem.*, 1987, **235**, 259.

427. P. Audebert, S. Sadki, F. Miomandre and G. Clavier, *Electrochem. Commun.*, 2004, **6**, 144.

428. P.T. Kissinger, C.R. Preddy, R.E. Shoup, W.R. Heineman, in Laboratory techniques in Electroanalytical Chemistry, O.T. Kissinger, W.R. Heineman (Eds.). 2nd Ed. (1996) Marcel Dekker, New York

429. S. Cosnier, A. Deronzier and J.C. Moutet, *J. Electroanal. Chem.*, 1985, **193**, 193.

430. S. Cosnier, A. Deronzier and J.C. Moutet, *J. Electroanal. Chem.*, 1986, **207**, 315.

431. S. Cosnier, A. Deronzier and J.-F. Roland, *J. Electroanal. Chem.*, 1990, **285**, 133.

432. M.A. Vorotynsev, M. Skompska, E. Pousson, J. Goux and C. Moise, *J. Electroanal. Chem.*, 2003, **552**, 307.

433. G. Bidan, In, *Proceedings of the Spring Meeting of the Electrochemical Society,* Toronto, Ont, Canada, 1985, p. 105.

434. G. Bidan, B. Divisia-Blohorn, M. Lapkowski, J.M. Kern and J.P. Sauvage, *J. Am. Chem. Soc.*, 1992, **114**, 5986.

435. A. Deronzier and J.C. Moutet, *Coord. Chem. Rev*, 1996, **147**, 339.

436. C. Odin and M. Nechtchein, *Synthetic Metals*, 1991, **41-43**, 2943.

437. S. Griveau, V. Albin, T. Pauporté, J.H. Zagal and F. Bedioui, *J. Mater. Chem.*, 2002, **12**, 225.

438. V. Vijayanathan, S. Venkatachalam and V.N. Krishnamurthy. *Synthetic Metals,* 2000, **114,** 273.

439. S Asavapiriyanont, G.K. Chandler, G.A. Gunawardena, D.Pletcher, *J. Electroanal. Chem.*, 1984, **177**, 229.

440. Z. Zhang and G. Shi, *J. Electroanal. Chem.*, 2004, **569**, 197.

441. A.J. Downard and D. Pletcher, *J. Electroanal. Chem.*, 1986, **206**, 139.

442. R.E. Nofttle and D. Pletcher, *J. Electroanal. Chem.*, 1987, **227**, 229.

443. T.F. Otero and E.D. Larreta-Azelain, *Polymer,* 1988, **29**, 1522.

444. S. Trevin, F. Bedioui, M.G. Gomez Villegas and C. Bied-Charreton, *J. Mater. Chem.*, 1997, **7**, 923.

445. A. Goux, F. Bedioui, L. Robbiola and M. Pontie, *Electroanalysis*, 2003, **15**, 696.

446. T. R. I. Cataldi, D. Centonze and G. Ricciardi, *Electroanalysis*, 1995, **7**, 312.

447. T. R. I. Cataldi, E. Desimoni, G. Ricciardi and L. Francesco, *Electroanalysis*, 1995, **7**, 435.

448. D.E. Raymond and D.J. Harrison, *J. Electroanal. Chem.* 1990, **296**, 269.

449. K.Tanaka, T. Shichiri, S. Wang and T. Yamabe, *Synthetic Metals*, 1988, **24**, 203.

450. M. Takakubo, *J. Electroanal. Chem.*, 1989, **258**, 303.

451. F. Hahn, B. Beden, M.J. Croissant and C. Lamy, *Electrochim. Acta,* 1986, **31**, 335.

452. M.K. Amini, S. Shahrokhian and S. Tangestaninejad, *Anal. Lett.*, 1999, **32**, 2737.

453. S.B. Saidman, *Electrochim. Acta*, 2003, **48,** 1719.

454. C.-L. Lin, C.-C. Lee and K.-C. Ho, *J. Electroanal. Chem.*, 1995, **397**, 211.

455. F. D'Souza, *J. Porphyrins Phthalocyanines*, 2002, **6**, 285.

456. G. Inzelt, V. Kertesz and A.-S. Nyback, *J. Solid State Electrochem.*, 1999, **3**, 251.

457. E. Sabatani and I. Rubenstein, *J. Phys. Chem.:* A., 1987, **91**, 6663.

458. J. Wang, J.L.L. Paz and M. Jiang, *Langmuir*, 1999, **15**, 1884.

459. D.L. Pilloud, X. Chen, P.L. Dutton and C.C. Moser, *J. Phys. Che*m.: B, 2000, **104**, 2868.

460. S. Griveau, M. Gulppi, J. Pavez, J.H. Zagal and F. Bedioui, *Electroanalysis*, 2003, **15**, 779.

461. G. Mengoli and M. Musiani, *Electrochim. Acta*, 1986, **31**, 201.

462. T.J. O'Shea and S.M. Lunte, *Anal. Chem.*, 1994, **66**, 307.

463. M.K. Halbert and R.P. Baldwin, *Anal. Chem.*, 1985, **57**, 591.

464. F. Beck, *Electrochim. Acta*, 1988, **33**, 839.

465. R. Lapuente, F. Cases, P. Garcés, E. Morallon, J.L. Vázquez, *J. Electroanal. Chem.*, 1998, **451**, 163.

466. S. Gutherrez-Granados, F. Bedioui and J. Devynck, *Electrochim. Acta*, 1993, **38**, 1747.